RUSSIAN ACADEMY OF SCIENCES
NATIONAL GEOPHYSICAL COMMITTEE

РОССИЙСКАЯ АКАДЕМИЯ НАУК
## НАЦИОНАЛЬНЫЙ ГЕОФИЗИЧЕСКИЙ КОМИТЕТ

NATIONAL REPORT

for the
International Association of
Volcanology and Chemistry of the Earth's Interior
of the
International Union of Geodesy and Geophysics
2011–2014

НАЦИОНАЛЬНЫЙ ОТЧЕТ

для
Международной ассоциации
вулканологии и химии недр Земли
Международного
геодезического и геофизического союза
2011–2014

Москва   2015   Moscow
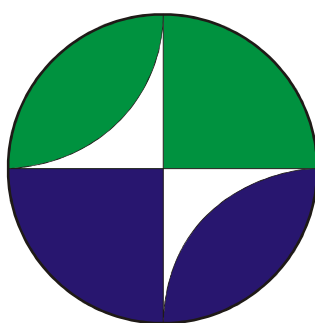
**Presented to the XXVI General Assembly
of the
International Union of Geodesy and Geophysics**

**К XXVI Генеральной ассамблее
Международного геодезического и геофизического
союза**

RUSSIAN ACADEMY OF SCIENCES

National Geophysical Committee

NATIONAL REPORT

for the
International Association of
Volcanology and Chemistry of the Earth's Interior
of the
International Union of Geodesy and Geophysics
2011–2014

Presented to the XXVI General Assembly
of the
IUGG

2015
Moscow

In the present National Report, major results are given of research conducted by Russian scientists in 2011–2014 on the topics of the International Association of Volcanology and Chemistry of the Earth's Interior (IAVCEI) of the International Union of Geodesy and Geophysics. Kamchatka Peninsula with its famous Klyuchevskaya Group of volcanoes is the most volcanically active area in Russia and one of the most active in the world. Majority of researches and scientific results on Volcanology and Geochemistry of the Earth's Interior during 2011–2014 were achieved in this region including recent data on new Tolbachik fissure eruption in 2012–2013. Besides it, the scientific results on the magmatism outside Russia, which were achieved by Russian scientists, are also included in this review. Major achievements in the chemistry of the Earth, geothermy, geodynamics, geochronology and deep mantle structure are featured. The studies as for the single volcanoes as well the regional observations are outlined. The theoretical and applied efforts connected to the volcanological processes are considered. The main conclusions are illustrated by summarized figures. All the required references are given.

В данном Национальном отчете представлены основные результаты исследований, проводимых российскими учеными в 2011—2014 гг., по темам, соответветствующим направлениям деятельности Международной ассоциации вулканологии и химии недр Земли (МАВХНЗ) Международного геодезического и геофизического союза (МГГС). Полуостров Камчатка с его знаменитой Ключевской группой вулканов являются наиболее вулканически активной областью России и одной из самых активных в мире. Основные результаы исследований по вулканологии и химии недр Земли в 2011—2014 гг. были получены в данном регионе, включая недавние данные по новому трещинному извержению вулкана Толбачик в 2012—2013 гг. Кром того, в отчет включены полученные российскими учеными научные результаты по магматизму за пределами России. В отчете представлены основные достижения по геохимии, геотермии, геодинамике, геохронологии и глубинному строению мантии. Описаны исследования как для отдельных вулканов, так и для целых регионов. Рассмотрены теоретические прикладные вопросы вулканических процессов. Основные выводы приведены на сводных иллюстрациях. Приведены все требуемые ссылки.

CONTENT

INTRODUCTION

T.G. Churikova, tchurikova@mail.ru, *National Geophysical Committee, Russian Academy of Sciences, Moscow, Russia. Institute of Volcanology and Seismology, Far East Division, Russian Academy of Sciences, Petropavlovsk-Kamchatsky, Russia*

This report submitted to the International Association of Volcanology and Chemistry of the Earth's Interior (IAVCEI) of the International Union of Geodesy and Geophysics (IUGG) contains results obtained by Russian volcanologists and geochemists in 2011-2014. In the report prepared for the XXVI General Assembly of IUGG (Prague, Czech Republic, 22 June - 2 July 2015), the results are briefly outlined of basic research in volcanology, geochemistry, isotopic systematics, geodynamics, geothermy, as well as in some other disciplines.

The period from 2011 to 2014 was still difficult for Russian volcanologists and geochemists. Owing to economic reasons scientific career in Russia is still believed to be lacking in prestige. Thus recruiting younger scientists for fundamental research in volcanologists and geochemists actually failed. Economic difficulties were redoubled by difficulties arising from reorganizing the Russian Academy of Sciences, Russian science and the educational system of Russia initiated by the leaders of the country. The number of Russian scientists in governing bodies of IUGG, IAVCEI, IASPEI, and their commissions is decreasing. In spite of the difficulties, Russian scientists participated in practically all conferences of the International Association of Volcanology and Chemistry of the Earth's Interior (IAVCEI), in the General Assemblies, international projects and international centers.

Even in such difficult conditions high scientific potential, great experience in research and the traditions of Russian volcanologists and geochemists allowed obtaining a number of fundamentally important new results in the period under review. Many of them are presented in the following sections of this report.

One of the most pronounced events in Russian volcanology during reviewing period was the IVS 50th anniversary Fissure Tolbachik Eruption (FTE-50) in 2012-13, named in honor of 50th anniversary of the Institute of Volcanology and Seismology of the Far East Division of Russian Academy of Sciences. At the present time the special issue of JVGR on 2012-13 Tolbachik eruption is in preparation. The most valuable and important results on this eruption available to present time are presented in this report.

In the reviewed period several volcanoes of the Kurile-Kamchatka arc were erupted. Volcanoes Shiveluch, Klyuchevskoy, Bezymianny, Karymsky are erupting regularly and these volcanoes were erupting during 2011-2014 with a frequency several times per year. Additionally during this time were erupted several volcanoes which were not active during several decades. This is such volcanoes as Kizimen volcano (last phreatic eruption was in 1928-29; there is no any deposits after this eruption) which was erupted from 9th of December 2010 to 9th of December 2013, Zhupanovsky volcano (last eruption was in 1956-57) started erupting from 24th of October 2013 and continue up to now, and Tolbachik fissure eruption FTE-50 (last eruption was in 1975-76) was continue from 27th November 2012 to September 2013. We also include in present report new data on the Koryaksky volcano which was erupted from December 2008 to the beginning 2010 (the previous eruption was in December 1956 – March 57 and last volumetric lava flows occur 3-3.5 Ka).

The present report includes five chapters that describe the achievements of Russian scientists. Three of them have regional character and present the results by regions – Kamchatka Peninsula, Kurile arc and investigations that were done outside Russia. Additionally two chapters present the results on mineral deposits connected to volcanic processes and general theoretical questions in volcanology. Inside these chapters we roughly split all results by subjects on Geology, Geochemistry, Geophysics and Geochronology. Each of the sections has a list of the most interesting and important scientific papers published in 2011–2014 including publications

prepared in cooperation of Russian scientists and their colleagues from other countries. Many presentations also accompanied by figures that summarize the main results of investigations.

For a number of reasons not all results obtained by Russian scientists on the problems of volcanologists and geochemists of the Earth's interior in 2011-2014 are included in this report. At the same time it is hoped that authors may present these results at symposia of IUGG XXVI General Assembly and at future IAVCEI meetings.

1. VOLCANOLOGICAL AND GEOCHEMICAL STUDIES IN KAMCHATKA AREA

1.1. Klyuchevskaya Group of Volcanoes and Central Kamchatka Depression

T.G. Churikova, tchurikova@mail.ru, *National Geophysical Committee, Russian Academy of Sciences, Moscow, Russia. Institute of Volcanology and Seismology, Far East Division, Russian Academy of Sciences, Petropavlovsk-Kamchatsky, Russia*

The Klyuchevskaya Group of Volcanoes (KGV, Fig. 1.1.1) has been the foremost object of volcanological research in Russia since the early 1930s. The beginnings of these researches were associated with the names of such outstanding scientists as academicians F.Yu. Levinson-Lessing, A.N. Zavaritsky, V.I. Vlodavets, corresponding member of the USSR Academy of Sciences B.I. Piip, S.I. Naboko, and others. Several volcanological expeditions worked in the KGV during the period from 1931 to 1935; the Kamchatka Volcanological Station of the USSR Academy of Sciences was inaugurated in the village of Klyuchi near the northern foot of Klyuchevskoy Volcano on September 1, 1935. The Station has been conducting continuous valuable observations of the KGV volcanoes since that time. This research has expanded since the Laboratory of Volcanology of the USSR Academy of Sciences with its Kamchatka Volcanological Station were set up in 1945–1962 and afterward successfully continued in the 1960s after the Institute of Volcanology of the Siberian Branch (SB) of the USSR Academy of Sciences was set up in the city of Petropavlovsk-Kamchatsky. By the present time the study of the KGV volcanoes has been conducted for nearly 80 years. Fundamental scientific results have emerged from the comprehensive study of major eruptions. These include the paroxysmal summit eruption of 1944–1945 on Klyuchevskoy, the disastrous eruption and directed explosion of the andesitic volcano Bezymianny in 1955–1956, and the Great Tolbachik Fissure Eruption GTFE of 1975–1976, which is the greatest basaltic eruption to have occurred in Kamchatka during historical time.
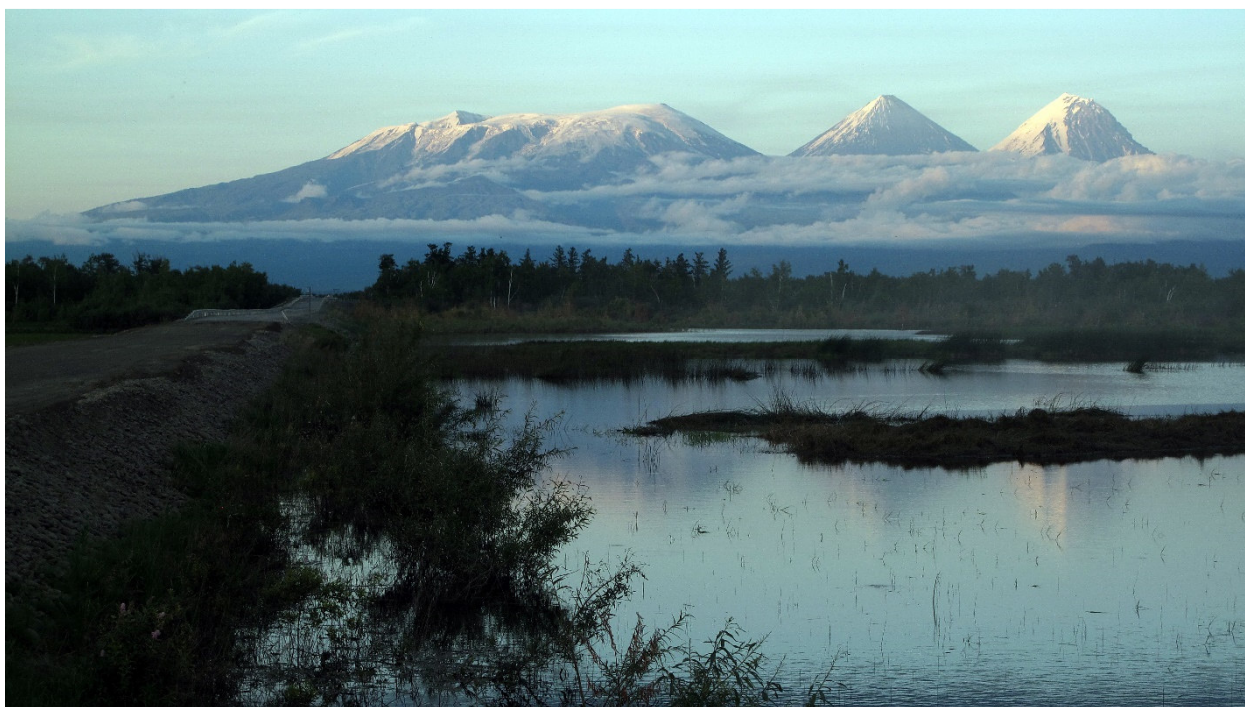
Fig. 1.1.1. Klyuchevskaya Group of Volcanoes (view from the West): from left to right are volcanoes: Ploskie Sopky (Krestovsky and Ushkovsky), Klyuchevskoy and Kamen. (Photo by B. Gordeychik and T. Churikova).

The most intense Holocene activity in Kamchatka is found in KGV (Fig. 1.1.1) of the Central Kamchatka Depression with Klyuchevskoy volcano (4750 m) being the most productive arc volcano in the world (63×10^6 tons magma/year). Additionally it was shown previously (Kersting and Arculus, 1995; Tsvetkov et al., 1989; Turner et al., 1998), that the amount of the sedimentary component is limited, offering the chance to investigate a relatively simple system. All these advantages make the Klyuchevskaya Group one of the best volcanic laboratories not only for Russian scientist, but also for one of the best volcanic places in the world.

In this section we will consider the investigations done by Russian volcanologists, geochemists and geophysists in the area of Klyuchevskaya Group.

1.1.1. Fissure Tolbachik Eruption (FTE-50) in 2012-13
1.1.1.1. The eruption history and the first eruption parameters

Gordeev E.I., gordeev@kscnet.ru**, Murav'ev Ya.D.,** murjd@kscnet.ru**, Samoilenko S.B., Volynets A.O.,** a.volynets@gmail.com**, Mel'nikov D.V.,** dvm@kscnet.ru**, Dvigalo V.N.,** dvig@kscnet.ru**, Demianchuk Yu.,** demyanchuk.yu@yandex.ru**, Belousov A., Belousova M.,** belousov@mail.ru**, Chirkov S.A., Melekestsev I.V.** *Institute of Volcanology and Seismology, Far East Division, Russian Academy of Sciences, Petropavlovsk-Kamchatsky, Russia*
Senyukov S, ssl@emsd.ru*, Kamchatka Branch of Geophysical Surveys RAS, Petropavlovsk-Kamchatsky, 683006, Russia*
Edwards B., edwardsb@dickinson.edu*, Department of Earth Sciences, Dickinson College, Carlisle, Pennsylvania 17013, USA*
Izbekov P.E., pavelizbekov@gmail.com*, Geophysical Institute, University of Alaska, Fairbanks, AK 99775, USA*

The eruption occurred within the Tolbachik regional zone of cinder cones approximately 900 km^2 in size and 70 km long. The centers of the present-day eruption are located to the north and closer to Plosky Tolbachik Volcano as compared with the centers of the Great Tolbachik Fissure eruption (Fig. 1.1.1.1.1).
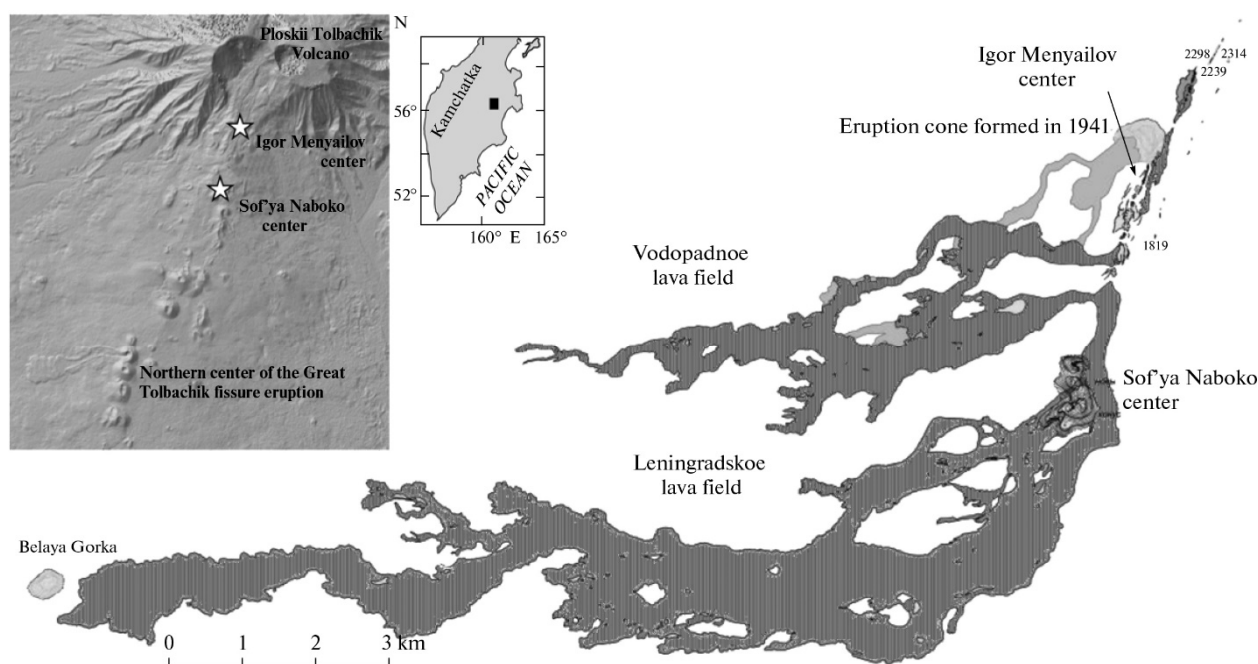
Fig. 1.1.1.1.1. Schematic location of the latest eruption and centers and map of lava flows for December 13, 2012.

At 17 h 15 min local time (5 h 15 min UTC) on November 27, 2012, lava started erupting from the submeridional fault formed south of Tolbachik Volcano. The fault zone extended for approximately 6 km between altitudes of 2200 and 1500 m. On November 28, lava flowing from two centers was accompanied by ash ejections with its distribution in the NNE direction for a distance of approximately 100 km. The period of November 29–30 was marked by moderate explosions, lava eruption from the upper eruptive center, intense lava flowing, and rapid movement of lava flows in the lower part of the fault. On December 1, activity in the upper center ceased. The length and area of the lava flow that erupted from the upper center amounted to 9 km and 5.6 km^2, respectively. From the beginning of December, the eruption became localized in the lower part of the fracture accompanied by an outflow of liquid Hawaiian-type lava from the fissure approximately 1 km long at altitudes of 1500–1600 m.

The lavas form variably shaped corded pahoehoe and pillow structures to form a system of lava channels. The maximal measured temperature of the melt was approximately 1100°C. The calculated in the field density of lavas with temperatures of 1100°C and water contents ranging from 0 to 1 wt % that erupted on the first day of the event varied from 2.65 to 2.58 g/cm^3. Densities of 2.7 to 2.63 g /cm^3 characterized lavas with the same parameters from the lower part of the fissure. The effective viscosity was 104 and 1.5–3.0 × 10^2 Pa at the beginning of eruption and in January 2013, respectively.

Lava flowing and effusion started at 20h on November 27, 2012, few hours after the eruption started. The eruption was preceded by a swarm of low-magnitude earthquakes (maximal M = 2.25) that occurred at shallow depths (approximately 5 km) 15 hours prior to eruption.

Its initial stage characterized by the intense outflow of moderately viscous lavas, which formed two spacious fields named Vodopadnoe and Leningradskoe (Fig. 1.1.1.1.1). The table presents the data on these fields.

Parameters of lava flows according to aerosurveying data of December 13, 2012

Parameter	Vodopadnoe	Leningradskoe
Area, km^2	5.654	17.035
Volume, km^3	0.027	0.208
Average thickness, m	4.8	12.2

The eruption was accompanied by the formation of cinder cones near both centers, with an integral volume of 0.008 km^3 estimated for December 13, 2012.

A peculiar feature of the latest eruption is its effusive mode with the volumetric coefficient of explosiveness (ratio between ash and lava volumes) being equal only to approximately 3%. Ash ejections were observed at the initial stage of the eruption, when the upper center was in action. They accompanied extension of fissures and lava intrusion into dead ice and permafrost on the southern slope of the Plosky Tolbachik Volcano. Ash was documented approximately 100 km away from the eruption, the rate of ash deposition amounted to 500 g/m^2.

The eruption started with the outflow of high-K aluminous trachybasaltic andesites (Fig. 1.1.1.1.2). The lavas of the initial stage differ from the varieties that previously erupted in the Tolbachik regional zone primarily in the high silica content. Later, at the beginning of December, the erupted products became more mafic. The SiO$_2$ content decreased by 2%. Eruption of such rocks was in progress during the entire subsequent period until the end of January. Lavas that erupted since mid-December exhibit larger plagioclase phenocrysts, some of which are up to 1 cm across and 1–2 mm thick, and the occurrence of olivine crystals (approximately 1 mm across) is also larger as compared with their counterparts in older lavas.
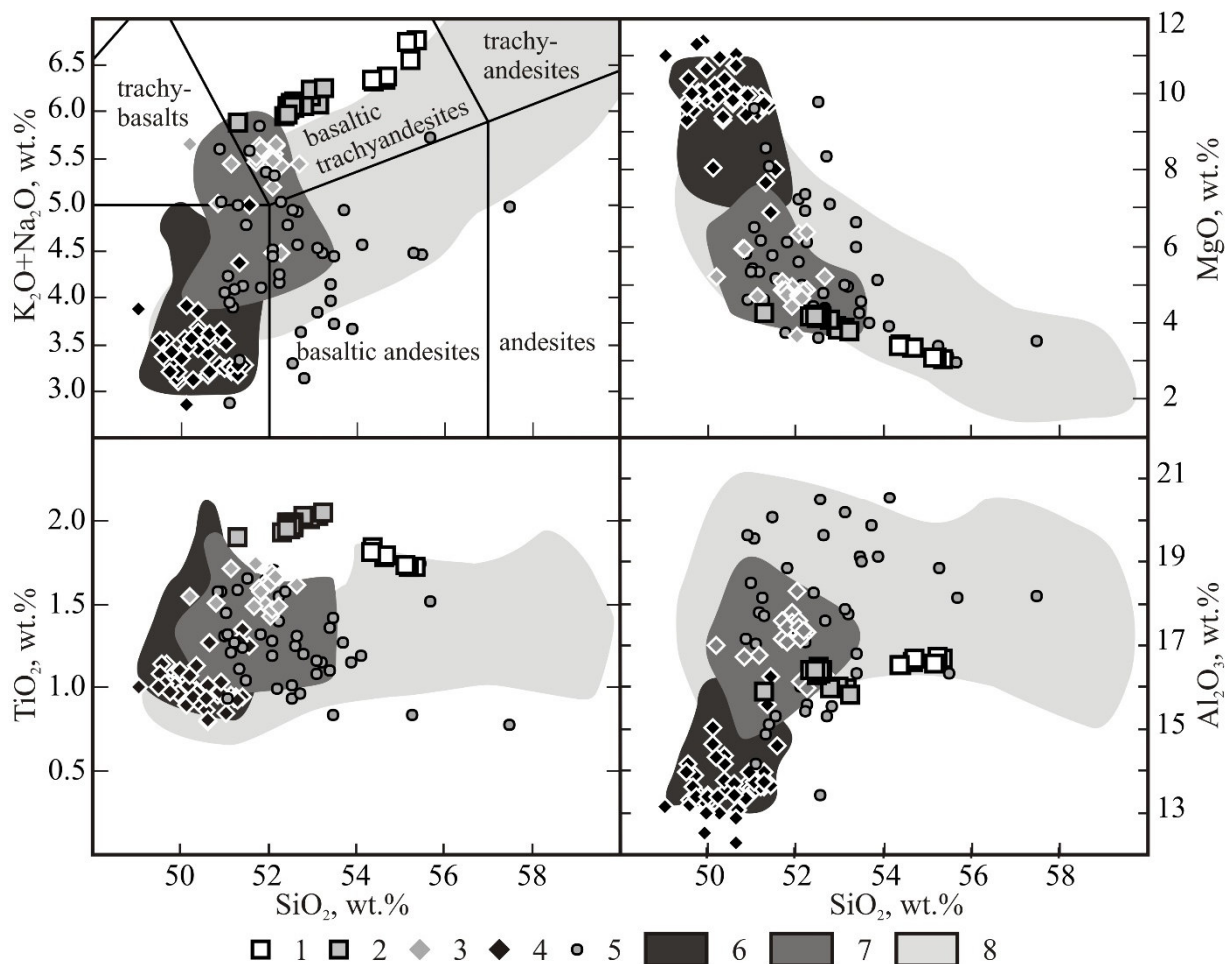
Fig. 1.1.1.1.2. Harker diagrams for FTE-50 volcanic rocks. Trachyandesites-basalts (*1–2*) FTE-50: *1*—Menyailov Vent, *2*—Naboko Vent; (*3–4*) eruption of 1975-76: *3*—Southern Vent, *4*—Northern Vent; (*5*) Plosky and Ostry Tolbachik stratovolcanoes; (*6–7*) Tolbachinsky Dol: *6*—high-Mg, *7*—high-Al volcanic rocks; (*8*) Ploskie Sopky volcanic rocks. The reference compositions of rocks from Tolbachinsky Dol, Ostry and Plosky Tolbachik volcanoes and Ploskie Sopky see in Volynets at al., 2013. Discrimination lines on $K_2O + Na_2O – SiO_2$ diagram—after Le Maitre, 1989.

This approximation done on the volumes of lava fields estimated for November 29, 2012, and December 13, 2012, from aerophotographs and satellite images obtained on March 6, 2013 (data of the EO-1 NASA satellite) yields the following values: the maximal volume of erupted material $B = 0.38$ km^3, the maximal discharge at the initial stage of the eruption $W = 250$ m^3/s, and duration of the eruption 140 days. The real magma discharge at the beginning of eruption (according to aero surveying on November 29, 2012) exceeds 400 m^3/s. Such a significant difference between the calculated and real discharge values is explained by eruption at the initial stage along the entire fissure 4–5 km long, whereas the approximation formula is valid for the channel with a constant section.

The emission of sulfur dioxide (SO_2) during the first days of eruption (November 27–28) was 5×10^4 t. The cloud containing this gas moved in the northwesterly direction under the influence of meteorological factors and on November 28, it was located above the southern coast of the East Siberian Sea being 190 000 km^2 in size.

The Scientific Council of the Institute of Volcanology and Seismology (Far East Branch, Russian Academy of Sciences) came to a decision to name the eruption under consideration the Tolbachik fissure eruption of the 50th Anniversary of IVS (TFE-50); the upper and lower eruption centers are named in honor of Igor Menyailov and Sof'ya Naboko, respectively.

Gordeev, E. I., Murav'ev, Y. D., Samoilenko, S. B., Volynets, A. O., Mel'nikov, D. V., & Dvigalo, V. N. (2013). The Tolbachik fissure eruption of 2012–2013: Preliminary results. Doklady Earth Sciences, 452(2), 1046-1050. Doi: 10.1134/S1028334X13100103

Gordeev, E. I., Muravyev, Y. D., Samoylenko, S. B., Volynets, A. O., Mel'nikov, D. V., Dvigalo, V. N., & Melekestsev, I.V. (2013). First results from the 2012-2013 Tolbachik Fissure eruption. Bulletin of the Volcanological Society of Japan, 58(2). http://www.researchgate.net/publication/259368312_First_Results_from_the_2012-2013_Tolbachik_Fissure_Eruption

Edwards, B., Belousov, A., Belousova, M., Volynets, A., Melnikov, D, Chirkov, S, Senyukov, S, Gordeev, E., Muraviev, Ya., Izbekov P., & Demianchuk Yu. (2013). Another Great Tolbachik Eruption? Eos Trans. AGU, 94(21), 189. Doi: 10.1002/2013EO210002

Belousov A., Belousova M. (2013). Tolbachik volcano: Hawaiian eruptions at Kamchatka. Priroda 10, 59-67. (In Russian). http://www.ras.ru/publishing/nature.aspx

1.1.1.2. Propagation style controls lava-snow interactions

Edwards B., edwardsb@dickinson.edu, *Department of Earth Sciences, Dickinson College, Carlisle, Pennsylvania 17013, USA*

Belousov A., Belousova M., belousov@mail.ru, *Institute of Volcanology and Seismology, Far East Division, Russian Academy of Sciences, Petropavlovsk-Kamchatsky, Russia*

Unique field observations of interactions between snowpack and advancing basaltic lava flows during the 2012–13 eruption at Tolbachik volcano were presented. Our observations show that lava–snow heat transfer is slow, and that styles of lava propagation control snowpack responses. 'A'a and sheet lava flows advance in a rolling caterpillar-track motion on top of the rigid, snowpack substrate with minor lava–snow interaction. In contrast, pahoehoe lava propagates by inflation of lobes beneath/inside the snowpack, producing rigorous lava–snow interaction via meltwater percolation down into the incandescent lava causing production of voluminous steam, rapid surface cooling and thermal shock fragmentation. The textures produced by pahoehoe–snowpack interactions are distinctive and, where observed at other sites, can be used to infer syn-eruption seasonality and climatic conditions (Figs. 1.1.1.2.1 and 1.1.1.2.2).
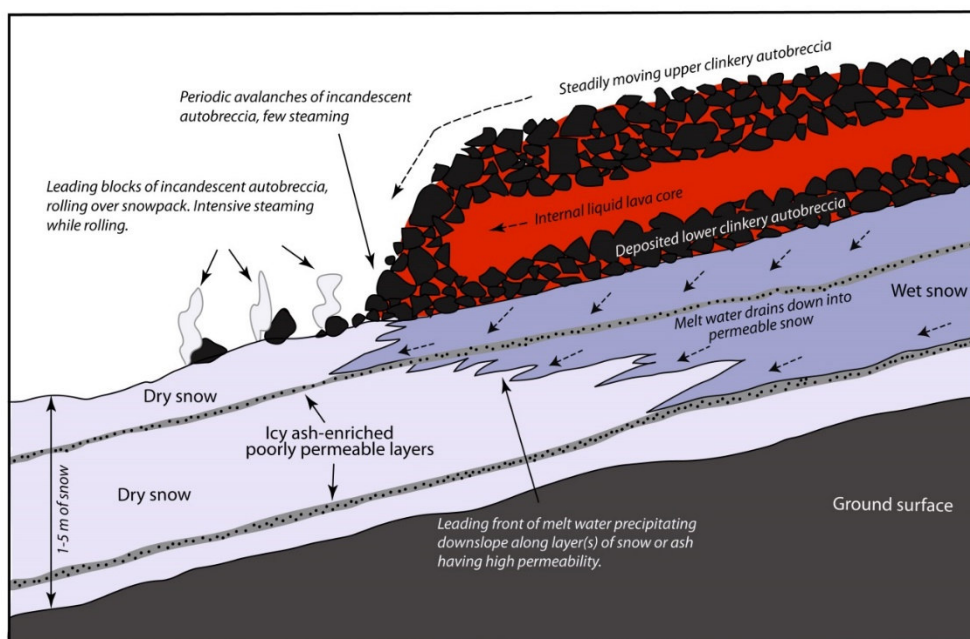
Fig. 1.1.1.2.1. Schematic sketch showing a cross-sectional view along the front of an `a`a flow advancing in tractor-tread style over thick snowpack with little obvious effect.
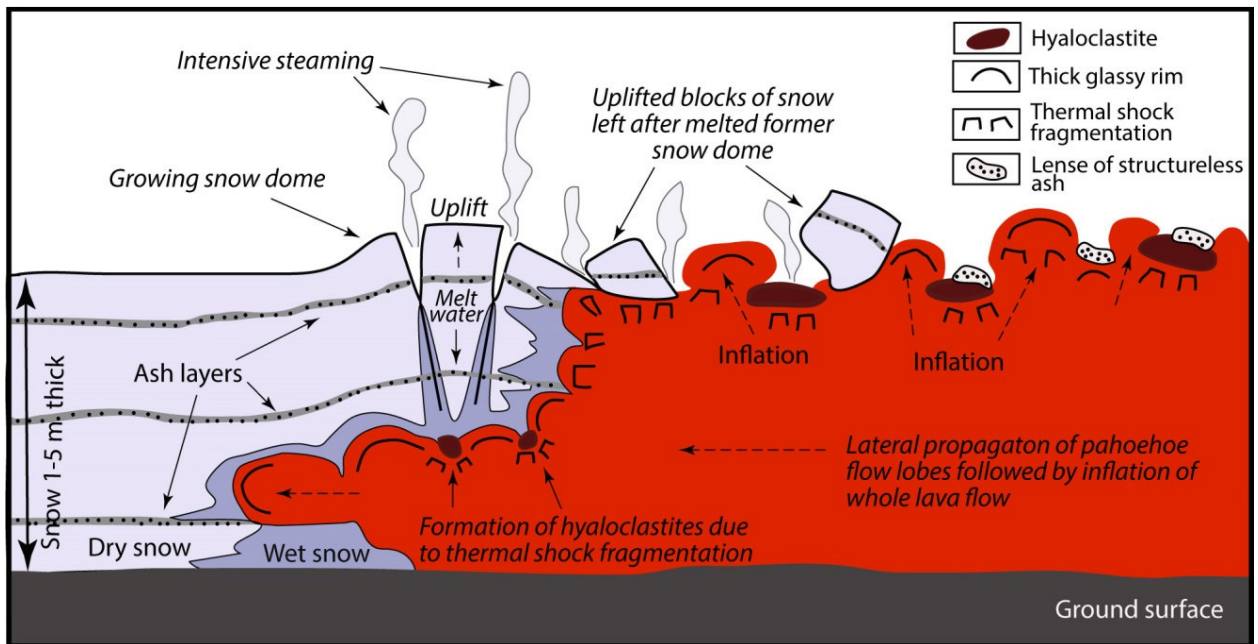
Fig. 1.1.1.2.2. Schematic sketch showing cross-sectional view along the front of pahoehoe flow advancing via inflation beneath/inside thick snow pack.

Edwards, B, Belousov, A., & Belousova, M. (2014). Propagation style controls lava-snow interactions. Nature Communications, 5: 5666. Doi: 10.1038/ncomms6666

Belousov, A., Behncke, B., & Belousova, M. (2011). Generation of pyroclastic flows by explosive interaction of lava flows with ice/water-saturated substrate. Journal of Volcanology and Geothermal Research, 202(1–2), 60-72. Doi: http://dx.doi.org/10.1016/j.jvolgeores.2011.01.004

1.1.1.3. Monitoring of the volcanic rock compositions during the 2012-2013 FTE

Volynets A.O., a.volynets@gmail.com, *Institute of Volcanology and Seismology, Far East Division, Russian Academy of Sciences, Petropavlovsk-Kamchatsky, Russia. GZG, Abteilung Geochemie, Universität Göttingen, Goldschmidtstrasse 1, 37077 Göttingen, Germany*

Melnikov D.V., dvm@kscnet.ru, **Belousov A.B.,** belousov@mail.ru, **Belousova M.G.,** belousov@mail.ru**, Chirkov S.A., Gordeev E.I.., Muraviev Ya.D., Demianchuk Yu.V., Samoilenko S. B., Dvigalo, V. N., Melekestsev I.V.,** *Institute of Volcanology and Seismology, Far East Division, Russian Academy of Sciences, Petropavlovsk-Kamchatsky, Russia*

Senyukov S, ssl@emsd.ru*, Kamchatka Branch of Geophysical Surveys RAS, Petropavlovsk-Kamchatsky, 683006, Russia*

Yakushev A., antemp@inbox.ru, **Griboedova I.,** irinagriboedova@ramlbler.ru, *Institute of Geology of Ore Deposits, Petrography, Mineralogy and Geochemistry RAS, Staromonetnyi pereulok 35, Moscow 119017, Russia*

Edwards B., edwardsb@dickinson.edu*, Department of Earth Sciences, Dickinson College, Carlisle, PA, 17013, USA*

Izbekov P.E., pavelizbekov@gmail.com*, Geophysical Institute, University of Alaska, Fairbanks, AK 99775, USA*

Tolstykh M., *Vernadsky Institute of Geochemistry and Analytical Chemistry RAS, Russia*

Tolbachinsky Dol (TD) is the southern part of the largest zone of monogenetic volcanism in Kamchatka, which is superimposed on the Klyuchevskoy group of composite volcanoes at the northern end of the Kamchatka volcanic arc (Fig. 1.1.1.3.1). At its northern end, TD intersects the

edifice of the Upper Pleistocene Plosky Tolbachik stratovolcano. TD has formed by numerous eruptions of high-alumina, sub-alkaline basalt and basaltic andesite throughout the Holocene, and since 2 ka also by high-Mg, medium-K basalt. The most recent prior activity took place here in 1975-76, in an eruption that is known as the Great Fissure Tolbachik Eruption (GFTE). The extensive research on the GFTE produced a series of papers and a monograph on the volcanology and petrology of the eruption (GFTE…, 1984; Fedotov et al., 1991; Volynets et al., 1978 and many others). The volume of the erupted products was 2.2 km^3, and the area covered by lava flows was ~45 km^2. This event started in July 1975 with a highly explosive eruption of high-Mg basalts from the 'Northern Breakthrough' and lasted about 2 months. Then the center of activity moved to the south and the eruption continued from the 'Southern Breakthrough' by the effusion of the high-alumina, sub-alkaline basalts and basaltic andesites until its end in December 1976. Volcanic rocks with compositions intermediate between the high-Mg and high-Al basalts were erupted during the short period at the end of the Northern Breakthrough and beginning of the Southern Breakthrough activity (Volynets et al., 1978). After almost 36 years of quiescence a new fissure eruption began on 27 November 2012 in the TD approximately 5 km north of the Northern Breakthrough. It lasted 9 month and was named the "IVS 50th anniversary Fissure Tolbachik eruption" (here – 2012-2013 fissure eruption of Tolbachik volcano; FTE).
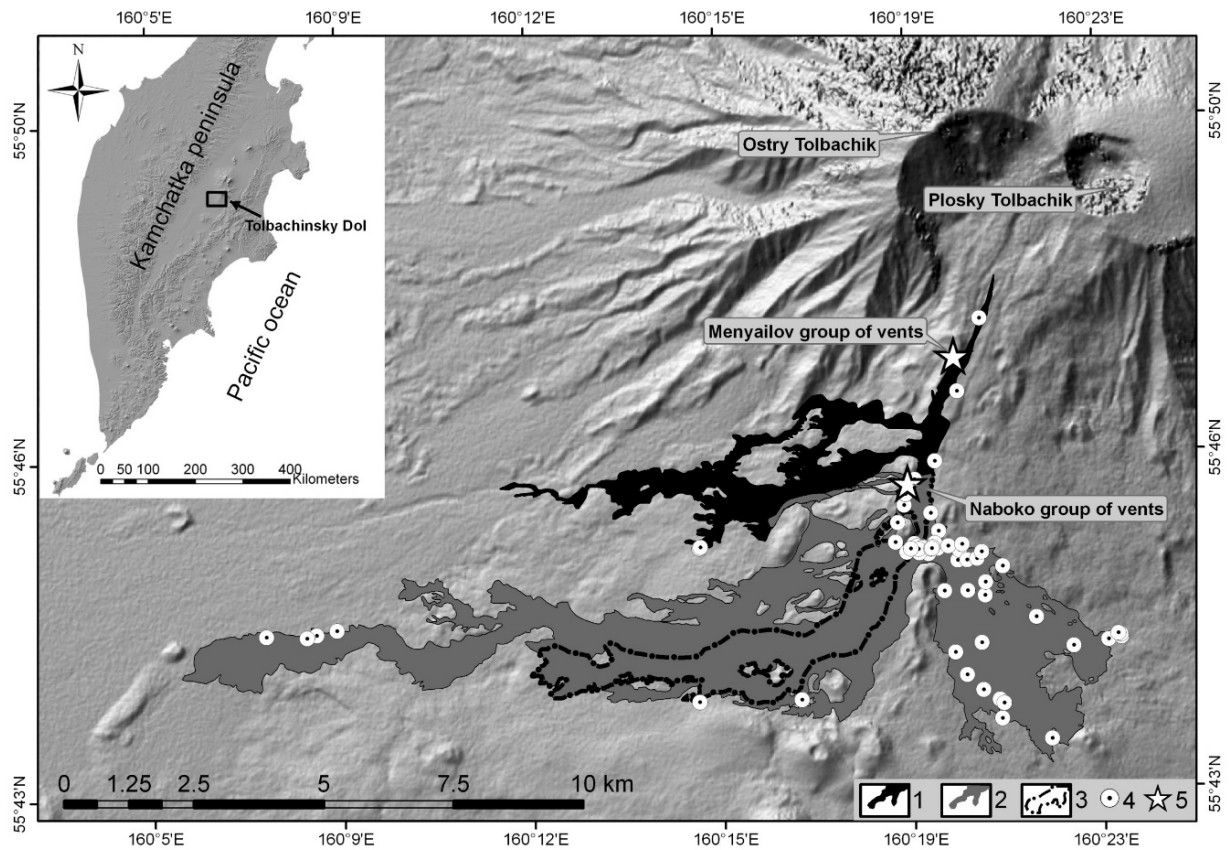
Fig. 1.1.1.3.1. Scheme of the 2012-2013 Tolbachik eruption lava flows distribution. Legend: 1 – Menyailov group of vents lava flows; 2 – Naboko group of vents lava flows; 3 – Menyailov group of vents lava flows, later in most parts overlapped by the Naboko group of vents lavas; 4 – sampling sites; 5 – location of centers of activity. This scheme is based on satellite images TERRA ASTER (NASA, JPL), EO-1 ALI (NASA) interpretation and field work observations. Topographic base – DEM SRTM X-band (DLR).

Fig. 1.1.1.3.2. Field photographs of the Menyailov group of vents activity on November 29, 2012 (A) and the activity of the Naboko group of vents in January 2013 (B). At the lower picture two smaller vents activity is clearly seen: simultaneous explosions producing ash clouds from one vent (to the left) and lava gushing from another vent (to the right). The latter finally remained as the main vent and a 123 m high cinder cone was built here.

The new eruption started from a fissure that opened on 27 November and formed the Igor Menyailov group of vents, which are located at N 55°47′9″/E 160°19′39″ at an elevation of 1900 m a.s.l. on the upper south slopes of Plosky Tolbachik stratovolcano (Fig. 1.1.1.3.1, 1.1.1.3.2A). About 18 hours later (Melnikov et al., submitted to JVGR) a second fissure opened further down the slope that eventually formed the Sofia Naboko group of vents at N 55°46′6″/E 160°18′59″ at an elevation of 1650 m a.s.l. (Fig. 1.1.1.3.2B). The Menyailov vents were active during the first three days of the eruption (27-30 November). After that the focus of the eruptive activity shifted exclusively to the Naboko vents and continued from there until the end of eruption in September 2013. Composition of lava, bombs and cinder, erupted during this event, were constantly monitored in the course of the eruption. Full set of results of this work are submitted to the Journal of Volcanology and Geothermal Research. Products of this eruption are represented by high alumina basaltic trachyandesites with higher alkalies and titanium contents than in all previously studied rocks of the Tolbachinsky Dol volcanic field. Rocks erupted during the first three days (27-30 November) from the Menyailov group of vents are the most silica- and alkali-rich (SiO_2 concentrations up to 55.35 wt. percent and K_2O up to 2.67 wt. percent). From December onwards, when the eruptive activity moved from the Menyailov vents to the Naboko group of vents, silica content dropped by 2 wt. percent; concentrations of MgO, TiO_2 and Mg# increased; K_2O, Na_2O concentrations and K_2O/MgO ratio decreased (Fig. 1.1.1.3.3). From this moment, until the end of the eruption the composition of rocks remained constant and homogeneous, no systematical compositional differences between lava, bombs and scoria samples were evident. Trace element distributions in the rocks of the Menyailov and Naboko vent lavas are relatively uniform; Menyailov lavas have slightly higher Th, Nb, Hf, Y, and HREE concentrations than the Naboko vent lavas at more or less constant element ratios (Fig. 1.1.1.3.4). Concentrations of Nb, Ta, Zr, Hf, and Y in rocks of both vents are higher than in typical arc-front lavas, reflecting variable source enrichment by these elements. The 2012-2013 FTE lavas have lower Mg#, higher FeO, TiO_2 and alkali concentrations and higher K_2O/MgO ratio than lavas produced by all of the large stratovolcanoes located in the Central Kamchatka Depression (Klyuchevskoy, Bezymianny, Kamen, Shiveluch). Similar evolution trends are observed in the Ploskie Sopky volcanic massif (Churikova, 1993), although the 2012-2013 FTE products still have higher alkali and Ti concentrations. Geochemical, petrological observations and modeling are in agreement with the newly erupted material being derived from remnant high-Al magma from the 1975-76 eruption with only slight amounts of cooling (less than 1℃ per year) during the intervening 36 years.
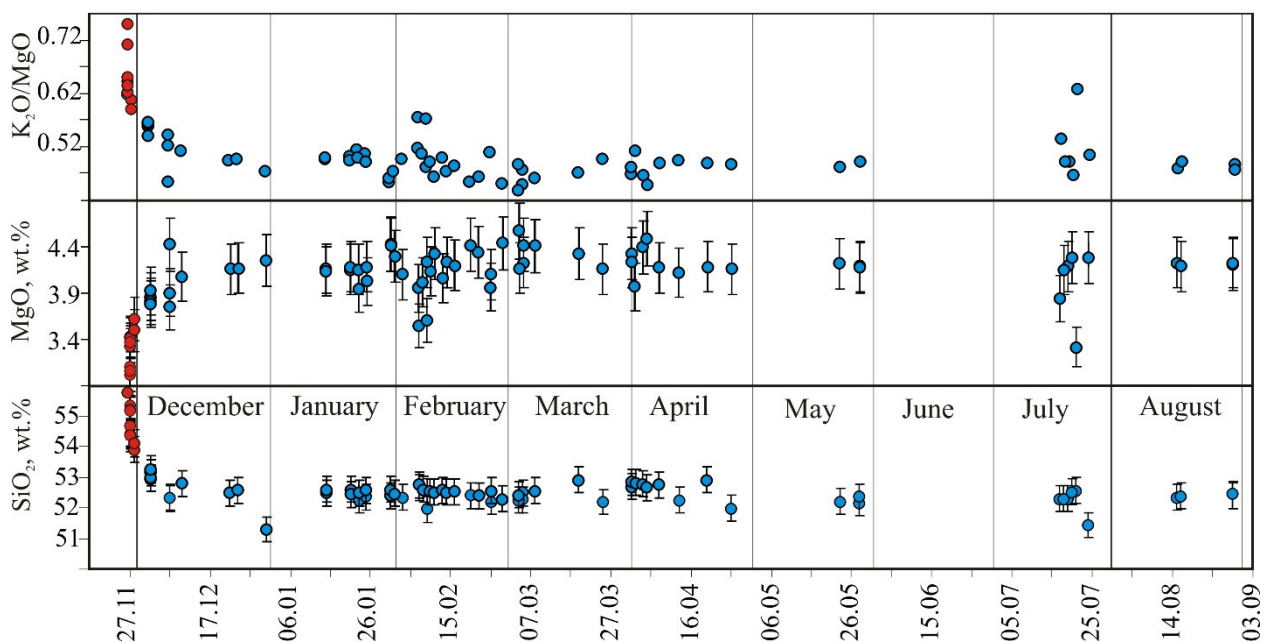
Fig. 1.1.1.3.3. Evolution of composition of rocks during the eruption. The vertical axis represents time. Black symbols – Menyailov vent, white symbols – Naboko vent.
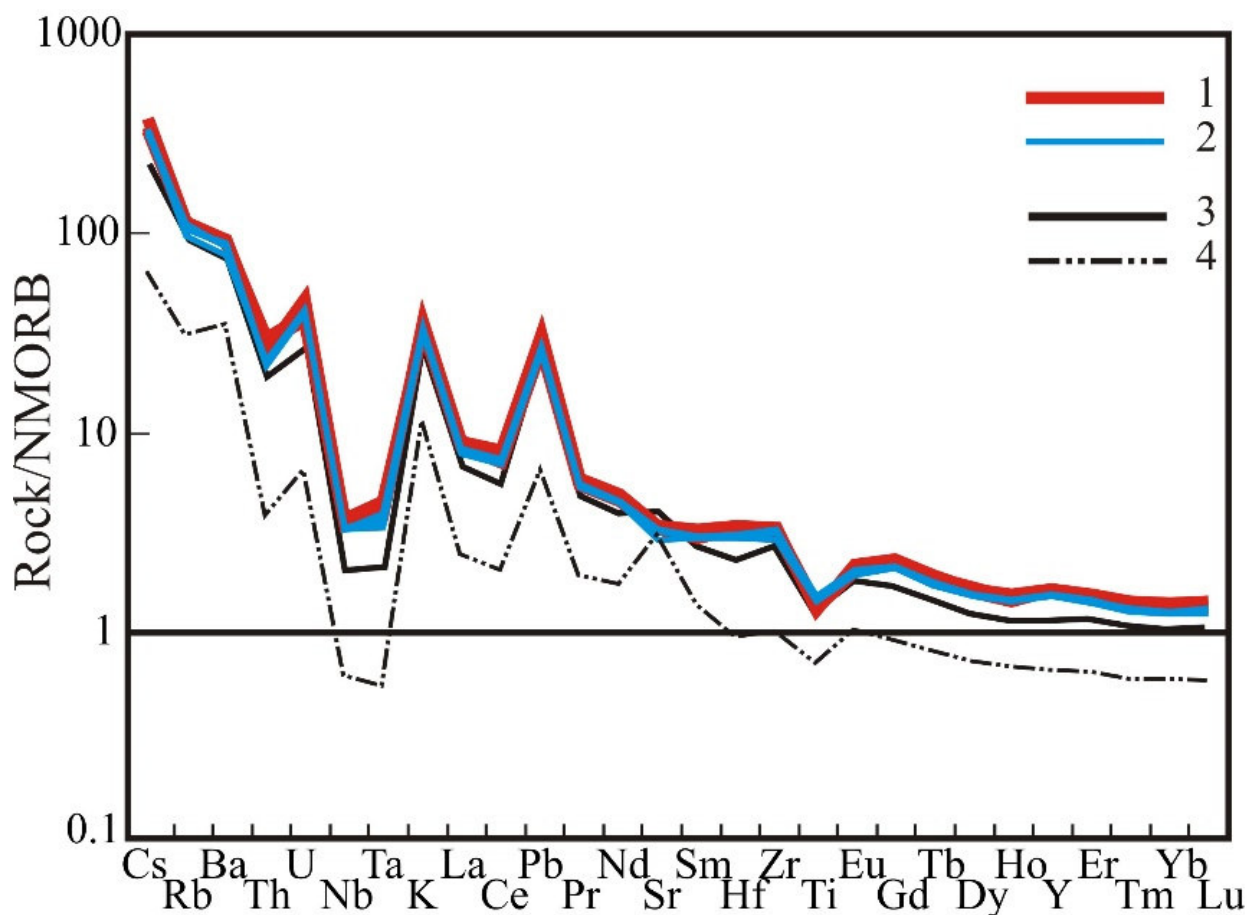
Fig. 1.1.1.3.4. Distribution of REE and other incompatible microelements in 2012-2013 Tolbachik fissure eruption volcanic rocks. Legend: 1-2 – 2012-2013 Tolbachik fissure eruption: 1 – Menyailov Vent, 2 – Naboko Vent; 3-4 – GFTE: 3 – Southern Breakthrough, 4 – Northern Breakthrough. Concentrations of elements in N-MORB after (Sun and McDonough, 1989).

Edwards, B, Belousov, A., Belousova, M., Volynets, A., Melnikov, D., Chirkov, S., Senyukov, S., Gordeev, E., Muraviev, Ya., Izbekov P., & Demianchuk Yu. (2013). Another "Great Tolbachik" Eruption? // Eos Transactions AGU, 94(21), 189-191. Doi: 10.1002/2013EO210002

Gordeev, E. I., Murav'ev, Y. D., Samoilenko, S. B., Volynets, A. O., Mel'nikov, D. V., & Dvigalo, V. N. (2013). The Tolbachik fissure eruption of 2012–2013: Preliminary results. Doklady Earth Sciences, 452(2), 1046-1050. Doi: 10.1134/S1028334X13100103

Volynets, A. O., Melnikov, D. V., & Yakushev, A. I. (2013). First data on composition of the volcanic rocks of the IVS 50th anniversary Fissure Tolbachik eruption (Kamchatka). Doklady Earth Sciences, 452(1), 953-957. Doi: 10.1134/S1028334X13090201

Gordeev, E. I., Muravyev, Y. D., Samoylenko, S. B., Volynets, A. O., Mel'nikov, D. V., Dvigalo, V. N., & Melekestsev, I.V. (2013). First results from the 2012-2013 Tolbachik Fissure eruption. Bulletin of the Volcanological Society of Japan, 58(2). http://www.researchgate.net/publication/259368312_First_Results_from_the_2012-2013_Tolbachik_Fissure_Eruption

Volynets, A. O., Melnikov, D., Yakushev, A., & Tolstykh, M. (2013). Petrology and geochemistry of the New Tolbachik Fissure Eruption volcanic rocks and their evolution during the first two weeks of eruption. Forecasting Volcanic Activity - Reading and translating the messages of nature for society. IAVCEI 2013 Scientific Assembly, July 20-24, Kagoshima, Japan. http://www.kazan.or.jp/iavcei2013/iavcei_hp/PDF/1A1_3B-O3.pdf

Volynets, A., Edwards, B., Melnikov, D., Yakushev, A., & Griboedova, I. Monitoring of the volcanic rock compositions during the 2012-2013 fissure eruption at Tolbachik volcano, Kamchatka. Journal of Volcanology and Geothermal Research. (In review).

Melnikov, D., & Volynets, A. Remote sensing and petrological observations on the 2012-2013 fissure eruption at Tolbachik volcano, Kamchatka: implications to the reconstruction of the eruption chronology. Journal of Volcanology and Geothermal Research. (In review).

Belousov, A., Belousova, M., Edwards, B., Volynets, A., & Melnikov D. Overview of the precursors and dynamics of the 2012-13 basaltic fissure eruption of Tolbachik volcano, Kamchatka, Russia. Journal of Volcanology and Geothermal Research. (In review).

1.1.1.4. Aerial photogrammetric monitoring of Tolbachik eruption 2012-13

Dvigalo V.N., dvig@kscnet.ru, *Institute of Volcanology and Seismology, Far East Division, Russian Academy of Sciences, Petropavlovsk-Kamchatsky, Russia*

Shevchenko A.V., shevchenko@kscnet.ru**, Svirid I.Yu.,** svirid@kscnet.ru, *Institute of Volcanology and Seismology, Far East Division, Russian Academy of Sciences, Petropavlovsk-Kamchatsky, Russia. Vitus Bering Kamchatka State University (KamGU), Petropavlovsk-Kamchatsky, Russia*

Based on aerial photogrammetric observations we quantified the parameters for the Tolbachik Fissure Eruption (TFE) of 2012–2013 for the period between November 27, 2012 and June 5, 2013. The largest lava discharge was in the first two days (440 m^3/sec), when there was a maximum amount of active lava vents along the whole new fissures. In the following two weeks, the lava discharge decreased (140 m^3/sec in average). From the second part of December 2012 to June 2013, the lava discharge was close to 18 m^3/sec. From November 27, 2012 (the beginning of the eruption) to June 5, 2013 the erupted lava covered over 35.23 km^2, its volume was 0.52 km^3. According to our preliminary estimations the total volume of lava deposits at the end of the eruption (September 17, 2013) comprises 0.55–0.65 km^3.

We revealed that TFE 2012–2013 was primarily effusive. The volume of pyroclastic deposits is not more than 0.1 km^3 in 1.5 km from the new fissures area. We made maps to show the location of the fissured zone, the main vents, and lava flows on the slope of Plosky Tolbachik Volcano.

The comparative analysis of the 2012–2013 TFE and the 1975–1976 Great Tolbachik Fissure Eruption (GTFE) allows to reveal some characteristic features for the new eruption: the onrush of eruptive process (TFE began 15 hour after seismic precursor, whereas GTFE began 10 days after swarm of volcanic earthquakes), the absence of continuous initial explosive phase and also more close location of eruption zone. The basement of Plosky Tolbachik Volcano was not involved in TFE 2012–2013, at that several days before the GTFE there was a bit of crystal-lapilli and Pele's hair ejected from its summit pit crater, and by the end of the eruption due to the subsidence the volume of the pit crater increased from 0.022 km^3 to 0.347 km^3.

We also note the contrast between the predominantly explosive character of the GTFE initial phase and the exclusively effusive activity during the first few days of the 2012–2013 TFE. The discharge rate of lava during the first 2 days of the 2012–2013 TFE was an order of magnitude greater than the discharge rate of solid material during the generation of the first cinder cone in the GTFE. The above facts are very likely to indicate that the initial period in the 2012–2013 TFE followed the "fluid hammer" scenario. We can conclude based on the character of the 2012–2013 TFE fissure zone that this "fluid hammer" was around the Menyailov Vents where the fissure zone is the widest and where the first lava flows were discharged. Subsequently, when the fissure zone opened, the magmatic material propagated along the zone southward down the slope until it reached an altitude of 1700 m and formed the larger lava flows and cones in those locations during quieter eruption behavior.

Dvigalo, V. N., Svirid, I. Y., & Shevchenko, A. V. (2013). The first quantitative estimates of parameters for the Tolbachik Fissure Eruption of 2012–2013 from aerophotogrammetric observations. Journal of Volcanology and Seismology, 8(5), 261-268. Doi: 10.1134/S0742046314050029

Svirid, I.Yu. (2014). The 2012–2013 fissure Tolbachik eruption, Kamchatka. 1st International Workshop on Volcano Geology: abstracts book. July 7-11, 2014, Madeira, Portugal, 154-158. http://www.kscnet.ru/ivs/bibl/sotrudn/svirid/abstractbook_wvg2014_svirid.pdf

1.1.1.5.   Minerals in Tolbachik eruption 2012-13

Diamonds and accessory minerals in products of the 2012-2013 FTE

Gordeev E.I., Karpov G.A., karpovga@kscnet.ru, **Anikin L.P., Flerov G.B.,** flerov@kscnet.ru, **Ovsyannikov A.A., Chubarov V.M., Dunin-Barkovsky R.L. Sokorenko A.V. Sidorov E.G.,** *Institute of Volcanology and Seismology, Far East Division, Russian Academy of Sciences, Petropavlovsk-Kamchatsky, Russia*
Silaev V.I., Rakin V.I., Petrovskii V.A., *Institute of Geology, Komi Republic, Science Center, Urals Branch, Russian Academy of Sciences, ul. Pervomaiskaya, 54, Syktyvkar, 167982 Russia*
Vasil'ev E.G., *Gornyi National Institute of Mineral Resources, Vasil'evskii ostrov, 21 liniya, 2, St. Petersburg 199106 Russia*
Krivovichev S.V., Filatov S.K., filatov.stanislav@gmail.com, *St. Petersburg University, Universitetskaya nab. 7/9, St. Petersburg, 199034 Russia*
Antonov A.V., *Karpinskii All-Russia Scientific-Research Geological Institute, Srednii pr. 74, St. Petersburg, 199106, Russia*

Based upon the studies of the ejecta of the 2012-2013 Fissure Tolbachik Eruption named after the 50th Anniversary of the IVS FEB RAS, first discovered microdiamonds and their accessory minerals have been characterized. Complex studies of crystal-morphological, spectroscopic, thermal and isotope-geochemical properties of those diamonds have been conducted. Diamond grains are yellowish-bluish in color, of cubic-octahedral habit, sized 250 up to 700 mcm (Fig. 1.1.1.5.1).

Fig. 1.1.1.5.1. Crystal morphology of the Tolbachik diamonds. Arrows indicate: a-e – pits of diffusive depletion; f – sculpture of equiponderant etching pits on the cube face; g – anatomic structure of a cubic-octahedron individual; h – a typical twin.

SME analyses has revealed that most diamonds are well formed isometric, plane-faced and sharp-edged monocrystals. Crystal cubic faces often host rather large pits of diffusive depletion

(15-80 mcm), and etching pits sized 1-5 mcm (Fig. 1.1.1.5.2). Occasionally, xenomineral coatings can be found on the diamond surfaces (mostly within the etching pits). By their composition, these coatings can be divided into silicate, alumosilicate, silicate-oxide and sulfate. Notable is high contents of Fe, Ni and Cu admixtures in them (Fig. 1.1.1.5.2).

Fig. 1.1.1.5.2. Coatings and films of alumosilicates (*a–c*), quartz and sulfates (*d*), and native metals (*e*, *f*) on the surface of Kamchatka diamonds. SEM stands for images made by elastically reflected electrons.

Considered have also been the peculiarities of various accessory minerals: native metals (Cu, Fe, Al), their alloys, as well as Ti-bearing corundum, moissanite, garnet (almandine), globular hematite, spinellides (Fig. 1.1.1.5.3).
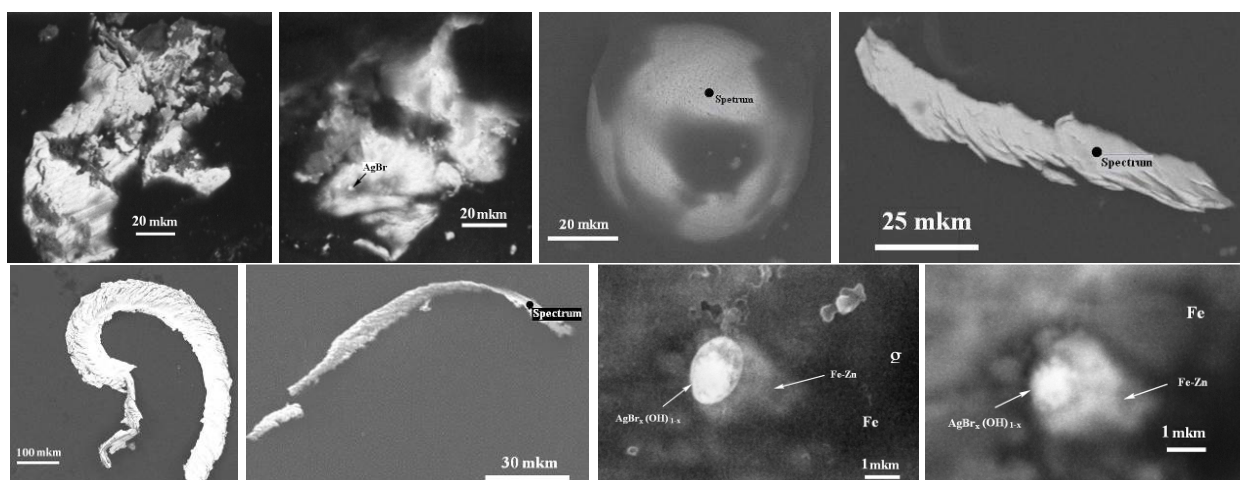
Fig. 1.1.1.5.3. Particles of native iron: a–f – pure and containing SiMnCr-admixtures; g, h – pure iron with enclosures of $AgBr_x(OH)_{1-x}$ and zinc-bearing iron. SEM images, backscattered electron (a–f, h) and secondary electron analysis (g).

Phase diagnostics of the diamond grains was carried out by X-ray and Raman spectroscopy. The resulting X-ray photographs exhibit all the three main reflections from (111), (220), and (311) in diamond structure. Ultramicroblock structure and texturing of the diamond phase have been reported. The elementary cell parameter as found from the X-ray diagram was 0.3556 (3) nm, which is in agreement with data for a sufficiently perfect crystalline diamond phase. The Raman spectra which were recorded using a red laser in the 200–3000 cm^{-1} range and a resolution of 1.6 cm^{-1}, showed a single strong line at 1332 cm^{-1} which is consistent with a diamond. Spectra excited by a 785 nm laser show a broader line peaking at 1370 cm^{-1}; its intensity varies between 1 and 70% of the diamond line intensity at 1332 cm^{-1}. The resulting spectra showed two series of absorption lines differing by their nature. IR-spectroscopy has shown that the Tolbachik diamonds and low- to medium-Ni, with absolutely non-aggregated structural Ni defects, which attests to relatively low temperatures of crystallization and absence of mantle anneal. Tolbachik diamonds are peculiar by the isotopically light carbon that is not typical for monocrystal diamonds and is closely related to the carbon in the Brazil carbonado whose formation is known to be associated with the fluid-rich mantle melts or with the fluids proper.

The results acquired suggest that in contrast to diamonds from kimberlite, lamproite, and tuffisite deposits, the Tolbachik diamonds are not xenogenic with respect to the lavas and exhalations that brought them to the surface. Hypothesized is also their genesis due to "shock"-crystallizing mechanisms occurring within the gas-phase. Based on all these considerations, we suggest classifying the Tolbachik diamond occurrences as a genetic type that was unknown previously; we think it would be reasonable to call it the volcanogenic-eruptive or Tolbachik type.

Gordeev, E. I., Karpov, G. A., Anikin, L. P., Krivovichev, S. V., Filatov, S. K., Antonov, A. V., & Ovsyannikov, A. A. (2014). Diamonds in lavas of the Tolbachik fissure eruption in Kamchatka. Doklady Earth Sciences, 454(1), 47-49. Doi: 10.1134/S1028334X14010097

Karpov, G. A., Silaev, V. I., Anikin, L. P., Rakin, V. I., Vasil'ev, E. A., Filatov, S. K., Petrovskii V.A. & Flerov, G. B. (2014). Diamonds and accessory minerals in products of the 2012–2013 Tolbachik Fissure Eruption. Journal of Volcanology and Seismology, 8(6), 323-339. Doi: 10.1134/S0742046314060049

Karpov, G. A., Anikin, L. P., Flerov, G. B., Chubarov, V. M., & Dunin-Barkovsky, R. L. (2014). Mineralogical and petrograpic features of diamond-containing ejecta of the 2012–2013

Tolbachik Fissure Eruption. Volcanism and related processes. Annual regional scientific conference dedicated to the Volcanologist Day. Proceedings of the conference. March 27-28, 2014, Petropavlovsk-Kamchatsky. Petropavlovsk-Kamchatsky: Institute of volcanology and seismology FED RAS, 283–288. (In Russian). http://www.kscnet.ru/ivs/publication/volc_day/2014/art43.pdf

Anikin, L. P., Sokorenko, A. V., Ovsyannikov, A. A., Sidorov, E. G., Dunin-Barkovsky, R. L., Antonov, A. V., Chubarov, V. M. (2013) Finding diamonds in lavas Tolbachik eruption of 2012-2013 years. Volcanism and related processes. Annual regional scientific conference dedicated to the Volcanologist Day. Proceedings of the conference. March 29-30, 2013, Petropavlovsk-Kamchatsky. Petropavlovsk-Kamchatsky: Institute of volcanology and seismology FED RAS, 20-23. (In Russian). http://www.kscnet.ru/ivs/publication/volc_day/2013/art3.pdf

Karpov, G. A., Silaev, V. I., Anikin, L. P., Flerov, G. B., & Petrovsky, V. A. (2014). A new genetic type of diamonds in association with native metals as found in ejecta of the 2012–2013 Tolbachik Fissure Eruption. Problems and perspectives of modern mineralogy (Yushkin Memorial Seminar–2014) Proceedings of mineralogical seminar with international participation Syktyvkar, Komi Republic, Russia 19–22 May 2014, Syktyvkar: Geoprint, 2014. 128-131. (In Russian). http://geo.komisc.ru/scientific-publication/proceedingofmeetings/meetings/237-yushkin2014/file

Unusual minerals in hot lava caves of Tolbachik eruption 2012-13

Belousov A., Belousova M., *Institute of Volcanology and Seismology, Far East Division, Russian Academy of Sciences, Petropavlovsk-Kamchatsky, Russia*

Fig. 1.1.1.5.4. Entrance into the biggest lava tube which is 350 m long

In June 2014, nine months after the end of Tolbachik eruption the investigations of new formed lava tubes were conducted. Two lava tubes with lengths 355 m and 150 m and width 10 m were visited and mapped, the temperature was 10-60 degrees C and there were no volcanic gases inside them. One more tube was too hot (>110 degrees C) and only the first 50 m were investigated (Fig. 1.1.1.5.4). Some tubes have temperatures 350 degrees C and more. The big white stalactites and stalagmites composed of sulfates and chlorides of K were found in the caves (Fig. 1.1.1.5.5). The lava tubes of this eruption are bigger than ones of 1975-76 eruption.

Fig. 1.1.1.5.5. Stalactites composed of sulfates and chlorides of K.

Belousov, A. B., & Belousova, M. G. (2014). Hot lava tubes of Tolbachik volcano and their unusual mineral formations. Vestnik DVO RAN, 5(177), 148-150. (In Russian). http://elibrary.ru/download/45837075.pdf

Oxysulfates of copper, sodium, and potassium in the lava flows of the 2012–2013 FTE

Karpov G.A., karpovga@kscnet.ru**, Vergasova L.P., Anikin L.P., Moskaleva S.V.,** *Institute of Volcanology and Seismology, Far East Branch, Russian Academy of Sciences, bul'var Piipa 9, Petropavlovsk-Kamchatsky, 683006, Russia*
Krivovichev S.V., Chernyat'eva A.P., Anikin L.P., Moskaleva S.V., Filatov S.K., filatov.stanislav@gmail.com**,** *St. Petersburg University, Universitetskaya nab. 7/9, St. Petersburg, 199034, Russia*

Samples from the surface of lava flows discharged by the 2012–2013 Tolbachik Fissure Eruption were found to contain oxysulfates of copper, sodium, and potassium:

$K_2Cu_3O(SO_4)_2$ (fedotovite), $NaKCu_2O(SO_4)_2$, and $Na_3K_5Cu_8O_4(SO_4)_8$. The last two phases have no naturally occurring or synthetic analogues that we are aware of. They form flattened crystals of prismatic to long-prismatic habits. The crystals of $Na_3K_5Cu_8O_4(SO_4)_8$ have a chemical composition corresponding to the empirical formula $Na_{2.22}K_{5.47}Cu_{8.02}S_{8.05}O_{36}$. An X-ray analysis of this compound showed that it has a monoclinic symmetry, $P2/c$, $a = 13.909(4)$, $b = 4.977(1)$, $c = 23.525(6)$ Å, $\beta = 90.021(5)°$, $V = 1628.3(7)$ Å^3. The crystal structure was determined by direct techniques and refined to yield R_1 for 3955 reflexes//web// with $F^2 > 4\sigma F$. The compound $NaKCu_2O(SO_4)_2$ also belongs to the monoclinic system, $P2/c$, $a = 14.111(4)$, $b = 4.946(1)$, $c = 23.673(6)$ Å, $\beta = 92.052(6)°$, $V = 1651.1(8)$ Å^3. The structure was determined by direct techniques to yield a tentative structural model that has been refined up to $R_1 = 0.135$ for 4088 reflexes with $F^2 > 4\sigma F$. The crystal structure of $Na_3K_5Cu_8O_4(SO_4)_8$ is based on chains of $[O_2Cu_4]^{4+}$ consisting of rib-coupled oxy-centered tetrahedrons of $(OCu_4)^{6+}$. The chains are surrounded by sulfate radicals, resulting in columns of $\{[O_2Cu_4](SO_4)_4\}^{4-}$ aligned along the b axis. The interchain space contains completely ordered positions of Na^+ and K^+ cations. The principle underlying the connection of $NaKCu_2O(SO_4)_2$ columns in the crystal structure of $\{[O_2Cu_4](SO_4)_4\}^{4-}$ is different, in view of the relation Na:K = 1 as contrasted with 3:5 for the compound $Na_3K_5Cu_8O_4(SO_4)_8$. The presence of oxy-centered tetrahedrons in the structure of these new compounds furnishes an indirect hint at the importance of polynuclear copper-oxygen radicals with centering oxygen atoms as forms of transport of copper by volcanic gases.

Karpov, G. A., Krivovichev, S. V., Vergasova, L. P., Chernyat'eva, A. P., Anikin, L. P., Moskaleva, S. V., & Filatov, S. K. (2013). Oxysulfates of copper, sodium, and potassium in the lava flows of the 2012–2013 Tolbachik Fissure Eruption. Journal of Volcanology and Seismology, 7(6), 362-370. Doi: 10.1134/S0742046313060031

1.1.2. Petrology and geochemistry of the volcanoes of Klyuchevskaya Group and Central Kamchatka Depression

1.1.2.1. Tolbachik volcanic massif

Petrology, geochemistry and isotope chemistry of the Tolbachik volcanic massif

T.G. Churikova, tchurikova@mail.ru, *Institute of Volcanology and Seismology, Far East Division, Russian Academy of Sciences, Petropavlovsk-Kamchatsky, Russia*
Gordeychik B., gordei@mail.ru, *Institute of Experimental Mineralogy, Russian Academy of Sciences, Chernogolovka, Russia*
Iwamori H., hikaru@jamstec.go.jp, **Nakamura H.**, hitomi-nakamura@jamstec.go.jp, **Haraguchi S.**, haraguti@sys.t.u-tokyo.ac.jp, **Miyazaki T.,** tmiyazaki@jamstec.go.jp, **Vaglarov B.S.,** bog@jamstec.go.jp, *Japan Agency for Marine-Earth Science and Technology, Yokosuka, Japan*
Ishizuka O., ishizuka@aist.go.jp, *Institute of Geology and Geoinformation, Geological Survey of Japan/AIST, Ibaraki, Japan*
Nishizawa T.[5], nishizawa.t.ad@m.titech.ac.jp, *Tokyo Institute of Technology, Tokyo, Japan*

The numerous of national and international publications were dedicated to Plosky Tolbachik volcano eruptions and adjacent monogenetic cones, which were erupted repeatedly during Holocene, including historical time. However, all these data mainly relates to monogenetic cones, but the information on stratovolcanoes itself practically absent. There are only few papers on Ostry and Plosky Tolbachik stratovolcanoes focusing on geology, petrography and some petrochemistry of the rocks. The modern geochemical and isotope studies of the stratovolcanoes were never achieved. In this report we present geological, petrographical, petrochemical, geochemical and some K-Ar data on the rocks of Tolbachik massif. The present report based on

representative collection of 154 samples from stratovolcanoes, dikes, monogenetic cones of different ages, including last 2012-13 eruption. Additionally our study included samples separately standing edifice of Povorotnaya mount, which age according to K-Ar dating is 0,306±0,01 Ma (Fig. 1.1.2.1.1).

Fig. 1.1.2.1.1. Tolbachik volcanic massif and mount Povorotnaya, view from the North.

The geological history of Tolbachik massif consists of four consecutive periods of volcano activity: basement formation about 0,086±0,016 Ma ago (according to K-Ar dating), growth of two sub-simultaneous stratovolcanoes, development of dike complex and formation of numerous cinder and cinder-lava monogenetic cones.
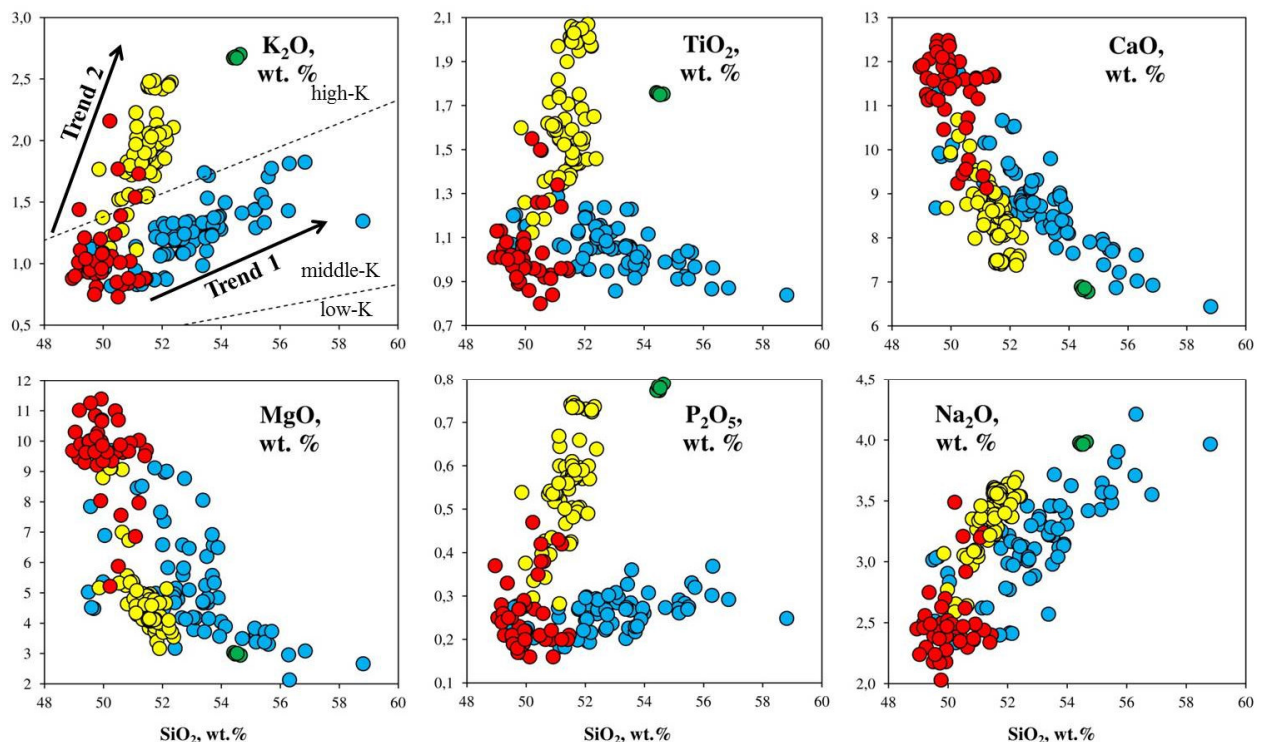
Fig. 1.1.2.1.2. SiO2 vs. major elements diagrams for Tolbachik massif rocks, Povorotnaya mount and KGV basement. 1975-76 Northern Breakthrough shown for comparison.

All rocks of Tolbachik massif belong to a medium-K and high-K calc-alkaline basalt–basaltic–andesitic series. In detail, however, there are some differences in the trends for major and trace elements. On all variation diagrams (Fig. 1.1.2.1.2) all samples split for three groups with formation of two different trends and one separate area. The first trend consists of medium-K basalts and basaltic andesites (Fig. 1.1.2.1.2, trend 1). It includes all samples of Tolbachik massif

basement, the lower parts of stratovolcanoes up to the elevation 2100 m, as well as all samples of Povorotnaya mount. This trend shows increasing K_2O and Na_2O and decreasing Al_2O_3, TiO_2, CaO, FeO, and MgO from basalts to basaltic andesites. The SiO_2 variation is the largest compared to other groups of samples.

The second medium-high-K trend includes the upper parts of stratovolcanoes higher than 2100-2500 m and the lavas of majority of cinder and cinder-lava cones. This trend is very steep and at SiO_2 variations only by 2.5% shows the sharp increase of alkalies, P_2O_5 and TiO_2 and sharp decrease in MgO, MnO, Fe_2O_3 and CaO (Fig. 1.1.2.1.2, trend 2).

The third group of rocks, which forms a separate area on all variation diagrams represented by basaltic andesites with SiO_2 54-55%, high alkalis, P_2O_5, TiO_2 and Fe_2O_3 at relatively low MgO and CaO. This group includes only the rocks of the first three days of 2012-13 eruption (so-called Menyailov Vent).
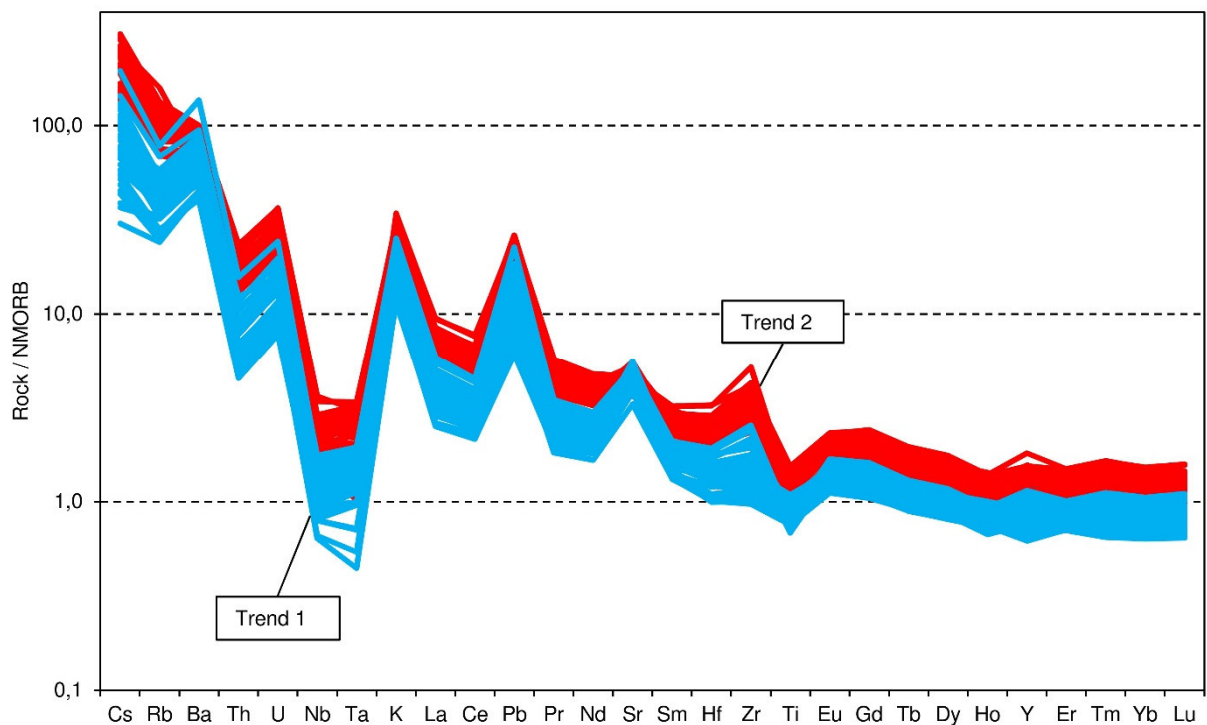
Fig. 1.1.2.1.3. NMORB-normalized trace element patterns for different volcanic complexes found at Tolbachik volcanic massif and Povorotnaya Mount. NMORB values after (Sun and McDonough, 1989).

Trace element patterns for all studied rocks have typical arc signatures with strong but variable LILE and LREE enrichment and low HFSE, which testify fluid influences. The samples of trend 1 have systematically lower values for REE, Nb and Ta compared to samples of trend 2 (Fig. 1.1.2.1.3). On trace element and trace element ratios binary diagrams the samples of two trends are also systematically different. The rocks of third group are mostly enriched in all incompatible elements not only inside the Tolbachik massif lavas, but also inside all rocks of Klyuchevskaya Group of Volcanoes. At the same time high-Mg basalts of 1975 eruption show the lowest patterns in all incompatible elements at Tolbachik massif. The samples from trend 1 and high-Mg basalts of 1975 are systematically depleted in Nb, Ta and REE compare to NMORB while the rocks of trend 2 and group 3 are systematically enriched.

Conclusions: (1) Volcanic activity at the area of Tolbachik massif started with formation of large basement, which was represented by middle-K Ol-bearing basalts and basaltic andesites including the augite-porphyric associations. Mantle source of these melts was depleted compare to N-MORB. This magma chamber was active also during first stages of stratovolcanoes formation. (2) Younger, upper parts both stratovolcanoes were influenced by different high-K

28

mantle source, which was enriched in alkalies, TiO_2, P_2O_5, and all incompatible trace elements. The rocks of this series are systematically enriched compared to N-MORB. The Holocene lavas of monogenetic cones also belong to this rock series. (3) The rocks of the Povorotnaya mount similar in petrography and chemical composition to the Tolbachik massif basement. Taking into account these data and data of K-Ar dating, we conclude that the Povorotnaya mount is the block of Tolbachik massif basement.

Churikova, T. G., Gordeychik, B. N., Iwamori, H., Nakamura, H., Ishizuka, O., Nishizawa, T., Haraguchi, S., Miyazaki, T., & Vaglarov, B. S. (2015). Petrological and geochemical evolution of the Tolbachik volcanic massif, Kamchatka, Russia. Journal of Volcanology and Geothermal Research. (In review).

Churikova, T. G., Gordeychik, B. N., Edwards, B. R., Ponomareva, V. V., & Zelenin, E. The Tolbachik volcanic massif: a review of the petrology, volcanology and eruption history prior to the 2012-2013 eruption. (2015). Journal of Volcanology and Geothermal Research. (In review).

Churikova, T., Gordeychik, B., Iwamori, H., Nakamura, H., Nishizawa, T., Haraguchi, S., Yasukawa, K., & Ishizuka, J. (2014). Petrology and geochemistry of the Tolbachik stratovolcano. 8-th Biennial Workshop on Japan-Kamchatka-Alaska Subduction Processes (JKASP-2014): Finding clues for science and disaster mitigation from International collaboration. Sapporo, Japan, 22-26 September 2014. http://hkdrcep.sci.hokudai.ac.jp/map/jkasp2014/pdf/R50.pdf

Mineralogy of the rocks from the Tolbachik volcanic massif

Flerov G.B., flerov@kscnet.ru*;* **Ananyev V.V., Ponomarev G.P.,** ponomarev@kscnet.ru*;* **Melekestsev I.V.***, Institute of Volcanology and Seismology, Far East Division, Russian Academy of Sciences, Petropavlovsk-Kamchatsky, Russia*

Based on whole rock and mineral composition analyses the petrological-geodynamical model of the magmagenesis of the volcanic manifestations in the area of Tolbachinsky Dol was elaborated. It was shown that the melt evolution of the Ostry and Plosky Tolbachik stratovolcanoes were similar while the basalts of the areal zone of the cinder and cinder-lava cones are systematically different from the stratovolcanoes. The main conclusions of this research is that the basaltic and trachybasaltic magmas are genetically not related and mixed during the period when the regime activity of the volcano was change from central to fissure types. The main process responsible for the rocks variations inside the basaltic and trachybasaltic fields is crystal differentiation. The existence of basalts and trachybasalts at the same magma system can be explained by the addition of the alkalies to the basaltic magma chamber and by the accumulation of these alkalies during fractional crystallization (Fig. 1.1.2.1.4).
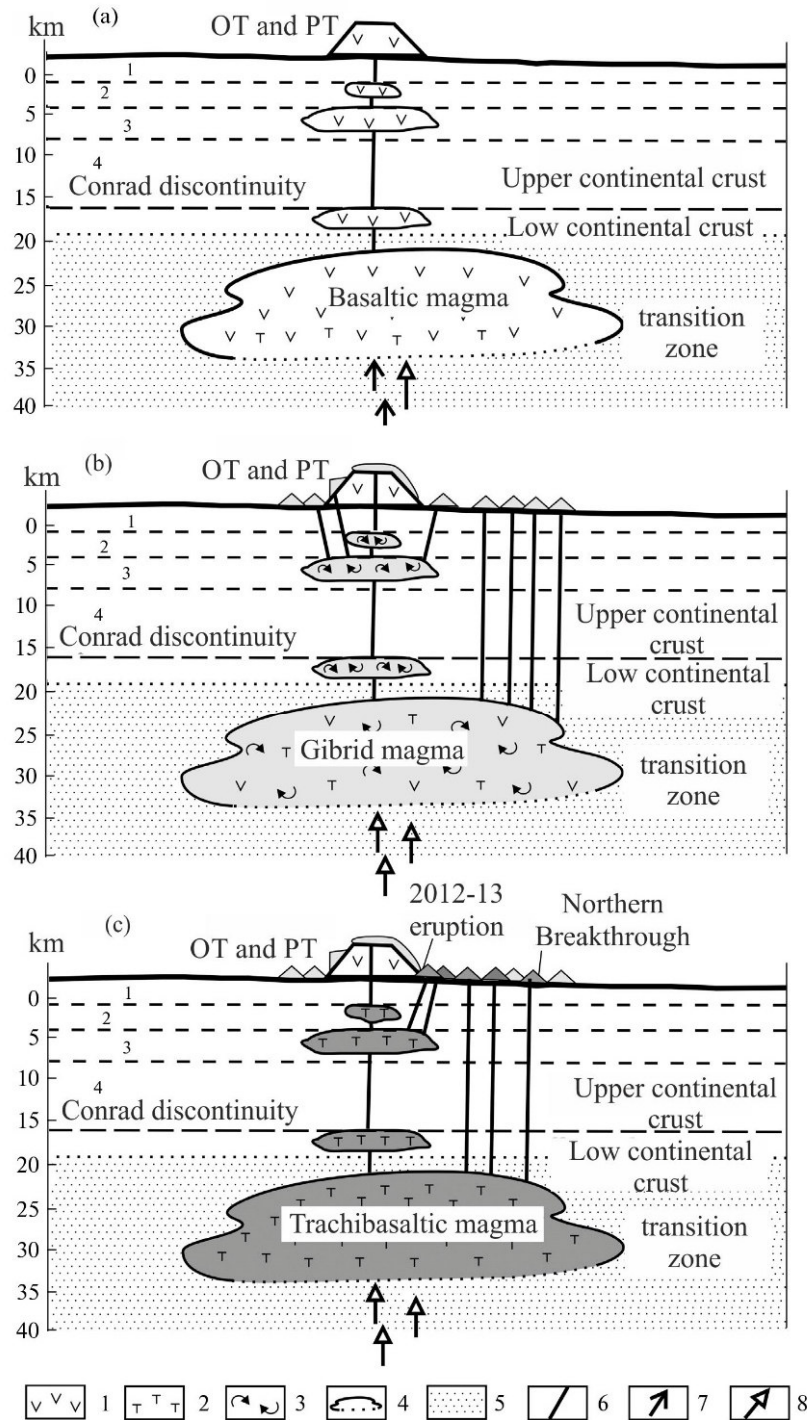
Fig. 1.1.2.1.4. Petrological-geodynamical model of the volcanic magmagenesis of the basaltic and trachybasaltic magma at the Tolbachinsky Dol area. (a) time of formation of the Ostry and Plosky Tolbachik stratovolcanoes; (b) first stage of the formation of fissure volcanic zone of the monogenetic cinder and cinder-lava cones; (c) second stage of the formation of fissure volcanic zone of the monogenetic cinder and cinder-lava cones. 1 – basaltic magma; 2 – trachybasaltic magma; 3 – magma of mixed composition; 4 – magma chambers; 5 – transition crust-mantle zone; 6 – magmatic columns; 7 – direction of the basaltic magma migration; 8 - direction of the trachybasaltic magma migration. Upper continental crust layers: (1) Quaternary volcanic rocks; (2) volcanic-sedimentary rocks of N1–N2 age; (3) – volcanic and intrusion rocks of the K–P age; (4) – crystalline basement of the Pz age. OT – Ostry Tolbachik, PT – Plosky Tolbachik.

Flerov, G. B., & Melekestsev, I. V. (2013). 2012-2013 eruption as result of continuous activity of the Tolbachik regional zone of cinder cones. Volcanism and related processes. Annual

regional scientific conference dedicated to the Volcanologist Day. Proceedings of the conference. March 29-30, 2013, Petropavlovsk-Kamchatsky. Petropavlovsk-Kamchatsky: Institute of volcanology and seismology FED RAS, 20-23. (In Russian). http://www.kscnet.ru/ivs/publication/volc_day/2013/art20.pdf

Flerov, G.B., Ananyev, V.V., & Ponomarev, G.P., Petrogenesis of the rocks from Ostry and Plosky Tolbachiks and the relationship of the volcanic manifestations of basaltic and trachybasaltic magmas at the Tolbachinsky Dol area (Kamchatka). Journal of Volcanology and Seismology. (In printing).

New mineral species in products of fumarole activity of the 1975-76 Tolbachik eruption

Vergasova, L.P., vlp@kscnet.ru, **Ananyev V.V.**, *Institute of Volcanology and Seismology, Far East Division, Russian Academy of Sciences, Petropavlovsk-Kamchatsky, 683006, Russia*
***Starova G.L., Filatov, S.K., Britvin, S.N.**, St. Petersburg University, Universitetskaya nab. 7/9, St. Petersburg, 199034, Russia*

Important aspect of the mineralogy of the Tolbachik volcanic massif is the diverse mineral population that forms after eruptions from secondary deposits at fumaroles. Minerals of volcanic exhalations represent a special genetic group. They are formed at surface pressure, elevated temperatures and with the participation of a fluid phase. The 1975-76 eruption was very productive with respect to such minerals and during the 35 years after this eruption more than 120 exhalation minerals have been identified, 32 of which were new (Table 1.1.2.1.1; Vergasova and Filatov, 2012) and 52 of which are the first reported occurrences in Kamchatka (Table 1.1.2.1.1). Minerals of exhalations were found at all cones of 1975-76 eruption, but the most varieties were found at cone 2. Most of them were also found around the crater zone.

The exhalation minerals mainly consist of lithophile (K, Na, Mg, Ca, Al, Si, Rb, Cs, P, V, C, O, F, Cl) and chalcophile (S, Cu, Zn, Pb, As, Se, Au, Bi, Te) elements, with lesser concentrations of Fe and Mo. Some ore elements like Cu, Pb and Zn are also present in these minerals, particularly the Cu-rich minerals (Table 1.1.2.1.1). The present-day volcanogenic–exhalation copper ore occurrence was detected at cone 2 of the 1975-76 eruption (Naboko and Glavatskikh, 1983). It was accompanied by As, V, Se, Bi, Te, and Au mineralization and large concentrations of Na, K and F (Vergasova et al., 2007).

Most of the new minerals occur in dispersed, fine-grained forms, and grains larger than 0.1 mm are rare. However, they can be spread across areas of up to several thousands of square meters (Naboko and Glavatskikh, 1992). Many new minerals are unstable in atmosphere and can disappear after cooling.

All new minerals can be divided on 7 groups: fluorides, chlorides, oxochlorides, carbonates, arsenates, vanadates, sulfates and oxysulfates, selenites, and oxyselenites. Most of them are anhydrous. Detailed classification was based on precise crystal structure determinations. The most common minerals at 1975-76 eruption are Ponomarevite and Tolbachite. It was found that isomorphism plays an important role in the chemistry of minerals from the exhalations. To date many of the new minerals have been synthesized. According to experimental data, the metals in fumaroles can be transported as chlorides, oxochlorides, oxo-centered complexes OA_4, and also can be transported in water-free conditions.

Copper appears to be closely connected to K and Na, and is transported with them as a gas phase. This suggests that crater areas of basaltic volcanism can be important for the formation of copper ore deposits (Vergasova and Filatov, 2012).

Table 1.1.2.1.1. New mineral species that were discovered in the fumarole deposits of the 1975-1976 Tolbachik eruption

Number	Name of mineral	Formula of mineral	References
		Fluoride	
1	Menyailovite	$Ca_4AlSi(SO_4)F_{13}*12H_2O$	[Vergasova et al., 2004]
		Chlorides and oxychlorides	
2	Tolbachite	$CuCl_2$	[Vergasova and Filatov, 1983]
3	Melanothallite	Cu_2OCl_2	[Vergasova and Filatov, 1982]
4	Ponomarevite	$K_4Cu_4OCl_{10}$	[Vergasova et al., 1988c]
5	Lesukite	$Al_2(OH)_5Cl*2H_2O$	[Vergasova et al., 1997a]
		Carbonates	
6	Chlorartinite	$Mg_2(CO_3)ClOH*3H_2O$	[Vergasova et al., 1998b]
		Arsenates	
7	Alarsite	$AlAsO_4$	[Semenova et al., 1994]
8	Coparsite	$Cu_4\mathbf{O_2}[(As,V)O_4]Cl$	[Vergasova et al., 1999a]
9	Urusovite	$Cu[AlAsO_5]$	[Krivovichev et al., 2000; Vergasova et al., 2000]
10	Filatovite	$K[(Al,Zn)_2(Al,Si)_2O_8]$	[Vergasova et al., 2004]
11	Bradaszekite	$NaCu_4(AsO_4)_3$	[Filatov et al., 2001]
12	Lammerite-b	$b-Cu_3(AsO_4)_2$	[Starova et al., 2011]
		Vanadates	
13	Leningradite	$PbCu_3(VO_4)_2Cl_2$	[Vergasova et al., 1990]
14	Averievite	$Cu_5(VO_4)_2\mathbf{O_2}*\mathbf{nMX}$	[Vergasova et al., 1988a; Starova et al., 1997]
		Sulphates and oxysulphates	
15	Pauflerite	$b-VOSO_4$	[Krivovichev et al., 2007]
16	Piypite	$K_4Cu_4\mathbf{O_2}(SO_4)_4*MeCl$	[Vergasova et al., 1984; Filatov and Vergasova, 1989]
17	Fedotovite	$K_2Cu_3\mathbf{O}(SO_4)_3$	[Vergasova et al., 1988b]
18	Kamchatkite	$KCu_3\mathbf{O}Cl(SO_4)_2$	[Vergasova et al., 1988a]
19	Klyuchevskite	$K_3Cu_3Fe^{3+}\mathbf{O_2}(SO_4)_4$	[Vergasova et al., 1989a]
20	Alumoklyuchevskite	$K_3Cu_3Al\mathbf{O_2}(SO_4)_4$	[Gorskaya et al., 1995]
21	Vlodavetsite	$AlCa_2(SO_4)_2F_2Cl*4H_2O$	[Vergasova et al., 1995a]
22	Nabokoite	$Cu_7Te\mathbf{O_4}(SO_4)_5*KCl$	[Popova et al., 1987]
23	Atlasovite	$Cu_6Fe^{3+}Bi^{3+}\mathbf{O_4}(SO_4)_5*KCl$	[Popova et al., 1987]
24	Vergasovaite	$Cu_3\mathbf{O}[(Mo,S)O_4][SO_4]$	[Bykova et al., 1998]
		Selenites and oxyselenites	
25	Sophiite	$Zn_2(SeO_3)Cl_2$	[Vergasova et al., 1989b]
26	Ilinskite	$NaCu_5\mathbf{O_2}(SeO_3)_2Cl_3$	[Vergasova et al., 1997b]
27	Bernsite	$KCdCu_7\mathbf{O_2}(SeO_3)_2Cl_9$	[Krivovichev et al., 2001]
28	Chloromenite	$Cu_8Zn\mathbf{O_2}(SeO_3)_4Cl_6$	[Vergasova et al., 1999b]
29	Georgbokiite	$Cu_5\mathbf{O_2}(SeO_3)_2Cl_2$	[Vergasova et al., 1999]
30	Parageorgbokiite	$b-Cu_5\mathbf{O_2}(SeO_3)2Cl_2$	[Vergasova et al., 2006]
31	Prewittite	$KPb_{1.5}ZnCu_6\mathbf{O_2}(SeO_3)_2Cl_{10}$	[Krivovichev, 2008]
32	Allochalcoselite	$Cu^+Cu^{2+}_5Pb\mathbf{O_2}(SeO_3)_2Cl_5$	[Vergasova et al., 2005]

Note: Oxygen of oxy-salts that is not included in acid radicals is highlighted in bold. Table taken from [Vergasova and Filatov, 2012].

Vergasova, L. P., & Filatov, S. K. (2012). New mineral species in products of fumarole activity of the Great Tolbachik Fissure Eruption. Journal of Volcanology and Seismology, 6(5), 281-289. Doi: 10.1134/S0742046312050053

Starova, G. L., Vergasova, L. P., Filatov, S. K., Britvin, S. N., & Ananyev, V. V. (2011). Lammirite-β $Cu_3(AsO_4)_2$ – a new mineral from fumaroles of the Great Fissure Tolbachic Eruption (Kamchatka, Russia). Zapiski RMO, 5, 46-51. (In Russian). http://www.minsoc.ru/articles.php?id=32&mid=21405&eid=2140503

Krivovichev, S. V., Filatov, S. K., Vergasova, L. P., & Kutuzova, R. S. (2012). Decomposition of Aluminosilicates and Accumulation of Aluminum by Microorganisms on Fumarole Fields of Tolbachik Volcano (Kamchatka Peninsula, Russia) // Minerals as Advanced Materials II (pp. 389-399): Springer Berlin Heidelberg.

Shuvalov, R. R., Vergasova, L. P., Semenova, T. F., Filatov, S. K., Krivovichev, S. V., Siidra, O. I., & Rudachevsky, N. S. (2013). Prewittite, $KPb_{1.5}Cu_6Zn(SeO_3)_2O_2Cl_{10}$, a new mineral from Tolbachik fumaroles, Kamchatka peninsula, Russia. Descripton and crystal structure. American Mineralogist. 98(2-3). 463-469.

Krivovichev, S., Filatov, S., & Vergasova, L. (2013). The crystal structure of ilinskite, NaCu5O2(SeO3)2Cl3, and review of mixed-ligand CuOmCln coordination geometries in minerals and inorganic compounds. Mineralogy and Petrology, 107(2), 235-242. Doi: 10.1007/s00710-012-0238-2

Krivovichev, S. V., Vergasova, L. P., Filatov, S. K., Rybin, D. S., Britvin, S. N., & Ananiev, V. V. 92013) Hatertite, $Na_2(Ca,Na)(Fe^{3+},Cu)_2(AsO_4)_3$, a new alluadite-group mineral from Tolbachik fumaroles, Kamchatka peninsula, Russia. European Journal of Mineralogy, 25(4), 683-691. Doi: 10.1127/0935-1221/2013/0025-2311

Vergasova, L. P., Semenova, T. F., Krivovichev, S. V., Filatov, S. K., Zolotarev, A. A., & Ananiev, V.V. (2014) Nicksobolevite, $Cu_7(SeO_3)_2O_2Cl_6$ - a new complex copper oxoselenite chloride from Tolbachik fumaroles, Kamchatka peninsula, Russia. European Jornal of mineralogy, 26(3), 439-449. Doi: 10.1127/0935-1221/2014/0026-2383

1.1.2.2. The petrological relationship between Kamen volcano and adjacent volcanoes of Klyuchevskaya group

Churikova T.G., tchurikova@mail.ru, *Institute of Volcanology and Seismology, Far East Division, Russian Academy of Sciences, Petropavlovsk-Kamchatsky, Russia*

Gordeychik B., gordei@mail.ru*, Institute of Experimental Mineralogy, Russian Academy of Sciences, Chernogolovka, Moscow region, 142432, Russia*

Ivanov B., ivanovbv@kscnet.ru, *Institute of Volcanology and Seismology, Far East Division, Russian Academy of Sciences, Petropavlovsk-Kamchatsky, Russia*

Wörner G., gwoerner@gwdg.de, *GZG Abteilung Geochemie, Universität Göttingen, Germany*

Data on the geology, petrography, mineralogy, and geochemistry of rocks from Kamen Volcano (Central Kamchatka Depression) are presented and compared with rocks from the neighboring active volcanoes. The rocks from Kamen and Ploskie Sopky volcanoes differ systematically in major elemental and mineral compositions and could not have been produced from the same primary melts. The compositional trends of Kamen stratovolcano lavas and dikes are clearly distinct from those of Klyuchevskoy lavas in all major and trace element diagrams as well as in mineral composition. However, lavas of the monogenetic cones on the southwestern slope of Kamen Volcano are similar to the moderately high-Mg basalts from Klyuchevskoy and may have been derived from the same primary melts. This means that the monogenetic cones of Kamen Volcano represent the feeding magma for Klyuchevskoy Volcano. Rocks from Kamen stratovolcano and Bezymianny form a common trend on all major element diagrams, indicating their genetic proximity. This suggests that Bezymianny Volcano inherited the feeding magma

system of extinct Kamen Volcano. The observed geochemical diversity of rocks from the Klyuchevskaya group of volcanoes can be explained as the result of both gradual depletion over time of the mantle N-MORB-type source due to the intense previous magmatic events in this area, and the addition of distinct fluids to this mantle source.

Like other KGV, Kamen Volcano overlies the large lava plateau of a shield volcano with its center below Ploskie Sopky Volcano. These lavas crop out mainly in the Studenaya and Khapitsa river valleys as well as near the Kozyrevsk and Klyuchi settlements. The age of these plateau lavas was determined by Ar–Ar dating to be 262–274 ka. The edifice of the Kamen stratovolcano formed after the emplacement of the plateau lavas (i.e. since ca. 260 ka) in two stages with different types of eruptions and erupted material. The first stage is characterized by an explosive regime with accumulation of thick pyroclastic deposits composed mainly of tuffs and tuffaceous breccias. The second stage of the stratovolcano was mainly effusive and is represented by thin lava flows that covered the early cone. Numerous dikes – lava flow conduits – also formed during this second stage. A similar sequence was suggested for the formation of Klyuchevskoy and Stariy Shiveluch stratovolcanoes. The sequence of activity of Kamen and its neighboring volcanoes is summarized in Fig. 1.1.2.2.1, based on geochronological evidence.

Ages and compositional series of the Klyuchevskaya group of volcanoes
(Central Kamchatka Depression)
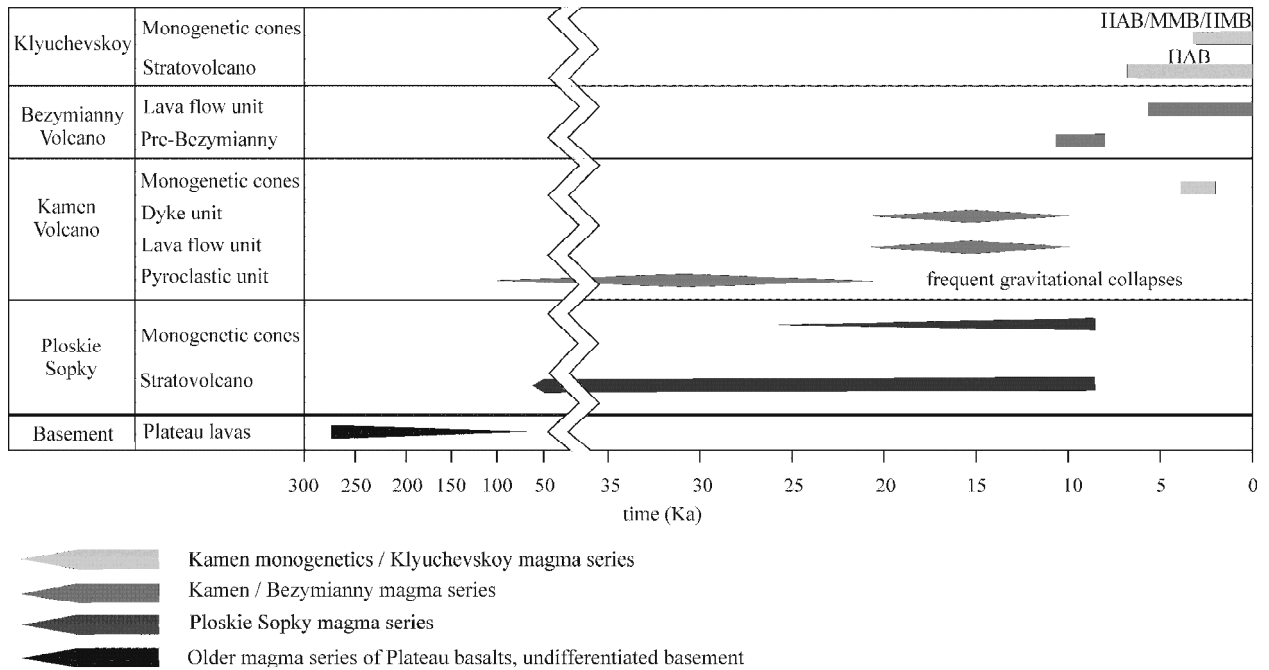
Fig. 1.1.2.2.1. Age-distribution diagram of Kamen Volcano and its surrounding stratovolcanoes and monogenetic centres. HAB — high-aluminium basalts; MMB — moderate-magnesium basalts; HMB — high-magnesium basalts.

Data from Kamen Volcano lavas show that major and trace elements as well as the mineral compositions of rocks from the stratovolcano and dikes are similar. This suggests that both suites crystallized from the same parental melts under comparable pressure–temperature (P–T) conditions and were derived from similar mantle sources. Similar Ol and Cpx Mg# in stratovolcano and dike rocks also suggest that both minerals are in equilibrium, but they do not fall on the mantle array. Low OlMg# and CpxMg# and low Ni and Cr concentrations in both minerals show that these magmas were significantly fractionated and do not represent primary melt compositions. This conclusion is confirmed by the absence of high-Cr Sp inclusions in Ol.

At the same time systematic differences in rock and mineral composition exist between Kamen stratovolcano/dikes and monogenetic cones, which simply reflect the different degrees of

differentiation of these suites. Most Ol from the more mafic monogenetic basaltic andesite cones are >Fo85, whereas Ol from more differentiated stratovolcano lavas are <Fo85. Cpx in monogenetic samples is also more magnesian than Cpx in Kamen stratovolcano/dikes. Pl compositions fall between the two Pl generations found in stratovolcano rocks: monogenetic cone Pl compositions are An60–75 while stratovolcano and dike Pl compositions are An40–55 and An75–90.
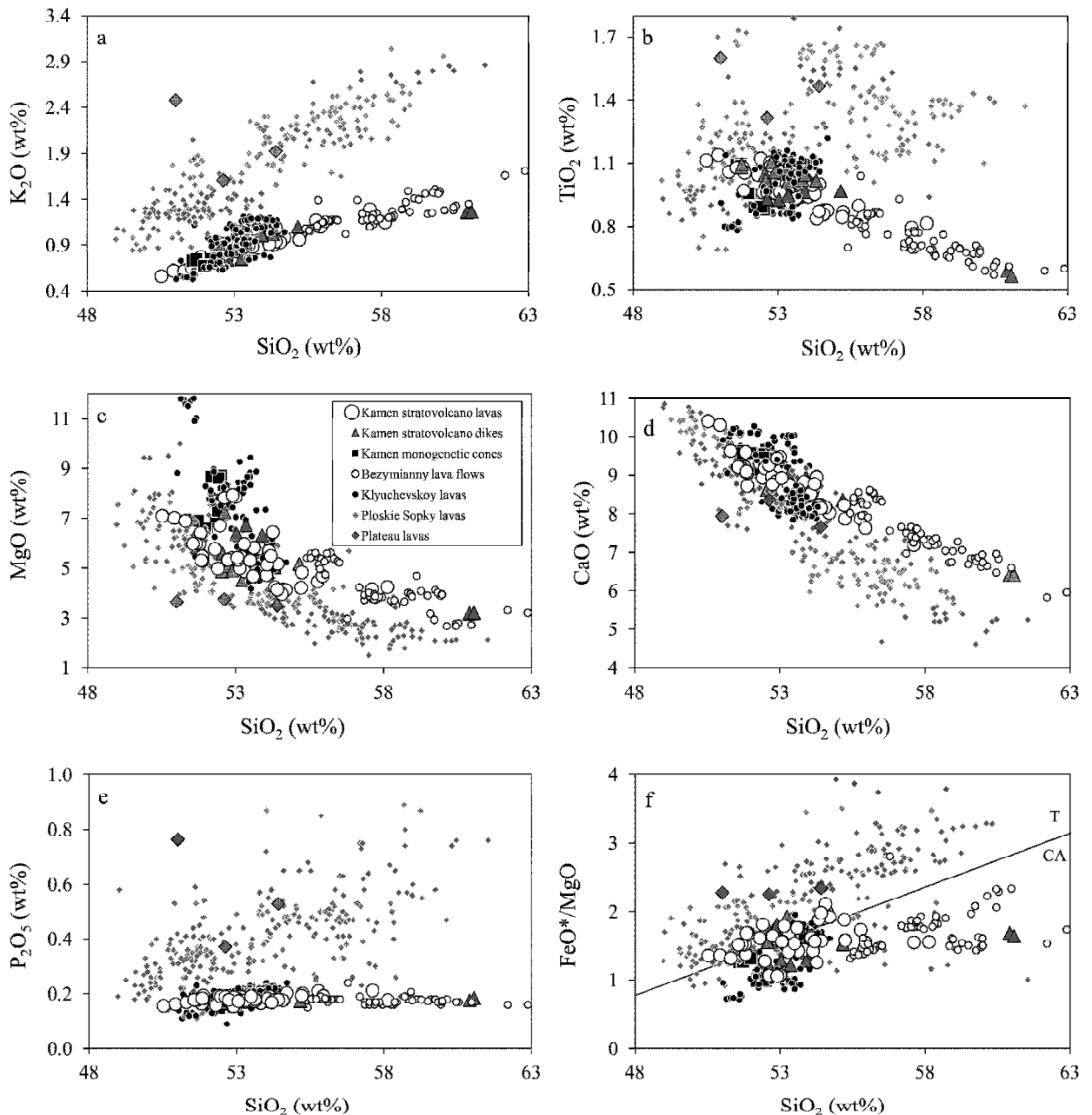
Fig. 1.1.2.2.2. Major elements (a–e) and FeO^*/MgO (f) vs. SiO_2 in rocks from Kamen Volcano and neighbouring volcanoes. Data for Ploskie Sopky rocks, Bezymianny lava flows, and Klyuchevskoy basaltic andesites are from (Churikova, 1993; Kersting and Arculus, 1994; Ozerov et al., 1997; Pineau et al., 1999; Churikova et al., 2001; Ishikawa et al., 2001; Dosseto et al., 2003; Bindeman et al., 2004; Almeev, 2005; Portnyagin et al., 2007; Turner et al., 2007).

Mineral assemblages in monogenetic cone rocks are very similar to those documented in Klyuchevskoy Volcano rocks. In contrast to samples from the stratovolcano and dikes, monogenetic cone Ol is more Mg-rich than is Cpx, suggesting that Cpx crystallized significantly later than Ol and that these minerals were not in equilibrium.

Kamen rocks exhibit major and trace element compositional trends that are distinct from those of Klyuchevskoy and Ploskie Sopky volcanoes but overlap with, and extend the mafic range of lavas from Bezymianny (Figs. 1.1.2.2.2, 1.1.2.2.3). Kamen rocks are also distinct from Klyuchevskoy and Ploskie Sopky rocks with respect to the CaO–Fo systematics in their Ol. Again, Ol from Bezymianny lavas falls on an extension of the Kamen Ol trend (Fig. 1.1.2.2.4).
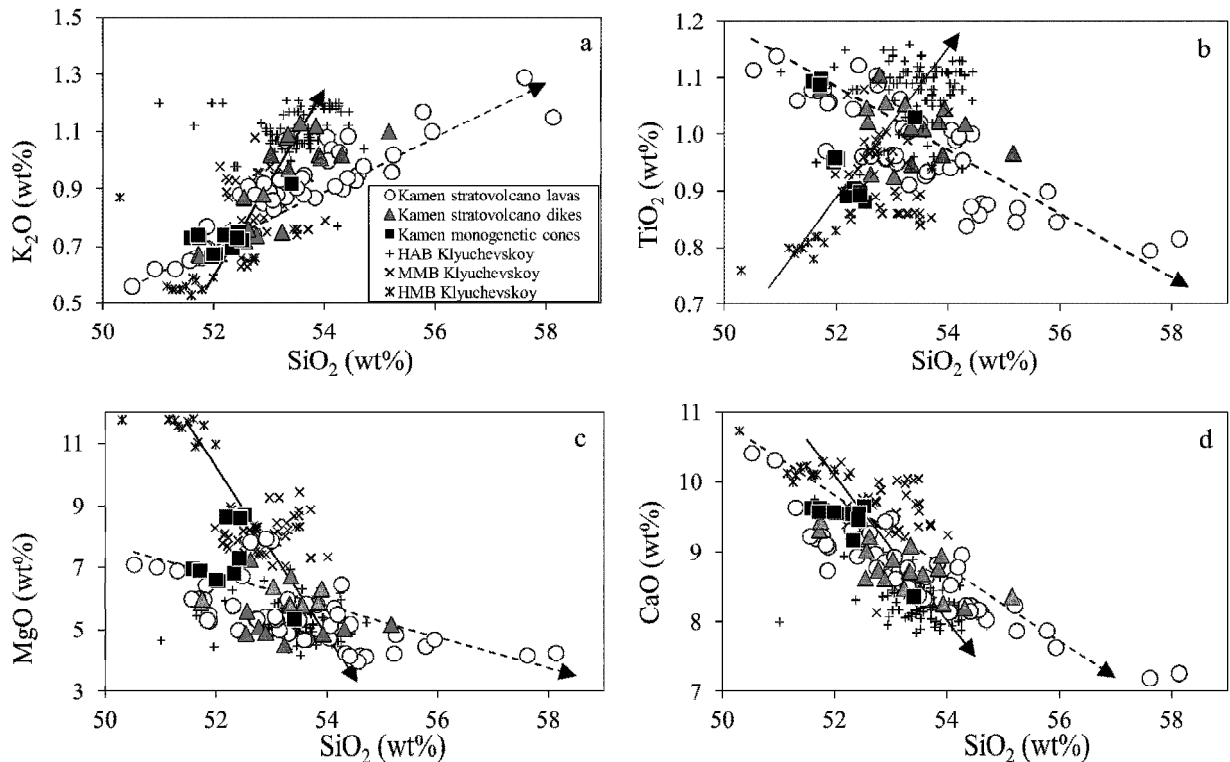
Fig. 1.1.2.2.3. Major elements vs. SiO_2 found in Kamen and Klyuchevskoy volcanic rocks. Data for Klyuchevskoy Volcano are from (Portnyagin et al., 2007). HAB — high-aluminium basalts; MMB — moderate-magnesium basalts; HMB — high-magnesium basalts. The black arrow indicates the evolutionary path of Klyuchevskoy melts; the dotted arrow shows the evolutionary path of the Kamen lavas.

Two more observations argue for a close genetic relationship between Kamen and Bezymianny magmas: (1) the occurrence of late-stage Hbl-rich lavas in the evolution of Kamen stratovolcano lavas and dike samples. Compositionally similar Hbl-rich rocks were also erupted at Bezymianny Volcano; and (2) the termination of Kamen Volcano activity 10–11 ka, which overlaps directly with the initiation of magmatism at Bezymianny about 10–11 ka ago (Fig. 1.1.2.2.1).

Samples similar to Klyuchevskoy HMB were not found at Kamen volcano. However, Kamen monogenetic cone lavas are close to the Klyuchevskoy MMB field on all major and trace element diagrams and in mineral compositions (Fig. 1.1.2.2.2), suggesting their genetic relationship.

From these observations, a direct genetic relationship is suggested between Klyuchevskoy MMB and monogenetic cones from Kamen, implying the same primary melts and mantle sources for these two volcanic series. These new data confirm an earlier suggestion based on field work (I.V. Melekestsev, A.P. Maksimov, pers. com.) and our own observations of the morphologies and ages of these cones: (1) they are situated on the slopes of Kamen Volcano and were active after Kamen Volcano activity had ended (i.e. after a series of gravitational collapses); (2) most of the Klyuchevskoy Volcano cinder and cinder–lava cones are situated at same distance (between 7 and 15 km) from the centre of the main edifice and thus overlap with the monogenetic cinder cones around Kamen, at a distance of 9 to 14 km from Klyuchevskoy; (3) the age of the studied cones is about 2–3.5 ka BP (unpublished data from O.A. Braitseva and V.V. Ponomareva), being a much

later occurrence relative Kamen volcano's ceased activity but coeval with the evolution of Klyuchevskoy (Fig. 1.1.2.2.1).
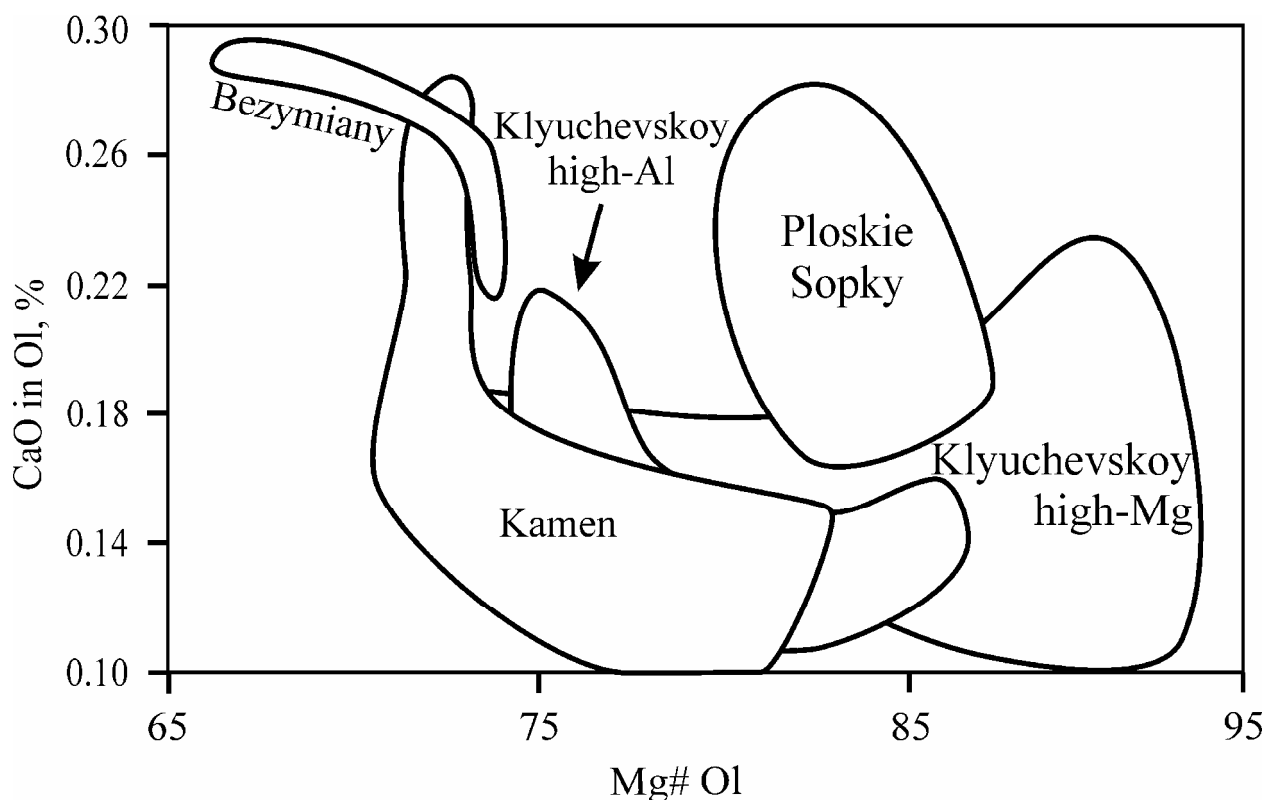
Fig. 1.1.2.2.4. CaO vs. Mg# in Ol for Klyuchevskaya group of volcanoes rocks. There is a trend from Klyuchevskoy through Kamen to Bezymianny volcanoes. Ol from the Ploskie Sopky Volcano form a field that is separate from this trend.

The rocks of Ploskie Sopky Volcano, the oldest of the KGV, form systematically different trends from all studied KGV on major and trace element diagrams and thus cannot have originated from the same magma source by fractional crystallization. They are enriched in K2O, TiO2, and P2O5 and depleted in MgO and CaO (Fig. 1.1.2.2.2). Ol from Ploskie Sopky Volcano is also highly enriched in CaO compared to Ol from all other KGV volcanoes studied (Fig. 1.1.2.2.4). Three samples of plateau lavas, which are older still, overlap with the Ploskie Sopky compositional field.

Some conclusions may obtained:

1) Data on major and trace elements in rocks from Kamen Volcano and neighbouring volcanoes fall into three distinct geochemical groups. Lavas from the Kamen stratovolcano and its dikes are distinct in their geochemical character from magmas erupted at Ploskie Sopky and Klyuchevskoy.

2) A close genetic relationship exists between Kamen and Bezymianny volcanoes in which the Bezymianny lavas comprise the more evolved part of the common trends. This Kamen–Bezymianny trend is dominated by fractional crystallization and magma mixing and is typical for many arc magma series. This trend suggests that Kamen Volcano shares the magma source and a common magma plumbing system with Bezymianny Volcano.

3) Monogenetic cinder and cinder–lava cones situated on the W–SW slopes of Kamen Volcano are compositionally similar and thus genetically related to Klyuchevskoy Volcano (MMB lavas).

4) Klyuchevskoy lavas are geochemically separate from the Kamen – Bezymianny rocks and define three distinct magma compositions that are not genetically related by simple low-pressure fractionation and/or mixing. Rather, these magmas either (a) represent high-P fractionated melts from a common arc basalt, or (b) are derived from the same mantle source with different

degrees of melting and magma mixing, or (c) are derived from distinct sources in the mantle wedge.

5) Ploskie Sopky Volcano rocks are systematically different from Kamen and Klyuchevskoy rocks in major elements and mineral composition; some are similar to the older plateau lavas. Thus they could not have originated from the same primary melts by fractional crystallization.

6) The geochemical diversity of KGV rocks and their relationship to underlying plateau lavas results from both (a) gradual depletion with time of the mantle NMORB-type source due to previous magmatic events, and (b) the addition of distinct and variable fluids to this mantle source.

7) Trace and volatile element ratios in rocks and melt inclusions show that the fluid composition can differ even between neighbouring volcanoes with rather similar mantle sources.

Churikova, T. G., Gordeychik, B. N., Wörner, G., & Ivanov, B. V. (2011). Variable fluids and mantle sources documented in the geochemistry of Kamen volcano and the Kluchevskaya volcanic group. 7th Biennual Workshop on Japan-Kamchatka-Alaska Subduction Processes: Mitigating Risk Through International Volcano, Earthquake, and Tsunami Science. JKASP-2011. Petropavlovsk-Kamchatsky, Russia. August 25-30, 2011. Abstracts. – Petropavlovsk-Kamchatsky: Institute of Volcanology and Seismology FEB RAS, Kamchatkan Branch of Geophysical Service RAS, 145-146. – http://www.kscnet.ru/ivs/slsecret/jkasp_2011/abstr/jkasp_2011.htm.

Churikova, T. G., Gordeichik, B. N., & Ivanov, B. V. (2012). Petrochemistry of Kamen volcano: A comparison with neighboring volcanoes of the Klyuchevskoy group. Journal of Volcanology and Seismology, 6(3), 150-171. Doi: 10.1134/S0742046312030037

Churikova T. (2012). Variable fluid sources across the Kamchatka arc: evidence from volatile and fluid mobile trace elements. Joint Symposium of Misasa-2012 and GEOFLUID-2. Dynamics and Evolution of the Earth's Interior: special emphasis on the role of fluids. March 18-21, 2012, Misasa, Tottori, Japan, 18. http://www.misasa.okayama-u.ac.jp/~symp/abstract.pdf

Churikova, T. G., Gordeychik, B. N., Ivanov, B. V., & Wörner, G. (2013). Relationship between Kamen Volcano and the Klyuchevskaya group of volcanoes (Kamchatka). Journal of Volcanology and Geothermal Research, 263, 3-21. Doi: http://dx.doi.org/10.1016/j.jvolgeores.2013.01.019

Churikova, T. G., Gordeychik, B. N., Wörner, G. (2014) Mantle and fluid sources below Klyuchevskoy-Kamen-Bezymianny line (Kamchatka) // GEOFLUID-3. Nature and Dynamics of fluids in subduction zones. Tokyo Institute of technology, 2014, Tokyo, 72.

1.1.2.3. Japanese-Russian project of study Klyuchevskoy volcano

Bergal-Kuvikas O., olgakuvikas@gmail.com, *Hokkaido University, Graduate School of Science, Department of Earth and Planetary Sciences, Japan. Institute of Volcanology and Seismology, Russia*

Nakagawa M, mnakagawa@mail.sci.hokudai.ac.jp, *Hokkaido University, Graduate School of Science, Department of Earth and Planetary Sciences, Japan*

Muravyev Y., murjd@kscnet.ru**, Malik N.,** maliknataliya@mail.ru**, Ovsyannikov A.,** oval@kscnet.ru, *Institute of Volcanology and Seismology, Russia*

Ishizuka Y., y.ishizuka@aist.go.jp, *Geological Survey of Japan, Japan*

Hasegawa T., hasegawt@mx.ibaraki.ac.jp, *Department of Earth Sciences, College of Science, Ibaraki University, Japan*

Uesawa S., uesawa@criepi.denken.or.jp, *Geosphere Science, CRIEPI, Japan*

In the frameworks of Japanese-Russian project the Klyuchevskoy volcano was studied. The Klyuchevskoy volcano is one of the famous and biggest volcano in the Eurasia (altitude ~ 4750

m, volume ~ 250 km^3). It is located in the Central Kamchatka Depression, in the northern part of the Eastern Volcanic Belt of Kamchatka. The Klyuchevskoy volcano is voluminous stratovolcano with numerous cinder cones. Based on the tephrochronological data the volcano has been formed 6000-7000 BP.

This research represents one of the part Japanese-Russian project investigation of Klyuchevskoy volcano. We will focus on the geological and petrological aspects. Field work was started in 2010 and continues three years. On the today, we have representative collected rocks including 104 samples of prehistorical eruptions and 106 samples of historical eruptions (from 1932 to recently eruptions in 2013). Representative collection of the samples allow us understand temporal changing of magma composition during historical time.

Klyuchevskoy volcanic group include 14 volcanoes and present us one of the active group at the Kurile-Kamchatka volcanic arc. Since 1697 to 1931 Klyuchevskoy volcano mainly had erupted on the summit. However new circle of activity was started in 1932 and continued approximately 80 years. The circle is characterized by combination of flank eruptions and summit activities. After the paroxysmal summit eruption in 1994, for volcano typically weak small explosions. However since 2003 new cinder cones was forming on the top and during to present day effusive and/or strombolian eruptions have been occurred until the present day.

Location of cinder cones are controlled by fracturing zone on the slopes of volcano. Most of cinder cones are located in Northeast and Southeast sectors. Relations between locations of cinder cones, lava volume, altitude and age testified about existence fissures or fracture zone on the slope of Klyuchevskoy volcano. Along fissures ages and altitude of flank eruptions are increasing.

Analysis of the location cinder cones suggests that flank eruptions had gone up to the summit from 450 m to 4500 m (summit) since 1932 until 1989. Consequently distance from central crater degrease with time. Clear dependence volume of volcanic material and years of eruptions not observed. However, most effusive eruptions existed in the beginning of the cycle.

Geochemical data of prehistoric eruptions have a relatively wide diapason of variations (51-54.5 wt. % SiO_2). Magma was characterized by more mafic and ferriferous compositions (4-12 wt % MgO, 8.7-10 wt % Fe_2O_3). In opposite, historical eruptions are characterized by more fractionating magma. The higher contents of SiO_2 52.5-55 wt %, Al_2O_3 14-18 wt %, Na_2O 2.7-3.8 wt. % are determined. Spatial magma variations in time (0-3000 BP) suggests that composition of rocks continuously changed from more depleted in past to more enriched in modern time (higher contents of Zr, Y, Ba, Sr, K_2O). Simple fractional crystallization not explain compositional variation of magma.

On the Klyuchevskoy volcano are defined two different magmatic suites: First suite is low K_2O. This group is characterized by lowest contents of K_2O (0.5-0.8 wt. %), high MgO (7-13 % wt. %), low contents of incompatible elements (Ba, Sr, Rb). For second suite is typical high contents of K_2O (0.8-1,2 wt %), highest Zr, Ba, Rb, TiO_2. Distribution of these magmatic groups in the time are irregular. Thus, since 3000 BP to 1500 BP low K_2O suite has been dominating. Since 1000 BP to present time high K_2O suite prevail. However, general pattern magma variations in time (0-3000 BP) shows that high K_2O suite dominate over low K_2O suite.

Relation between location of cinder cones and magma suites has a some tendency. Low K_2O suites are located on the lower slopes, in opposite high K_2O suite are located in the upper slopes and on the top of volcano. Additionally, low K_2O suite belong to fracturing zone with large concentration of cinder cones.

This topic show just first results of our research, main purpose of this presentation is show geochemical and petrological features of the prehistorical and historical eruptions. Now geochemical works are continuously. We will present ICP-MS and isotope data on the conference. Discuss about origin of the magma and causes of magmatic variations in space and time will be studying in the future.

Bergal-Kuvikas, O., Nakagawa, M., Muravyev, Ya., Malik, N., Ovsyannikov, A., Ishizuka, Yo., Hasegawa, N., & Uesawa, S. (2014). Japanese-Russian project of study Klyuchevskoy volcano (Kamchatka, Russia): First results of the geological and petrological investigations. 8-th Biennial Workshop on Japan-Kamchatka-Alaska Subduction Processes (JKASP-2014): Finding clues for science and disaster mitigation from International collaboration. Sapporo, Japan, 22-26 September 2014. http://hkdrcep.sci.hokudai.ac.jp/map/jkasp2014/pdf/R10-1.pdf

1.1.2.4. Geochemical studies of the Shiveluch volcanic massif

Gorbach N.V., n-gorbach@mail.ru**, Tembrel I.,** *Institute of Volcanology and Seismology, Far East Division, Russian Academy of Sciences, Petropavlovsk-Kamchatsky, Russia*
Portnyagin M.V., mportnyagin@ifm-geomar.de, *Vernadsky Institute of Geochemistry and Analytical Chemistry, Russian Academy of Sciences, Moscow, Russia. Leibniz Institute of Marine Sciences (IFM GEOMAR), Kiel, Germany*
Hauff F., fhauff@geomar.de, *Helmholtz Centre for Ocean Research Kiel (GEOMAR), Kiel, Germany*

Shiveluch is one of the largest (up to 1000 km^3) and most active volcanic centers in Kamchatka, which occupies a unique geodynamic setting close to the edge of the subducting Pacific plate at the Kurile–Kamchatka and Aleutian arc junction (Fig. 1.1.2.4.1). Volcanic massif has a long and complex eruptive history that started before 80 ka (Pevsner et al., 2014). It edifice includes the Late Pleistocene Old Shiveluch stratovolcano, partially destroyed by a large-scale sector collapse, and Young Shiveluch eruptive center, which has been active through the Holocene (Melekestsev et al., 1991).
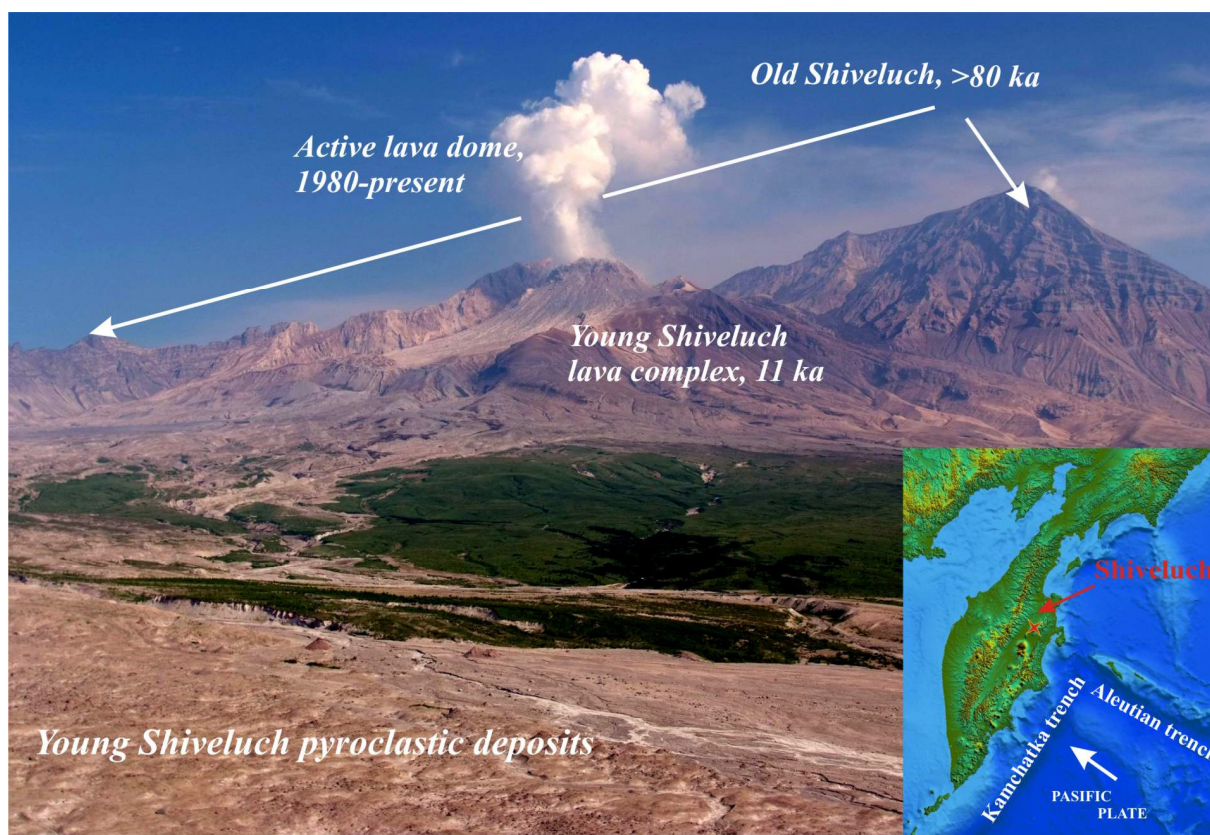
Fig. 1.1.2.4.1. Shiveluch volcanic massif, view to the northwest.

Geology and Petrology of the Lava Complex of Young Shiveluch Volcano, Kamchatka

Detailed geological and petrological–geochemical study of rocks of the lava complex of Young Shiveluch volcano made it possible to evaluate the lava volumes, the relative sequence in which the volcanic edifice was formed, and the minimum age of the onset of eruptive activity. The lavas of Young Shiveluch are predominantly magnesian andesites and basaltic andesites of a mildly potassic calc–alkaline series (SiO_2 =55.0–63.5 wt %, Mg# =0.56–0.69). Geologic relations and data on the mineralogy and geochemistry of rocks composing the lava complex led us to conclude that the magnesian andesites of Young Shiveluch volcano are of hybrid genesis and are a mixture of silicic derivatives and a highly magnesian magma that was periodically replenished in the shallow magma chamber. Geological lines of evidence of the mixing processes are provided by lavas of heterotaxitic structure and by the occurrence of melanocratic nodules in the lavas of the modern extrusive dome. The mineralogical lines of evidence are compositionally discrete groups of hornblende and plagioclase phenocryst cores and their sharp zoning, the occurrence of highly magnesian olivine in all rock varieties, the reaction relations of this mineral with pyroxenes and hornblende, and the reversed zoning of the pyroxenes.

From the viewpoint of geochemistry, magma mixing most significantly affected the Cr and Ni concentrations, which are the most contrasting in the primitive and evolved rocks. In the Cr vs. SiO_2 plot (Fig. 1.1.2.4.2), the trend predicted for the fractional crystallization of basaltic melt has a hyperbolic configuration and leads to a significant depletion of the melts in Cr (as well as Ni) during early crystallization stages. The data points of lavas from Young Shiveluch plot away from the crystallization trend and define diffuse linear trends, which suggests that these magmas were produced by the mixing of primitive basalt magma and evolved andesites.
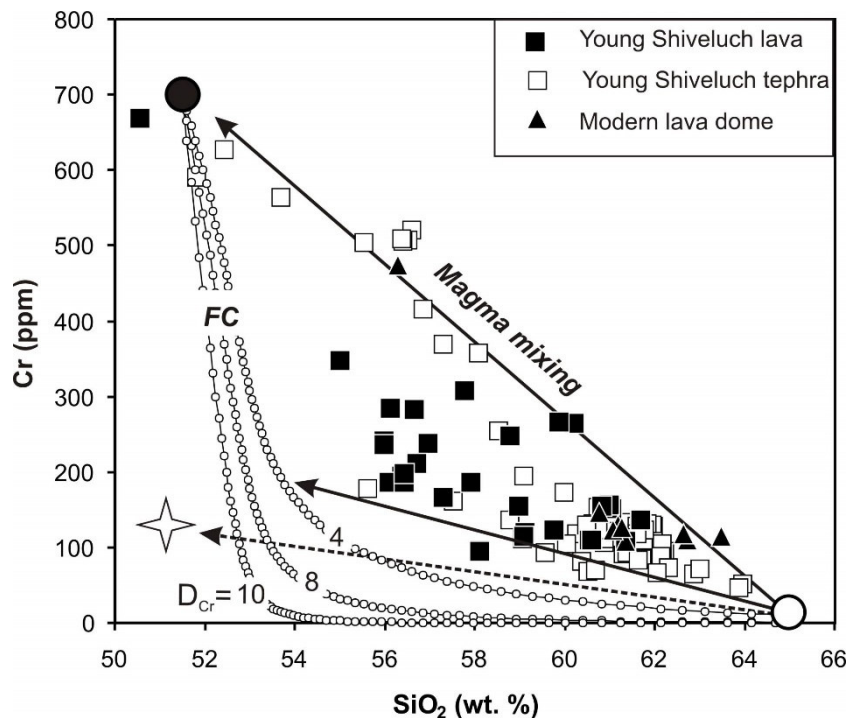
Fig. 1.1.2.4.2. Variations in the concentrations of SiO2 and Cr in lavas and pyroclastic rocks of Young Shiveluch volcano. Lava compositions are our data, compositions of pyroclastic rocks are according to (Ponomareva et al., 2007). Thin lines with circles show the model trends of fractional crystallization FC of basalt melt with initial concentrations of Cr = 700 ppm and SiO2 = 51.5 wt % (solid circle) at various values of the bulk partition coefficient D_{Cr} between minerals and melt. The calculations were made using the dependence between the SiO2 concentration and degree of crystallization, according to (Brophy, 2008). Heavy arrows show possible mixing trends of a differentiated magma with 65 wt % SiO2 (open circle) and (I) primitive basalt, and (II) basaltic andesite obtained by 35% crystallization of primitive melt. The dashed

line with an arrowhead shows the mixing trend of differentiated andesite and an average composition of high-Al basalt of the mildly-K series (star) of the Eastern Volcanic Front (Geochemical Types…, 1990).

The "adakitic" geochemical characteristics (Sr/Y > 50, Y < 18 ppm) of andesites of Young Shiveluch volcano are most clearly pronounced in the most evolved rock varieties and are produced by the fractional crystallization of an association of plagioclase and hornblende at the incomplete separation of plagioclase crystals from the fractionating magmas (Fig. 1.1.2.4.3).
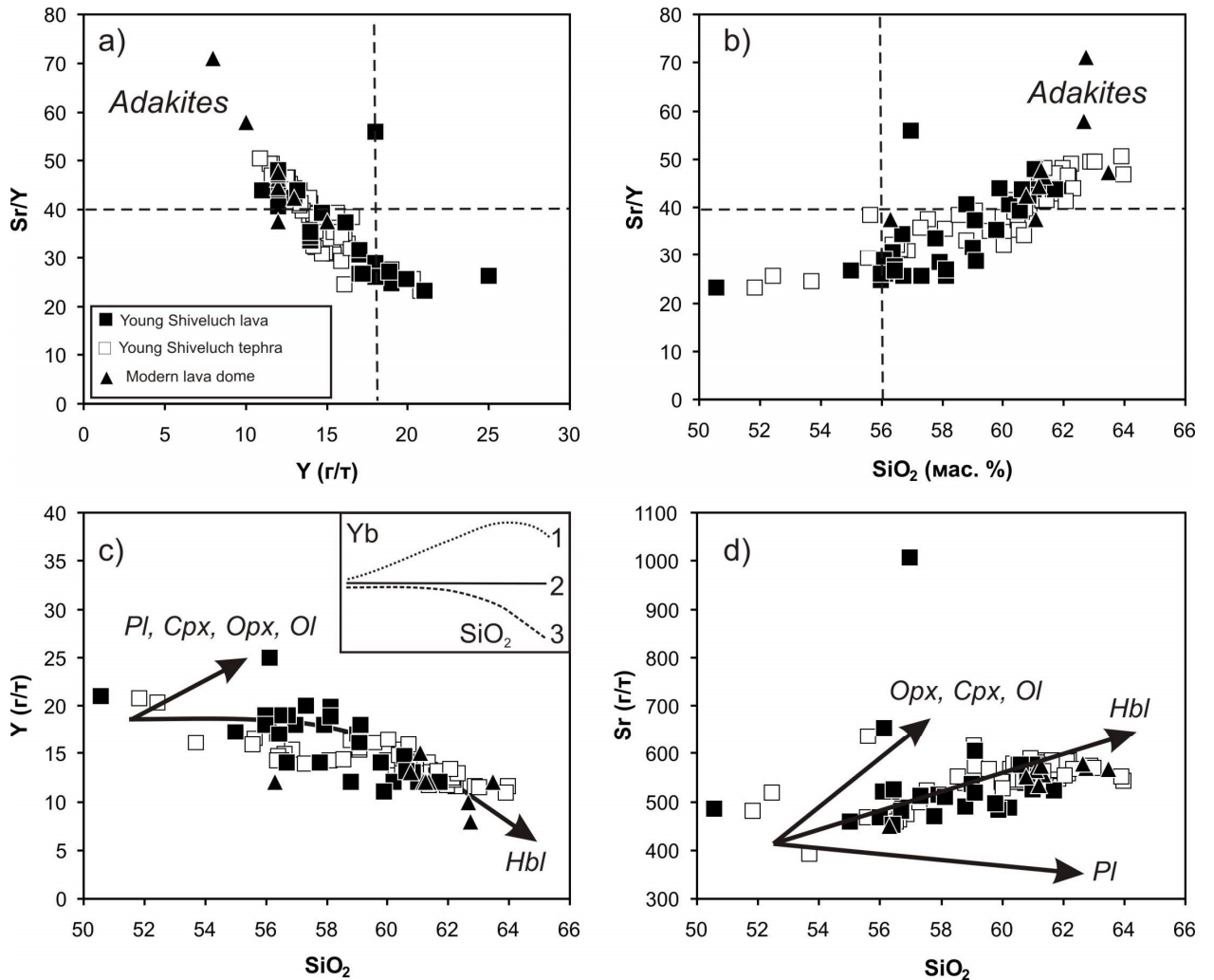
Fig. 1.1.2.4.3. Variations in the concentrations of SiO2, Sr, and Y in lavas and pyroclastic rocks of Young Shiveluch volcano. Lava compositions are our data, compositions of pyroclastic rocks are according to (Ponomareva et al., 2007). The field of adakite compositions (Y < 18 ppm, Sr/Y > 40, SiO2 > 56 wt %) is shown according to (Defant and Drummond, 1990). The inset in Fig. 1.1.2.4.3c shows trends for Yb (a close geochemical analogue of Y) in the crystallization course of basalt melt (1) without and (2) with amphibole under lower crustal conditions and (3) a trend based on data in (Brophy, 2008). The heavy arrows in Figs. 1.1.2.4.3c and 1.1.2.4.3d show the vectors of the melt compositional evolution during the crystallization of various phases.

Gorbach, N. V., & Portnyagin, M. V. (2011). Geology and petrology of the lava complex of Young Shiveluch Volcano, Kamchatka. Petrology, 19(2), 134-166. Doi: 10.1134/S0869591111020068
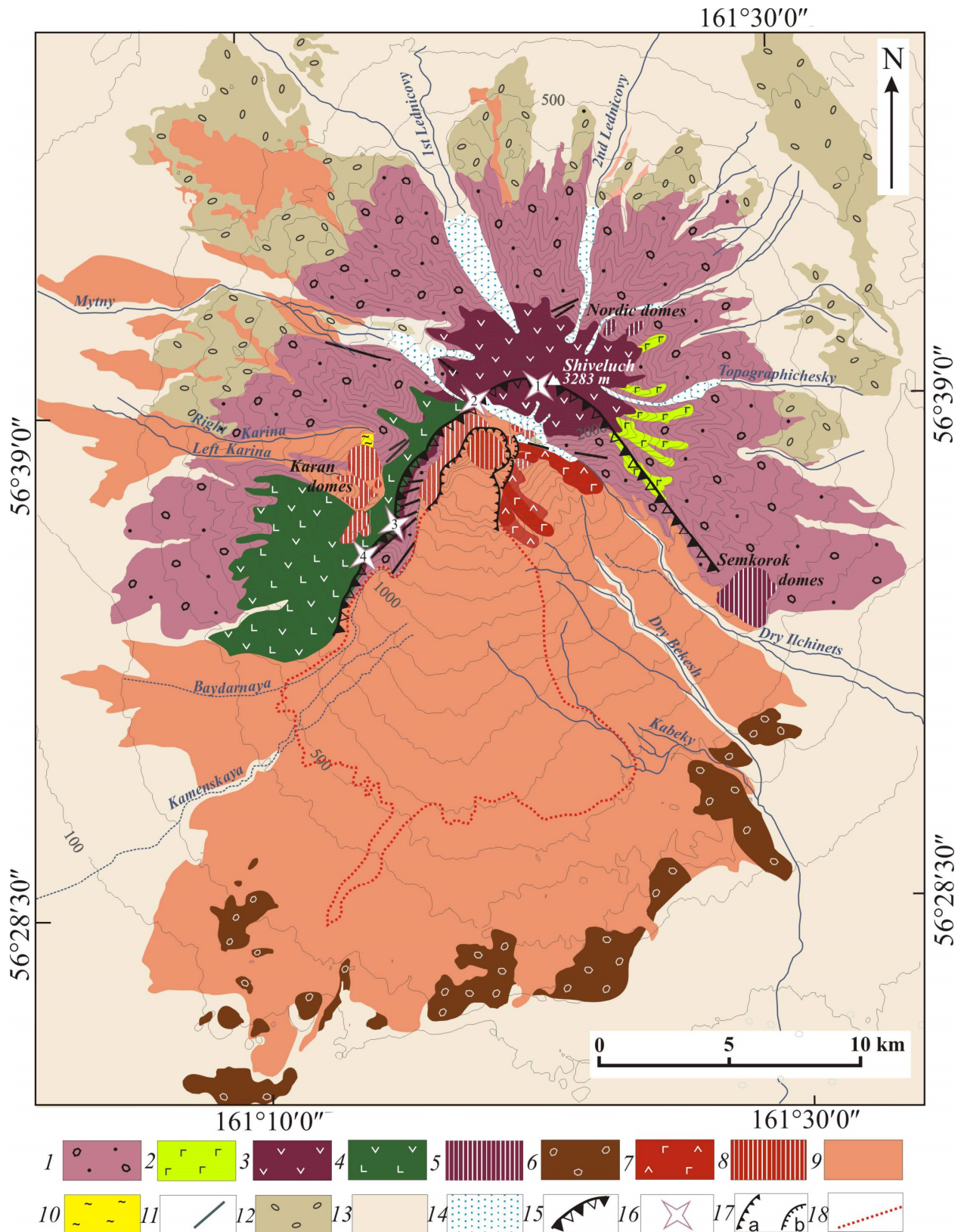
Fig. 1.1.2.4.4. Geological map of the Shiveluch volcanic massif compiled based on the 2006-2009 field observations and previously published data from Lopatin et al. (1979) and Melekestsev et al. (1991). The field of the Holocene proximal pyroclastic deposits is shown after Ponomareva et al. (2007). The field of proluvial deposits, moraines and expected Old Shiveluch sector collapse deposits allocated based on the interpretation of aerial photographs.

We report results of a new comprehensive geological mapping of the Late Pleistocene Old Shiveluch volcano. The mapping results and geochemical data on major and trace element composition of the volcanic rocks are used to characterize spatial distribution, eruptive sequence and volumetric relationships between different rock types of the volcano. Old Shiveluch volcano had been constructed during two main stages: initial explosive and subsequent effusive ones. Pyroclastic deposits of the initial stage are represented by agglomerate and psephytic tuffs with very few lava flows and form at least 60% of volume of the Old Shiveluch edifice. The deposits of the second stage are dominantly lava flows erupted from four vents: Central, Western, Baidarny and Southern, reconstructed from the field relationships of their lava flows. About 75% of the Old Shiveluch edifice, both pyroclastic deposits and lava, are composed of magnesian andesites (SiO_2=57.3-63.8 wt %, Mg#=0.53-0.57). The most abundant andesitic lavas were coevally erupted from the Central and Western vents in the central part of the edifice. Less voluminous high-Al basaltic andesites (SiO_2=53.5-55.7 wt %, Mg#=0.52-0.56) were produced by the Western, Baidarny and Southern vents situated in the south-western sector. Small volume high-Mg basaltic andesites (SiO_2=53.9-55.0 wt %, Mg#=0.59-0.64) occur in the upper part of the pyroclastic deposits.

Andesites of Old and Young Shiveluch Volcanoes have similar compositions, whereas Old Shiveluch basaltic andesites are compositionally distinctive from those of the Young Shiveluch by having lower Mg#, SiO_2, Cr and Ni, and higher Al_2O_3, FeO^T, CaO, TiO_2, and V contents at given MgO. Geochemical modeling suggests that the compositions of the intermediate Old Shiveluch magmas can be reasonably explained by simple fractional crystallization of olivine, clinopyroxene, plagioclase and magnetite (±hornblende) from water-bearing (~3 wt % H_2O) high-Mg# basaltic parental magma at intermediate to shallow crustal depths (<15 km). Mixing of evolved (SiO_2>60 creating the compositional diversity of the Old Shiveluch magmas compared to the Young Shiveluch ones. The pronounced change in the Shiveluch magma compositions could have been related to adjustments of the magma plumbing system beneath Old Shiveluch following the large scale sector collapse in the Late Pleistocene that enabled a common mixing of evolved and primitive magmas on the later, Holocene stage of the volcano evolution.

Old Shiveluch (1-6): 1 – Initial agglomerate tuffs of Hbl-Pl and Hbl-Px-Pl andesites, 2 – Initial Ol-Cpx-Pl basaltic andesites, 3 – lavas of Hbl-Pl and Hbl-Px-Pl andesites, rarely lavas Px-Pl± Hbl basaltic andesites, 4 – lavas of Px-Pl basaltic andesites, 5 – extrusive lavas of Hbl-Pl ±Px andesites, 6 – expected deposits of Old Shiveluch sector collapse.

Young Shiveluch and Karan domes (7-9): 7 – lavas of Ol-Cpx-Pl± Hbl basaltic andesites and andesites, 8 - extrusive lavas of Hbl-Pl and Hbl- Px- Pl andesites, rarely Ol-Hbl± Pl andesites, 9 – proximal pyroclastic deposits.

Other symbols (10-17)**:** 10 – block of terrigenous rocks**,** 11 – dikes, 12 – moraines**,** 13 – proluvial and lahar deposits, 14 – modern glaciers, 15 – collapse crater rim, 16- reconstructed Old Shiveluch vents (1 – Central, 2 – Western, 3 – Baidarny, 4 – Southern) 17 – crater of 1964 eruption, 18 - boundary of 1964 eruption deposits.
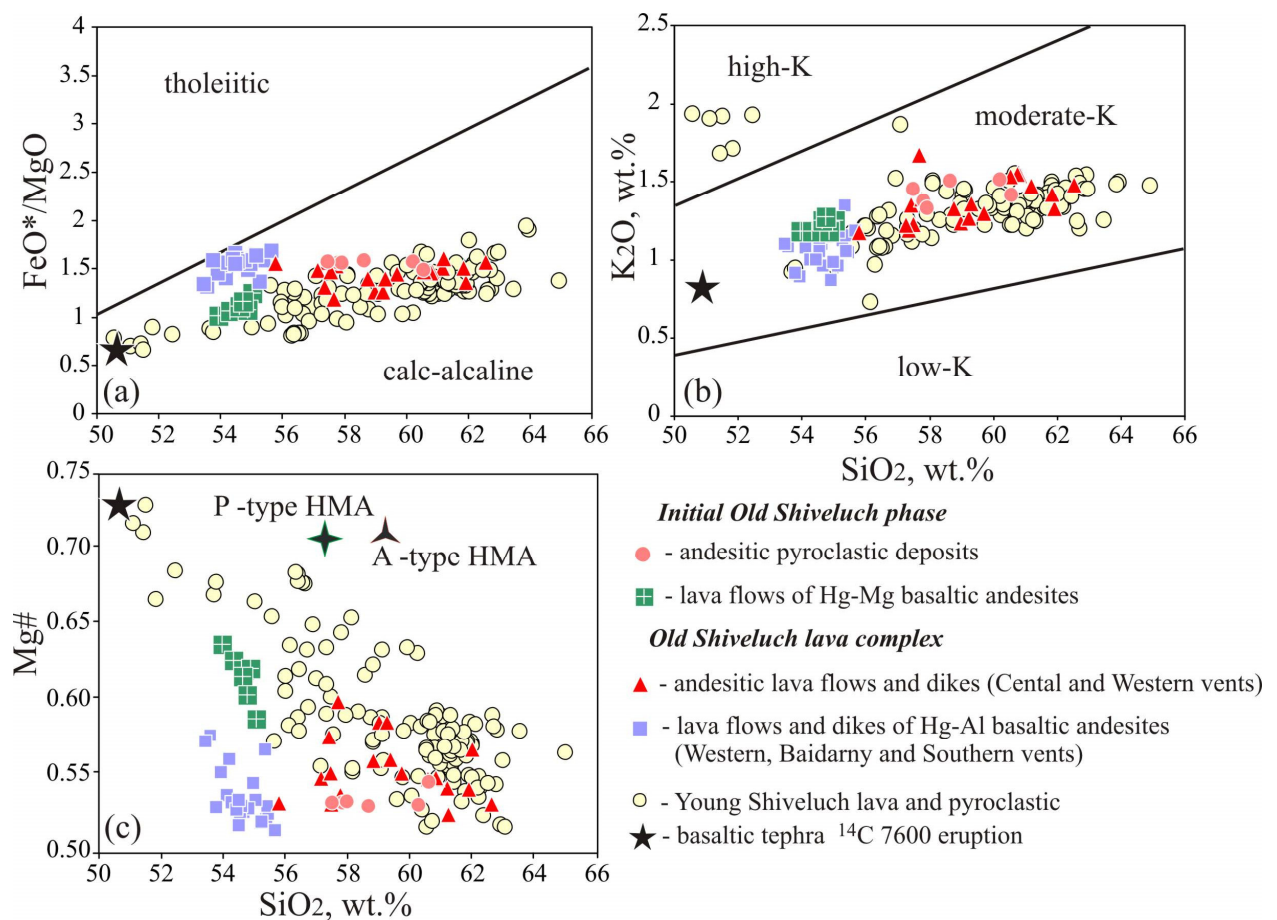
Fig. 1.1.2.4.5. Composition of Old Shiveluch rocks in SiO_2 – FeO^*/MgO (a), SiO_2–K_2O (b) and SiO_2–Mg# (c) diagrams. The compositions of Young Shiveluch lavas and pyroclastics (Volynets et al., 1997; Ponomareva et al., 2007 and Gorbach and Portnyagin, 2011), A- and P-type primitive high-magnesian andesites (Yogodzinski et al., 1994; 1998) are shown for comparison.

Gorbach, N., Portnyagin, M., & Tembrel, I. (2013). Volcanic structure and composition of Old Shiveluch volcano, Kamchatka. Journal of Volcanology and Geothermal Research, 263, 193-208. Doi: http://dx.doi.org/10.1016/j.jvolgeores.2012.12.012

Gorbach N. V., & Portnyagin M. V. Evolution of the Late Pleistocene Old Shiveluch Volcano, Kamchatka // 2nd Bilateral Workshop of KALMAR- Phase I: Kurile-Kamchatka and the Aleutian Marginal Sea-Island Arc Systems, Trier, Germany. May 16-20, 2011. P. 58-59.

Gorbach N. V., & Portnyagin M. V. (2011). Geochemistry and mineralogy of the Late Pleistocene Old Shiveluch volcano, Kamchatka. 7th Biannual Workshop on Japan-Kamchatka-Alaska Subduction Processes: Mitigating Risk Through International Volcano, Earthquake, and Tsunami Science. JKASP-2011. Petropavlovsk-Kamchatsky, Russia. August 25-30, 2011. Abstracts. – Petropavlovsk-Kamchatsky: Institute of Volcanology and Seismology FEB RAS, Kamchatkan Branch of Geophysical Service RAS, 260-261, http://www.kscnet.ru/ivs/slsecret/jkasp_2011/abstr/jkasp_2011.htm.

Sr-Nd isotopic composition of Shiveluch volcanic massif (Kamchatka)

Several hypothesis have been proposed regarding to the origin of Shiveluch magmas: 1) slab melting (Yogodzinski et al., 2001; Churikova et al., 2001; Münker et al., 2004); 2) two subducted slabs beneath Shiveluch which are responsible for variable magma compositions (Ferlito, 2011); 3) a highly depleted harzburgitic mantle source (Volynets et al., 1999); 4) low temperature mantle melting and large contribution from pyroxenite sources (Portnyagin et al., 2007; Portnyagin and Manea, 2008; Portnyagin et al., 2009; Nikulin et al., 2012). Melekestsev et al. (1991) proposed an extensive interaction of magmas with the lower crust. Published Sr-Nd

45

isotope data were obtained for Holocene Shiveluch rocks so far (Ivanov, 2008; Volynets et al., 2000, Churikova et al., 2001). Here we report new isotope data for rocks representing all major Shiveluch units and spanning age interval from the initial Late Pleistocene to historic eruptions.

The Old and Young Shiveluch rock have Sr and Nd isotopic compositions which are typical for the Quaternary volcanic rocks of Kamchatka and overlap data for three volcanic zones of Kamchatka (Fig. 1.1.2.4.6a). $^{87}Sr/^{86}Sr$ isotope ratios vary from 0.703215 to 0.703676. $^{143}Nd/^{144}Nd$ range from 0.513123 to 0.513045 (εNd = 9.5-7.9) and correlate negatively with Sr isotope ratios. Compared with Klyuchevskoi and Bezymianny, Shiveluch rocks have lower $^{87}Sr/^{86}Sr$ but similar $^{143}Nd/^{144}Nd$. The similar range of isotope compositions of Old and Young Shiveluch rocks suggests that these rocks originate from a common source, not from two distinct sources for Old and Young Shiveluch magmas (Ferlito, 2011). The difference in major element composition of the Old and Young Shiveluch magmas is likely related to different crystallization histories and increased role of magma mixing on the most recent stage of Shiveluch activity (Gorbach et al., 2013). With exception of high-K basalts erupted 3600 ^{14}C BP, Sr isotope ratios correlate with major elements in Shiveluch rocks and increase with increasing SiO_2 (Fig. 1.1.2.4.6b). All Shiveluch rocks, including high -K basalts, exhibit a strong positive correlation between $^{87}Sr/^{86}Sr$ and K_2O (Fig. 1.1.2.4.6c), Th/La (Fig. 1.1.2.4.6d), Th/Ta and La/Sm.
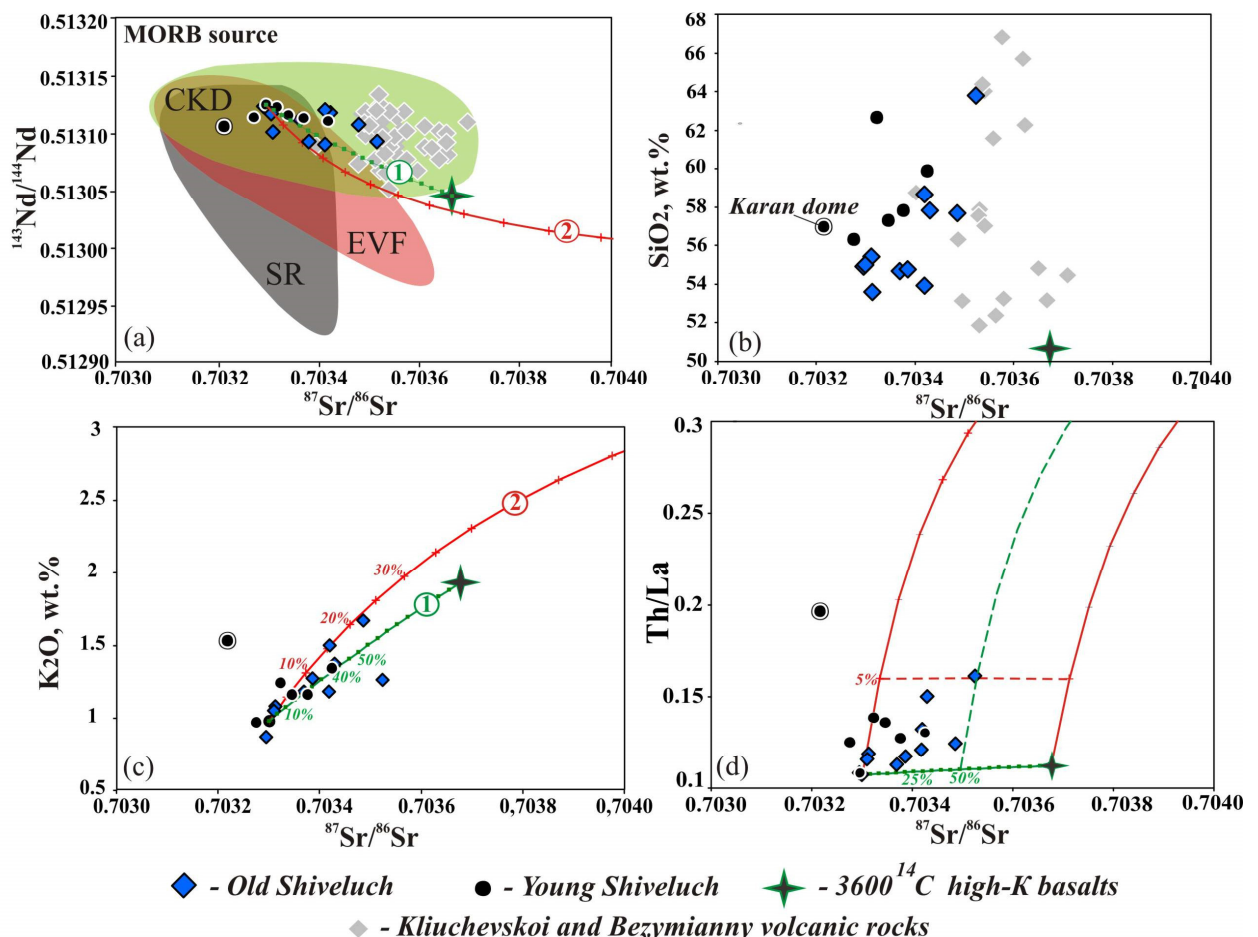
Fig. 1.1.2.4.6. Sr-Nd isotope systematics (a) and variations of $^{87}Sr/^{86}Sr$ vs. SiO_2, K_2O and Th/La (b-d) in Shiveluch rocks. Fields of Sredinny Range (SR), Eastern Volcanic Front (EVF); Central Kamchatka Depression (CKD) are shown after Churikova et al., (2001). On fig. (c) и (d) possible trends of amphibole-mica schists assimilation and mixing with mantle-derived high-K basalts are shown. The amphibole-mica schists composition are after Tararin et al. (2007; 2010).

The variability of Sr and Nd isotope ratios can reflect heterogeneous mantle source and/or crustal assimilation. In order to evaluate the potential effects of heterogeneous mantle source we calculated a mixing trend of the high-$^{143}Nd/^{144}Nd$ and low-$^{87}Sr/^{86}Sr$ Shiveluch basalts as depleted

end-member and 3600 ^{14}C BP high-K basalts as end-member derived from enriched mantle source (Portnyagin et al., 2007). To simulate crustal assimilation, amphibole-mica schists of Khavyvenskaya Rise were chosen as possible assimilant. Although the crust composition under Shiveluch is unknown, Khavyvenskaya Rise amphibole-mica schists can be present in the basement of the Central Kamchatka depression and, in particular, under the western sector of Shiveluch (e.g. Avdeiko et al., 2001). The amphibole-mica schists have ^{87}Sr/^{86}Sr= 0.70727, ^{143}Nd/^{144}Nd=0.512968, K_2O=4.3 wt. %, Th/La= 0.46 (Tararin et al., 2007; 2010).

The results of our modeling are shown in Fig. 1.1.2.4.6. Variations in Sr-Nd isotopic ratios and K_2O contents in Shiveluch rocks can be well explained by either mixing with high-K 3600 ^{14}C end-member or by assimilation of crustal rocks (trend 1 and 2 in Fig. 1.1.2.4.6a, c). The systematics of ^{87}Sr/^{86}Sr and Th/La ratios allows discriminating the effects of magma mixing and assimilation. This model suggests that both mixing with high-K basalts (up to 50 %) and crustal assimilation (less than 5 %) could contribute to the geochemical and isotopic variations of Shiveluch magma. Assimilation of about 2% of rocks is suggested for the Karan dome andesites, whose composition differs from typical Shiveluch compositions (Fig. 1.1.2.4.6a-d).

Gorbach N.V., Portnyagiv M.V., Hauff F. Sr-Nd composition of Shiveluch volcanic massif, Kamchatka. 8-th Biennial Workshop on Japan-Kamchatka-Alaska Subduction Processes (JKASP-2014): Finding clues for science and disaster mitigation from International collaboration. Sapporo, Japan, 22-26 September 2014. http://hkdrcep.sci.hokudai.ac.jp/map/jkasp2014/pdf/R26.pdf

1.1.3. Geophysical investigations of the Klyuchevskaya Group of volcanoes

1.1.3.1. The Peripheral Magma Chamber of Plosky Tolbachik

Fedotov S.A., karetn@list.ru. *Institute of Volcanology and Seismology, Far East Division, Russian Academy of Sciences, Petropavlovsk-Kamchatsky, Russia. Shmidt Institute of Physics of Earth, Russian Academy of Sciences, Moscow, Russia*
Utkin I.S., Utkina L.I., isutliut@mail.ru**,** *Shmidt Institute of Physics of the Earth, Russian Academy of Sciences, Moscow, Russia*

The Klyuchevskoy group of volcanoes (KGV) in Kamchatka is the most powerful existing island arc and subduction zone volcanic center. The Holocene volcanic activity in the southern part of the KGV is concentrated in a large basaltic volcano, Plosky Tolbachik (PT), altitude 3085 m and in its Tolbachik zone of cinder cones (TZ), length 70 km, which are similar to Hawaiian-type volcanoes and their rifts. A variety of different basalt types are erupted at a rate of 18×10^6 t/yr.

This research provides information on the PT peripheral magma chamber obtained by several independent methods. We used data on the evolution, eruptions, magma discharge, deformation, and earthquakes in the PT and TZ, as well as calculations that give the size of the PT flow-through magma chamber. The use of seismological and geodetic data places the chamber under the PT summit caldera, gives its transverse size as below 6 km, and the top of the chamber at a depth of 2 km. Our calculations give 4.9–5.8 km for the transverse chamber dimension, 3.2–3.9 km for its vertical dimension, 40–70 km^3 for chamber volume, and about 4 km for the depth of chamber center.

The information we provide makes the properties of this source of PT and TZ alumina-rich basalts clear, as well as those of the entire KGV complex plumbing system.

The Plosky Tolbachik (PT) basaltic volcano along with the Tolbachik zone of cinder cones (TZ) is and outstanding object of volcanological research and a major natural feature in the powerful Klyuchevskoy Group of Volcanoes (KGV) in Kamchatka. This is the third (by the

discharge of ejecta) volcanic center at the Kuril–Kamchatka arc and the one that shows the greatest similarity to Hawaiian-type volcanoes among the 70 active volcanoes at the arc.
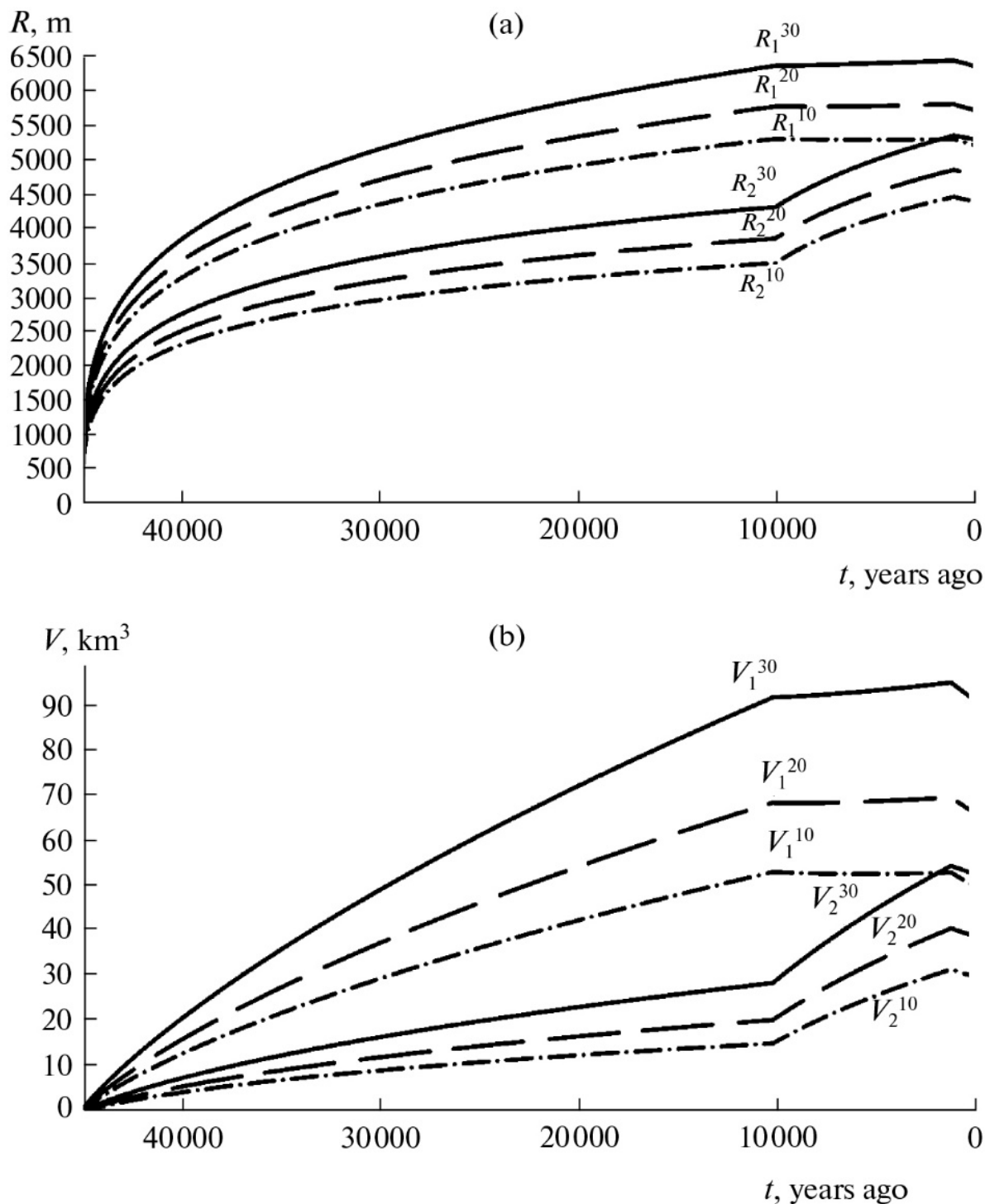
Fig. 1.1.3.1.1. Theoretical functions $R_1(t)$ and $R_2(t)$ for the length of the chamber's horizontal axis (a) in relation to time, $V_1(t)$ and $V_2(t)$ are chamber volumes of Plosky Tolbachik (b), the chamber having the shape of an ellipsoid with a vertical axis of revolution, since chamber origin (45000 years ago) until now. The vertical bar marks the present time. Continuous lines show the functions R_1^{30}, R_2^{30}, V_1^{30}, and V_2^{30}, 0 that were calculated assuming 30% (in weight) of the magma in the chamber being crystallized. Dashed lines show the functions R_1^{20}, R_2^{20}, V_1^{20}, and V_2^{20}, calculated by assuming 20% of the magma volume to be crystallized. Dashed-dotted lines show the functions R_1^{10}, R_2^{10}, V_1^{10}, V_2^{10} assuming that 10% of the magma volume is crystallized.

48

The paper make reference to numerous works that give accounts of multiyear comprehensive research of the KGV, PT, and TZ conducted using the methods of volcanology, seismology, geodesy, geophysics, petrology, geochemistry, and other disciplines. This research provide data obtained by volcanology, geodesy, and seismology concerning the properties of the PT and TZ and calculations for the PT peripheral magma chamber. The whole is a sequel to studies in the powerful and complex magmatic plumbing system for the KGV and in its geophysical model.

We obtained similar independent estimates for the location and dimensions of the PT peripheral magma chamber: it lies beneath the PT collapsed summit caldera, the top of the chamber is at a depth of 2 km, the transverse dimension of the chamber is 4.9–5.8 km, the vertical dimension is 3.2–3.9 km, the volume is 40–70 km^3, and the center of the chamber is at a depth of about 4 km (Fig. 1.1.3.1.1). The Great Tolbachik Fissure Eruption of 1975–76 (GTFE) caused 0.45 km^3 of alumina-rich basalts to be removed from the chamber. The above information will be useful for attacking the following problems.

There is scant information on the rise of deep mantle magmas toward the PT peripheral chamber. It is still unclear why the 1939–1941 eruption of alumina-rich basalts at the PT summit terminated in a breakthrough of deep-seated magnesian basalts in May 1941, while an opposite sequence of types of erupting basalts was observed during the GTFE.

There has been little research on pressure changes in the extensive and complex magmatic plumbing system for the KGV, which occurred after the PT summit caldera subsided by 200 m during the GTFE, to name one among other unresolved questions.

These questions can be part of further basic research on the KGV, its magmatic plumbing system, and the properties of magma chambers beneath volcanoes.

Fedotov, S. A., Utkin, I. S., & Utkina, L. I. (2011). The peripheral magma chamber of Ploskii Tolbachik, a Kamchatka basaltic volcano: Activity, location and depth, dimensions, and their changes based on magma discharge observations. Journal of Volcanology and Seismology, 5(6), 369-385. Doi: 10.1134/S0742046311060042

1.1.3.2. The movement of the magmas below Klyuchevskaya Group of volcanoes

Fedotov S.A., karetn@list.ru, *Institute of Volcanology and Seismology, Far East Division, Russian Academy of Sciences, Petropavlovsk-Kamchatsky, Russia. Schmidt Institute of Physics of Earth, Russian Academy of Sciences, Moscow, Russia*
Slavina L.B., Kuchay M.S., *Schmidt Institute of Physics of the Earth, Russian Academy of Sciences, Moscow, Russia*
Senyukov S.L., *Kamchatka Branch of Geophysical Service, Russian Academy of Sciences, Petropavlovsk-Kamchatsky, Russia*

Seismic and volcanic processes in the Northern group of volcanoes (NGV) of Kamchatka 2012–2013 accompanying the Tolbachik fissure eruption (TFE, lately called «50 years of IVS») and the Great Tolbachik fissure eruptions (GTFE) of 1975–1976, and also seismic activity during the period between these two large basalt eruptions in 1977–2012 are considered. Features of development of seismic processes, similarity and differences in behavior of seismicity of the main volcanoes of NGV – Plosky Tolbachik, Klyuchevskoy, Bezymianny and Shiveluch – are revealed. Features of distribution of earthquakes on depth, their migration in space and time in the NGV area connections of seismic and volcanic activity in NGV are considered. The description of the main features of seismic activity during preparation and development of GTFE of 1975–1976, development of swarms of the earthquakes preceding emergence of its Northern and Southern breaks is provided. Features of seismic activity during the long period between GTFE and TFE eruptions are studied. The description of the main features of development of the seismic activity

preceding and accompanying TFE in 2012–2013 is given. As a result of the conducted researches the main sources and channels of a magmatic feeding of volcanoes of NGV are revealed. It is shown that there is the main feeding channel in the mantle and the general intermediate magma center for all NGV. Depth of its location according to seismic data is 25–35 km. Ways-channels of magma outflow rise from this general intermediate center to active volcanoes Klyuchevskoy, Tolbachik, Bezymianny and Shiveluch. Existence of a layer of neutral buoyancy at depths 15–20 km under all NGV and existence of a source of an areal volcanism of magnesian basalts at North-East from the Klyuchevskoy volcano at depths ~ 20 km are shown. These data partially confirm the geophysical model of magmatic feeding system of Klyuchevskoy group of volcanoes constructed earlier in 2010. The presented data cover wider area of all NGV and are based on new observations (Fig. 1.1.3.2.1).
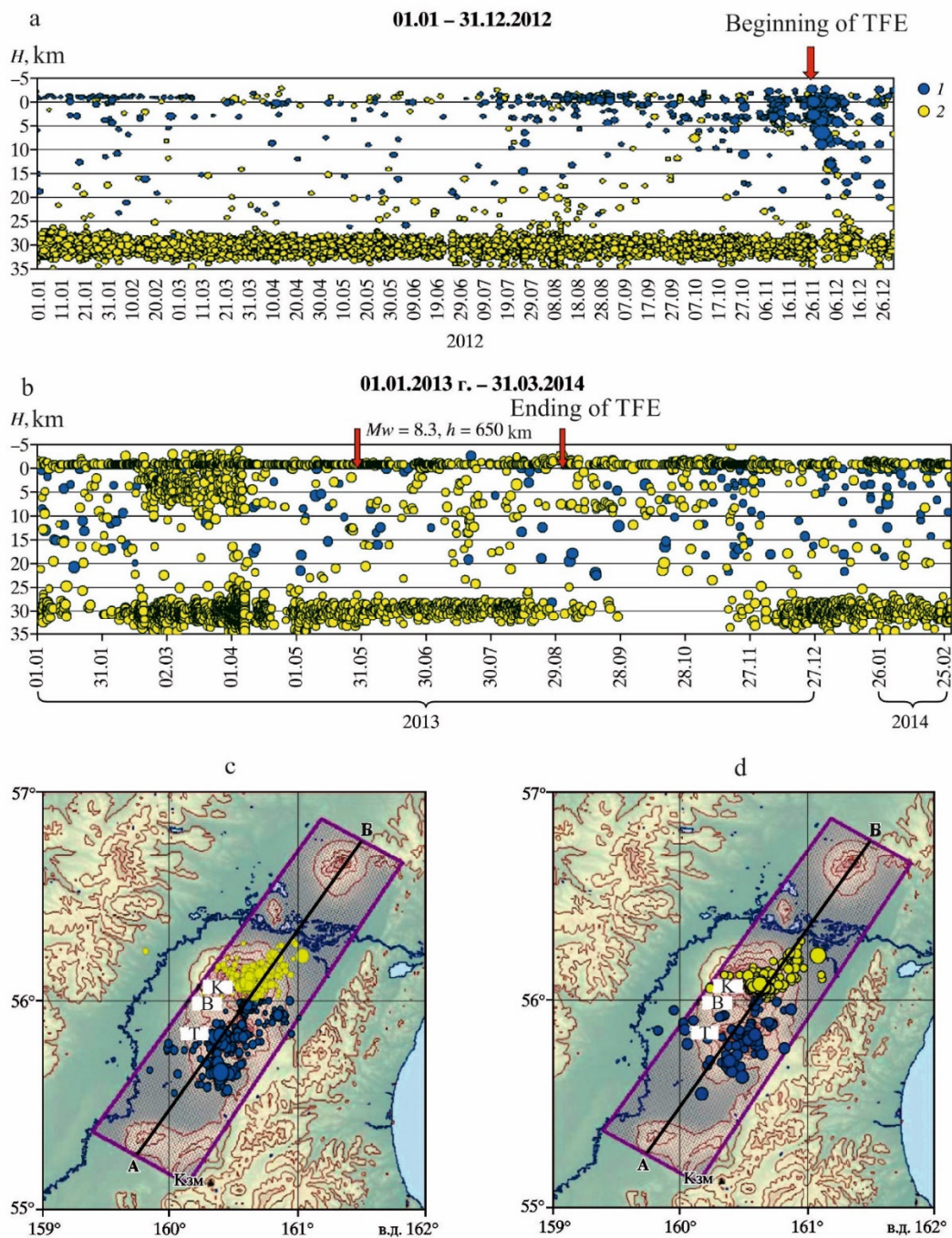
Fig. 1.1.3.2.1. The distribution of the seismic events in time and depth at NGV before and in the beginning of TFE 01.01–31.12.2012 (a) and during the eruption and the ending of TFE 01.01.2013 г. – 31.03.2014

(b) and related maps of the locations of the epicenters of earthquakes (*c*, *d*). *1* – the earthquakes of TFE in the area of the Plosky Tolbachik volcano; *2* – the earthquakes in the area of Klyuchevskoy volcano. K – Klyuchevskoy volcano, B – Bezymianny volcano, T – Tolbachik volcano. AB - line crossing from the southwest to the northeast the rectangle bounding the locality of the volcanoes.

Fedotov S. A., Slavina L. B., Senyukov S. L., & Kuchay M. S. (2014). Seismic processes and movement of the magmas, occurring at the Great Tolbachik fissure eruption 1975-1976 and the Tolbachik fissure eruption 2012-2013 (Kamchatka). Geofizicheskie process i biocfera, 13(3), 3-30. (In Russian). http://gpb.ifz.ru/fileadmin/user_upload/documents/journals/gpb/13-3/01_2014_N3_rus.pdf

1.1.4. Geochronology of the Klyuchevskaya Group of volcanoes

1.1.4.1.   Eruption 10,200 cal BP at Ploskie Sopky massif

Ponomareva V., vera.ponomareva1@gmail.com, *Institute of Volcanology and Seismology, Far East Division, Russian Academy of Sciences, Petropavlovsk-Kamchatsky, Russia*
Portnyagin M., mportnyagin@ifm-geomar.de**,** *Helmholtz-Zentrum für Ozeanforschung Kiel (GEOMAR), Kiel, Germany. V.I. Vernadsky Institute of Geochemistry and Analytical Chemistry, Moscow, Russia*
Nürnberg D., *Helmholtz-Zentrum für Ozeanforschung Kiel (GEOMAR), Kiel, Germany*
Krasheninnikov S., *V.I. Vernadsky Institute of Geochemistry and Analytical Chemistry, Moscow, Russia*
Derkachev A., *V.I.Il'ichev Pacific Oceanological Institute, Vladivostok, Russia*
Pendea I.F., *Department of Interdisciplinary Studies, Lakehead University, Orillia, ON, Canada*
Bourgeois J., *Department of Earth and Space Sciences, University of Washington, Seattle, WA, USA*
Reimer P. J., *School of Geography, Archaeology and Palaeoecology, Queen's University Belfast, Belfast, Northern Ireland, UK*
Garbe-Schönberg D., *Institute of Geoscience, Christian-Albrechts-University of Kiel, Kiel, Germany*

We report tephrochronological and geochemical data on early Holocene activity from Plosky volcanic massif in the Kliuchevskoi volcanic group (Fig. 1.1.4.1.1), Kamchatka Peninsula. Explosive activity of this volcano lasted for ~1.5 kyr, produced a series of widely dispersed tephra layers, and was followed by profuse low-viscosity lava flows. This eruptive episode started a major reorganization of the volcanic structures in the western part of the Kliuchevskoi volcanic group. An explosive eruption from Plosky (M~6), previously unstudied, produced tephra (coded PL2) of a volume of 10-12 km^3 (11-13 Gt), being one of the largest Holocene explosive eruptions in Kamchatka. Characteristic diagnostic features of the PL2 tephra are predominantly vitric sponge-shaped fragments with rare phenocrysts and microlites of plagioclase, olivine and pyroxenes, medium- to high-K basaltic andesitic bulk composition, high-K, high-Al and high-P trachyandesitic glass composition with SiO_2 = 57.5-59.5 wt%, K_2O = 2.3-2.7 wt%, Al_2O_3=15.8-16.5 wt%, and P_2O_5= 0.5-0.7 wt%. Other diagnostic features include a typical subduction-related pattern of incompatible elements, high concentrations of all REE (>10x mantle values), moderate enrichment in LREE (La/Yb~5.3), and non-fractionated mantle-like pattern of LILE.
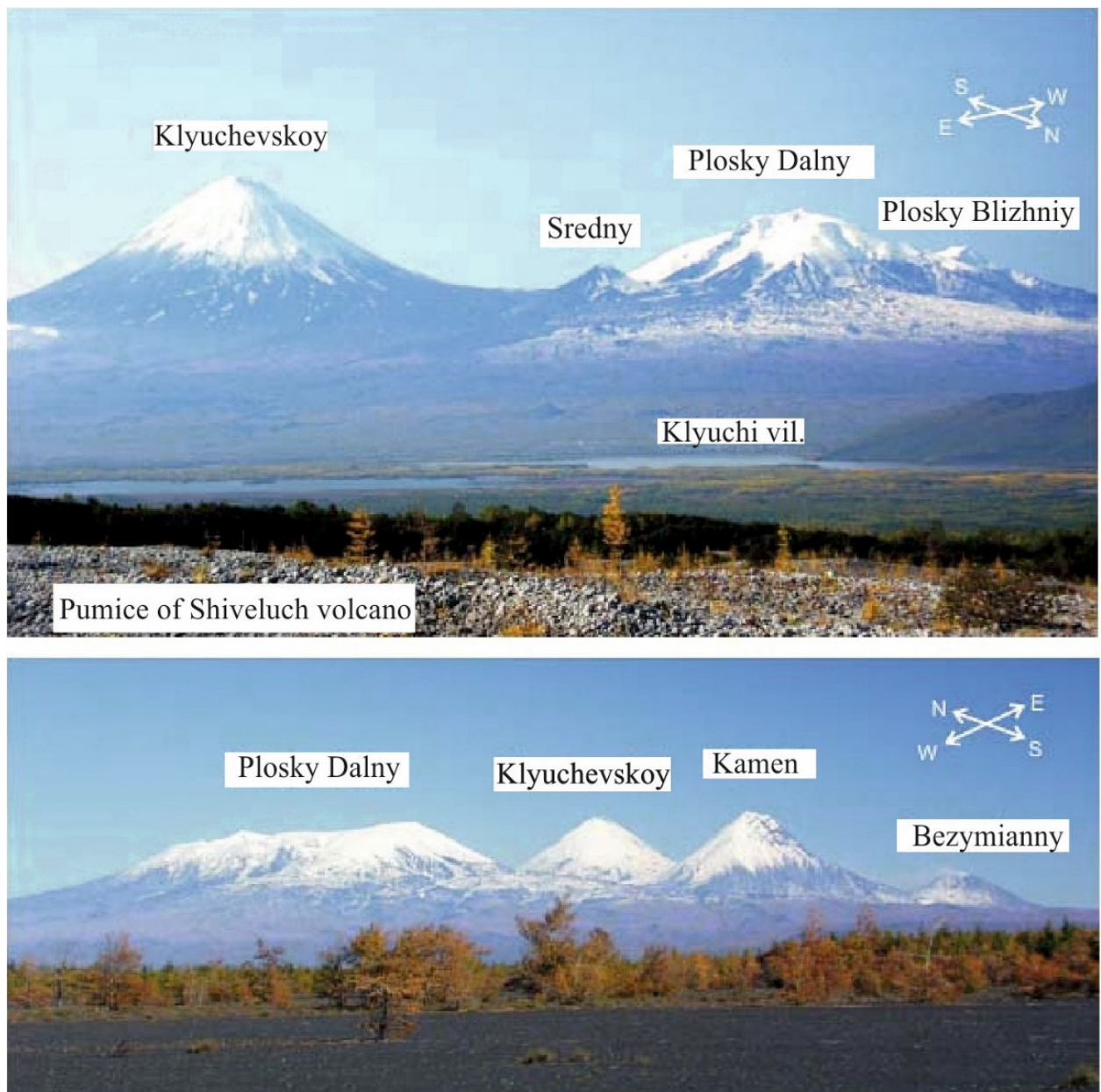
Fig. 1.1.4.1.1. Panorama photos of the Kliuchevskoi volcanic group including the Plosky volcanic massif, the latter made up by Ushkovsky (Plosky Dalny) and Krestovsky (Plosky Blizhniy) volcanoes. Upper photo view southward from the slope of Shiveluch volcano; lower photo view eastward from along the Kamchatka River valley. Photos by Philip Kyle.

Geochemical fingerprinting of the PL2 tephra with the help of EMP and LA-ICP-MS analyses allowed us to map its occurrence in terrestrial sections across Kamchatka and to identify this layer in Bering Sea sediment cores at a distance of >600 km from the source (Fig. 1.1.4.1.2). New high-precision ^{14}C dates suggest that the PL2 eruption occurred ~10,200 cal BP, which makes it a valuable isochrone for early Holocene climate fluctuations and permits direct links between terrestrial and marine paleoenvironmental records. The terrestrial and marine ^{14}C dates related to the PL2 tephra have allowed us to estimate an early Holocene reservoir age for the western Bering Sea at 1410±64 ^{14}C yrs. Another important tephra from the Early Holocene eruptive episode of Plosky volcano, coded PL1, was dated at 11,650 cal BP. This marker is the oldest geochemically characterized and dated tephra marker layer in Kamchatka to date, and is an important local marker for the Younger Dryas - early Holocene transition. One more tephra from Plosky, coded PL3, can be used as a marker northeast of the source at a distance of ~110 km.
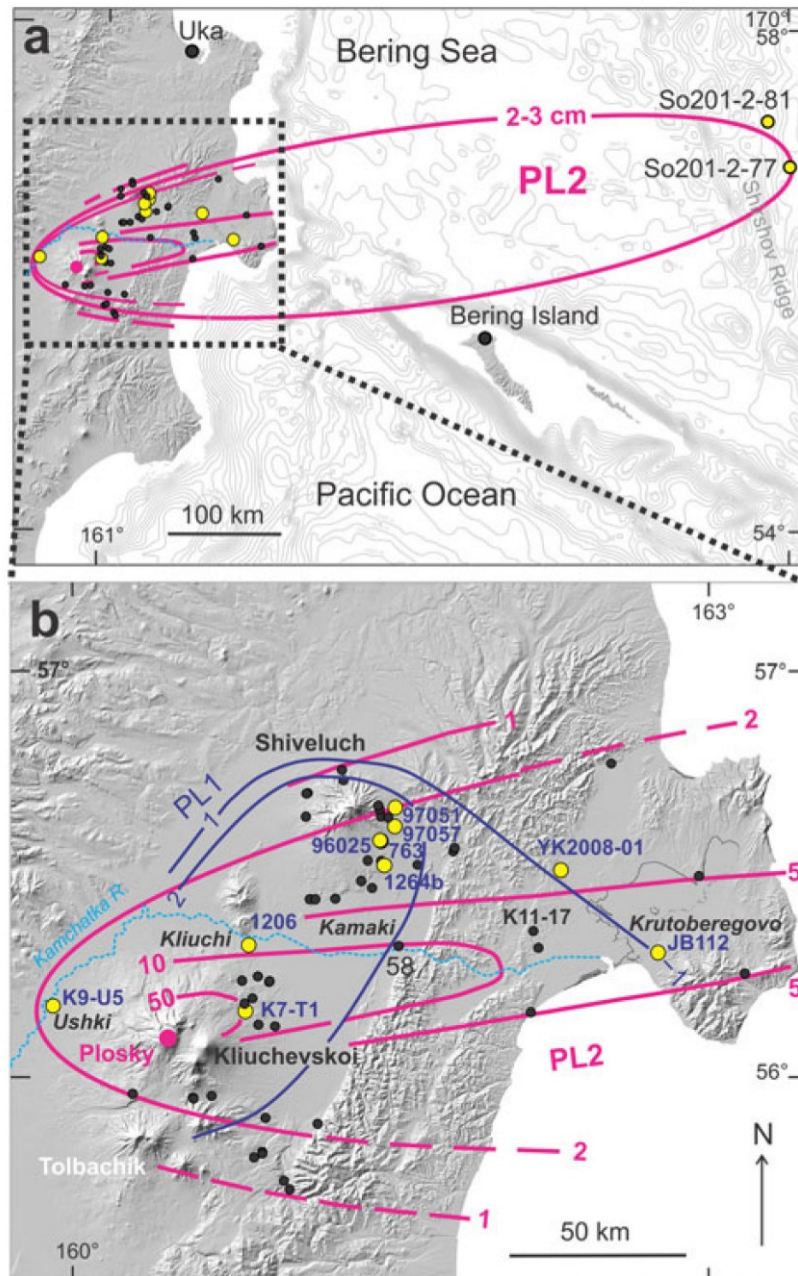
Fig. 1.1.4.1.2. Maps of dispersal of Plosky tephras. (a) Approximate position of a 2.5 cm isopach for PL2 tephra. Sites at Uka and on Bering Island are peat sections where no Plosky tephra has been found. (b) Enlarged inset from a showing isopach lines for PL2 (magenta) and PL1 (darkpurple); thickness in cm.

Ponomareva, V., Portnyagin, M., Derkachev, A., Pendea, I. F., Bourgeois, J., Reimer P. J., Garbe-Schönberg D., Krasheninnikov S., & Nürnberg D. (2013). Early Holocene M~6 explosive eruption from Plosky volcanic massif (Kamchatka) and its tephra as a link between terrestrial and marine paleoenvironmental records. International Journal of Earth Sciences, 102(6), 1673-1699. Doi: 10.1007/s00531-013-0898-0

1.1.4.2. Chronology of explosive eruptions of the Shiveluch volcano

Ponomareva V., vera.ponomareva1@gmail.com, *Institute of Volcanology and Seismology, Far East Division, Russian Academy of Sciences, Petropavlovsk-Kamchatsky, Russia*

Portnyagin M., mportnyagin@ifm-geomar.de**,** *Helmholtz-Zentrum für Ozeanforschung Kiel (GEOMAR), Kiel, Germany. V.I. Vernadsky Institute of Geochemistry and Analytical Chemistry, Moscow, Russia*

Nürnberg D., *Helmholtz-Zentrum für Ozeanforschung Kiel (GEOMAR), Kiel, Germany, V.I. Vernadsky Institute of Geochemistry and Analytical Chemistry, Moscow, Russia*

Derkachev A., *V.I.Il'ichev Pacific Oceanological Institute, Vladivostok, Russia*

Pevzner M., m_pevzner@mail.ru**,** *Geological Institute, Moscow, Russia*

Blaauw M., *School of Geography, Archaeology and Palaeoecology, Queen's University Belfast, Belfast, UK*

Kyle P. *Department of Earth and Environmental Science, New Mexico Institute of Mining and Technology, Socorro, NM, USA*

The ~16 ka long record of explosive eruptions from Shiveluch volcano (Kamchatka, NW Pacific) is refined using geochemical fingerprinting of tephra and radiocarbon ages. Volcanic glass from 88 prominent eruptions was analyzed by electron microprobe (Fig. 1.1.4.2.1). Eruption ages were estimated using 113 radiocarbon dates for proximal tephra sequence. These radiocarbon dates were combined with 76 dates for regional Kamchatka marker tephra layers into a single Bayesian framework taking into account the stratigraphic ordering within and between the sites. As a result, we report ~1700 high-quality glass analyses from 88 Shiveluch eruptions of known age. These define the magmatic evolution of the volcano and provide a reference for correlations with distal fall deposits. Shiveluch tephras represent two major types of magmas which have been feeding the volcano during the Late Glacial-Holocene time: Baidarny basaltic andesites and Young Shiveluch andesites. Baidarny tephras erupted mostly during the Late Glacial time (~16 - 12.8 ka BP) but persisted into the Holocene as subordinate admixture to the prevailing Young Shiveluch andesitic tephras (~12.7 ka BP - present). Baidarny basaltic andesite tephras have trachyandesite and trachydacite (SiO_2<71.5 wt. %) glasses. The Young Shiveluch andesite tephras have rhyolitic glasses (SiO_2>71.5 wt. %). Strongly calc-alkaline medium-K characteristics of Shiveluch volcanic glasses along with moderate Cl, CaO and low P_2O_5 contents permit reliable discrimination of Shiveluch tephras from the majority of other large Holocene tephras of Kamchatka. The Young Shiveluch glasses exhibit wave-like variations in SiO_2 contents through time that may reflect alternating periods of high and low frequency/volume of mafic magmas supply to deep magma reservoirs beneath the volcano. The compositional variability of Shiveluch glass allows geochemical fingerprinting of individual Shiveluch tephra layers which along with age estimates facilitates their use as a dating tool in paleovolcanological, paleoseismological, paleoenvironmental, and archaeological studies. Electronic tables accompanying this work offer a tool for statistical correlation of unknown tephras with proximal Shiveluch units taking into account sectors of actual tephra dispersal, eruption size and expected age. Several examples illustrate the effectiveness of the new database. The data are used to assign a few previously enigmatic wide-spread tephras to particular Shiveluch eruptions. Our finding of Shiveluch tephras in sediment cores in the Bering Sea at a distance of ~600 km from the source permits re-assessment of the maximum dispersal distances for Shiveluch tephras and provides links between terrestrial and marine paleoenvironmental records (Fig. 1.1.4.2.2).
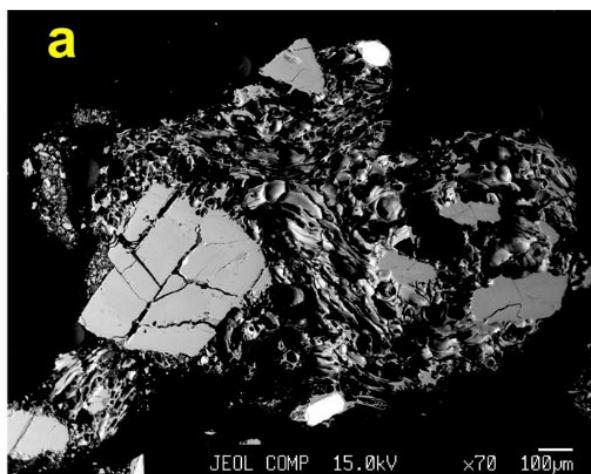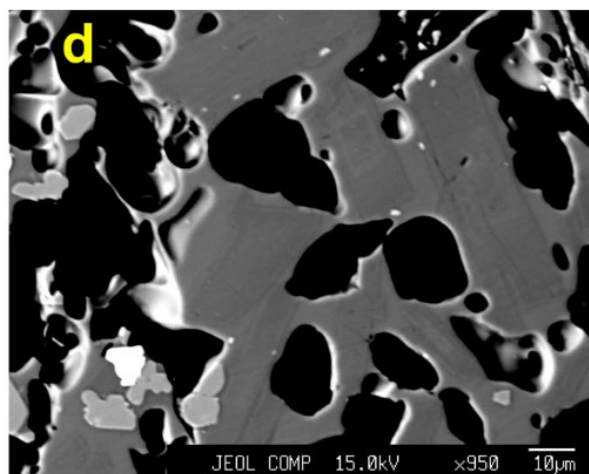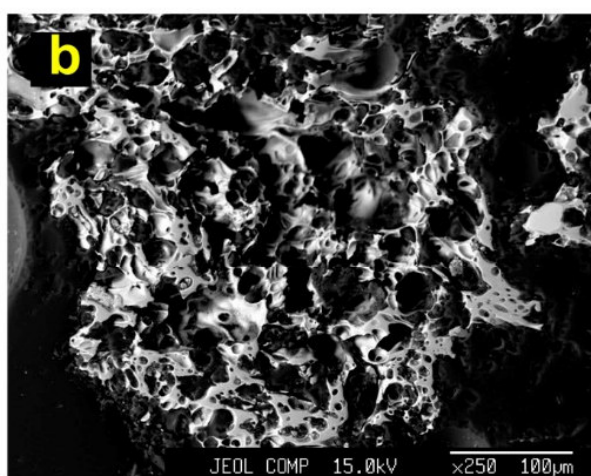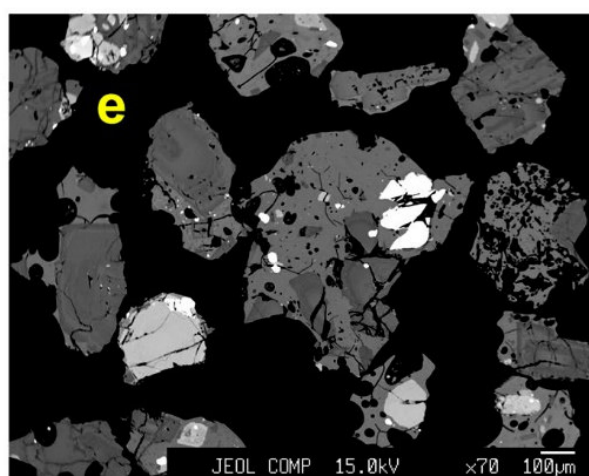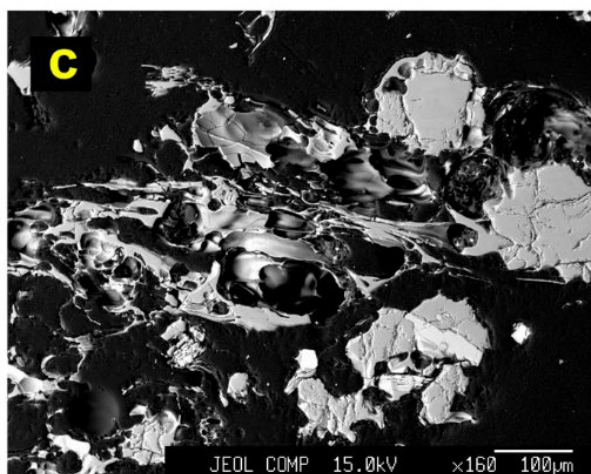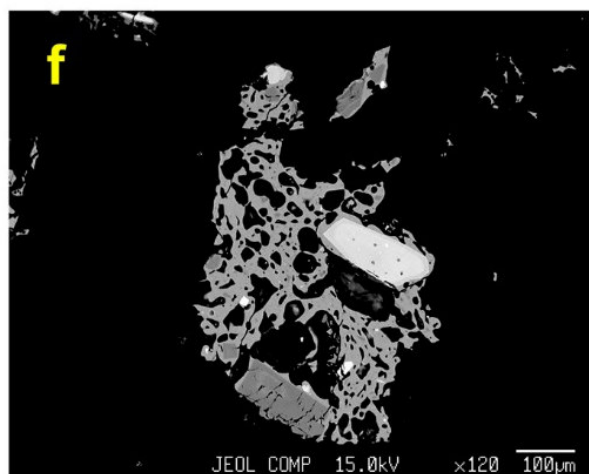
Fig. 1.1.4.2.1. Backscattered electron images of selected Shiveluch tephra. **a–c** Young Shiveluch pumiceous tephra: **a** SH1 (unit 4, sample 757-1), **b** SH2800 (unit b, sample 775-8), **c** early Holocene high-K pumice (sample 775-25); **d–f** cinders: **d** SHsp (unit 28, sample 757-20); **e** "dark package" (unit 46, sample K01-17); **f** Baidarny cinder (sample 97057-3). For stratigraphic position of the samples, see Online Resource 1.
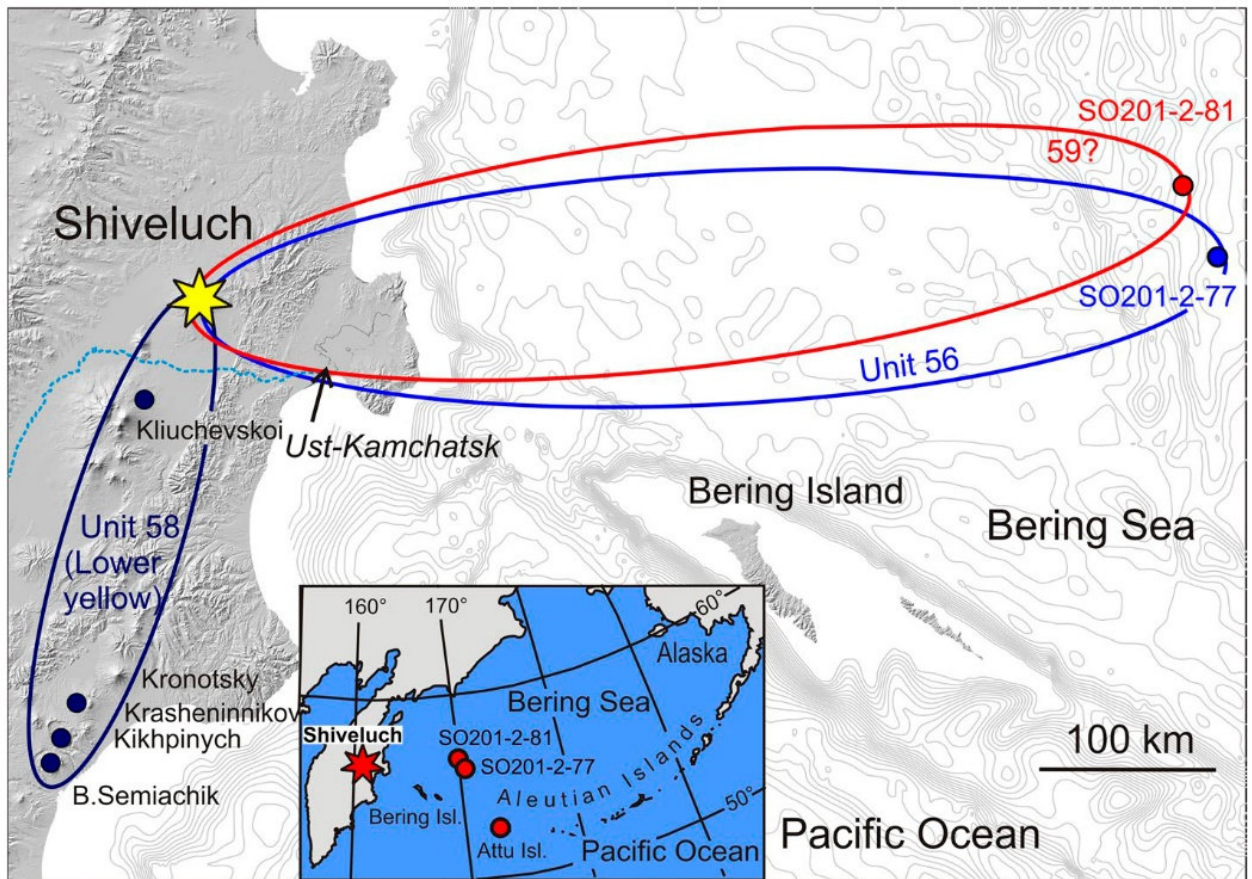
Fig. 1.1.4.2.2. Minimum dispersal of selected YSH tephras based on new correlations with distal sites. *Color circles* show locations of the analyzed distal tephra samples. *Ovals* of matching *colors* show minimum dispersal areas for tephra units 56, 59 and 58 ("*Lower yellow*"). Findings of YSH tephras in the marine cores SO201-2-81 and SO201-2-77 are the first ever findings of Shiveluch tephra in the marine sediments, which allow us to estimate the minimum dispersal of Holocene Shiveluch tephra at 560–580 km. *Inset* shows the location of Attu Island, where tephra samples attributed by Kyle et al. (2011) to Shiveluch likely come from another source

Ponomareva, V., Portnyagin, M., Pevzner, M., Blaauw, M., Kyle, P., & Derkachev, A. (2015). Tephra from andesitic Shiveluch volcano, Kamchatka, NW Pacific: chronology of explosive eruptions and geochemical fingerprinting of volcanic glass. International Journal of Earth Sciences, 1-24. Doi: 10.1007/s00531-015-1156-4
Kyle, P. R., Ponomareva, V. V., & Schluep R.R. (2011) Geochemical characterization of marker tephra layers from major Holocene eruptions in Kamchatka, Russia. International Geology Review, 53(9), 1059–1097, Doi: 10.1080/00206810903442162

1.1.5. Geological observations at the Klyuchevskaya Group of volcanoes

1.1.5.1. Aerial photogrammetric monitoring of active volcanoes and geothermal objects

Dvigalo V.N., dvig@kscnet.ru, **Melnikov D.V.,** dvm@kscnet.ru, **Melekestsev I.V.,** *Institute of Volcanology and Seismology, Far East Division, Russian Academy of Sciences, Petropavlovsk-Kamchatsky, Russia*
Shevchenko A.V., shevchenko@kscnet.ru, **Svirid I.Yu.,** svirid@kscnet.ru , *Institute of Volcanology and Seismology, Far East Division, Russian Academy of Sciences, Petropavlovsk-Kamchatsky, Russia, Petropavlovsk-Kamchatsky, Russia. Vitus Bering Kamchatka State University (KamGU), Petropavlovsk-Kamchatsky, Russia*

Aerial photogrammetric monitoring of the active volcanoes of Kamchatka has been carrying out at the Institute of Volcanology FESC USSR and the Institute of Volcanology and Seismology FEB RAS since 1973. Our team performs the entire work cycle: aerial photo survey, stereophotogrammetric processing of the photographic material, building the Digital Terrain Models and creating specialized topographic maps and plans. The photogrammetric processing of the aerial photographs provides high accuracy of the obtained qualitative and quantitative characteristics of the active volcanic objects. Using this method we can also estimate the effect of eruptions and detect their precursors. The majority of the studied objects now is too dangerous for direct observations due to high eruptive activity, therefore, the remote sensing, in particular photogrammetry, is the most appropriate way of monitoring them.

Aerial photogrammetric monitoring of the Shiveluch volcano
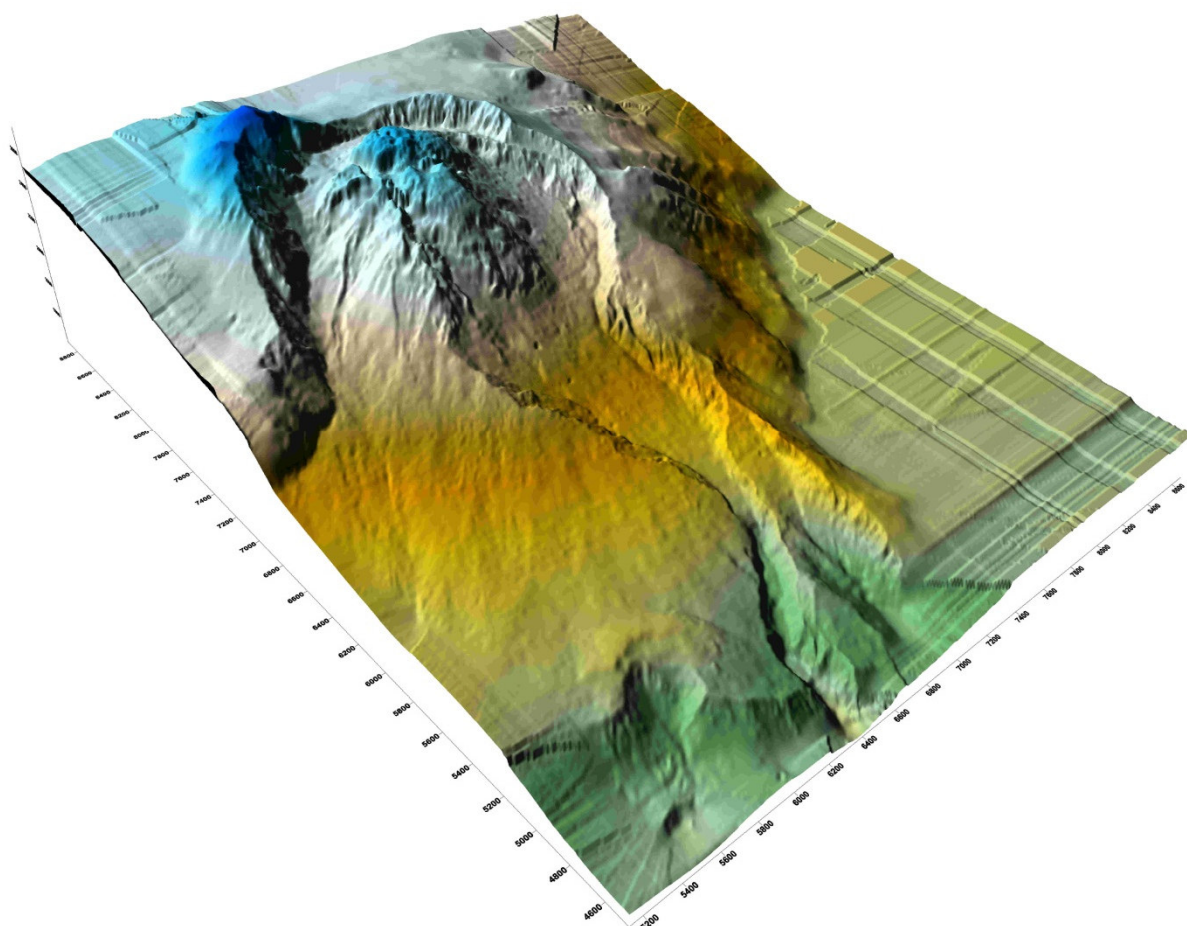
Fig. 1.1.5.1.1. Three-dimensional model of the Molodoy Shiveluch lava dome for July 12, 2012.

The detailed analysis of morphological features of the Molodoy Shiveluch Volcano lava dome showed that since 2001 the dome has grown mostly exogenously: numerous lava lobes and crease structures have been extruded at its different sectors. Using geomorphological interpretation of stereo imagery and aerial photogrammetric method we have made the morphological and volcanological descriptions of the lava dome, built Digital Terrain Models (Fig. 1.1.5.1.1) and obtained precise morphometric characteristics for the different stages of its growth. The crease structures detected at Molodoy Shiveluch were classified into three types: radial, bilaterally symmetrical and irregular. These crease structures are morphologically similar to those formed at Unzen Volcano during the 1990–1995 eruption. We supposed that the reason of change in type of

the dome growth from endogenous to predominantly exogenous may be in intensification of lava output, as well as in change of extrusive material physical properties due to increasing of SiO_2.

Also we defined that the role of gravitational processes was significant during recent period of Molodoy Shiveluch activity. Relatively loose material of exogenous lava lobes is subject to failures. Debris avalanches produce the greatest relief-forming effect in comparison with other processes at Molodoy Shiveluch. Thus one of the largest recent eruption of February 28, 2005 was triggered by partial failure of the dome (not less than 0.11 km^3 in volume). The largest partial failure (0.28 km^3) occurred on October 28, 2010, when the eruptive activity was low. Performed geomorphological analysis revealed the similarity of the 1964, 2005 and Upper Pleistocene post failure landforms.

Shevchenko, A.V. (2014). Exogenous dome growth at Molodoy Shiveluch Volcano, Kamchatka. 1st International Workshop on Volcano Geology: abstracts book. July 7-11, 2014, Madeira, Portugal, 132–136. http://www.kscnet.ru/ivs/bibl/sotrudn/zhevchenko/shevchenko_wvg2014.pdf

Shevchenko, A.V., Svirid, I.Yu., & Dvigalo, V.N. (2014). The formation of the exogenous dome at Molodoy Shiveluch Volcano. Volcanism and related processes. Annual regional scientific conference dedicated to the Volcanologist Day. Proceedings of the conference. March 27-28, 2014, Petropavlovsk-Kamchatsky. Petropavlovsk-Kamchatsky: Institute of volcanology and seismology FED RAS, 128–134. (In Russian). http://www.kscnet.ru/ivs/publication/volc_day/2014/art20.pdf

Shevchenko, A.V., & Svirid, I.Yu. (2014). Collapsing processes of the current lava dome at Molodoy Shiveluch Volcano. Natural environment of the Kamchatka. Materials XIII regional youth scientific conference, 15 April, 2014, Petropavlovsk-Kamchatsky. Petropavlovsk-Kamchatsky: Institute of volcanology and seismology FED RAS, 129-142. (In Russian). http://www.kscnet.ru/ivs/publication/young_conf/2014/1/art11.pdf

Aerial photogrammetric monitoring of the Kizimen Volcano
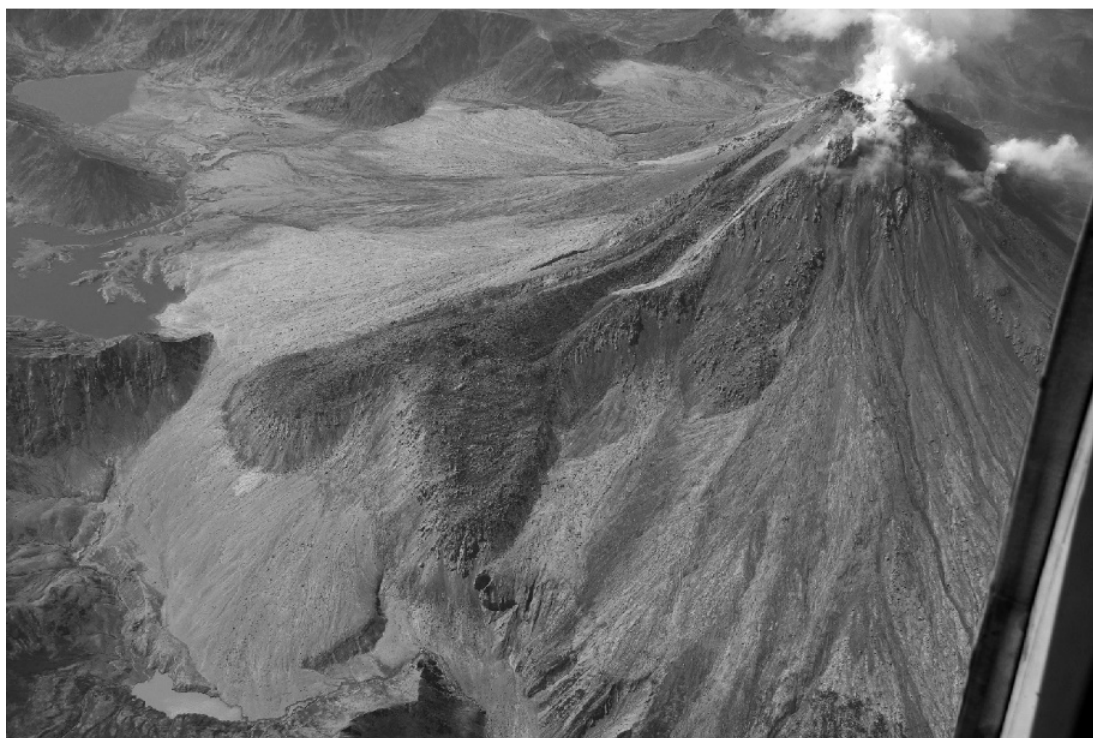
Fig. 1.1.5.1.2. 2010-12 eruption of the Kizimen volcano.

The detailed analysis of aerial photographs and space images for the Kizimen area allowed us to characterize the geologic and geomorphologic effects of the eruption over the 2010–2011 period. The total volume (>0.5 km^3) of the erupted material makes this eruption one of the most productive in Kamchatka over the past 200 years (Fig. 1.1.5.1.2).

The pyroclastics (tephra, deposits of the juvenile pyroclastic avalanches and incandescent debris avalanches) comprise >0.3 km^3. We defined the parameters of the very thick blocky lava flow: 3.052 km in length, up to 232 m in thickness, 2.163 km^2 in area, and about 0.195 km^3 in volume. With the exception of the tephra, which fell over an area of about 100000 km^2, the rest of the material was accumulated on the Kizimen cone and at its base (Fig. 1.1.5.1.3). The mean discharge rate was about 15 m^3/sec (29 t/sec) for 13 months (from November 11, 2010 to December 11, 2011).
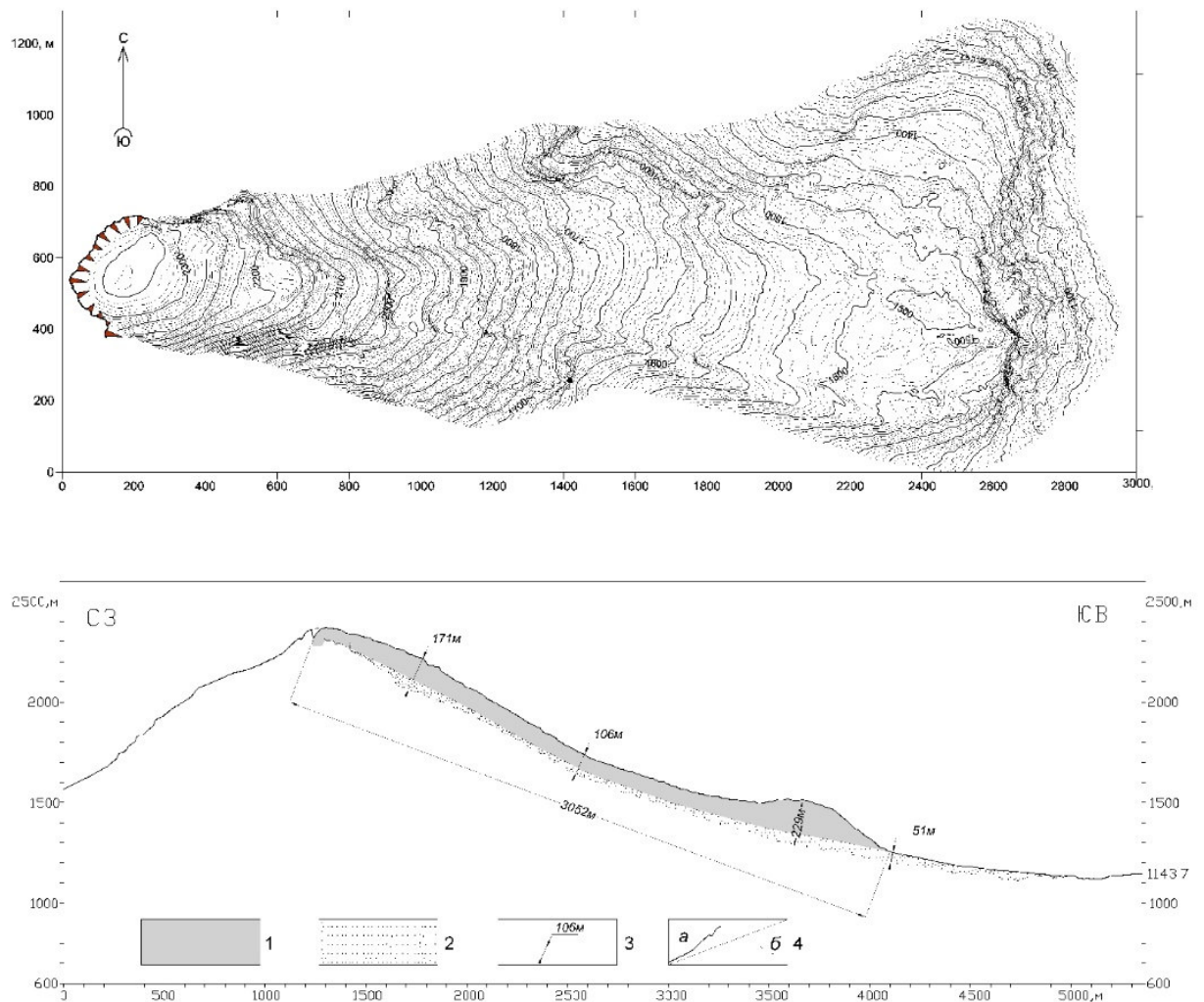
Fig. 1.1.5.1.3. The space distribution and thickness of the 2010-12 Kizimen eruption.

Dvigalo, V. N., Melekestsev, I. V., Shevchenko, A. V., & Svirid, I. Y. (2013). The 2010–2012 eruption of Kizimen Volcano: The greatest output (from the data of remote-sensing observations) for eruptions in Kamchatka in the early 21st century part I. The November 11, 2010 to December 11, 2011 phase. Journal of Volcanology and Seismology, 7(6), 345-361. Doi: 10.1134/S074204631306002X

Melnikov, D. V., Dvigalo, V. N., & Melekestsev, I. V. (2011). The 2010-2011 eruption of Kizimen volcano, Kamchatka: dynamics of eruptive activity and geologic-geomorphological impact (based on remote sensing data). Bulletin of Kamchatka regional association "Educational-

Scientific Center". Earth sciences, 2(18), 87-101. (In Russian). http://www.kscnet.ru/kraesc/2011/2011_18/art7.pdf

1.1.5.2. Volcanic activity of andesitic volcanoes

O. A. Girina, Nuzhdaev, *Institute of Volcanology and Seismology, Far East Division, Russian Academy of Sciences, Petropavlovsk-Kamchatsky, Russia*

Bezymianny volcano eruptions

Bezymianny Volcano is one of the most active volcanoes in the world. In 1955, for the first time in history, Bezymianny started to erupt and after six months produced a catastrophic eruption with a total volume of eruptive products of more than 3 km^3. Following explosive eruption, a lava dome began to grow in the resulting caldera. Lava dome growth continued intermittently for the next 57 years and continues today. During this extended period of lava dome growth, 44 Vulcanian-type strong explosive eruptions occurred between 1965 and 2012. This research presents a summary of activity at Bezymianny Volcano from 1956 to 2010 with a focus on descriptive details for each event.

Girina, O. A. (2013). Chronology of Bezymianny Volcano activity, 1956–2010. Journal of Volcanology and Geothermal Research, 263, 22-41. Doi: http://dx.doi.org/10.1016/j.jvolgeores.2013.05.002

Shiveluch volcano eruptions

The explosive eruption of Young Shiveluch volcano occurred on September 22, 2005. A 20-km long pyroclastic flow formed in the Baydarnaya Valley. Ash deposits from this eruption were observed in an area of the Northern volcanic group of Kamchatka.

Girina, O. A., & Nuzhdaev, A. A. (2014). On some features peculiar to the September 22, 2005 eruption of Young Shiveluch Volcano, Kamchatka. Journal of Volcanology and Seismology, 8(4), 218-227. Doi: 10.1134/S0742046314040034

1.1.6. Petrophysical studies of the Bezymianny volcano rocks

Ladygin V.M., Frolova Yu.V., skalka@geol.msu.ru, *M.V. Lomonosov Moscow State University, Moscow, Russia*
Girina O.A., girina@kscnet.ru, *Institute of Volcanology and Seismology, Far East Division, Russian Academy of Sciences, Petropavlovsk-Kamchatsky, Russia*

This research presents results from a study of lava flows that were discharged by Bezymianny Volcano at different times, from old (about 3500 years ago) to recent ones (1985–1989). We provide detailed descriptions of the composition, structure, and petrophysical properties for the main types of constituent rocks, which are andesites and basaltic andesites. It was found that porosity is the leading factor that controls rock properties, while the effects of structural and mineralogical features are less prominent. We demonstrate the variation in the properties of rocks that compose the lava flows in relation to their ages: the older a rock is, the higher its density and strength and the lower its porosity is.

Ladygin, V. M., Girina, O. A., & Frolova, Y. V. (2012). Petrophysical features of lava flows from Bezymyannyi Volcano, Kamchatka. Journal of Volcanology and Seismology, 6(6), 341-351. Doi: 10.1134/S074204631206005X

1.2. Eastern volcanic front

1.2.1. Recent eruptions in the Eastern volcanic front

1.2.1.1. Koryaksky Volcano eruption 2008-2010

Water contaminated by fresh tephra as a natural hazard factor

Melekestsev I.V., annasm@kscnet.ru**, Kartasheva E.V., Kirsanova T.P., Kuz'mina A.A.**
Institute of Volcanology and Seismology, Far East Division, Russian Academy of Sciences, Petropavlovsk-Kamchatsky, 683006, Russia

Fig. 1.2.1.1.1. Three eruptive vents in the northwestern sector of the Koryaksky summit portion in January 2009. Photographed by A.V. Sokorenko.

This study is the first to show, using data from the eruption of Koryaksky Volcano, Kamchatka that began in December 2008 and continued through 2009 that the water in permanent and temporary streams that start on the slopes of the volcanic cone and in temporary lakes when contaminated with fresh tephra is a specific hazard factor related to long-continued hydrothermal–phreatic eruptions on that volcano. This water is characterized by increased acidity (pH 4.1–4.35) and large amounts (up to 50–100 cm^3/liter) of solid suspension and is unfit for drinking and irrigation. When combined with tephra, it probably produced mass destruction of a number of animals who lived on the slopes and at the base of the volcano. The water contaminated with tephra is an important component of the atmospheric mud flows occurring on Koryaksky Volcano; for

several future years it will be a potential source for enhancing the acidity of ground water in the volcanic edifice.
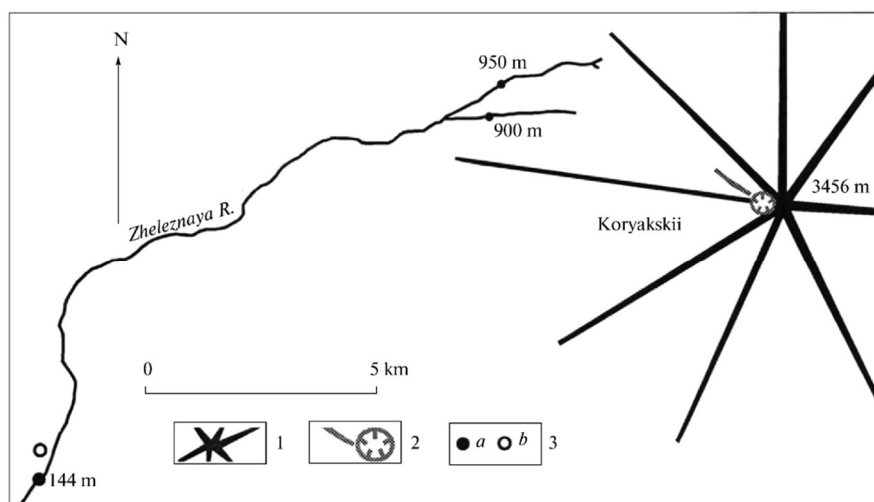
Fig. 1.2.1.1.2. Water sampling sites (the Zheleznaya River and its left tributary): (1) Koryaksky edifice, (2) western crater and eruptive fissure responsible for the 1956–1957 and 2008–2009 eruptions on Koryaksky, (3) water sampling sites (a) and the well (b).

Table 1.2.1.1.1. Chemical analyses of water sampled in the Koryaksky area (in $\mu g/dm^3$), hardness in meq/l)

Parameter	Feature sampled				MPC for drinking water	Order of concentration value (mean for Kamchatka)	Analysis method
	well LGA	950	900	144			
pH	7.6	4.2	4.35	4.15	from 6 to 9	from 6 to 7	potentiometry
Salinity	83.5	83.21	35.42	64.34	1000	<100	calculation
hardness	0.223	1.04	0.13	0.8	7	n	AAS
aluminum		<0.3	1.35		0.5	0.0n	photometry
boron	<0.1	<0.1	<0.1	<0.1	0.5	0.n	potentiometry
iron	<0.005	0.8844	0.5542	0.245	0.3	0.n	AAS
manganese	<0.005	0.071	0.0024	0.0406	0.1	0.0n	AAS
copper	<0.001	0.0096	0.0149	0.0069	1	0.00n	AAS
nickel	<0.005	0.0249	0.0148	0.0186	0.1	0.00n	AAS
nitrates	1.51	<0.1	<0.1		45	n · 10	photometry
lead	<0.01		0.0131	0.0256	0.3	0.00n	AAS
sulfates	2.86	57.64	16.33	43.2	500	n · 100	titrimetric analysis
fluorides	<0.1	0.2	<0.1		1.2	0.n	potentiometry
chlorides	1.64	0.71	2.13	2.8	350	n · 100	titrimetric analysis
zinc	<0.005	0.0048	0.0022	0.0075	5	0.0n	AAS
lithium	<0.001	<0.01	<0.01	<0.005	0.03	0.00n	FES
cobalt	0.0117	0.016	0.0058	0.0202	0.1	0.00n	AAS
ammonia	<0.1	<0.1	<0.1	<0.1	2	0.n	photometry
silica	8.32	7.93	3.25	2.4	10	n · 10	photometry
sodium	4.86	0.368	0.807	0.22	200	n · 10	FES
nitrite	<0.01	<0.01	<0.01	<0.1	3	0.00n	photometry
hydrocarbonate	31.73	3.9	10	4.88		n · 100	potentiometry
potassium	1	0.192	0.34	0.35		n	FES
calcium	3.27	16.83	1.6	14.4		n · 10	AAS
magnesium	0.73	2.43	0.49	0.97		n	AAS

Note: The chemical analyses of the samples were made at the Analytical Center IV&S FED RAS by Researchers E.V. Kartasheva and Junior Researcher A.A. Kuz'mina. The data for comparison (average for Kamchatka) were based on long-term observations of water compositions observable in the drinking water supply system. AAS stands for atomic absorption spectrometry, FES for flame emission spectrophotometry,

well LGA denotes a water sample from the well in the Shiveluch LGA (at the base of Koryaksky Volcano), depth 110 m, 950 denotes a water sample from the Zheleznaya River at 950 m altitude, 900 denotes a water sample from the tributary of the Zheleznaya at 900 m altitude, 144 is a water sample from the Zheleznaya at 144 m altitude.

Melekestsev, I. V., Kartasheva, E. V., Kirsanova, T. P., & Kuz'mina, A. A. (2011). Water contaminated by fresh tephra as a natural hazard factor: The 2008–2009 eruption of Koryaksky Volcano, Kamchatka. Journal of Volcanology and Seismology, 5(1), 17-30. Doi: 10.1134/S0742046311010064

Koryaksky volcano: the recent state and its recent activity

Gordeev E.I., Droznin V.A., Dubrovskaya I.K., Muravyev Ya.D., murjd@kscnet.ru**, Ovsyannikov A.A.** *Institute of Volcanology and Seismology, FEB RAS, Petropavlovsk-Kamchatsky, Russia*

Presented the results of studying of the weak explosive gas-ashed eruption of the Volcano Koryaksky occurring since December, 2008 on the beginning of 2010. Based on the previous eruption of a volcano in 1956–1957, it is possible to allocate separate fumarolic or Koryaksky type of eruption.

High resolution thermal cameras were used in observations of gas and ash plumes during eruption the Koryaksky volcano in March 2009. Our results provide the thermal structure of gas and ash flows. The structure of the eruption column consists of several individual plumes. The vertical velocity of plume rise was estimated at 5.5–7 m/s. The eruption column or plume can be conventionally divided into three parts: a highly convective region, a buoyant region, and a region of horizontal motion. The temperature of the plume is higher than that of the surrounding atmosphere by 3–5°C for the horizontal motion region and by about 20°C for the buoyant region. The velocity at the buoyant region is 5–7 m/s. For the boundary between highly convective and buoyant regions, where the plume diameter is known, the vapor mass flow and the heat capacity of the thermal jet flow can be determined from the heat balance equation. The mass flow of the overheated vapor, which has a temperature of 450°C and comprises a gas and ash eruption plume, was estimated to be $Q = 35$ kg/s. The total mass of water vapor over the period of eruption (100 days) is estimated at $3 \cdot 10^5$ t. The total thermal energy of the eruption amounted to 10^9 MJ.
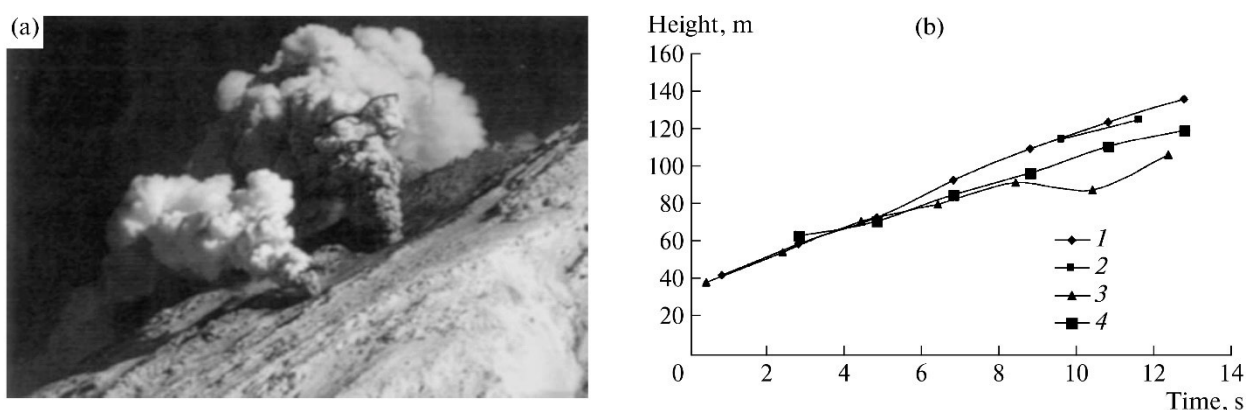
Fig. 1.2.1.1.3. Photograph of the gas and ash eruption plume taken at a distance of 6.3 km from the observation site (a). The heads of plumes are marked with a black line; (b) growth of the plume rise height; (1, 2) lower vent; (3, 4) upper vent.

Gordeev, E. I., Droznin, V. A., Dubrovskaya, I.,K., Muravyev, Ya, D., & Ovsyannikov A. A. (2011) Volcan Koryaksky: the recent state and its activity 2008–2010. Vestnik DVO RAN, 3(157), 25-34. (In Russian). (In Russian). http://elibrary.ru/download/60259377.pdf

Ashes from the eruption of Koryaksky Volcano

Maximov A.P., Anikin L.P., Vergasova L.P., Ovsyannikov A.A., Chubarov V.M. *Institute of Volcanology and Seismology FEB RAS Petropavlovsk-Kamchatsky, 683006, Russia*
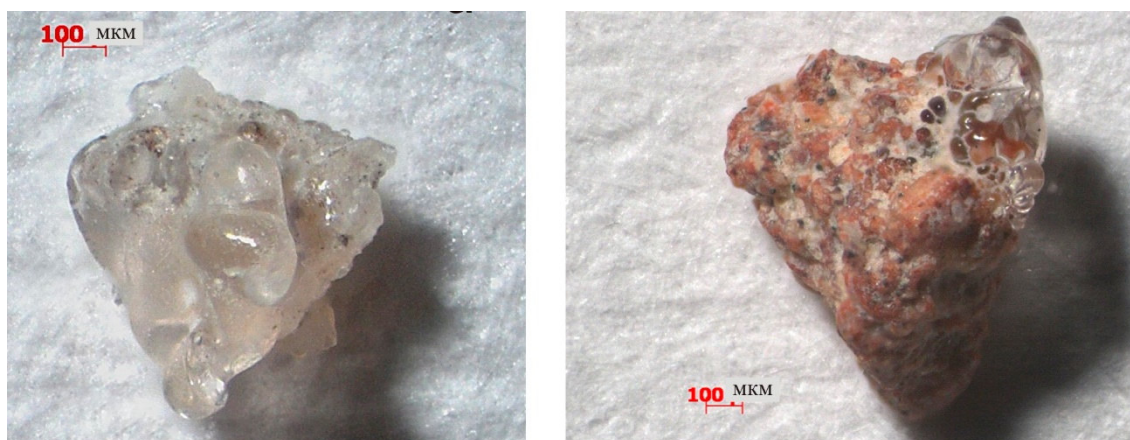
Fig. 1.2.1.1.4. The particles of silica gel from the ashes of the eruption of the volcano Koryaksky: single particle of silica gel and particle of oxidized rock with kidney-shaped build-up silica gel. Photos taken with a stereomicroscope Discovery V12.
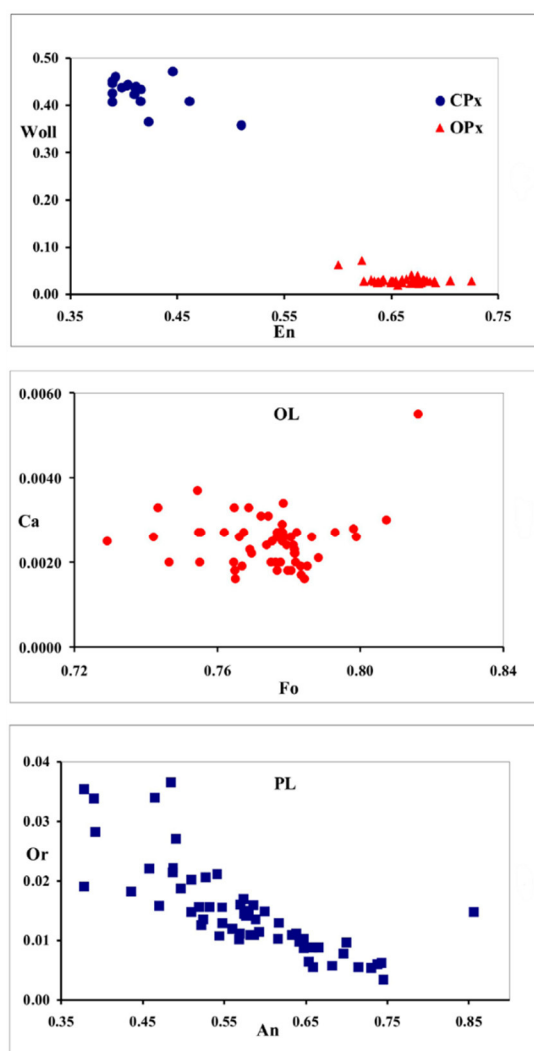
Fig. 1.2.1.1.5. Diagrams compositions of rock-forming minerals in the ashes of the eruption of the volcano Koryaksky 2009.

The paper presents results of granulometric, chemical and mineral analysis of ash from the Koryaksky 2009 eruption. Ash is fine grained with no traces of fresh volcanic glass. There is a wide range of minerals of various genesis: common magmatic minerals, various accessories and minerals of hydrothermal genesis. The article provides the conclusion of mixed genesis of ash and the hydrothermal nature of the volcano activity.

Maximov, A. P., Anikin, L. P., Vergasova, L. P., Ovsyannikov, A. A., & Chubarov, V. M. (2011). Ashes from the 2009 eruption of Koryaksky volcano and distinguishing features of their genesis. Bulletin of Kamchatka regional association "Educational-Scientific Center". Earth sciences, 2(18), 73-86. (In Russian). http://www.kscnet.ru/kraesc/2011/2011_18/art6.pdf

1.2.1.2. Kizimen eruption 2010-2013

The history of the eruption

Malik N.A., malik@kscnet.ru*,* **Ovsyannikov A.A.,** oval@kscnet.ru, **Maximov A.P.,** maximov@kscnet.ru**, Aninov V.V.***,* **Gordeev E.I.,** gordeev@kscnet.ru**, Girina O.A.,** girina@kscnet.ru**, Droznin V.A.,** dva@kscnet.ru**, Murav'ev Ya.D.,** murjd@kscnet.ru*,* **Manevich A.G.,** lav217@kscnet.ru*,* **Mel'nikov D.V.,** dvm@kscnet.ru**, Nuzhdaev A.A., Demyanchuk Yu.V.,** demyanchuk.yu@yandex.ru, *Institute of Volcanology and Seismology, Far East Division, Russian Academy of Sciences, Petropavlovsk-Kamchatsky, 683006, Russia*

Fig. 1.2.1.2.1. (upper left) Regional location of Kizimen on Kamchatka Peninsula, Russia; red square indicates area of enlarged map. (lower right) Local set ting of Kizimen among neigh boring volcanoes. Regional map was found on the internet, authorship unknown. Local map was provided by Droznin Valery

(Institute of Volcanology and Seismology, Russian Academy of Sciences, Far Eastern Branch). Figure taken from (Bulletin of the Global Volcanism Network. Volume 36, Number 10, October 2011).

One of the active Holocene volcanoes of the Kurile-Kamchatka arc - Kizimen Volcano (N 55º08′, E 160º20′, alt. 2375 m) - is located on the eastern edge of the Central Kamchatka Depression (CKD), in the area of Schapinsky graben and midway between the eastern volcanic front (EVF) and CKD at the latitude of the Klyuchevskaya Group (Fig. 1.2.1.2.1). In historical time only one eruption was documented in 1928 visually. But probably this eruption was very poor and no any deposits were found. Their volcanic products are represented by pyroclastic deposits and lava flows of basalt-dacite composition. One permanent fumarole at W slope of volcano is known since 1825.

Fig. 1.2.1.2.2. New summit fumaroles at Kizimen volcano. Photo done from the south 20.11.2011 by A.V. Sokorenko.

The seismic activity before new 2010-2013 eruption started at 2009. In October 2010 two new fumaroles at the volcano summit occur (Fig. 1.2.1.2.2). The first ash fall was documented at November 12 2010. The intensive explosive activity was documented at October 10-14 with ash plumes up to 1 km and pyroclastic flows (Fig. 1.2.1.2.3). Than ash activity was continue and the active explosions started at December 10 2010. Simultaneously with this eruption large lahar (17-18 km long) was formed in December 13 at Poperechny and Levaya Schapina rivers. To the end of 2011 Kizimen ash covers area about 300 thousand km^2. The estimated mass of ash for this period (December 2010 – March 2011) was about 10 million tons. Numerous pyroclastic flows mainly at SE slope of volcano are characteristic feature of this eruption (Fig. 1.2.1.2.4.). The chemical composition of ash and lapilli is high-Al andesites and dacites.

The first lava flow occurs in February 2011. The explosive eruption was continuing up to the end of 2011 when the pyroclastic flows were moved to NE slope of volcano. The future activity was represented by effusive events and by lava flow squeezing. At September 2011 the lava front was on the elevation 1300 m, and the lava flow was 2.5 km long. At March 2012 the lava front was on the elevation 1100-1200 m, and the lava flow was 3.1 km long (Fig. 1.2.1.2.5) and it's

thickness was 50-100 m. The velocity of the lava flow front was about 4-12 m/day. This effusive stage of eruption was continuing up to September 2012 when it was switched on extrusive-effusive phase.

Fig. 1.2.1.2.3. View of explosive Kizimen eruption of 5.01.2011 from the west. The permanent fumarole is left of crater. Photo by E.S. Vlasov.

Fig. 1.2.1.2.4. Pyroclastic flow 26.01.2011. Photo by S.A. Chirkov.

Eruption of Kizimen volcano finished on December 09, 2013. Activity of the volcano changed with time: in 2012-2013, there was effusive eruption from mid-January 2011, till September 2012, and extrusive-effusive eruption from September 2012, till September 2013.

Fig. 1.2.1.2.5. Lava flow, photo done by Malik N.A. April 30 2012: 1 — lava front, 2 — edge of lava flow, 3 — fresh lava flow.

Lava flow composition is andesites with SiO_2 from 56.3 to 63.5% at constant FeO*/MgO, which covers all earlier known SiO_2 values for the Kizimen lavas of different ages (Churikova et al., 2001, 2007, 2013). Composition of volcanic glass from the 2010-2011 eruptions from Kizimen is also identical to that from its largest pre-historic eruptions (Ponomareva et al., 2012).

The main rock-forming minerals in Kizimen eruption 2010-2013 are plagioclase (An_{50-85}) and hornblende (F/FM — 0.25–0.40). Other phenocrysts are represented by Opx (En_{64-78}), Aug ($En_{43-48.5}$ Fs_{13-18} $Woll_{34.5-42}$), Ol ($Fo_{72-76.5}$), Mt (6–14% TiO_2), and Ilm. Two different volcanic glasses were measured in these rocks – one with SiO_2=77% and K_2O=4%, second one with SiO_2=77% and K_2O=4%, which was explained by the liquation process.

Malik, N. A., & Ovsyannikov, A. A. (2011). The eruption of the Kizimen volcano in October 2010 – March 2011. Bulletin of Kamchatka regional association "Educational-Scientific Center". Earth sciences, 1(17), 7-10. (In Russian). http://www.kscnet.ru/kraesc/2011/2011_17/art1.pdf

Malik, N. A., Maximov, A. P., & Ananyev, V. V. (2012). Eruption of Kizimen volcano in 2010-2012 and its products. Volcanism and related processes. Annual regional scientific conference dedicated to the Volcanologist Day. Proceedings of the conference. March 29-30, 2012, Petropavlovsk-Kamchatsky. Petropavlovsk-Kamchatsky: Institute of volcanology and seismology FED RAS, 64-70. (In Russian). http://www.kscnet.ru/ivs/publication/volc_day/2012/art10.pdf

Gordeev, E., Droznin, V., Malik, N., & Muravyev, Y. (2012) Kizimen Volcano, Kamchatka, Russia: 2010-2012 Eruptive Activity. American Geophysical Union, Fall Meeting, December 3-7, 2012, San Francisco, California. Abstract #V33D-2896G

Churikova, T. G., Ivanov, B. V., Eichelberger, J., Wörner, G., Browne, B., & Izbekov, P. (2013). Major and trace element zoning in plagioclase from Kizimen Volcano (Kamchatka): Insights into magma-chamber processes. Journal of Volcanology and Seismology, 7(2), 112-130. Doi: 10.1134/S0742046313020024

Gordeev, E. I., & Girina, O. A. (2014). Volcanoes and their hazard to aviation. Herald of the Russian Academy of Sciences, 84(1), 1-8. Doi: 10.1134/S1019331614010079

Girina, O. A., Manevich, A. G., Melnikov, D. V., Nuzhdaev, A. A., Demyanchuk, Yu. V. (2014). Activity of Kamchatkan Volcanoes in 2012-2013 and Danger to Aviation. 8-th Biennial Workshop on Japan-Kamchatka-Alaska Subduction Processes (JKASP-2014): Finding clues for science and disaster mitigation from International collaboration. Sapporo, Japan, 22-26 September 2014. http://hkdrcep.sci.hokudai.ac.jp/map/jkasp2014/pdf/R16.pdf

Ponomareva, V. V., Portnyagin, M. V., & Melnikov, D. V. (2012). Composition of tephra from modern (2009-2011) eruptions of the Kamchatka and Kurile islands volcanoes. Bulletin of Kamchatka regional association "Educational-Scientific Center". Earth sciences, 2(20), 23-37. (In Russian). http://www.kscnet.ru/kraesc/2012/2012_20/art5.pdf

Emission of the volcanic ash amount into the at atmosphere

Gordeev E.I., gordeev@kscnet.ru, **Firstov P.P.,** firstov@emsd.ru, *Institute of Volcanology and Seismology, Far East Division, Russian Academy of Sciences, Petropavlovsk-Kamchatsky, 683006; Kamchatka Branch, Geophysical Service, Russian Academy of Sciences, Petropavlovsk-Kamchatsky, 683006, Russia*

Kulichkov S.N., snk@ifaran.ru, *Obukhov Institute of Atmospheric Physics, Russian Academy of Sciences, Moscow, 119017, Russia*

Makhmudov E.R., *Kamchatka Branch, Geophysical Service, Russian Academy of Sciences, Petropavlovsk-Kamchatsky, 683006, Russia*

The IS44 station operates at the observation point of Nachiki on the Kamchatka peninsula, which is part of the International Monitoring System (IMS), and it helps verify compliance with the Comprehensive Nuclear Test-Ban Treaty (CTBT). The Kamchatka Branch, Geophysical Service, Russian Academy of Sciences (KB GS RAS), has a station operating in the village of Paratunka. Both of these stations allow one to monitor strong explosive eruptions of andesitic volcanoes (Fig. 1.2.1.2.6).

Both kinematic and dynamic parameters of acoustic signals accompanying the eruptions of the Bezymianny volcano (at a distance of 361 km from Nachiki) in 2009–2010 and the Kizimen volcano (at a distance of 275 km) on December 31, 2011, are considered. A low-frequency rarefaction phase 60 s in length has been revealed in the initial portion of the record of acoustic signals accompanying such strong eruptions. It is shown that the rarefaction phase occurs due to the rapid condensation of superheated juvenile vapor that enters the atmosphere during such explosions. The amount of volcanic ash emitted into the atmosphere has been estimated within $(3.2–7.3)\ 10^6\ \mathrm{m}^3$ on the basis of acoustic signals recorded during the eruptions under consideration.
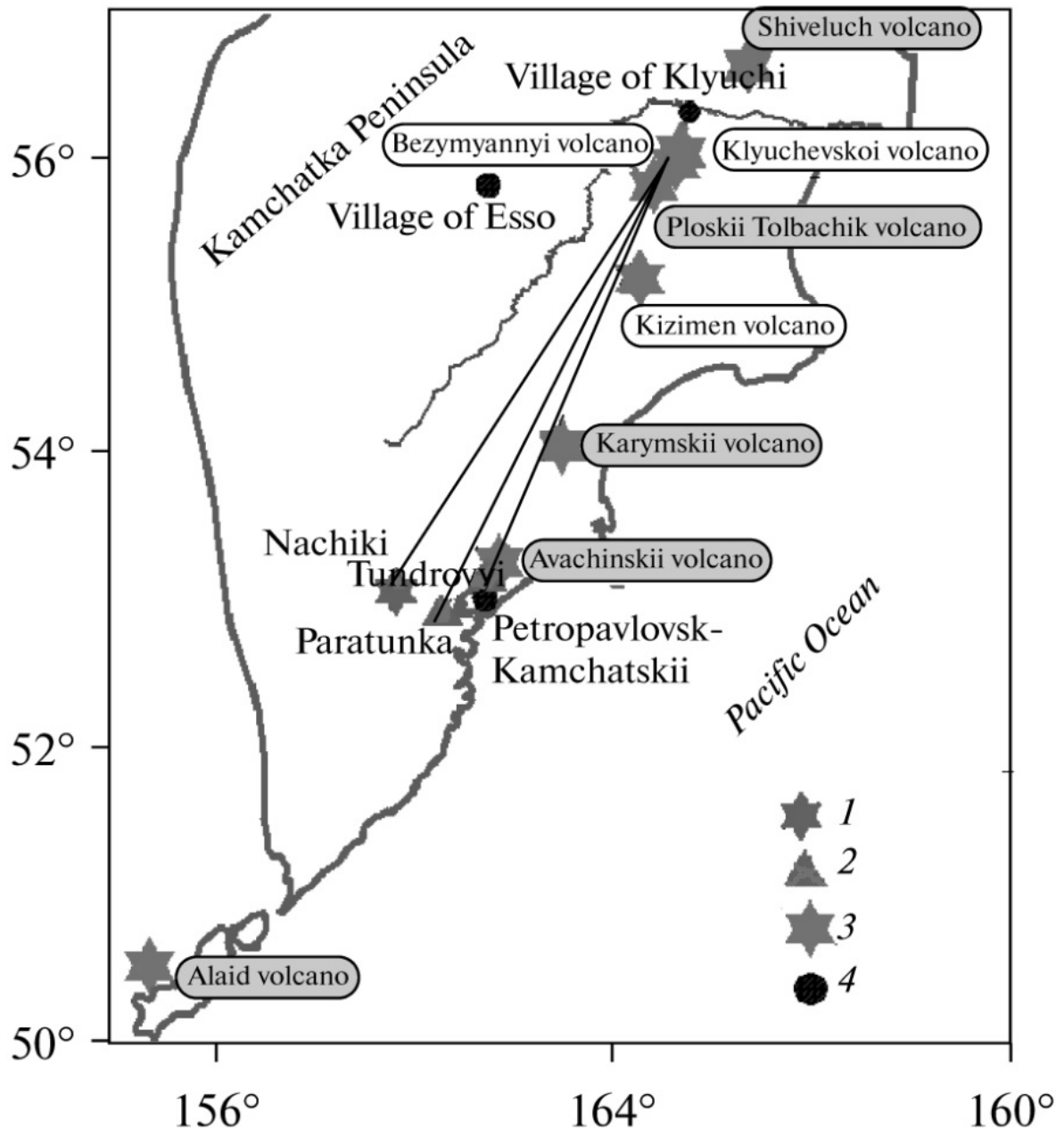
Fig. 1.2.1.2.6. Layout of acoustic stations and Kamchatka active volcanoes; (1) IS44 station (Nachiki), (2) stationary stations (Paratunka and Tundrovyi), (3) active volcanoes, and (4) populated areas.

Gordeev, E. I., Firstov, P. P., Kulichkov, S. N., & Makhmudov, E. R. (2013). Infrasonic waves from volcanic eruptions on the Kamchatka peninsula. Izvestiya, Atmospheric and Oceanic Physics, 49(4), 420-431. Doi: 10.1134/S0001433813030080

Eruption of Kizimen volcano in 2009-2013 in seismic data and visual observations

Firstov P.P. firstov@emsd.ru, **Shakirova A.A.,** shaki@emsd.ru, **Arbugaeva O.A.,** *Kamchatka Branch, Geophysical Service, Russian Academy of Sciences, bul'v. Piip 9, Petropavlovsk-Kamchatsky, 683006 Russia*

Eruption of andesitic volcano Kizimen in 2010-2013 was recorded for the first time of detailed seismological observations in Kamchatka. Different forms of activity of the volcano is well diagnosed by satellite images in the infrared spectrum and seismic effects. Quasi-periodic

appearance of micro earthquakes generated by the front of the lava flow when it moves down the slope was observed first for Kamchatka volcanoes eruptions with andesitic lava.

Kizimen eruption was preceded by long seismic preparation for one year and eight months, when in the region of the volcano were recorded volcano-tectonic (VT) earthquakes with energy class K>5 (K = lgE, J). According to the catalog of earthquakes of 2010 seismicity increased significantly in the area of the volcano. By late April, the accumulated conditional strain reached a value of $2*10^6$ Dzh$^{0.5}$ then until October observed its monotonic increase, and then there were two intervals amplification of seismic activity (Fig. 1.2.1.2.7). The first occurred in mid-October, when there were a series of shallow earthquakes with K>10. In November 2010 there was a second activation of seismicity with four earthquakes with K>10. The total value of the conditional strain in 2010 was $8*10^6$ Dzh$^{0.5}$. Powerful explosions with emission of ash to a height of 10 km occurred 12 and 31 December 2010 (Fig. 1.2.1.2.7b).

The space-time seismicity of the Kizimen volcano points to the restructuring of the stress field area under the influence of viscous magma rising to the dyke with a complex configuration before the eruption. Preparation of eruption was slow, indicating sluggish processes in the magma chamber.
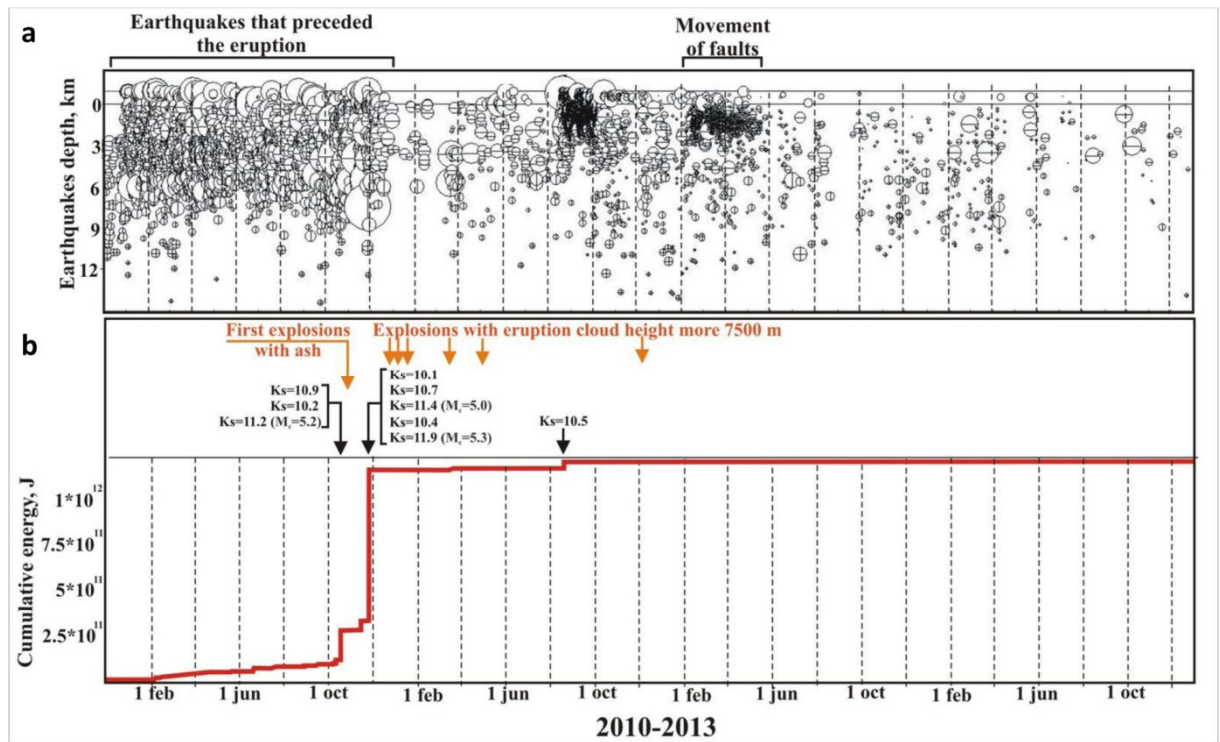
Fig. 1.2.1.2.7. Distribution focuses depth of volcano-tectonic earthquakes preceding and accompanying Kizimen eruption (a) and conventional strain graph (b).

After the eruption and during the formation of a lava flow in 2011 VT earthquakes continued to occur (Fig. 1.2.1.2.7a), and their focuses in a northeast direction from the volcano with a depth of 0 to 5 km were clearly gravitated to the fault NW-trending (Fig. 1.2.1.2.8). It is possible that seismic activity of these structures related to the establishment of isostatic equilibrium associated with the appearance of excess weight in the form of lava flow of more than 1 km^3 on the eastern slope of the volcano.
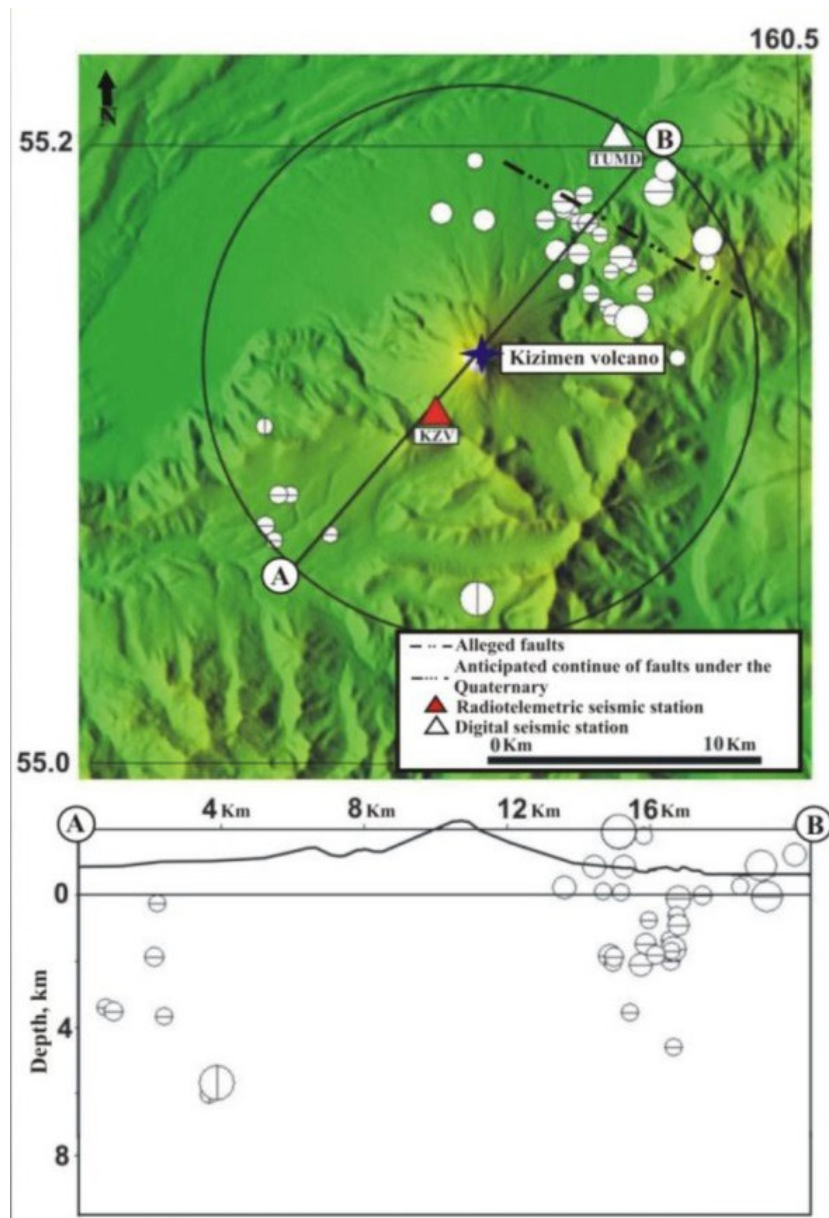
Fig. 1.2.1.2.8. VT earthquakes in 2011 gravitated to the fault NW-trending.

Shortly after the start of the eruption thermal anomaly was observed on satellite images up to 25 pixels (January 2011). In March 2011 on the slopes of the volcano was seen lava flow. With the advent of lava flow explosive activity decreased significantly and in April 2011 the number of pixels of the thermal anomaly has been declining. Increased thermal anomalies up to 25 pixels in December 2011 - April 2012 due to the formation of the second tongue of the lava flow.

Since October 2011 a second lava flow tongue began to form. During the formation of a second tongue temperature of thermal anomalies reached 75-80ºC. Area of the lava flow equal 1.16 km^2 by 5 September 2011, the flow area has increased almost in double and amounted to 2.16 km^2 to December 11, 2011. In November 2011 - January 2012 the formation of a lava flow stopped and PF recorded mainly, area deposits amounted 13.12 km^2 by 11 December 2011.

Squeezing lava flow resumed at the end of January 2012, which ceased its motion in June 2012 and then began to form apical extrusion. This is confirmed by the presence of thermal anomalies, dedicated to the top of the volcano. In April-May 2012 temperature of thermal anomalies decreased 10°C and the number of pixels has decreased dramatically. With the start of squeezing extrusion temperature rose to 30º-50ºC. Thermal anomaly was recorded continuously until June, and then appeared in the September-October 2013.

Pressing viscous andesitic lava and lava flow was accompanied by unusual seismic activity not previously observed during eruptions of andesitic volcanoes of Kamchatka. Seismic stations KZV and TUMD recorded quasiperiodic appearance of microearthquakes similar in form and with the same amplitude, with duration from tens of minutes to tens of days. Microearthquakes with quasiperiodicity from 8 to 50 seconds and energy class K = 2.0 - 5.5 started to be recorded continuously from May 13, 2011. A distinctive feature of this seismicity is quasistability of earthquakes maximum amplitude on longer time intervals.

Legitimate statistically significant changes in arrivals of seismic waves at seismic stations KZV and TUMD are observed for earthquakes mode "drumbeats". Increase t_{S-P} at station KZV from 0.7 to 1.5 s with an root-mean-square error RMSE = 0.2 s, and a decrease tTUMD-tKZV from 0.9 to 0.5 s with RMSE = 0.1 s indicate that the earthquake epicenters naturally removed from the station KZV and approach the station TUMD. The spatial location of the lava flow and seismic stations distinctly indicate that micro-earthquakes were generated by the movement of the viscous front of lava flow. Appearance of regime «drumbeats» agrees well with a photography of the lava flow and thermal anomalies.

Firstov, P. P., & Shakirova, A. A. (2011). Seismic phenomena accompanying Kizimen volcano eruption in 2011. Bulletin of Kamchatka regional association "Educational-Scientific Center". Earth sciences, 2(18), 7-13. (In Russian). http://www.kscnet.ru/kraesc/2011/2011_18/art1.pdf

Shakirova, A. A. (2011). Regime «DRUMBEATS» during the eruption of volcano Kizimen in 2011. Research in the field of Earth sciences. Materials of the IX regional youth conference, December 1-2, 2011. Petropavlovsk-Kamchatsky: IVS FEB RAS, 201-212. (In Russian). http://www.kscnet.ru/ivs/publication/young_conf/2011/1/art18.pdf

Shakirova, A. A. (2012). Lava flow of Kizimen volcano as a generator seismicity seismicity «DRUMBEATS». Research in the field of Earth sciences. Materials of the X regional youth conference, November 28-29, 2012. Petropavlovsk-Kamchatsky: IVS FEB RAS, 127-139. (In Russian). http://www.kscnet.ru/ivs/publication/young_conf/2012/1/art11.pdf

Firstov, P. P., & Shakirova, A. A. (2012). Eruption of Kizimen volcano in 2009-2012 and its manifestation in the seismic effects. Volcanism and related processes. Annual regional scientific conference dedicated to the Volcanologist Day. Proceedings of the conference. March 29-30, 2012, Petropavlovsk-Kamchatsky. Petropavlovsk-Kamchatsky: Institute of volcanology and seismology FED RAS, 76-81. (In Russian). http://www.kscnet.ru/ivs/publication/volc_day/2012/art12.pdf

Firstov, P. P., Shakirova, A. A., Arbugaeva O. A. (2013). Activity of the Kizimen volcano during May 2012 —March 2013 in seismic data and visual observations. Volcanism and related processes. Annual regional scientific conference dedicated to the Volcanologist Day. Proceedings of the conference. March 29-30, 2013, Petropavlovsk-Kamchatsky. Petropavlovsk-Kamchatsky: Institute of volcanology and seismology FED RAS, 130-138. (In Russian). http://www.kscnet.ru/ivs/publication/volc_day/2013/art19.pdf

Firstov P., Shakirova A. Eruption of Kizimen volcano in 2009-2013 in seismic data and visual observations. 8-th Biennial Workshop on Japan-Kamchatka-Alaska Subduction Processes (JKASP-2014): Finding clues for science and disaster mitigation from International collaboration. Sapporo, Japan, 22-26 September 2014. http://hkdrcep.sci.hokudai.ac.jp/map/jkasp2014/pdf/R37.pdf

Pre-eruption deformation caused by dike intrusion beneath Kizimen volcano

Ji L., *Second Crust Monitoring and Application Center, China Earthquake Administration, Xi'an, Shaanxi, China*
Lu Z. lu@usgs.gov, **Dzurisin D.,** Cascades Volcano Observatory, U.S. Geological Survey, Vancouver, WA, USA

Senyukov S., ssl@emsd.ru, **Nuzhdina I.N., Droznina S.J., Garbuzova V.T., Kozhevnikova T.Y., Sobolevskaya O.V.** Kamchatkan Branch of Geophysical Survey, Russia Academy of Sciences, Petropavlovsk-Kamchatsky, Russia
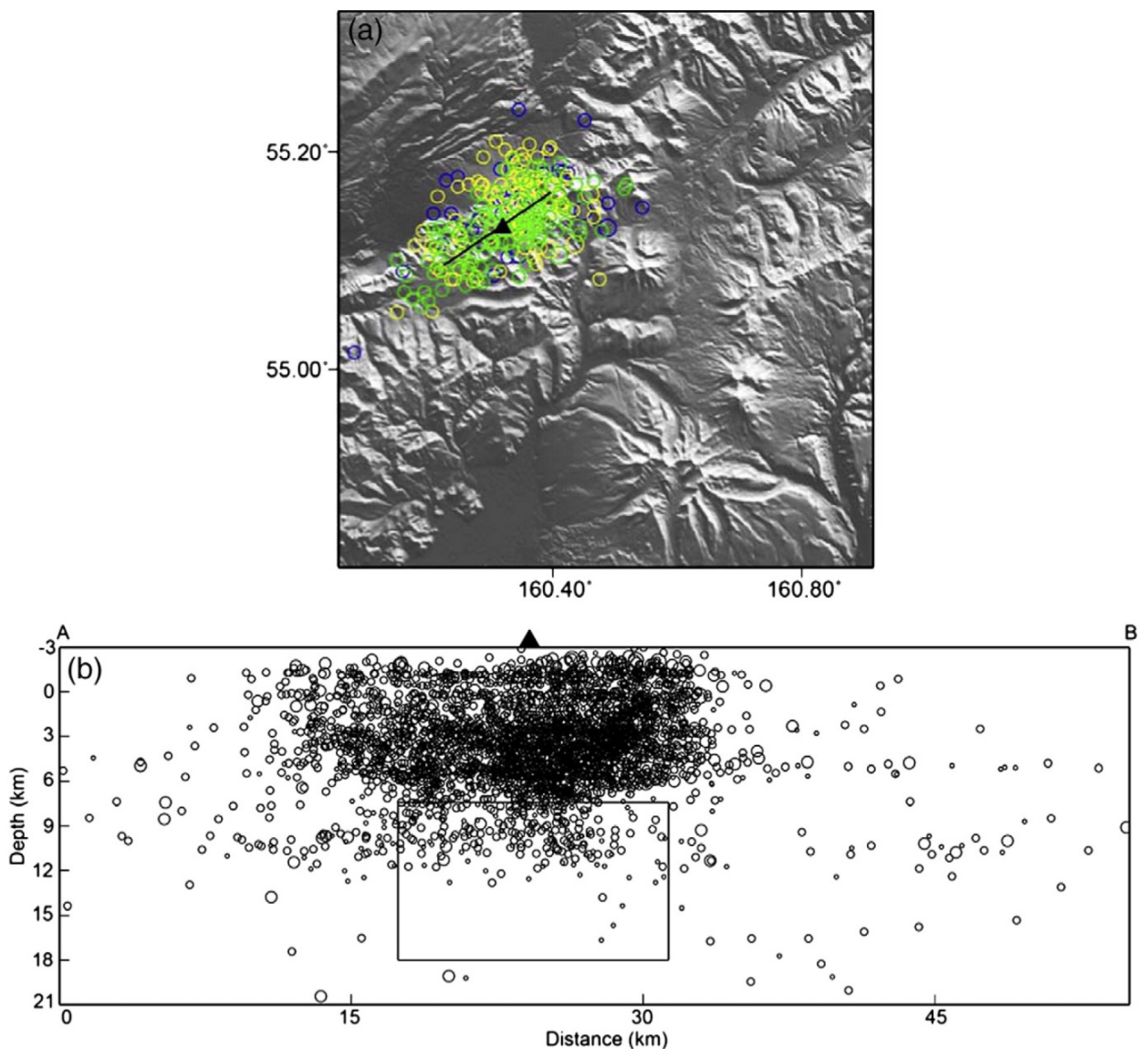
Fig. 1.2.1.2.9. (a) Epicentral distribution of earthquakes near Kizimen. Blue, yellow, and green circles represent earthquakes that occurred during July–December 2009, January–June 2010, and July 2010–November, 2011, respectively. For clarity, only earthquakes with ML > 3 are shown. (b) Cross-section showing the depth distribution of earthquakes recorded from July 2009 to November 2010. Hypocenters were projected onto profile A–B (see Fig. 4b at Ji et al., 2013). Kizimen volcano is marked with black triangle, with surface projection of best-fit dike indicated by black line. Rectangle below shows boundaries of best-fit dike prior to its ascent to the surface.

Interferometric synthetic aperture radar (InSAR) images reveal a pre-eruption deformation signal at Kizimen volcano, Kamchatka, Russia, where an ongoing eruption began in mid-November, 2010. The previous eruption of this basaltic andesite-to-dacite stratovolcano occurred in 1927–1928. InSAR images from both ascending and descending orbital passes of Envisat and ALOS PALSAR satellites show as much as 6 cm of line-of-sight shortening from September 2008 to September 2010 in a broad area centered at Kizimen. About 20 cm of opening of a nearly vertical dike provides an adequate fit to the surface deformation pattern. The model dike is approximately 14 km long, 10 km high, centered 13 km beneath Kizimen, and strikes NE–SW. Time-series

analysis of multi-temporal interferograms indicates that (1) intrusion started sometime between late 2008 and July 2009, (2) continued at a nearly constant rate, and (3) resulted in a volume expansion of 3.2×107 m^3 by September 2010, i.e., about two months before the onset of the 2010 eruption. Earthquakes located above the tip of the dike accompanied the intrusion. Eventually, magma pressure in the dike exceeded the confining strength of the host rock, triggering the 2010 eruption (Fig. 1.2.1.2.9.). Our results provide insight into the intrusion process that preceded an explosive eruption at a Pacific Rim stratovolcano following nearly a century of quiescence, and therefore have implications for monitoring and hazards assessment at similar volcanoes elsewhere.

Ji, L., Lu, Z., Dzurisin, D., & Senyukov, S. (2013). Pre-eruption deformation caused by dike intrusion beneath Kizimen volcano, Kamchatka, Russia, observed by InSAR. Journal of Volcanology and Geothermal Research, 256, 87-95. Doi: http://dx.doi.org/10.1016/j.jvolgeores.2013.02.011

Senyukov, S. L., Nuzhdina, I. N., Droznina, S. J., Garbuzova, V. T., Kozhevnikova, T. Y., & Sobolevskaya, O. V. (2011). Seismicity of the volcano Kizimen. Problems of complex geophysical monitoring of the Russian Far East. III scientific-technical conference. Petropavlovsk-Kamchatsky, October 9–15, 2011, 144–148. (In Russian). http://www.emsd.ru/files/konf111009/pdf/sb/Sekciya_Monitoring/Senyukow2.pdf

Senyukov, S. L. (2013). Monitoring and prediction of volcanic activity in Kamchatka from seismological data: 2000–2010. Journal of Volcanology and Seismology, 7(1), 86-97. Doi: 10.1134/S0742046313010077

1.2.1.3.   New activity of the Zhupanovsky volcano

Samoilenko S.B., samsergey@kscnet.ru, **Mel'nikov D.V.,** dvm@kscnet.ru, **Chirkov S.A., Manevich A.G.,** lav217@kscnet.ru*, Institute of Volcanology and Seismology, Far East Branch, Russian Academy of Sciences, Petropavlovsk-Kamchatsky, Russia*

Zhupanovsky volcano (N 53º35′9″, E 159º8′3″, alt. 2958 m) composed by four fused stratovolcanoes of basalt-dacite composition forming a mountain chain (Fig. 1.2.1.3.1). Active Holocene cone is third one. This cone is composed by the phreatic deposits as well as by lava flows and have 2 craters, one with diameter 300 m and depth 100 m, second one with diameter 80 m and depth 40 m. In historical time this cone was erupted 6 times with last eruption in 1956-57. Series of fumaroles with temperatures from 93°C to 430°C are active permanently at second and third cones.

According to KVERT data (http://www. kscnet.ru/ivs/kvert/van/ index.php?n=2013-25) a moderate explosive phreatic eruption of the Zhupanovsky volcano occurred at 15h October 23, 2013 (UTC) with fissure opening at the elevation 2600 m. According to thermal imaging survey obtained by Flir ThermaCAM P 640 equipment the gas temperature in this fumarole was 170°C. Ash explosions rose up to 5 km a.s.l. and ash plumes extended for about 120 km mainly to the east and south-east of the volcano covering area about 120 km^2. A thickness of ash was about 15-20 cm at the volcano summit and less on some distance out of volcano (Fig. 1.2.1.3.2). The amount of ash was estimated as 100 thousands of tons (0.07-0.08 km^3 at the measured ash density 1.4 kg/m^3).
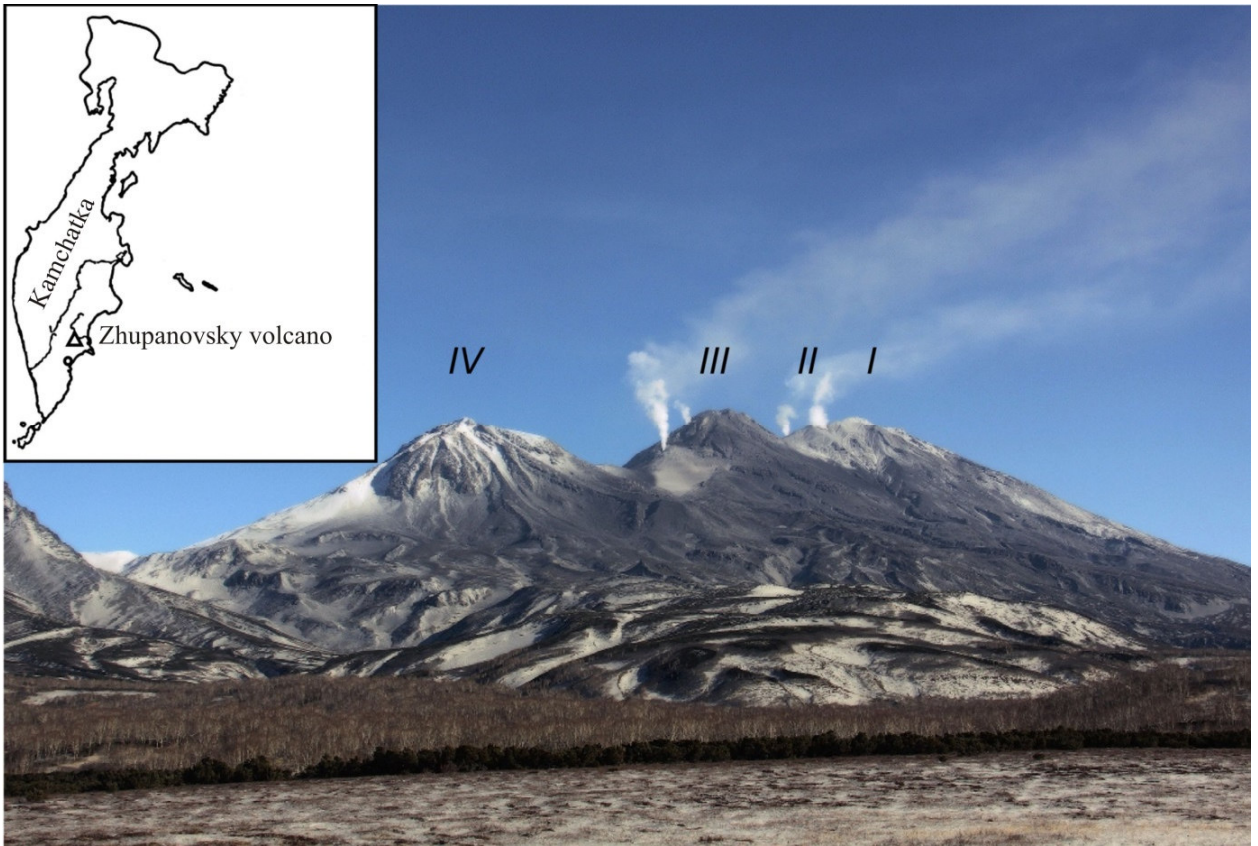
Fig. 1.2.1.3.1. View on Zhupanovsky volcano from the south. Numbers of cones are shown by Roman numerals. Photo by Samoilenko S.B.

Fig. 1.2.1.3.2. Ash deposits on the slopes of third cone of the Zhupanovsky volcano in October 23-24, 2013. Photo by Samoilenko S.B.

More active explosive eruption of Zhupanovsky volcano began on June 06, 2014 and continues at least up to March 2015. This time it was the summit eruption (Fig. 1.2.1.3.3) from the smaller crater. According to Russian pilots and Tokyo VAAC (http://ds.data.jma.go.jp/svd/vaac/data/vaac_list.html) data the eruptive column rise up to 6 km a.s.l. According to KVERT data (Girina et al., 2013, 2015) ash explosions rose up to 8-10 km a.s.l. on June 19, September 05 and 07, October 11, November 07 and 22; in the other days – up to 5-6 km a.s.l. Ash plumes extended for about 1000 km mainly to the eastern directions of the volcano. Ash falls occurred at Petropavlovsk-Kamchatsky on September 07. Activity of the volcano during this time was dangerous to international and local aviation. Ash thickness in 6 km from the volcano crated was less than 5 mm and less than 1 mm out of volcano cone. Fumarole activity increased. The fissure with numerous fumaroles of 140°C crossed the volcano summit from W to E at the elevation about 2600 m at the distance 1.4 km. On the space image Landsat 7 ETM+ (NASA, USGS) from 16.06.2013 seven main fumaroles could be distinguished on the volcano summit along the fissure.

Fig. 1.2.1.3.3. Ash cloud, view on Zhupanovsky volcano from north June 13, 2014. Photo by D. Melnikov.

13th of June Zhupanovsky volcano had two types of activity: permanent fumarole activity and explosive events each 20-40 min. Remote measurements of SO_2 using the equipment MobileDOAS with USB2000+ spectrometer show that during permanent activity average gas consumption was 720 tonn/day (±10%), and during explosive events 1510 tonn/day (±9%). Till now this eruption has explosive character and has magmatic or phreato-magmatic nature.

Samoilenko, S. B., Mel'nikov, D. V., Chirkov, S. A., & Manevich, A. G. (2014). Activation of Zhupanovsky volcano in 2013-2014. Bulletin of Kamchatka regional association "Educational-Scientific Center". Earth sciences, 1(23), 21-26. (In Russian). http://www.kscnet.ru/kraesc/2014/2014_23/art2.pdf

Girina, O. A., Manevich, A. G., Melnikov, D. V., Nuzhdaev, A. A., Demyanchuk ,Yu. V., & Petrova, E. (2013). Explosive Eruptions of Kamchatkan Volcanoes in 2012 and Danger to Aviatio. EGU General Assembly 2013. Geophysical Research Abstracts. Vienna, Austria: 2013. V. V15. № 6760-1, http://meetingorganizer.copernicus.org/EGU2013/EGU2013-6760-1.pdf

1.2.2. G□□h□mi□□l studi□s □f th□E□st□rn v□l□□ni□fr□nt

1.2.2.1.   Th□stud□□f □□r□m□t□rs □f m□gm□ti□□r□□□ss□s

Timina T. Y., Kovyazin S. V., Tomilenko A. A. *timina@igm.nsc.ru, Sobolev Institute of Geology and Mineralogy, Siberian Branch, Russian Academy of Sciences, Novosibirsk, Russia*

This work considers the studies of melt and fluid inclusions in spinel of ultramafic rocks in the mantle wedge beneath Avacha volcano (Kamchatka). The generations of spinel were identified: 1 is spinel (Sp-I) of the "primary" peridotites, has the highest magnesium number (#0.69-0.71), highest contents of Al_2O_3 and lowest contents of Cr_2O_3 (26.2-27.1 and 37.5-38.5 wt %, respectively), and the absence in it of any fluid and melt inclusions; 2 is spinel (Sp-II) of the recrystallized peridotites, has lower magnesium number (Mg# 0.64-0.61) and the content of Al_2O_3 (18-19 wt %), a higher content of Cr_2O_3 (45.4-47.2 wt %) and the presence of primary fluid inclusions; 3 is spinel (Sp-III) that is characterized by the highest content of Cr_2O_3 (50.2-55.4 wt %), the lowest content of Al_2O_3 (13.6-16.6 wt %), and the presence of various types of primary melt inclusions. The data obtained indicate that metasomatic processing of "primary" peridotites occurred under the influence of high concentrated fluids of mainly carbonate-water-chloride composition with influx of the following petrogenic elements: Si, Al, Fe, Ca, Na, K, S, F, etc. This process was often accompanied by a local melting of the metasomatized substrate at a temperature above 1050 °C with the formation of melts close to andesitic.
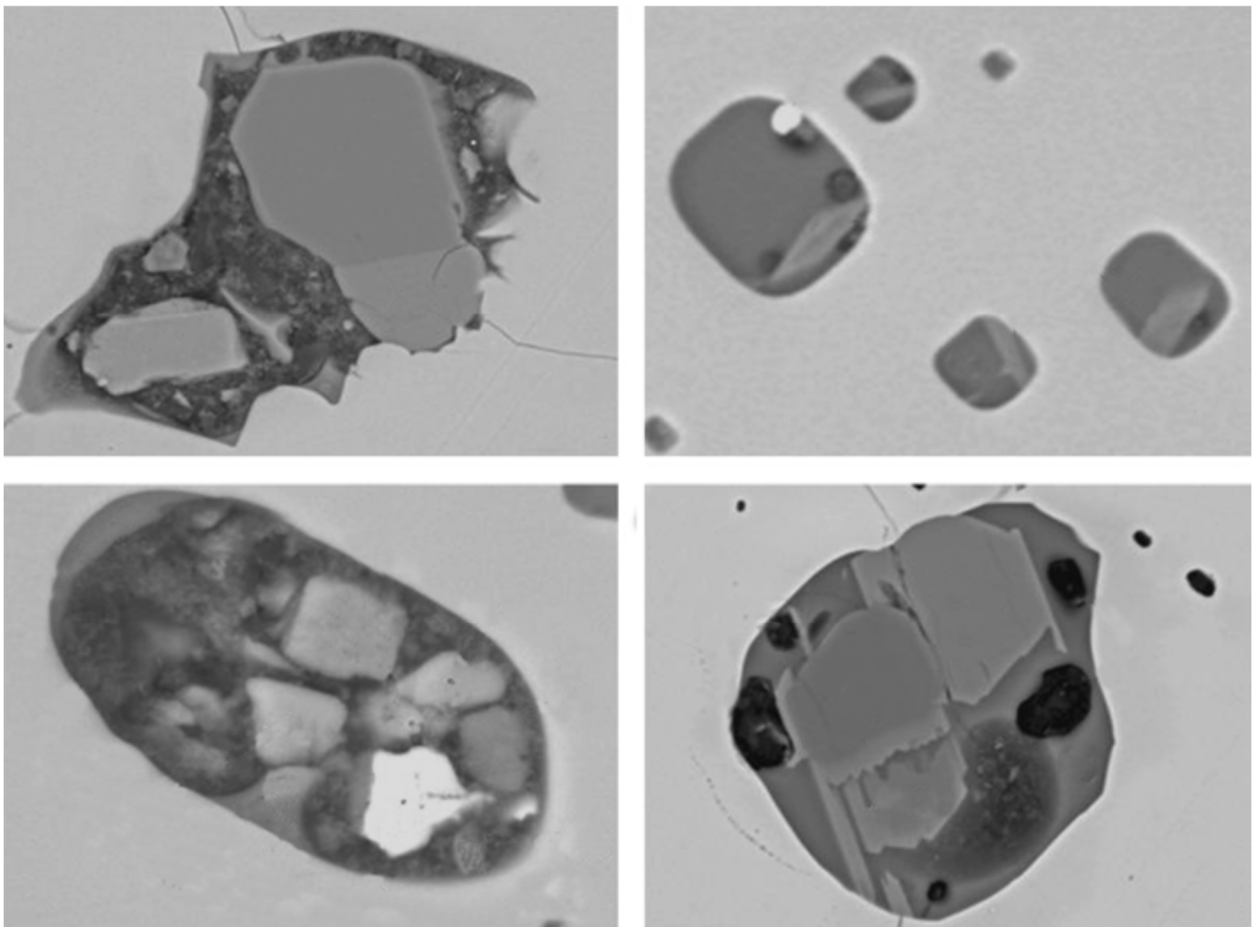
Fig. 1.2.2.1.1. Reflected electron microphotos of primary fluid and melt inclusions in spinel of peridotite xenoliths from Avacha volcano. (a) is combined crystal–fluid inclusion, (b) is normal melt inclusions, (c) is an anomalous melt inclusion, (d) is a combined melt inclusion. Ol is olivine, Cpx is clinopyroxene, Amph is amphibole, Ca is calcite, Anh is anhydrite, Qu is quartz, Fl is fluorite, Fe-phase is an unidentified iron-

bearing phase, Ca, Cl-phase is an unidentified calcium and chlorine-bearing phase, Sulf is sulfide, Gl is glass, is water–saline–fluid isolation, V is a gaseous phase. *L*H2O+salt

Timina, T. Y., Kovyazin, S. V., & Tomilenko, A. A. (2012). The composition of melt and fluid inclusions in spinel of peridotite xenoliths from Avacha volcano (Kamchatka). Doklady Earth Sciences, 442(1), 115-119. Doi: 10.1134/S1028334X12010229

1.2.2.2. Gorely volcano mineralogy

Gavrilenko M., max.gavrilenko@gmail.com*, Institute of Volcanology and Seismology, Far East Division, Russian Academy of Sciences, Petropavlovsk-Kamchatsky, Russia. Department of Earth and Planetary Sciences, Rutgers, The State University of New Jersey, Piscataway, NJ, United States*
Herzberg C., *Department of Earth and Planetary Sciences, Rutgers, The State University of New Jersey, Piscataway, NJ, United States.*
Portnyagin M., mportnyagin@ifm-geomar.de*, Vernadsky Institute of Geochemistry and Analytical Chemistry, Moscow, Russia. Leibniz Institute of Marine Research, IFM-GEOMAR, Kiel, Germany*
Ozerov A., ozerov@ozerov.ru, *Institute of Volcanology and Seismology, Far East Division, Russian Academy of Sciences, Petropavlovsk-Kamchatsky, Russia*
Tolstikh M.L., Naumov V.B., Kononkova N.N., *Vernadsky Institute of Geochemistry and Analytical Chemistry, Moscow, Russia*

Source Lithology inferred from olivine composition

Kamchatka peninsula (Russia) is an island-arc with a complex geological history and structure. It has three distinct volcanic fronts, the origin of which is still debated. Moreover, a junction with the Aleutian Arc (at ~56°N) complicates the understanding of geodynamics at the region.

However, the south part (from ~53°N) of Kamchatka peninsula is thought to be a "textbook case" of subduction zone with relatively rapid (over 8 cm/yr) near-normal convergence and a steep (over 50°) angle of subduction. Kamchatka is unusual in the world because its volcanoes contain a significant amount of primitive high MgO lavas that are rich in olivine crystals. Furthermore, high precision contents of Ni, Ca, and Mn can help to constrain the source lithology. Straub et al. (2008) reported high Ni contents on olivines from a limited number of samples from the Mexican Volcanic Front, and concluded that pyroxenite melting was important. Portnyagin et al. (2009) reported high precision Ni, Ca, and Mn contents of olivines from a wide range of volcanoes from Kamchatka, and similarly concluded that pyroxenite melting is widespread (Fig. 1.2.2.2.1). We have extended the work of Portnyagin et al. (2009) by analyzing olivine phenocrysts from volcanoes in the southernmost Kamchatka peninsula. Our work confirms that there are regional variations in olivine phenocryst composition that likely arises from variations in pyroxenite composition, the amount of peridotite melt that mixes with pyroxenite melts, and a variable role played by magnetite fractionation. We conclude that pyroxenite melting is likely to be important in subduction zones world-wide, but its significance has been underestimated because of the general rarity of olivine-bearing high MgO lavas.
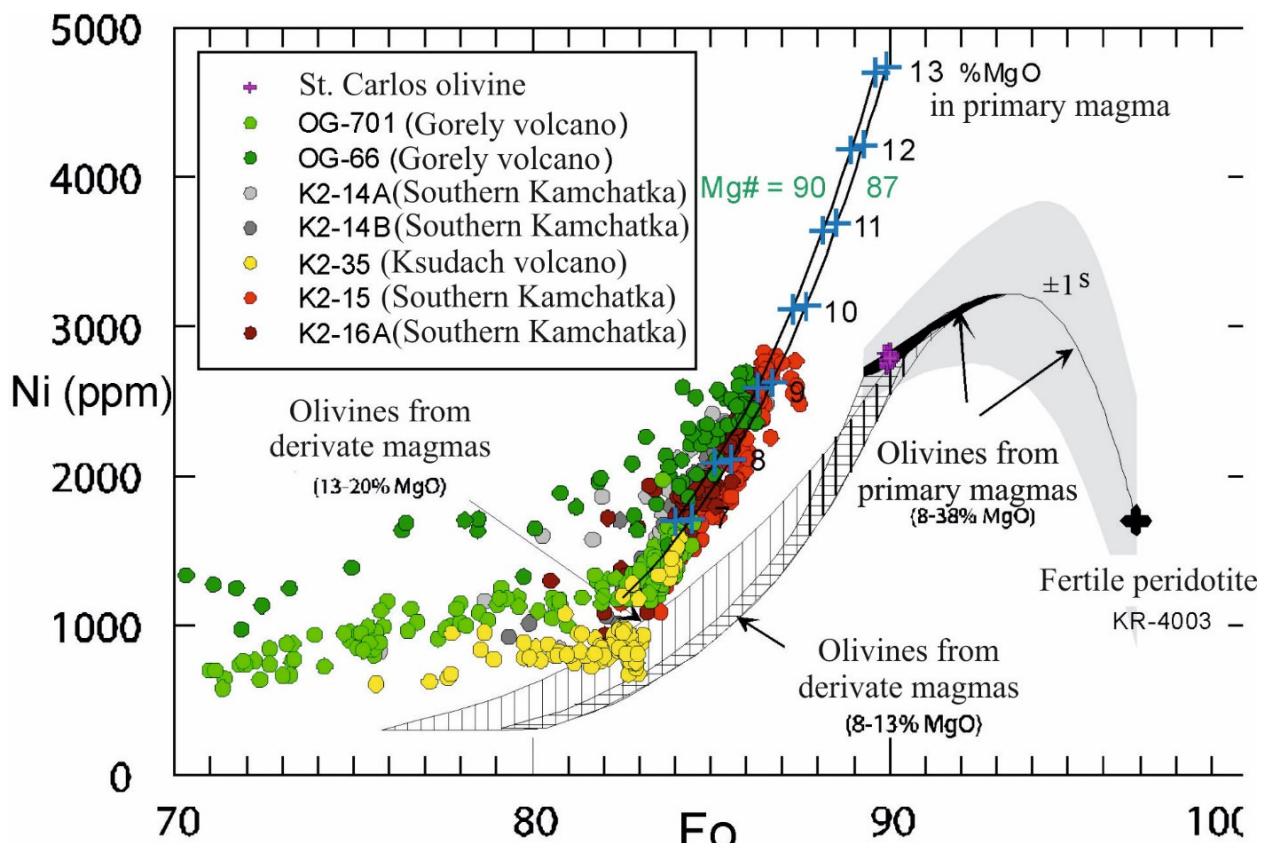
Fig. 1.2.2.2.1. Ni-Fo (Ol) diagram for the olivine composition from the basalts of Gorely volcano. The genetic fields of olivines were obtained by melting modelling of the fertile peridotite KR-4003 (according to Herzberg, 2011).

Gavrilenko, M., Herzberg, C., Portnyagin, M., & Ozerov A. (2012). Identification of Source Lithology at South Segment of Kamchatka Subduction Zone. American Geophysical Union, Fall Meeting, December 3-7, 2012, San Francisco, California. Abstract #V31A-2761.

Melt inclusion study

Melt inclusions in olivine and plagioclase phenocrysts from rocks (magnesian basalt, basaltic andesite, andesite, ignimbrite, and dacite) of various age from the Gorely volcanic center, southern Kamchatka, were studying by means of their homogenization and by analyzing the glasses in 100 melt inclusions on an electron microprobe and 24 inclusions on an ion probe. The SiO_2 concentrations of the melts vary within a broad range of 45–74 wt %, as also are the concentrations of other major components. According to their SiO_2, Na_2O, K_2O, TiO_2, and P_2O_5 concentrations, the melts are classified into seven groups. The mafic melts (45–53 wt % SiO_2) comprise the following varieties: potassic (on average 4.2 wt % K_2O, 1.7 wt % Na_2O, 1.0 wt % TiO_2, and 0.20 wt % P_2O_5), sodic (3.2% Na_2O, 1.1% K_2O, 1.1% TiO_2, and 0.40% P_2O_5), and titaniferous with high P_2O_5 concentrations (2.2% TiO_2, 1.1% P_2O_5, 3.8% Na_2O, and 3.0% K_2O). The melts of intermediate composition (53–64% SiO_2) also include potassic (5.6% K_2O, 3.4% Na_2O, 1.0% TiO_2, and 0.4% P_2O_5) and sodic (4.3% Na_2O, 2.8% K_2O, 1.3% TiO_2, and 0.4% P_2O_5) varieties. The acid melts (64– 74% SiO_2) are either potassic (4.5% K_2O, 3.6% Na_2O, 0.7% TiO_2, and 0.15% P_2O_5) or sodic (4.5% Na_2O, 3.1% K_2O, 0.7% TiO_2, and 0.13% P_2O_5). A distinctive feature of the Gorely volcanic center is the pervasive occurrence of Krich compositions throughout the whole compositional range (silicity) of the melts. Melt inclusions of various types were sometimes found not only in a single sample but also in the same phenocrysts. The sodic and potassic types of the melts contain different Cl and F concentrations: the sodic melts are richer in Cl, whereas the potassic melts are enriched in F. We are the first to discover potassic melts with very high F concentrations (up to 2.7 wt %, 1.19 wt % on average, 17 analyses) in the Kuriles and

Kamchatka. The average F concentration in the sodic melts is 0.16 wt % (37 analyses). The melts are distinguished for their rich ness in various groups of trace elements: LILE, REE (particularly HREE), and HFSE (except Nb). All of the melts share certain geochemical features. The concentrations of elements systematically increase from the mafic to acid melts (except only for the Sr and Eu concentrations, because of active plagioclase fractionation, and Ti, an element contained in ore minerals). The paper presents a review of literature data on volcanic rocks in the Kurile–Kamchatka area in which melt inclusions with high K_2O concentrations ($K_2O/Na_2O > 1$) were found. Krich melts are proved to be extremely widespread in the area and were found on such volcanoes as Avachinsky, Bezymianny, Bol'shoi Semyachik, Diky Greben', Karymsky, Kekuknaisky, Kudryavyi, and Shiveluch and in the Valaginsky and Tumrok Ranges.

Tolstykh, M. L., Naumov, V. B., Gavrilenko, M. G., Ozerov, A. Y., & Kononkova, N. N. (2012). Chemical composition, volatile components, and trace elements in the melts of the Gorely volcanic center, southern Kamchatka: Evidence from inclusions in minerals. Geochemistry International, 50(6), 522-550. Doi: 10.1134/S0016702912060079

1.2.2.3. Plagioclase zonation from the Kizimen volcano

Churikova T., tchurikova@mail.ru, **Ivanov B.,** ivanovbv@kscnet.ru, *Institute of Volcanology and Seismology, Far East Division, Russian Academy of Sciences, Petropavlovsk-Kamchatsky, Russia*
Wörner G., gwoerner@gwdg.de. *GZG Abteilung Geochemie, Universität Göttingen, Germany.*
Eichelberger J., jeichelberger@usgs.gov, *University of Alaska Fairbanks, Department of Geology and Geophysics Reichardt Building, Alaska, U.S.A. Currently at: U.S. Department of the Interior, U.S. Geological Survey, Office of Communication, 119 National Center, Reston, Va., 20192, USA*
Browne B., bbrowne@fullerton.edu, *Department of Geological Science, California State University, Fullerton, CA, USA*
Izbekov P., pavel@gi.alaska.edu, *Geophysical Institute, University of Alaska, Fairbanks, AK, USA*

The data on the geochemistry of the rocks of Kizimen Volcano and results of microprobe studies of major and trace elements in plagioclase grains from acid lavas and basalt inclusions are presented. The characteristics of the Kizimen Volcano are the following: (1) basalt inclusions are abundant in acid lavas; (2) banded, mixed lavas occur; (3) the distribution curves of rare-earth elements of acidic lavas and basalt inclusions intersect; (4) Sr–Nd isotope systematics of the rocks and inclusions do not indicate mixture with crustal material; (5) plagioclase phenocrysts are of direct and reverse zonation; (6) olivine and hornblende, as well as acid and mafic plagioclases, coexist in the rocks. The studies revealed that the rocks are of a hybrid nature and originated in the course of repeated mixture of acid and mafic melts either with chemical and thermal interaction of melts or exclusively thermal ones. Study of the major- and trace-element distribution in zonal minerals provides an informative tool for understanding the history of the generation and evolution of melts in a magma chamber (Fig. 1.2.2.3.1).

Based on textural evidence from plagioclase growth zones and major, minor and trace element contents, we conclude that:

1) All rocks of Kizimen volcano, including mafic enclaves, are hybrids and represent mixture of mafic and acid endmembers in different proportions. These end-members are likely to be derived melts from the same parental melt by crystal fractionation including amphibole.

2) The unusual negative correlation of Mg with An in high-An plagioclase can be explained by fractional crystallization of the high-Al basalt with Pl-only fractionation or by nonlinear behavior of Kd_{Mg} in Pl-melt system.
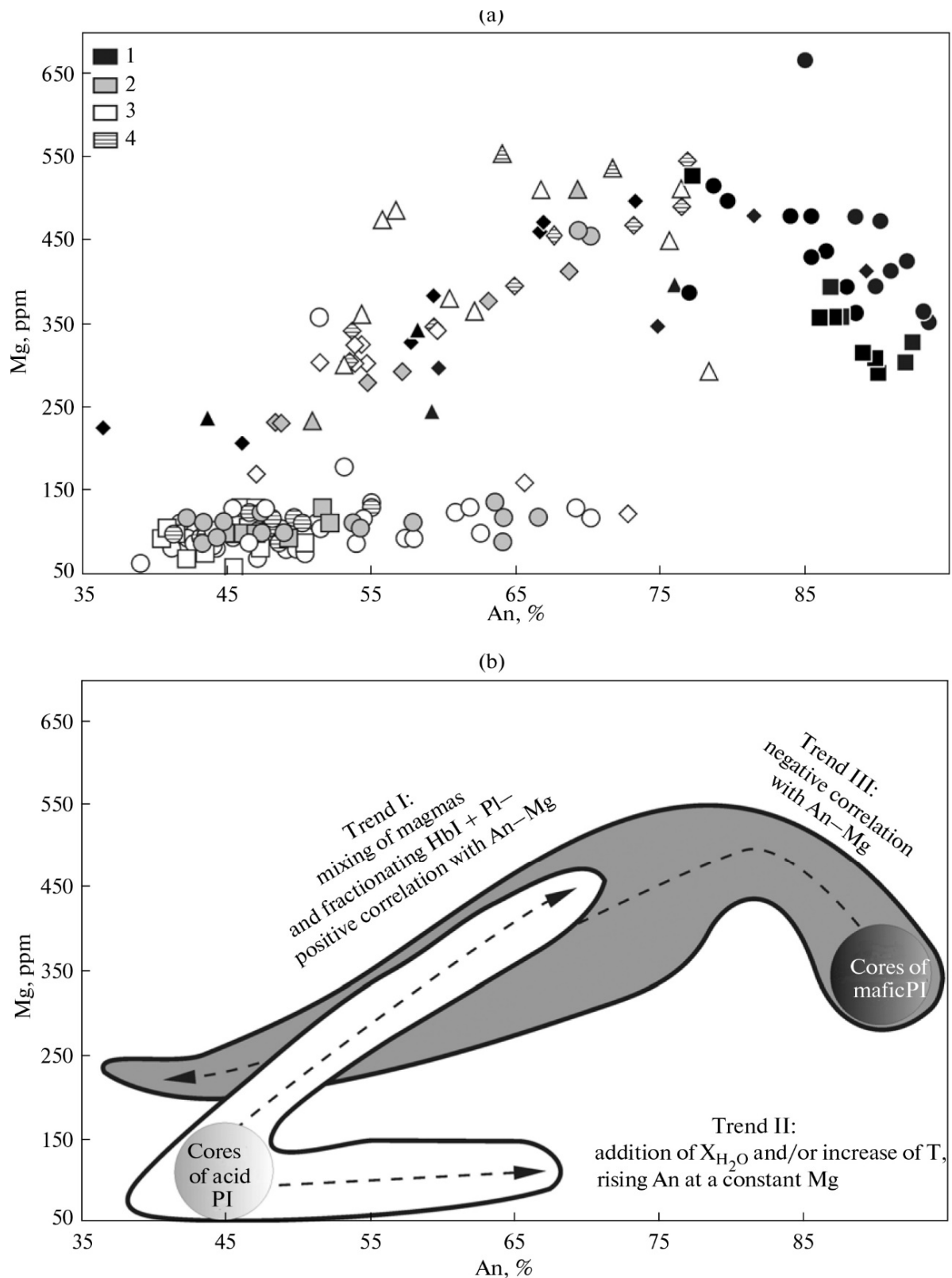
Fig. 1.2.2.3.1. A diagram of the Mg content in plagioclase versus its An number (a). The symbol shape designates the positions of points inside a crystal: squares denote the center, circles denote intermediate zones, diamonds denote rims, and triangles denote microlites. (1) Pl-1 from mafic inclusions; (2) Pl-2 from mafic inclusions; (3) Pl-1 from host dacite lava; (4) Pl-2 from host dacite lava. The scheme of crystal evolution is shown by arrows from the centers to the margins of the grains (b). The gray fields correspond to high-An (mafic) plagioclases from basalt and basaltic andesite inclusions in lavas; the white fields show the evolution of low-An (acid) plagioclases from both lavas and their inclusions.

3) Incomplete mixing maintains the physical identity of distinct, though somewhat hybridized, end-members. While (incomplete) chemical mixing is abundant, we also observe evidence for the transport of heat (or increased water content) only in the variation of An content in plagioclase at constant trace element concentrations.

4) The trend within mafic enclaves toward more mafic compositions with time at Kizimen indicates that generation (by fractional crystallization) of the evolved dacite is not keeping pace with mafic recharge and outputs are likely directly triggered by inputs.

Using petrological experiments, an investigation of the pre-eruptive conditions (T, P and fO_2) of dacite magma erupted during the KZI cycle (12,000–8,400 years ago) of Kizimen Volcano was achieved. This cycle is the earliest, most voluminous, and most explosive eruption cycle in the Kizimen record. Titanomagnetite-ilmenite geothermometry calculations require that the dacite existed at a temperature of 823 ±20°C immediately prior to eruption. Hydrothermal, water-saturated experiments on KZI dacite pumice reveal that at those temperatures the dacite was stable between 125-150 MPa. This estimate corresponds to a structural discontinuity between Miocene volcaniclastic rocks and Pliocene-Pleistocene volcanic rocks at a depth of 5-6 km beneath the Kizimen edifice, which may have facilitated the accumulation of dacitic magma below Kizimen during the KZI cycle.

Browne, B., Izbekov, P., Eichelberger, J., & Churikova, T. (2010). Pre-eruptive storage conditions of the Holocene dacite erupted from Kizimen Volcano, Kamchatka // International Geology Review, 52(1), 95-110. Doi: 10.1080/00206810903332413
Churikova, T. G., Ivanov, B. V., Eichelberger, J., Wörner, G., Browne, B., & Izbekov, P. (2013). Major and trace element zoning in plagioclase from Kizimen Volcano (Kamchatka): Insights into magma-chamber processes. Journal of Volcanology and Seismology, 7(2), 112-130. Doi: 10.1134/S0742046313020024

1.2.3. Geophysical investigations of the Klyuchevskaya Group of volcanoes

1.2.3.1. Nuclear-geophysical investigations of thermal areas in the Nalychevo

Firstov P.P., *Kamchatkan Branch of Geophysical Survey RAS, Petropavlovsk-Kamchatsky, Russia*
Rashidov V.A., *Institute of Volcanology and Seismology FEB RAS, Petropavlovsk-Kamchatsky, Russia*
Melnikova A.V., Shulzhenkova V.N., *Kamchatka Bering State University, Petropavlovsk-Kamchatsky, Russia*

In July 2010 the scientists from Kamchatkan Branch of Geophysical Survey RAS, Institute of Volcanology and Seismology FEB RAS and students from Kamchatka Bering State University carried out geomagnetic and nuclear-geophysical investigations at two thermal travertine areas: young – «Kotel» and modern anthropogenic – «Grifon Ivanova». The thermal areas are located in the valley of the Goryachaya River being the part of the 15-20 thousand years old Nalychevo hydrothermal system. The thermal waters of Nalychevo hydrothermal system are carbonaceous sodium-chloride with high concentration of arsenic and boron. The thermal travertine area «Kotel» was named for travertine dome, and thermal area «Grifon Ivanova» was given that name because of an anthropogenic grifon, named after the soviet hydrogeologist V.V. Ivanov. The thermal area «Kotel» is ~ 180×200 m, and the thermal area «Grifon Ivanova» is 90×100 m. In each of 501 observation points the vector magnitude of magnetic inductance, magnetic susceptibility and the dose rate of γ-radiation were sequentially measured. Volumetric activity of Rn in subsoil air was measured in 73 boreholes. Geomagnetic research revealed that travertine dome «Kotel» is located within the zone of negative magnetic field (ΔT)a. The map of magnetic susceptibility shows zonal

distribution of various types of sediments. The maximum value of magnetic susceptibility in the south-western and east-southeastern parts of the travertine area «Kotel» coincide with those from the anomalous magnetic field. Laboratory analysis of sampled rocks revealed that travertines are almost non-magnetic rocks. 2.5D magnetic modeling showed that within the thermal area «Kotel» that cause anomalies are located at the depth of 15-25 m in argillic and detritus-pebbly sediments. Research revealed that local anomalies of γ-radiation with values 20-30 mR/hr were caused by high radium concentration which deposited in travertine cover in zones of unloading of thermal waters. The authors also detected volumetric activity of Rn that reached 78.6 kBq/m^3 in the subsoil air. High values were caused by both emanating collectors with high concentration of Ra and fracture zones. Numerous travertine formations, as cup-shaped so dome-shaped, revealed within the thermal area «Kotel» are located along radiating cracks observed both in relief and in geophysical fields. We didn`t reveal significant anomalies of magnetic field (ΔT)a produced by natural source within the thermal area «Grifon Ivanova». Anomaly, observed on Grifon Ivanova, is caused by casing tube and with iron-rich rocks modified by hydrothermal influence developed in zone of the borehole. Anomalies with γ-radiation at the thermal area «Grifon Ivanova» stretch northeastward. There are two local anomalies with values 8-10 mR/hr: the first is located within the Grifon`s zone; another is about 90 m away from it. We suppose that this is a zone where radium-bearing minerals deposit into evolving modern travertine cover. Studied thermal areas are ideal natural laboratory for various 4D surveys which are currently developing at the hydrothermal regions.
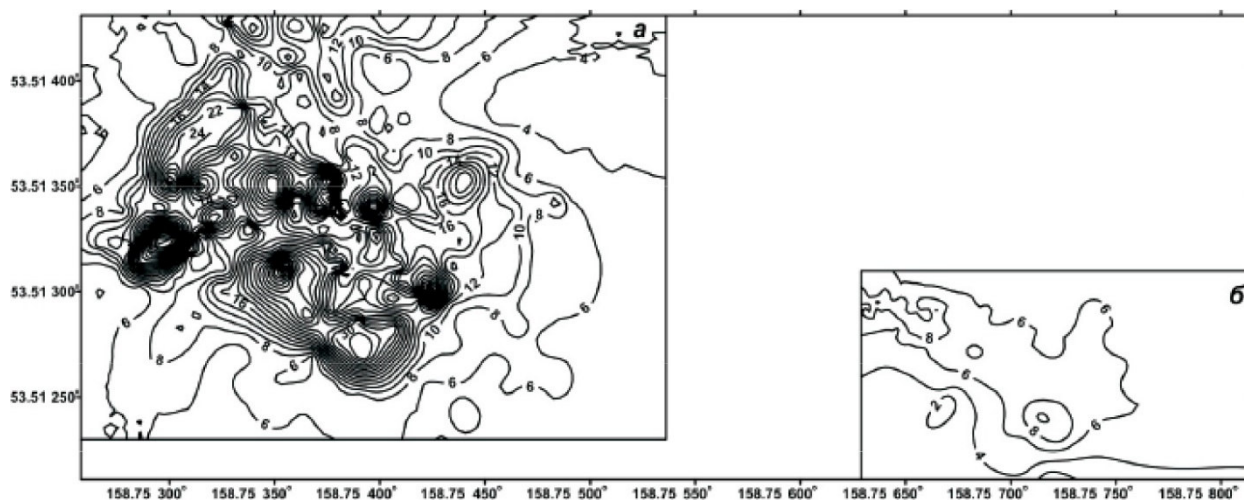
Fig. 1.2.3.1.1. Gamma-field levels map of the thermal area «Kotel» (a) and the thermal area «Grifon Ivanova» (b), μR/h.

Firstov, P. P., Rashidov, V. A., Melnikova, A. V., Andreev, V. I., & Shulzhenkova, V. N. (2011). Nuclear-geophysical investigation in Nalychevo nature park, Kamchatka. Bulletin of Kamchatka regional association "Educational-Scientific Center". Earth sciences, 1(17), 91-101. (In Russian). http://www.kscnet.ru/kraesc/2011/2011_17/art8.pdf

Firstov, P. P., Rashidov, V. A., Melnikova, A. V., Andreev, V. I., & Shulzhenkova, V. N. (2011). Geomagnetic and nuclear-geophysical investigations of thermal travertine areas in the Nalychevo hydrothermal system, Kamchatka. 7th Biennual Workshop on Japan-Kamchatka-Alaska Subduction Processes: Mitigating Risk Through International Volcano, Earthquake, and Tsunami Science. JKASP-2011. Petropavlovsk-Kamchatsky, Russia. August 25-30, 2011. Abstracts. – Petropavlovsk-Kamchatsky: Institute of Volcanology and Seismology FEB RAS, Kamchatkan Branch of Geophysical Service RAS, 294-297, http://www.kscnet.ru/ivs/slsecret/jkasp_2011/abstr/abs134.pdf

1.2.3.2.   The deep structure of the southern Kamchatka volcanic zone

Moroz Yu.F., morozyf@kscnet.ru, **Samoilova O.M.** *Institute of Volcanology and Seismology FEB RAS, Petropavlovsk-Kamchatsky, Russia*

We discuss the interpretation method and results of magnetotelluric soundings in combination with other geological and geophysical data. The interpretation method was developed by studying possible distortions in MTS curves using 3D-numerical modeling of the magnetotelluric field. Deep conductivity was studied by using longitudinal MTS curves below a period of 400 s, which are nearly unaffected by the induction effect due to marine electrical currents. Transverse curves were used to obtain more detail for the geoelectric model. Inversion of average longitudinal MTS curves resulted in a geoelectric section of the lithosphere down to a depth of 60 km. Anomalies of high conductivity in the lithosphere were detected and were found to produce certain effects in gravity and seismic velocities. MTS and seismic tomography data were used to determine the possible origin of the high conductivity anomaly and to estimate rock porosity and the concentration of magma melts.

Moroz, Y. F., & Samoilova, O. M. (2013). The deep structure of the southern Kamchatka volcanic zone from geophysical data. Journal of Volcanology and Seismology, 7(2), 99-111. Doi: 10.1134/S074204631302005X

1.2.3.3. Application of georadar profiling (GPR) at Kamchatka region

Pavlova V.Yu., Lungun O.A., Konstantinova T.G. *Vitus Bering Kamchatka State University (KamGU), Petropavlovsk-Kamchatsky, Russia*
Delemen I.F., delemen@kscnet.ru, *Institute of Volcanology and Seismology FEB RAS, Petropavlovsk-Kamchatsky, Russia*

GPR is one of the recent and fast developing methods of control of ground conditions. This method useful tool to solve series of engineering-geological problems, which is very actual for Kamchatka with volcanic deposits, earthquake deformations and numerous engineering-geological problems. *Institute of Volcanology and Seismology FEB RAS in cooperation with Vitus Bering Kamchatka State University (KamGU)* use this method to predict natural hazards in most populated areas of the Kamchatka Peninsula, especially around Petropavlovsk-Kamchatsky city.

Another application of GPR at Kamchatka is connected to observation of the caprock on geothermal power stations such as Mutnovsky geothermal power station. The study of caprock of any geothermal deposits is the most important task of geothermic geology which helps to use use natural heat more effectively. This method is very useful as on the stage of exploration drilling of the geothermal reservoir as well as during geophysical detalization of the geothermal deposits.

Pavlova V.Yu., Delemen I.F. (2014). Georadar investigations of zone of discharge of thermal water at the site Karymshinskii hydrothermal system (Kamchatka) Volcanism and related processes. Annual regional scientific conference dedicated to the Volcanologist Day. Proceedings of the conference. March 27-28, 2014, Petropavlovsk-Kamchatsky. Petropavlovsk-Kamchatsky: Institute of volcanology and seismology FED RAS, 214–220. (In Russian). http://www.kscnet.ru/ivs/publication/volc_day/2014/art34.pdf
Lungul, O. A., Pavlova, V. Yu. (2012). Clarification of seismic conditions and landslide hazard at the site of treatment facilities at Chavycha cape (Chavycha cape, Kamhatka Peninsula). Research in the field of Earth sciences. Materials of the X regional youth conference, November 28-29, 2012. Petropavlovsk-Kamchatsky: IVS FEB RAS, 85-100. (In Russian). http://www.kscnet.ru/ivs/publication/young_conf/2012/1/art8.pdf

1.2.4. Geochronology of the Eastern volcanic front

1.2.4.1. Multi-cyclic magma generation in Gorely eruptive center

Seligman A., Bindeman I., Geological Sciences, 1272 University Of Oregon, Eugene, OR 97403, USA

Jicha B., Department Of Geoscience, University Of Wisconsin-Madison, Madison, WI 53706, USA

Ellis B., Institute Of Geochemistry and Petrology, Department Of Earth Sciences, Eth Zurich, Switzerland

Ponomareva V., Leonov V., *Institute of Volcanology and Seismology, Far East Division, Russian Academy of Sciences, Petropavlovsk-Kamchatsky, Russia*
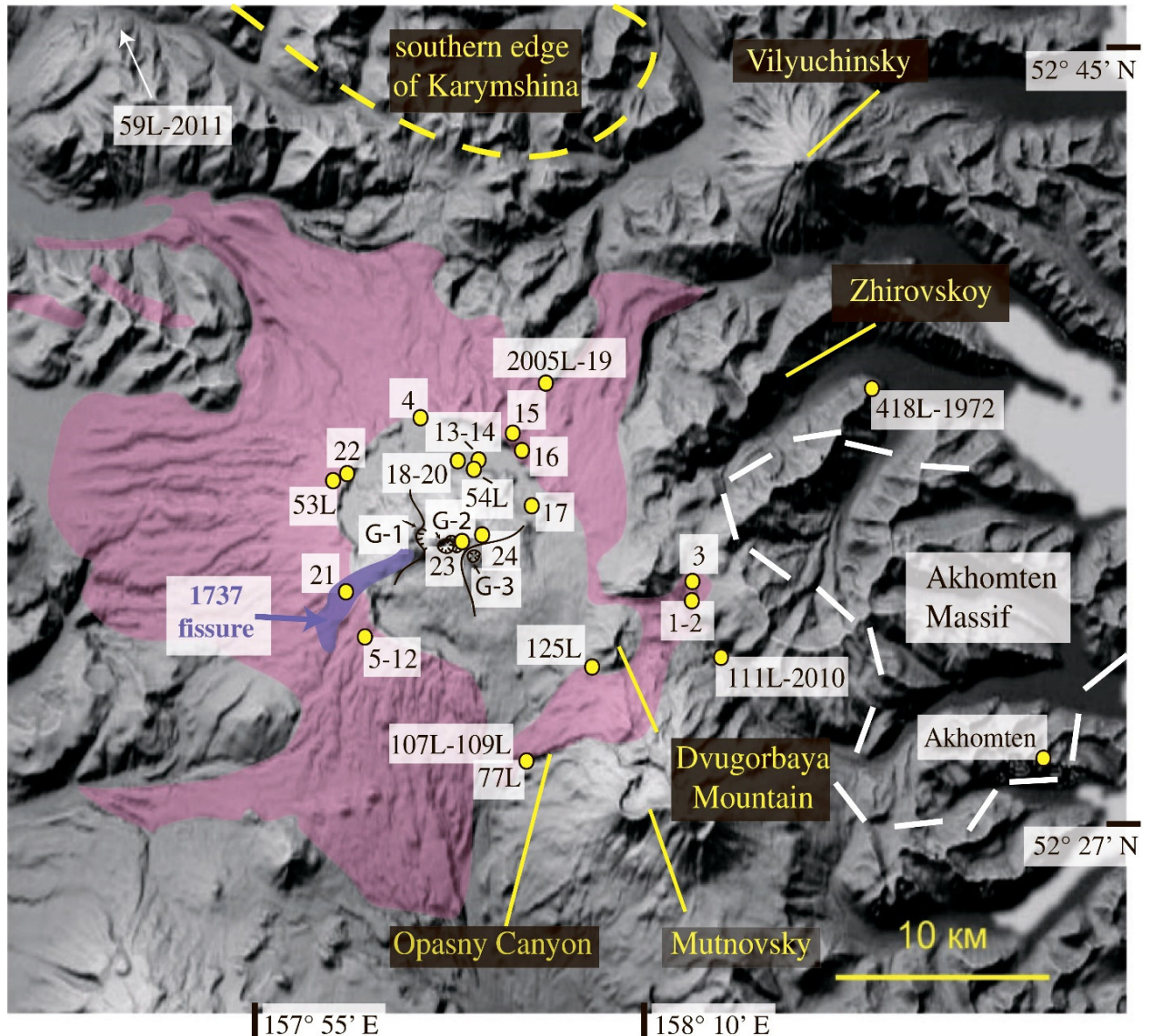
Fig. 1.2.4.1.1. Digital elevation map of Gorely volcano and its surrounding caldera, showing the extent of the ignimbrites and pumice, which are described in this study (shaded in pink), and the location of the studied samples. The sample names have been abbreviated (e.g. '11G-3' is written as '3', and '77L-144' is written as '77L'). The locations of Opasny Canyon, Mutnovsky volcano, Zhirovskoy volcano, Dvugorbaya Mountain, and Vilyuchinsky volcano are indicated. White dashed lines denote outcrops of the Akhomten Massif, and yellow dashed lines denote the extent of the southern edge of the Karymshina caldera. G-1, G-2, and G-3 refer to the Gorely-1, Gorely-2, and Gorely-3 cones, respectively.
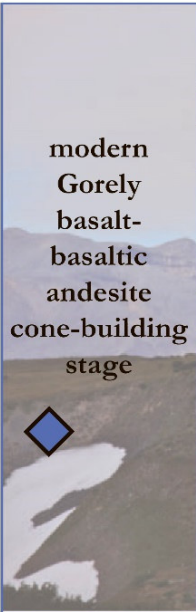
modern Gorely basalt-basaltic andesite cone-building stage (◆)	18th century fissure eruption (11G-21)
	11G-12 (~0.8 ka tephra)
	11G-23 (~1.5 ka lava)
	~2 ka lavas (11G-24, 11G-4, 07L-54)
	11G-20 (~4 ka tephra)
	11G-19 (~5 ka tephra)
	~7 ka lavas and tephras (11G-18, 11G-17, 11G-14, 11G-13, 11G-7)
	~8 ka tephras (11G-10, 11G-9, 11G-8)
	lava of early monogenetic cone (~20 ka; 11G-5)
(●)	late dacite ignimbrite eruption (~38 ka) (77L-144, 11G-3a/b, 07L-53)
	gap in dated material
early dacite ignimbrite eruptions (●)	109L-2010 (227±19 ka; $^{40}Ar/^{39}Ar$)
	125L-2000 (~227 ka)
	11G-1/2 (~300 ka)
	107L-2010 (332±6 ka; $^{40}Ar/^{39}Ar$)
	2005L-19 (361±8 ka; $^{40}Ar/^{39}Ar$) (Bindeman et al., 2010)
(▲)	pra-Gorely dacite lavas (~700 ka) (11G-6, 11G-15, 11G-16)
	Zhirovskoy basalt-andesite lava flows (0.7–0.8 Ma) (Sheimovich & Karpenko, 1996)
(□)	Karymshina rhyolite Ignimbrites (~1.8 Ma) (Bindeman et al., 2010)
(×)	nearby 4 Ma Qtz-biotite rhyolite Tuffs (111L-2010, 418L-1972, 59L-11)
(+)	Akhomten Granite Massif (89L-19; 11.2 Ma; U-Pb)
	Achaivayam-Valaginsky Arc (45-50 Ma) (Soloviev et al., 2002a, 2002b; Hourigan et al., 2009; Konstantinovskaya, 2003)
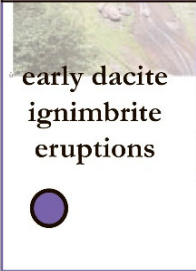
Fig. 1.2.4.1.2. Section illustrating the volcanic stratigraphy below Gorely volcano. Symbols and colors for each layer, where appropriate, are the same as those used in subsequent figures. The image behind the modern Gorely stage shows the current Gorely cone, with steam emanating from the top. The image behind the ignimbrite series shows the sampling location in Opasny Ravine.

The Kamchatka Peninsula is home to some of the most frequent and prolific subduction related volcanic activity around the world, with the largest number of caldera-forming eruptions relative to the size of the volcanic arc. Gorely volcano, located behind the currently active Eastern Volcanic Front, has a topographically prominent Late Pleistocene caldera (13 x 12 km - estimated to have produced >100km^3 of magma), which is now almost completely filled by a central cone.

We report new 40Ar/39Ar ages and geochemical and isotopic characteristics of newly recognized Mid-Pleistocene ignimbrite units of large but unknown volume sourced from the Gorely eruptive center. These ignimbrites have crystallinities of 9 to 24% and most are quartz-, amphibole-, and zircon-undersaturated. Additionally, we studied 32 eruptive units, including tephrochronologically-dated Holocene tephra, and pre- and post-caldera lava sequences, to understand the petrogenetic and temporal evolution of this long-lived arc volcano. Materials erupted prior to those that formed the modern Gorely edifice, including the voluminous ignimbrites and eruptions of the "pra-Gorely" stage, consist primarily of dacite, while sequences of the modern Gorely edifice are represented by basalt to basaltic andesite. MELTS modeling shows it is possible to obtain silicic compositions near those of the evolved ignimbrite compositions, strictly through 60-75% fractional crystallization at 1 kbar and NNO oxygen fugacity. However, newly compiled major element compositions for Gorely yield two separate bimodal peaks in our SiO2-frequency diagram, showing a prominent Daly-gap, with a deficiency in andesite. Trace element concentrations and ratios define two parallel trends, one for more silicic and another for more mafic sequences, indicating different parental melts. Additionally, delta18Omelt values reconstructed from coexisting plagioclase and clinopyroxene phenocrysts range from a low value of 4.85 ‰ to a normal value of 6.22 ‰, with low values ranging throughout the known lifespan of Gorely and the lowest value being from the first known ignimbrite to erupt, indicating episodic but temporally decreasing crustal assimilation of previously hydrothermally-altered material. 87Sr/86Sr and 143Nd/144Nd isotopic ratios range from 0.70328 to 0.70351 and 0.51303 to 0.51309 respectively, also suggesting incorporation of surrounding crust, although these trends are random throughout the lifespan of Gorely. The combination of light and diverse delta18O values as well as elevated 87Sr/86Sr and low 143Nd/144Nd ratios, and the bimodal nature of erupted material suggest derivation from older and isotopically diverse, low-delta18O country-rocks, such as the neighboring 11 Ma Akhomten granitic Massif, which shows prominent ranges in delta18O, 87Sr/86Sr, and 144Nd/143Nd values overlapping with Gorely magmas. In addition, the presence of glomerocrysts and mafic enclaves in the majority of Gorely thin sections indicate a period of crystal settling and subsequent intrusion of hot, primitive basalt that likely triggered an eruption. Finally, elevated Nb concentrations suggest these magmas are not sourced strictly through subduction, and may involve a decompression component, likely caused by delamination. Our results argue against a long-lived batholithic scale magma body under Gorely, and rather demonstrates an incremental view of silicic magma generation at so-called "long-term eruptive centers" consisting of magmatic and hydrothermal activity in Kamchatka and worldwide. We demonstrate that large volume (10-100 km^3 per eruption) isotopically distinct silicic magma can be generated rapidly between largely cone-building phases of volcanic activity through a combination of delamination, fractional crystallization, assimilation of older country rocks, shallow crustal assimilation of hydrothermally altered but otherwise similar older material. These transient shallow silicic magma chambers empty nearly completely in ignimbrite eruptions after 103-105 years of assembly.

Seligman, A., Bindeman, I., Jicha, B., Ellis B., Ponomareva, V., & Leonov V. (20140. Multi-Cyclic and Isotopically-Diverse Silicic Magma Generation in an Arc Volcano: Gorely Eruptive Center, Kamchatka, Russia. Journal of Petrology, 55(8), 1561-1594. Doi: 10.1093/petrology/egu034

1.2.5. Geological studies of the Eastern volcanic front

1.2.5.1. Aerial photogrammetric monitoring

Dvigalo V.N., dvig@kscnet.ru, *Institute of Volcanology and Seismology, Far East Division, Russian Academy of Sciences, Petropavlovsk-Kamchatsky, Russia*
**Shevchenko A.V.,** shevchenko@kscnet.ru**, Svirid I.Yu.,** svirid@kscnet.ru, *Institute of Volcanology and Seismology, Far East Division, Russian Academy of Sciences, Petropavlovsk-*

Kamchatsky, Russia. Vitus Bering Kamchatka State University, Petropavlovsk-Kamchatsky, Russia

Aerial photogrammetric monitoring of the active volcanoes of Kamchatka has been carrying out at the Institute of Volcanology FESC USSR and the Institute of Volcanology and Seismology FEB RAS since 1973. Our team performs the entire work cycle: aerial photo survey, stereophotogrammetric processing of the photographic material, building the Digital Terrain Models and creating specialized topographic maps and plans. The photogrammetric processing of the aerial photographs provides high accuracy of the obtained qualitative and quantitative characteristics of the active volcanic objects. Using this method we can also estimate the effect of eruptions and detect their precursors. The majority of the studied objects now is too dangerous for direct observations due to high eruptive activity, therefore, the remote sensing, in particular photogrammetry, is the most appropriate way of monitoring them.

Maly Semyachik Volcano

We have studied the Troitsky crater of Maly Semyachik Volcano using photogrammetric processing and interpretation of data from aerial imagery since 1946 and 1950. We used all available data from aerial survey and previous investigations, which resulted in rather detailed morphodynamic analysis. We have obtained the precise morphometric characteristics of the crater and revealed new parameters of the crater lake. Over the period 1950–2012 the water level of the lake increased by 53.3 m (Fig. 1.2.5.1.1.). The processing of the most detailed aerial images allowed us to estimate the volume of scree material from the crater's inner walls. Over the period 1968–2012 the volume of the scree material comprised up to 17 % of the lake's increasing volume.
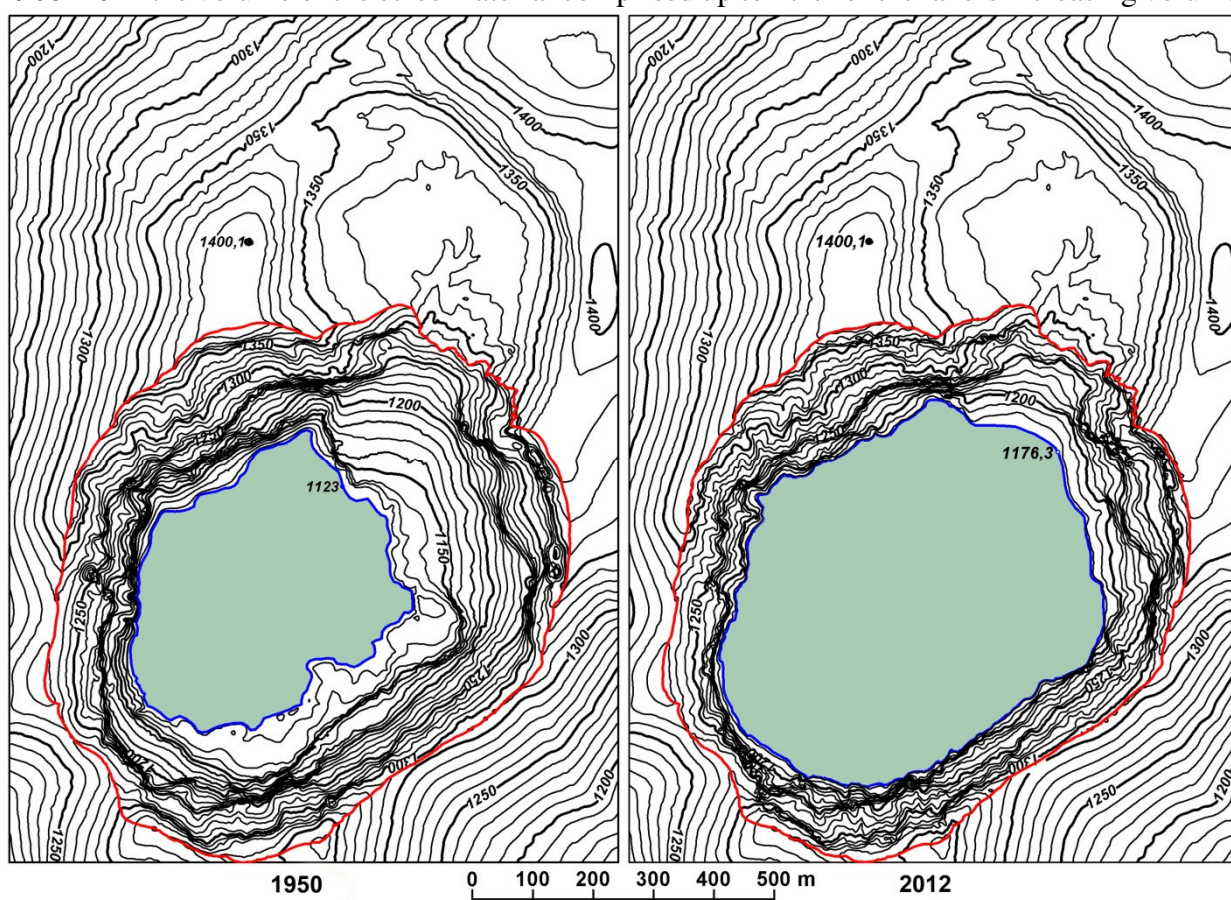
Fig. 1.2.5.1.1. Topographic maps of Troitsky crater of Maly Semyachik Volcano.

We find out lack of reliable data on explosive activity at Maly Semyachic Volcano over 1945–1946. The crater lake was formed in early 40s of the 20th century inside the already existing crater, which had been formed rather due to collapse-subsidence processes than as a result of previously suggested explosive processes of more than 400 years ago.

The investigation also revealed a possible inverse correlation between the activity of Maly Semyachik and Karymsky volcanoes.

Svirid, I. Yu., Shevchenko, A. V., & Dvigalo, V. N. (2013). Investigation of Maly Semyachik Volcano (Kamchatka) activity using morphodynamic data from the Troitsky crater. Bulletin of Kamchatka regional association "Educational-Scientific Center". Earth sciences, 2(22), 129-143. (In Russian). http://www.kscnet.ru/kraesc/2013/2013_22/art12.pdf

Svirid, I. Yu., & Shevchenko, A. V. (2013). Formation of the Troitsky crater and Zelyonoye lake at Maly Semyachik Volcano (Kamchatka). Materials of the XI regional youth conference, November 26, 2013. Petropavlovsk-Kamchatsky: IVS FEB RAS, 67-76. (In Russian). http://www.kscnet.ru/ivs/publication/young_conf/2013/1/art5.pdf

The Valley of Geysers

Over the past 33 years three mud flows have occurred at the Valley of Geysers in Kamchatka: October 4, 1981; June 3, 2007, and January 3-4, 2014. We defined the morphometric parameters of these mud flows. Viktor Dvigalo has made a precise prediction of the place of formation of the January, 3-4, 2014 mud flow. We suggested that mud flow hazard in the Valley of Geysers is underestimated: if people were on the walking rout, that was covered with the January, 3-4, 2014 mud flow, fatalities would have been inevitable. At the present time the most hazardous is the new dammed lake, which was formed by the damming of Geysernaya river with the January, 3-4, 2014 mud flow deposits. The risk of fatalities for the tourists becomes very high.

Dvigalo, V. N., Svirid, I. Yu., Shevchenko, A. V., & Jarkov, R. V. (2014). Mud flows in the Kamchatkan Valley of Geysers: monitoring and prediction based on photogrammetric research. III International Conference «Debris Flows: Disasters, Risk, Forecast, Protection»: proceedings, Yuzhno-Sakhalinsk, September 22–26, 2014. *Yuzhno-Sakhalinsk: Sakhalin Department of Far East Geological Institute FEB RAS, 101-104. (In Russian).* http://debrisflow.fegi.ru/ru/proceedings.pdf

1.2.5.2. Thermohydrodynamic modelling of the Valley of Geysers

Kiryukhin A.V., *avk2@kscnet.ru*, **Rychkova T.V.,** *Institute of Volcanology and Seismology, Far East Division, Russian Academy of Sciences, Petropavlovsk-Kamchatsky, Russia*

The formation of the hydrothermal system in the Valley of Geysers is shown to be governed by a structure of radial and circular faults of above-intrusion zone of a partially melted magmatic body with an epicenter near the Upper-Geyser Field, while the hydrothermal system is shown to receive its water from elevations of +500 to +900 m abs (according to isotopic data). The catastrophic landslide of June 3, 2007, was just a stage in the general scenario of the gradual hydrothermal transformation of the inclined Geyser unit (Q 34grn), building up the roof of the hydrothermal reservoir, with a gradual decline of slide resistance. The slide was triggered by the increased pressure in the hydrothermal and magmatic systems and the saturation of the Geyser unit by moisture during spring flood. According to the data of continuous regime thermohydrodynamic observations carried out in the Valley of Geysers with the use of HOBO-loggers of temperature and pressure since July 2007 to April 2010, the mean time between eruptions of Velikan geyser was 348 minutes. The intensification of precipitation input directly into the geyser pool causes a

short-time increase in the time between eruptions (up to the maximum of 32 h). According to observations at the "Plotina" gage, the total estimated mean annual discharge of thermal springs (by chlorine ion) in the Valley of Geysers is 263 kg/s; the discharge of thermal springs is governed by the level of Poldprudnoe Lake and its seasonal variations exceed 40%.
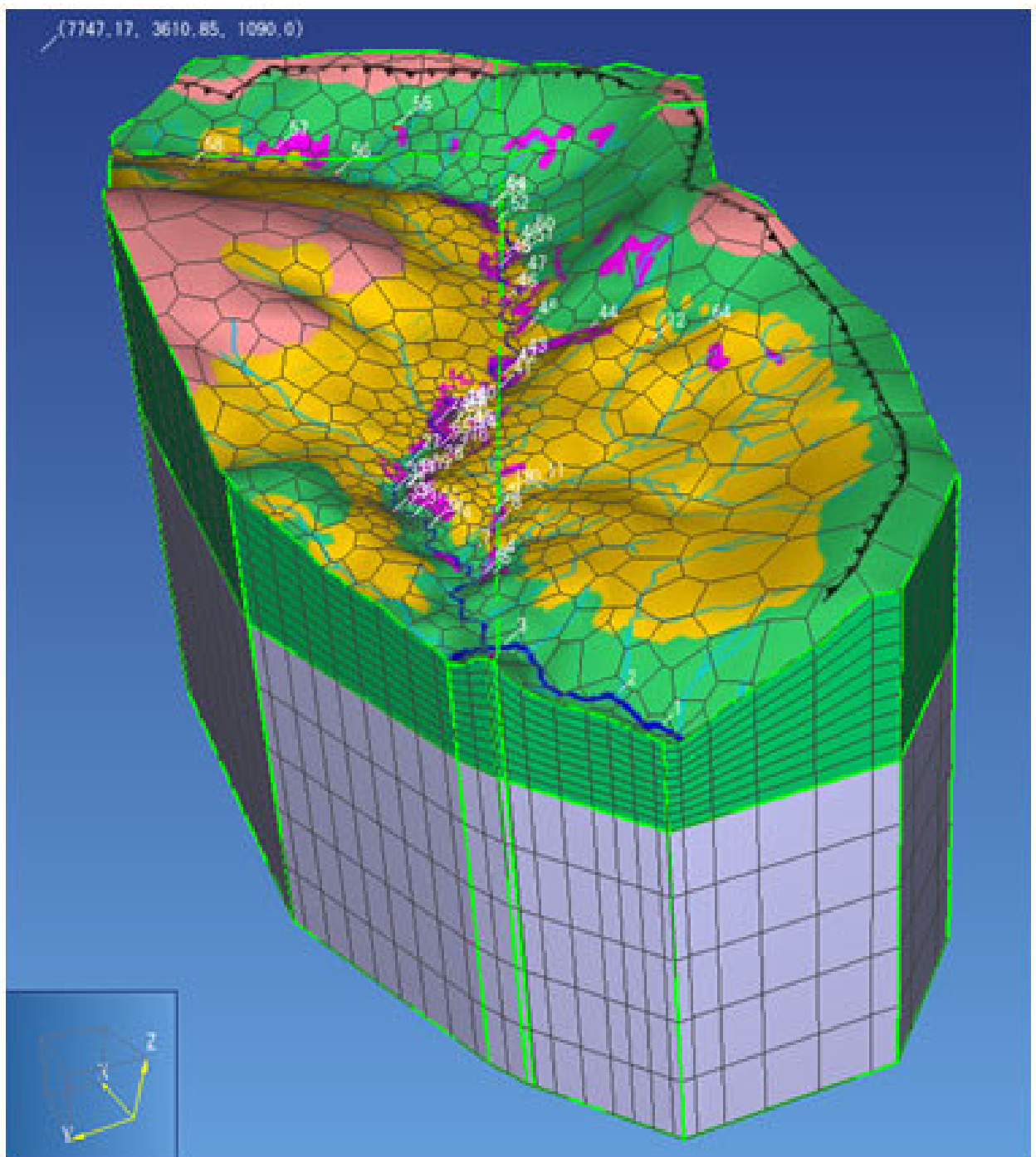
Fig. 1.2.5.2.1. Geometry of model and computational grid for thermohydrodynamic modelling of the Valley of Geysers.

Kiryukhin, A. V., & Rychkova, T. V. (2012). Functioning of natural and natural-engineering systems formation conditions and natural state of the hydrothermal system in the Valley of Geysers (Kronotsky Nature Reserve, Kamchatka). Water Resources, 39(7), 722-736. Doi: 10.1134/S0097807812070056

1.2.5.3.   Numerical simulation of a tsunami in Karymskoe lake

Torsvik T., *Bergen Center for Computational Science, Uni Research, Bergen, Norway*
Paris R., *CNRS-GEOLAB, Clermont-Universit´e, 4 rue Ledru, 63057 Clermont-Ferrand, France*
Didenkulova I., *Laboratory of Wave Engineering, Institute of Cybernetics, Tallinn, Estonia.*
Department of Nonlinear Geophysical Processes, Institute of Applied Physics, Nizhny Novgorod, Russia
Pelinovsky E., *Department of Nonlinear Geophysical Processes, Institute of Applied Physics, Nizhny Novgorod, Russia*
Belousov A., Belousova M., *Earth Observatory of Singapore, Nanyang Technological University, Singapore. Institute of Volcanology and Seismology, Far East Division, Russian Academy of Sciences, Petropavlovsk-Kamchatsky, Russia*

Karymskoe caldera lake is a nearly circular body of water with a diameter of approximately 4 km and a depth of up to 60 m. The sublacustrine, Surtseyan-type eruption in the lake on 2–3 January 1996 included a series of underwater explosions. A field survey conducted the following summer showed signs of tsunami wave runup around the entire coastline of the lake, with a maximum of 29m runup at the north shore near the source of the eruption, and 2–5m runup at locations on the east and south shore far away from the source. The tsunami has been simulated using the numerical long wave model COULWAVE, with input from reconstructed realistic pre-eruption bathymetry. Estimated result for wave runup are of the same order of magnitude as field measurements, except near the source of the eruption and at a few locations where analysis show significant wave breaking.
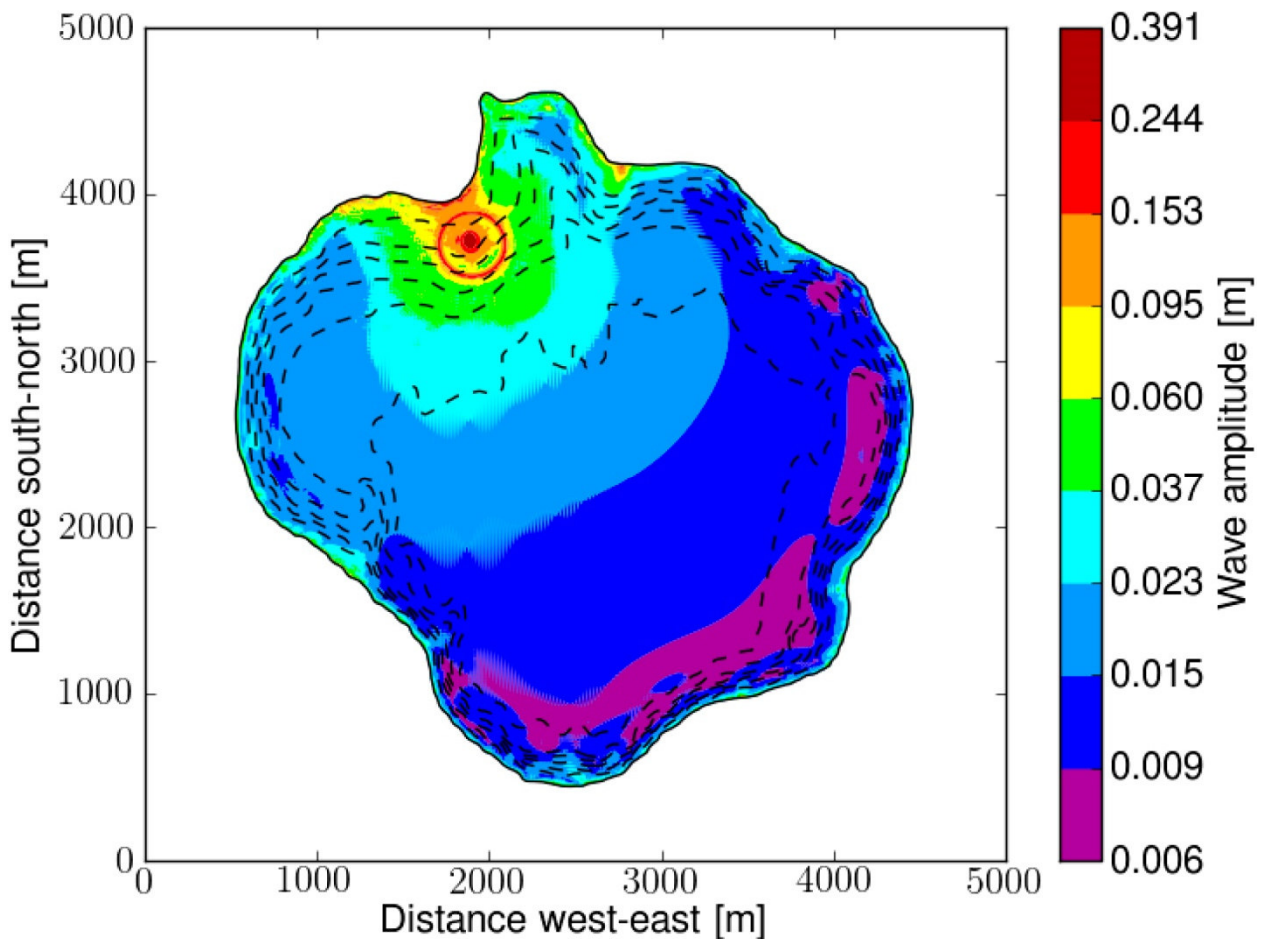
Fig. 1.2.5.3.1. Simulated maximum wave amplitude in Karymskoe lake during the 1996 eruption. The bathymetry is represented by dashed lines, which are drawn at 10 m depth intervals.

Torsvik, T., Paris, R., Didenkulova, I., Pelinovsky, E., Belousov, A., & Belousova, M. (2010) Numerical simulation of a tsunami event during the 1996 eruption in Karymskoye lake, Kamchatka, Russia. Natural Hazards and Earth System Science, 10(11), 2359-2369. Doi: 10.5194/nhess-10-2359-2010

1.2.5.4.   Uzon volcano caldera (Kamchatka): a unique natural laboratory

Kontorovich A.E., Bortnikova S.B., Kashirtsev V.A., Kostyreva E.A., Fomin A.N., *United Institute of Geology, Geophysics and Mineralogy, SB RAS, Novosibirsk, Russia*
Karpov G.A., *Institute of Volcanology and Seismology, Far East Division, Russian Academy of Sciences, Petropavlovsk-Kamchatsky, Russia*

Oil shows from the thermal springs of the Uzon volcano caldera have been studied by gas chromatography–mass spectrometry methods. Based on the composition and distribution of biomarker molecules, their genetic identity with the organic matter of Pliocene–Quaternary deposits has been established. It has been shown that the Uzon caldera is a unique natural laboratory of the present-day oil formation from the organic matter of Pliocene–Quaternary sediments. It has been stated that attempts to consider the compounds forming these oil shows as a product of hydrothermal abiogenic synthesis are absolutely unfounded.

Kontorovich, A. E., Bortnikova, S. B., Karpov, G. A., Kashirtsev, V. A., Kostyreva, E. A., & Fomin, A. N. (2011). Uzon volcano caldera (Kamchatka): A unique natural laboratory of the present-day naphthide genesis. Russian Geology and Geophysics, 52(8), 768-772. Doi: http://dx.doi.org/10.1016/j.rgg.2011.07.002

1.3.   Sredinny Range

1.3.1. Petrological and geochemical studies on the Sredinny Range rocks

1.3.1.1.   Volcanic centres of the Sredinny Range in the back arc of Kamchatka

Flerov G.B., [flerov@kscnet.ru,](mailto:flerov@kscnet.ru) **Koloskov A.V.,** [kolosav@kscnet.ru,](mailto:kolosav@kscnet.ru) **Melekestsev I.V., Puzankov M. Yu.,** puzankov@kscnet.ru, **Filosofova T.M.,** *Institute of Volcanology and Seismology FED RAS, Petropavlovsk-Kamchatski, Russia*
Perepelov A.B., [region@igc.irk.ru,](mailto:region@igc.irk.ru) **Shcherbakov Yu.D.,** [scherb@igc.irk.ru,](mailto:scherb@igc.irk.ru) *Vinogradov Institute of Geochemistry, Siberian Branch, Russian Academy of Sciences, Irkutsk, Russia*

Petrology and mineralogy of the Belogolovsky Massif in Kamchatka's Sredinny Range

The rock associations which represented by several petrochemical series of different alkalities are widely developed among the late Cenozoic volcanic rocks of the Kurile-Kamchatka island arc. These series are characterized by different rock compositions and magmagenesis. The joint manifestation of such series of rocks of different alkalinity was found in Belogolovsky massif of late Pliocene – early Pleistocene age, which is located in the Sredinny Range of Kamchatka. Six rock associations were identified from normal to moderate alkality (Fig. 1.3.1.1.1).
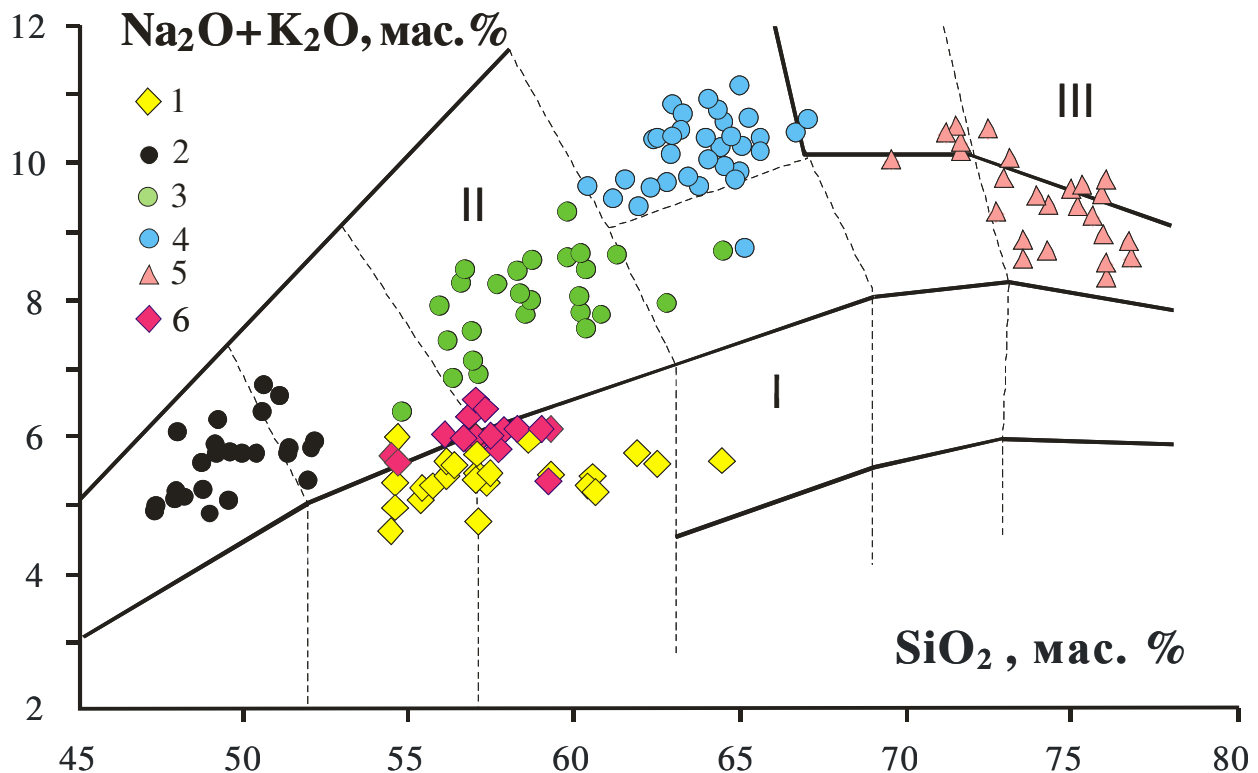
Fig. 1.3.1.1.1. Belogolovsky complex: 1 – basaltic andesites, andesites, dacites; 2 – trachybasalts, basaltic trachyandesites; 3 – trachyandesite, trachydacites; 4 – trachytes; 5 – trachyrhyolites, comendites; 6 – rock of Rassoshina complex. I – a normal alkalinity rock, II – moderately alkaline, III – alkaline.

A geological and petrologic model for the generation of the Belogolovsky Late Pliocene to Early Pleistocene volcanic massif was proposed. The evolution of volcanic products and the mineralogic composition of rocks of varying alkalinities provide evidence that the sources of parent magmas are spatially independent and reside at different depths. We identified two petrochemical series of rocks with varying alkalinities, viz., normal and moderate. Crystallization differentiation is the leading process that is responsible for the generation of the initial melts that give rise to the range of rocks within a series. The magmatic activity at the Belogolovsky massif started from the eruptions of the basaltic magma of normal alkality in geodynamic setting of compression which is typical for the island arc volcanism. The formation of rock with enriched alkalies (intraplate rocks) took place in rift mode. The evolution of the alkaline basaltic magma occurred stepwise, producing autonomous daughter melts with the following compositions: trachybasalt-trachyandesite-trachyte-trachyrhyolite and comendite. These melts were localized in inter-mediate magma chambers at different depths. The magma mixing processes in intracrust magma chambers are responsible for the formation of intermediate rocks.

Flerov, G. B., Perepelov, A. B., Puzankov, M. Y., Koloskov, A. V., Filosofova, T. M., & Shcherbakov, Y. D. (2014). The space-time relationships between volcanic associations of different alkalinities: The Belogolovskii massif in Kamchatka's Sredinnyi Range. Part 1. The geology, mineralogy, and petrology of volcanic rocks. Journal of Volcanology and Seismology, 8(3), 135-155. Doi: 10.1134/S0742046314030026

Kekuknai Volcanic Massif

The evolution of the Quaternary Kekuknai volcanic massif (the western flank of the Sredinnyi Range in Kamchatka) has been subdivided into five stages: (1) the pre-caldera trachybasalt– basaltic andesite, (2) the extrusive trachyandesite–trachydacite, (3) the early trachybasalt, (4) the middle hawaiite–mugearite (with occasional occurrences of basaltic

andesites), and (5) the late trachybasalt–hawaiite–mugearite (with occasional andesites) of areal volcanism (Fig. 1.3.1.1.2). On the basis of petrologic data we identified the island arc and the intraplate geochemical types of rocks in the massif. The leading part in petrogenesis was played by dynamics of the fluid phase with a subordinated role of fractional crystallization and hybridism.
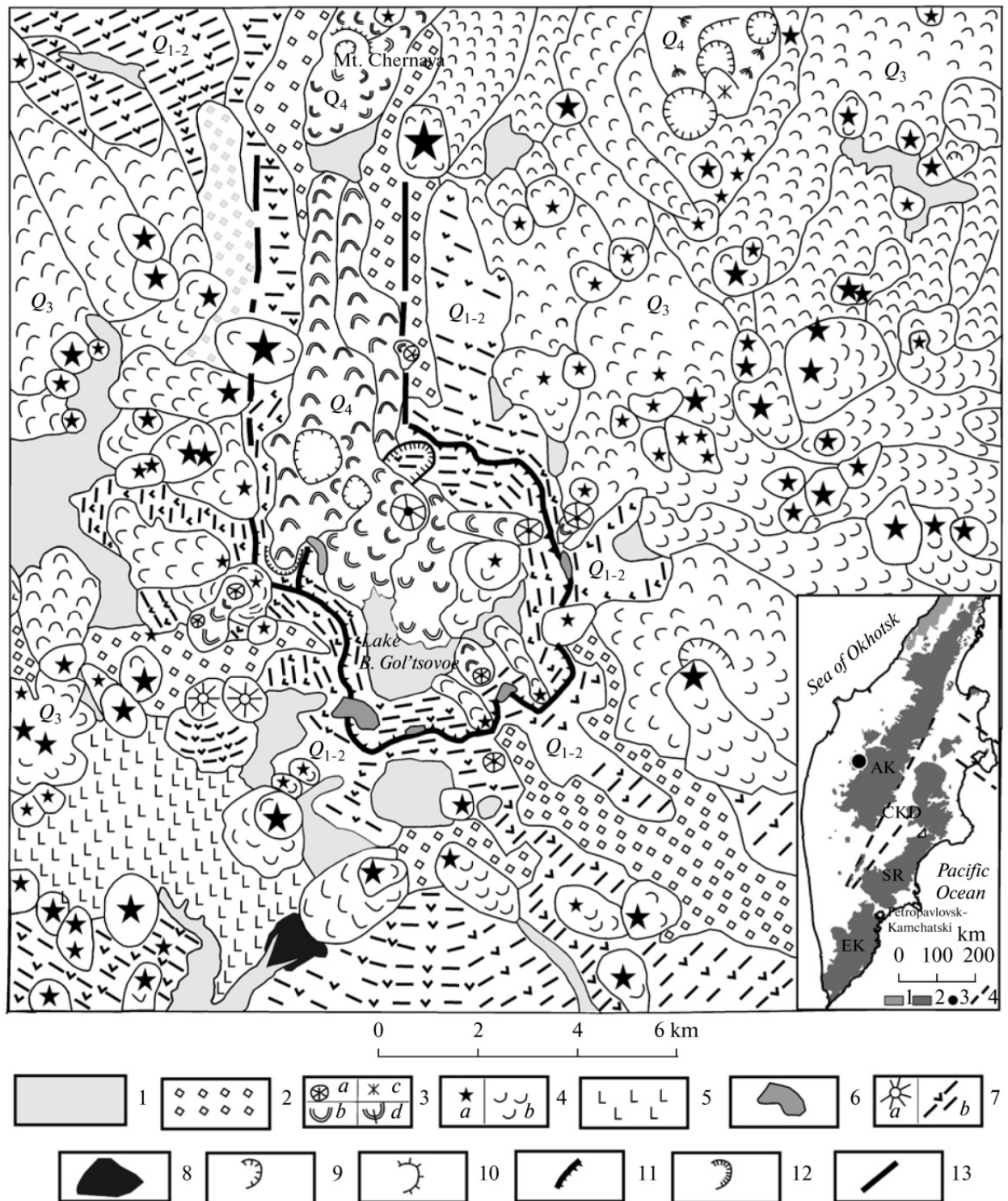
Fig. 1.3.1.1.2. Geological–geomorphological map of the Kekuknai volcanic massif. (1) Accretion deposits of various origins: fluvioglacial, alluvial, lacustrine, etc. (2) moraines of the second phase of Late Pleistocene glaciation (3) eruptive centers (a, c) and flows (b, d) of trachybasalt–andesite, hawaiite–mugearite (a, b) and dacite–rhyolite (c, d) composition of the late stage of Holocene areal volcanism (Q4); (4) eruptive centers (a) and flows (b) of trachybasalt (the early stage of areal volcanism) and hawaiite–mugearite (the middle stage of areal volcanism), of Middle–Late Pleistocene age ( ); (5) plateau basalts of

95

Middle–Late Pleistocene age (Q2 –); (6) trachyandesite–trachydacite extrusions of Early–Middle Pleistocene age (Q1–2); (7) eruptive centers (a) and fragments of destroyed volcanic edifices (b) of trachybasalt–andesite basalt of the pre-caldera stage of Early–Middle Pleistocene age (Q1–2); (8) volcanic rocks of Miocene–Pliocene basement (N1–2); (9) explosive craters, maars, funnels of phreatic explosions on lava flows; (10) volcanic domes; (11) escarp of the volcanic–tectonic caldera; (12) faults, landfalls; (13) inferred faults. Insert: position of the Kekuknai volcanic massif in the map of different-aged volcanic belts of the Kamchatka island-arc system. 1, E1– volcanic belt of western Kamchatka; 2, E3–N1 and N2–Q volcanic belts of Kamchatka (SR, Sredinny Range, SK south and EK eastern Kamchatka; 3, Kekuknai volcanic massif; 4, conventional boundaries of the central Kamchatka depression (CKD) and Aleutian–Kamchatka junction (AK).

Successive saturation of rocks with the fluid phase in the course of melt evolution stopped at the time of caldera generation when most fluid mobile elements and silica had been extracted. The geological and petrologic data attest to the formation of the massif in the environment of a backarc volcanic basin during the beginning of rifting with active participation of mantle plume components.

The Kekuknai massif was formed in the course of tectono–magmatic activity that involved the origin of a shield volcano and a caldera depression with associated emplacement of extrusions that terminated in intense post-caldera areal volcanism. The mineralogical compositions of the massif's rocks have been considered in detail. The use of previously known and newly developed indicator properties of rock-forming minerals allowed the reconstruction of the general picture of the magmatic melt evolution and conditions of rock crystallization (various fluid and water saturation levels, as well as the oxidation state of the system). Essentially island-arc or intraplate characteristics of the massif's rock compositions are found at different stages of development of a single fluid–magmatic system. Decompression evolution of the parent deep-seated basanitic magma occurred via occurrence in intermediate magma chambers of daughter magmas of trachybasalt (pre-caldera stage) or hawaiite (areal volcanism) composition. Subsequent emanate–magmatic differentiation of these melts, combined with crystallization differentiation under changing P–T– conditions, resulted in the formation of the entire diversity of the Kekuknai rocks.

Koloskov, A. V., Flerov, G. B., Perepelov, A. B., Melekestsev, I. V., Puzankov, M. Y., & Filosofova, T. M. (2011). Evolution stages and petrology of the Kekuknai volcanic massif as reflecting the magmatism in Backarc zone of Kuril-Kamchatka island arc system. Part 1. Geological position and geochemistry of volcanic rocks. Journal of Volcanology and Seismology, 5(5), 312-334. Doi: 10.1134/S074204631104004X

Koloskov, A. V., Flerov, G. B., Perepelov, A. B., Melekestsev, I. V., Puzankov, M. Y., & Filosofova, T. M. (2013). The evolutionary stages and petrology of the kekuknai volcanic massif reflecting the magmatism in the backarc zone of the kuril-kamchatka island arc system. Part II. petrologic and mineralogical features, petrogenesis model. Journal of Volcanology and Seismology, 7(2), 145-169. Doi: 10.1134/S0742046313020048

1.3.1.2. Oxygen isotopes and clinopyroxene-melt thermobarometry in Miocene-Quaternary volcanic rocks from Sredinny Range, Kamchatka

Volynets A., a.volynets@gmail.com, *Institute of volcanology and seismology FEB RAS, Petropavlovsk-Kamchatsky, Russia*
Wörner G., gwoerne@gwdg.de, **Przybilla R.,** rprzybi1@gwdg.de, *Geowissenschaftliches Zentrum, Georg-August-Universität Göttingen, Germany*

The Sredinny Range of Kamchatka (SR) is located at the back-arc of the contemporary Kamchatka subduction zone (Avdeiko et al., 2006; Churikova et al., 2001; many others). The Benioff zone at the south end of the Range (below Khangar volcano) lies at 350 depth; further to the north it is not constrained by geophysical data (Gorbatov et al., 1997). Active volcanism in

Kamchatka, which is driven by Pacific plate subduction, is mostly concentrated at the Eastern volcanic front and in the Central Kamchatka Depression; Shiveluch is the northernmost active volcano. Volcanic rocks from both zones demonstrate typical island-arc features (Volynets, 1994; Churikova et al., 2001). In Pliocene-Miocene times, the present SR back arc was in the position of the active front of the island arc system (Avdeiko et al., 2006; Volynets et al., 2010). Volcanic rocks, erupted at that time, have typical island-arc signature and are represented by extensive effusive plateau-like lava fields. These Miocene-Pliocene plateaubasalts formed from high degrees of fluid-induced melting (>20%, fluid amount – 1.5-4%; Volynets et al., 2010). Due to the gradual accretion of parts of paleo-Kronotsk arc from the south to the north of Miocene SR (Pevzner et al., 2009), accompanied by slab roll-back and formation of a new trench, volcanic rocks of so-called "hybrid" type started to erupt in the SR as stratovolcanoes, monogenetic cinder cones and lava flows (Volynets et al., 2010). These Quaternary rocks show HFSE enrichment but still have relatively high fluid-mobile/immobile element ratios and were formed due to the lower degrees of mostly decompression melting (8-10%) with lower amount of fluid involvement (<2%) in the back-arc (Volynets et al., 2010). A very intriguing feature of the studied rocks is the similarity of slab fluid compositions in rocks for all age groups for the whole Sredinny Range. This suggests that surprisingly similar fluids segregated from the same Pacific Plate below the arc front during the Late Miocene-Pliocene and the back-arc in the Quaternary. Oxygen isotope data have the potential to constrain the amounts of slab component contributing to arc lavas, and possibly even the part of the slab from which these fluids/melts are derived (Bindeman et al., 2005). Kamchatka has been described lately as a region of highly variable $\delta^{18}O$ values (Bindeman et al., 2004, 2005; Dorendorf et al., 2000; Pokrovsky and Volynets, 1999; Pineau et al., 1999; Duggen et al., 2007; Auer et al., 2008, etc.). The source for high $\delta^{18}O$ in volcanic rocks is attributed to the addition of high $\delta^{18}O$ slab fluids to the magma generation zone (Dorendorf at al., 2000), sediment melts and/or crustal contaminants, dependent on other petrological features of the rocks (Bindeman et al., 2005).

We investigated samples from Sredinny Range (SR) of Kamchatka (Quaternary Alnej volcano, Sedanka, Kekuknajsky and Right Ozernaya monogenetic lava fields, Tobeltsen and Nilgimelkin cinder cones (north SR), as well as Miocene-Pliocene plateau basalts of Left and Right Ozernaya rivers, Dvuh'urtochnoe plateau and Kruki Ridge, Fig.1.3.1.2.1). Composition of olivine in selected rock samples is Fo65-87 in plateau lavas and Fo60-85 in monogenetic lava samples. Measured $\delta^{18}O_{olivine}$ values vary from 5.47 to 7.78 ‰, and are substantially higher than mantle values ($\delta^{18}O_{olivine}$~5-5.5‰, Eiler, 2001). Calculated $\delta^{18}O_{melt}$=6.17-8.48 ‰ ($\delta^{18}O_{melt}$= $\delta^{18}O_{olivine}$+0.7). The observed variations cannot be connected to the fractional crystallization processes, which is confirmed by the absence of correlations with Mg# and SiO_2 content in the whole rocks. Oxygen isotope composition also does not correlate with the age of the studied rocks and with the geographic location of the volcanic edifices (from the south to the north of SR): high $\delta^{18}O$-olivines are found both in young and old rocks, in the southern and northern parts of SR.

Depending on the other geochemical characteristics of the rocks, subduction fluids (Dorendorf et al., 2000), sediment melts and/or crust material contamination (Bindeman et al., 2005) have been suggested as heavy oxygen isotope sources for the island-arc volcanic rocks. SR volcanic rocks have mantle-like $^{87}Sr/^{86}Sr$ (0.7028-0.70336, Volynets et al., 2010) and non-radiogenic lead isotope composition (for ex. $^{206}Pb/^{204}Pb$ ~ 18.2, Volynets et al., 2010). Neogene plateau basalts are characterized by the strong positive correlation of $\delta^{18}O$ with Ba/Th, Ba/Nb, Sr/Yb, U/Nb ratios, and weak positive correlation with $^{206}Pb/^{204}Pb$ and $^{87}Sr/^{86}Sr$ (Fig. 1.3.1.2.2). Quarternary volcanic rocks do not show any of these features. Instead, in Quaternary rocks we observe positive correlation between $\delta^{18}O$ and Ta/Yb, Zr/Y ratios and alkalis content. (Harmon and Hoefs, 1995) mention that alkaline OIB rocks tend to be enriched of the heavy oxygen isotopes compared to the tholeitic OIBs, and (Pokrovsky and Volynets, 1999) report positive correlation of the O isotopes with K_2O concentrations in the alkaline rocks, but the variations reported in these rocks, are much smaller than observed in SR rocks. Therefore, high $\delta^{18}O$ in the rocks of the two age groups we refer to the two different scenarios. Miocene-Pliocene plateau basalts of the

Sredinny Range are the result of the mixing between the strongly depleted MORB-type mantle with the subduction fluid, impregnant by the heavy oxygen. The source of the Quaternary volcanic rocks must be 1) basic; 2) HFSE-enriched and 3) carry heavy oxygen. This kind of signature might appear as a result of the massive fluid influx leading to the serpentinization of the mantle wedge. The other opportunity is an additional source of the heavy oxygen (with $\delta^{18}O \sim 10\text{-}15\ \%_o$), resulting from the assimilation of the ancient subducted material reworked.
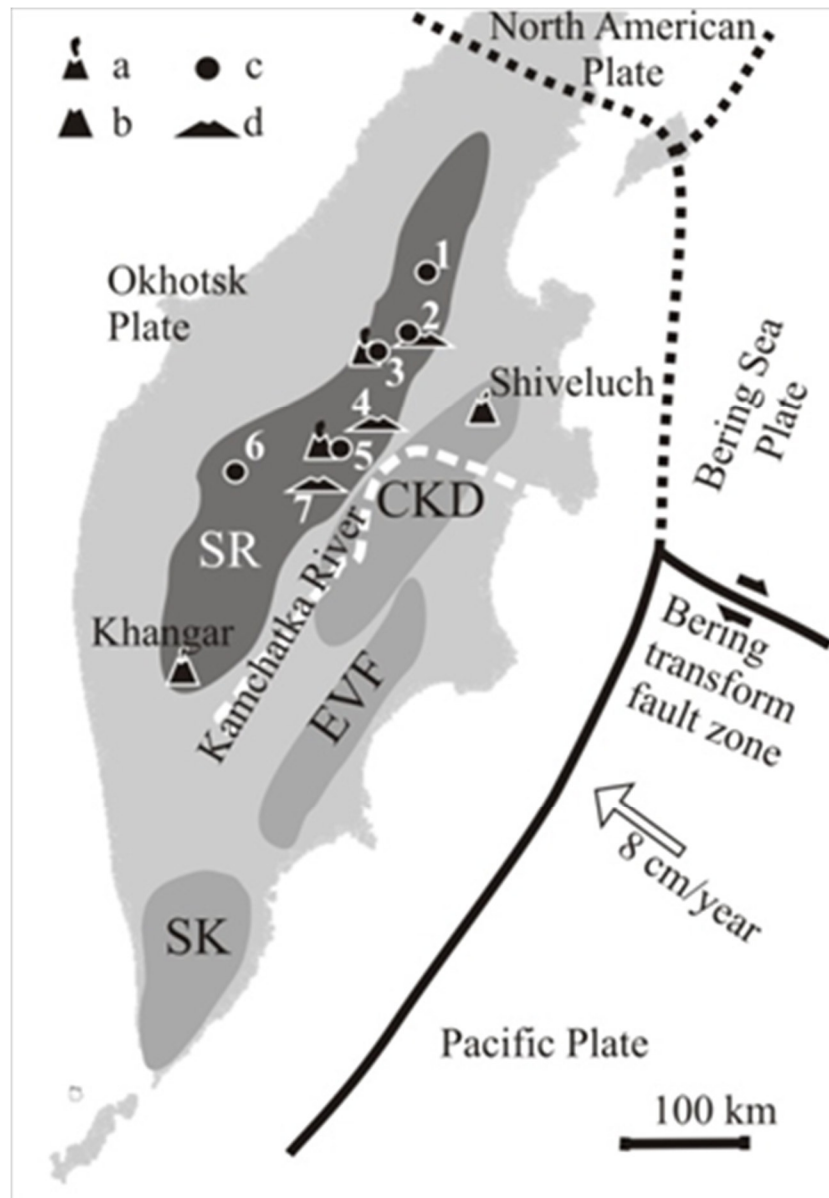
Fig. 1.3.1.2.1. General plate tectonic setting of Kamchatka and area studied. The outlines of the volcanic zones are from http://kamchatka.ginras.ru/ (Sredinny Range active volcanism zone after (Pevzner 2006)). Plate boundaries after DeMets et al. (1990), Zonenshain and Savostin (1979) and Lander et al. (1994). White arrow shows the Pacific-Okhotsk convergence after Scholl (2007). SR - Sredinny Range, CKD - Central Kamchatka Depression, EVF - Eastern Volcanic Front, SK – South Kamchatka. Locations of the studied samples in the Sredinny Range: 1 - Nylgimelkin cone, 2 – Right Ozernaya monogenetic lava field, Left and Right Ozernaya plateau, 3 - Sedanka monogenetic lava field, 4 - Dvuh'urtochnoe plateau, 5 - Alnej-Chashakondzha massif, 6 - Kekuknajsky monogenetic lava field, 7 - Kruki Ridge. Sampled edifices: a) – active stratovolcanoes and shield volcanoes; b) – extinct volcanoes; c) – Quaternary monogenetic centers (cinder cones and lava flows); d) – Miocene-Pliocene plateau.
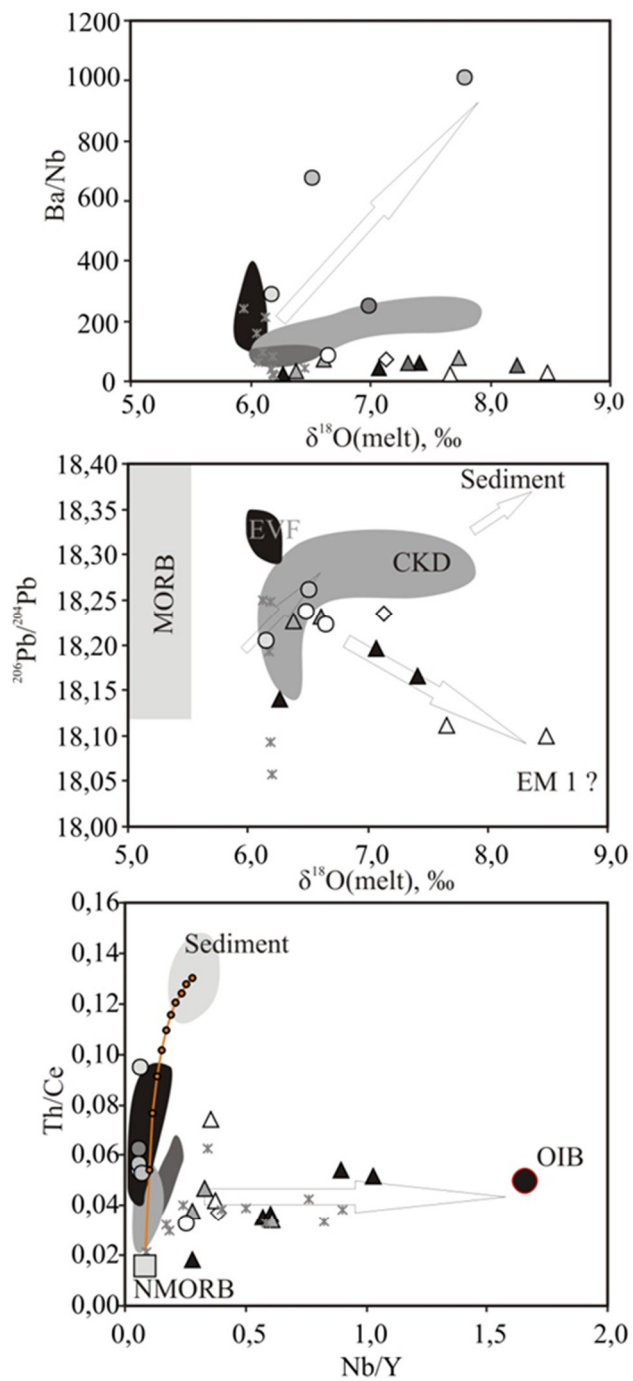
Fig. 1.3.1.2.2. Composition of oxygen isotopes compared to 206/204Pb and Ba/Nb ratio and modeling of the source compositions on a base of Th/Ce and Nb/Y systematic. Fields of Eastern volcanic front (EVF, black), Central Kamchatka Depression (light grey), Bakening (dark grey) and Ichnisky volcano (grey

crosses) are shown on a base of the unpublished data of Churikova T., Dorendorf F. and Wörner G. Orange line represents mixing ling of NMORB and sediment. Other symbols are described in the legend.

Differences in the geochemical characteristics of Miocene-Pliocene and Quaternary rocks are most likely caused by the different geodynamic settings of magma generation. Therefore, we should be able to discriminate these rocks as well in terms of magmatic temperatures and/or melting conditions (H_2O, fO_2). Higher temperatures should be found at decompression melting and lower – at fluid-induced melting. To check this hypothesis we studied compositions of minerals in volcanic rocks from both age groups and tried to estimate temperatures and pressures of crystallization. Pyroxenes in all studied samples are represented by augites and salites, in Right Ozernaya plateaubasalts also by diopside. Cpx from Holocene monogenetic lava flow from Sedanka area are enriched by Ca and Ti (up to 5.3 wt % TiO_2). Rocks of the monogenetic cinder cones of Right Ozernaya river and basaltic andesites of Dvuh'urtochnoe plateau also contain orthopyroxene (bronzite and hypersthene); Mg and transitional pigeonites are found in Kruki ridge basalts.

To calculate the equilibrium conditions for clinopyroxene-melt system (Putirka, 2008) the melt composition has been modeled by Ol extraction from the whole-rock composition of the corresponding sample until the equilibrium with Cpx in the resulting melt. This approach was necessary because we did not work with the melt inclusions, while whole-rock compositions, obviously, were affected by the composition and set of phenocrysts and therefore not in equilibrium with Cpx anymore. In most cases the amount of the extracted olivine was 5-8%, composition Fo80-82, what is in accordance with the microprobe analyses (the exception was Kruki Ridge basalt sample, where all measured Ol were Fe-rich and for the calculation we used Fo58). In Miocene-Pliocene plateau lavas the equilibrium conditions, calculated by (Putirka, 2008) geothermometer, are: Left Ozernaya river plateau (in average): 1145±42°C and 2.2±2.2 kBar; Dvuh'urtochnoe plateau: 1070±42 °C and 1.5±2.2 kBar; Kruki Ridge: 1114±42°C and 4.2±2.2 kBar; Right Ozernaya plateau (by two samples): 1100-1140±42°C and 3.7-2.8±2,2 kBar (Fig. 1.3.1.2.3). The pressure estimates are done for the dry conditions.

For the Quaternary monogenetic cones and lava flows the results on equilibrium P-T conditions divided into two groups, depending on the composition of the Px used for calculation. The clinopyroxenes of the first group have roughly the same composition as Cpx from Neogene plateau basalts, and give the following estimates of temperature and pressure: monogenetic cones of Right Ozernaya river (by two samples): 1100-1116±42°C and 3,9-3.2±2.2 kBar; Alney volcano: 1127±42°C and 3.4±2.2 kBar; Nylgimelkin cone 1111±42°C and 3.1±2.2 kBar; Sedanka area (3 samples): 1000-1100±42°C and 0-3.5±2.2 kBar; Kekuknajsky area 1133±42°C and 6.4±2.2 kBar (Fig. 1.3.1.2.3). These conditions are similar to the calculated for the Miocene-Pliocene plateau lavas and, most likely, reflect the sub-surface crystallization processes. The second group of Cpx from the Quaternary basalts has been found in Sedanka and Kekuknajsky monogenetic field areas. These clinopyroxenes are characterized by the elevated alumina content (Al2O3 6-11 wt.%, compared to average 3 % (maximum up to 6%) in the pyroxenes from the first group) and sodium (Na2O>1% in a contrast to 0.2-0.6 % in both groups respectively) (Fig. 1.3.1.2.4). Calculated Cpx-melt equilibrium conditions for these pyroxenes are 1183-1140±42°C and 11.6-24.9±2.2 kBar (Sedanka area); 1163-1200±42°C and 10.8-18±2.2 kBar (Kekuknajsky area) (Fig. 1.3.1.2.3). Similar results for the temperature were calculated for the Ol-melt equilibrium in basalt sample from Kekuknajsky area (with whole-rock composition used for the melt composition) 1248±43°C (by (Putirka, 2008) geothermometer). The calculated pressure estimates for these samples correspond to approximately 54-100 km depth. Also, in the same samples we have found the inclusions of high-Al, high-Mg Sp in Ol (Al_2O_3 >25 wt %, Mg#>30). Unfortunately, Sp was re-equilibrated during the cooling, but the temperature estimates made by several quasi-equilibrium compositions also give us the high values (1280-1292 ± 30°C by (Ponomarev & Puzankov, 2012) geothermometer). High alumina concentrations in these Px and Sp confirm deeper conditions of phenocrysts crystallization in Quaternary basalts than in Miocene-Pliocene plateau basalts.

100
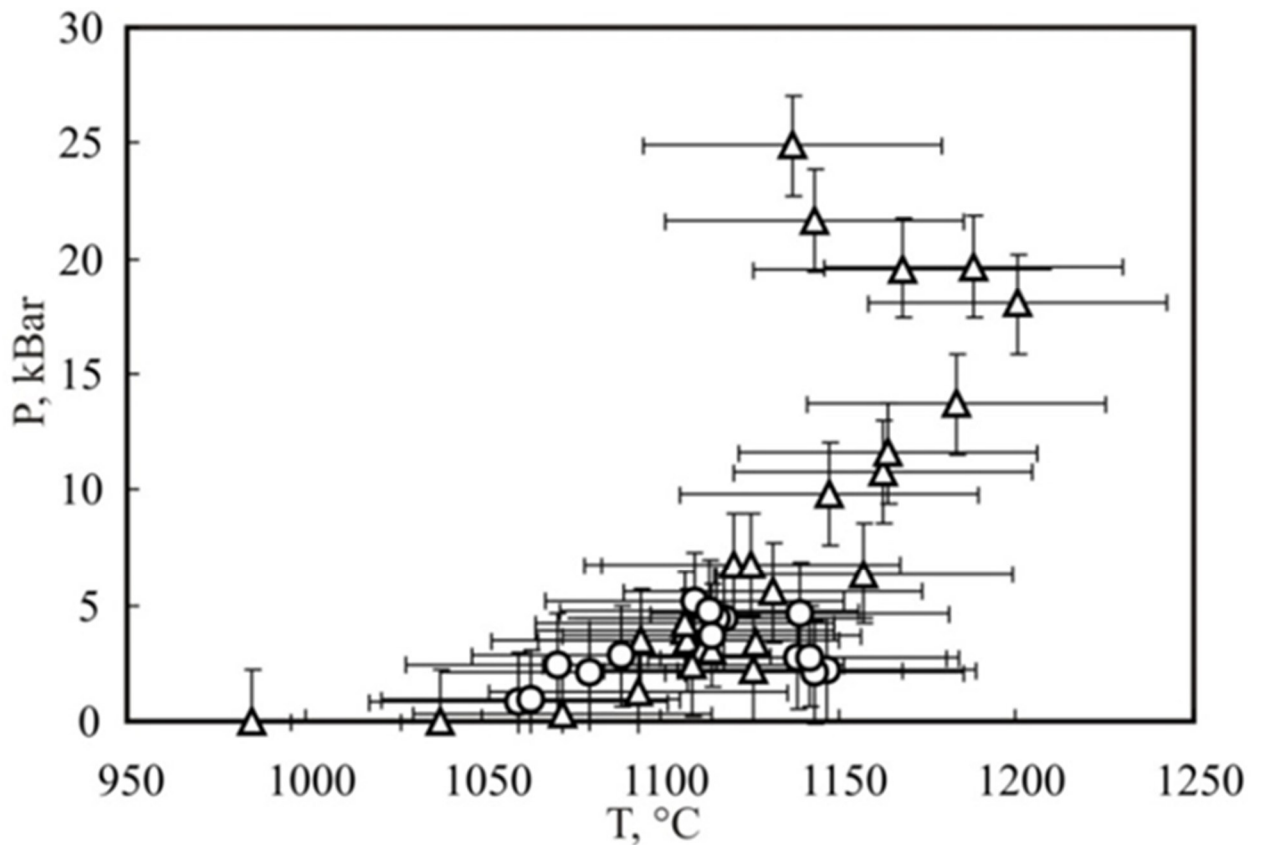
Fig. 1.3.1.2.3. Calculated phenocrysts' and microlites' crystallization pressure and temperature by Cpx-melt equilibrium (Putirka, 2008). Legend: triangles – Quaternary monogenetic cones and stratovolcanoes with hybrid type of incompatible elements distribution; circles – Miocene-Pliocene plateau basalts with typical island-arc signatures. Horizontal and vertical lines represent error bars.
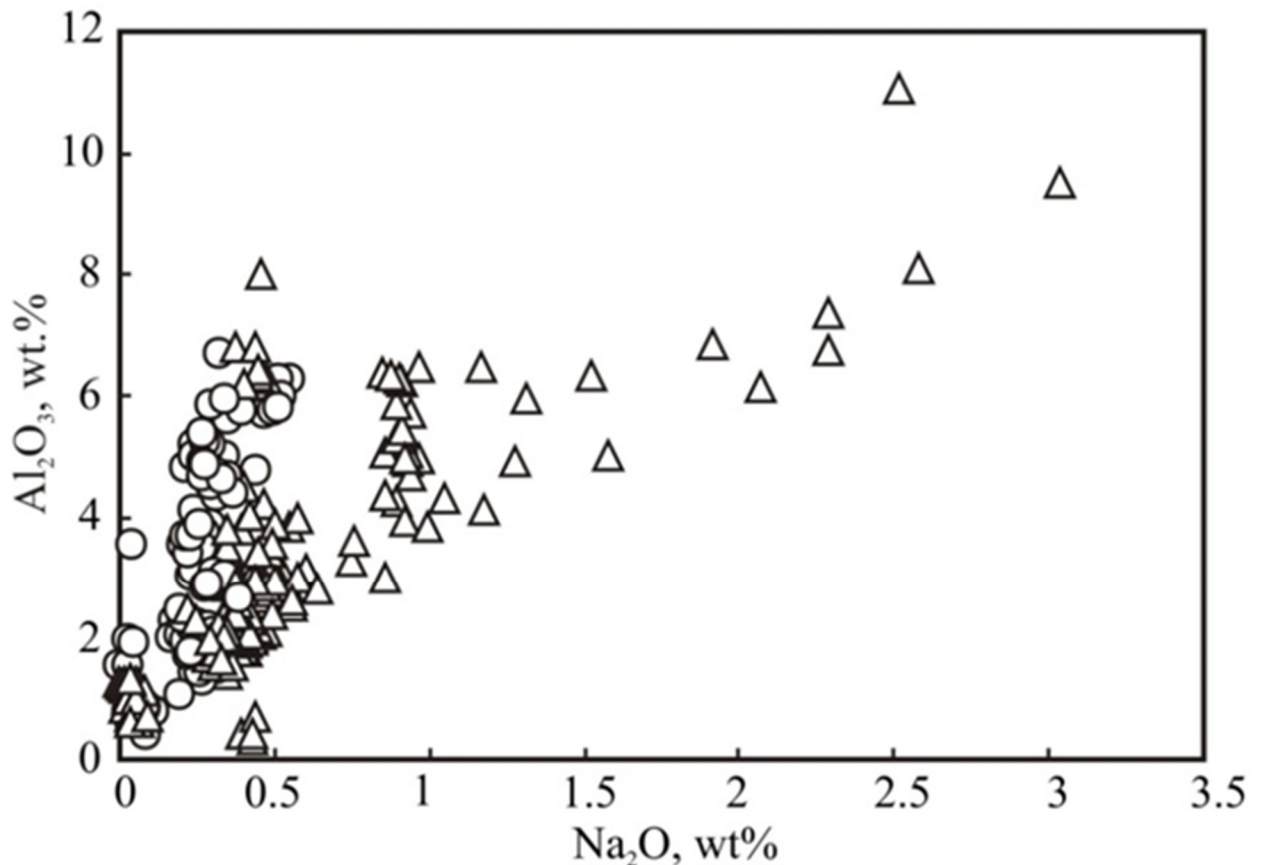
Fig. 1.3.1.2.4. Al2O3 vs. Na2O in clinopyroxenes from Sredinny Range. Legend same as in Fig. 1.3.1.2.3.

Therefore, the obtained set of data of clinopyroxene compositions in Sredinny Range basalts confirm the hypothesis, that the crystallization in Quaternary basalts with hybrid type of incompatible elements distribution started at higher temperatures and pressures than in Miocene-Pliocene plateau basalts with typical island-arc signatures.

Volynets, A., Wörner, G., Kronz ,A., Griboedova, I., & Babansky, A. (2014) Composition of pyroxenes in Miocene-Quaternary basalts of the Sredinny Range of Kamchatka: Implications to the crystallization conditions. 8-th Biennial Workshop on Japan-Kamchatka-Alaska Subduction Processes (JKASP-2014): Finding clues for science and disaster mitigation from International collaboration. Sapporo, Japan, 22-26 September 2014. http://hkdrcep.sci.hokudai.ac.jp/map/jkasp2014/proglist.html.

Volynets, A., Wörner, G., Kronz, A., Griboedova, I., Babansky, A. (2013) Pyroxenes from the Miocene-Quaternary basalts of the Sredinny Range of Kamchatka: composition and crystallization conditions. VII International conference "Volcanism, biosphere and ecological problems". Abstract volume: Maykop, ASU. P. 22-25. (In Russian).

Volynets, A., Wörner, G., Kronz, A., Ponomarev, G. (2012) Crystallization conditions of the Miocene-Quaternary volcanic rocks of Sredinny Range of Kamchatka inferred from mineralogical data. Contemporary problems of geochemistry: abstract volume of the conference. Irkutsk, SB RAS Sochava Institute of geography publishing group. Vol. 2. P. 35-37. (In Russian). http://www.igc.irk.ru/images/Conf_IGC-2012/Tezis/Tom-2.pdf

Volynets A., Wörner G., Przybilla R. (2012) Oxygen isotopic composition of the Miocene-Quaternary volcanic rocks of the Sredinny Range of Kamchatka and compositions of the magma sources // Contemporary problems of geochemistry: abstract volume of the conference. Irkutsk, SB RAS Sochava Institute of geography publishing group. Vol. 2. P. 38-40. (In Russian). http://www.igc.irk.ru/images/Conf_IGC-2012/Tezis/Tom-2.pdf

Volynets, A., Wörner, G., & Przybilla, R. (2011). Oxygen isotopes in Miocene-Quaternary volcanic rocks from Sredinny Range, Kamchatka. 7th Biennual Workshop on Japan-Kamchatka-Alaska Subduction Processes: Mitigating Risk Through International Volcano, Earthquake, and Tsunami Science. JKASP-2011. Petropavlovsk-Kamchatsky, Russia. August 25-30, 2011. Abstracts. – Petropavlovsk-Kamchatsky: Institute of Volcanology and Seismology FEB RAS, Kamchatkan Branch of Geophysical Service RAS, 168-169. http://www.kscnet.ru/ivs/slsecret/jkasp_2011/abstr/abs74.pdf

1.4. Regional studies at Kamchatka peninsula

1.4.1. Geochemical investigations

1.4.1.1. Geodynamical model of adakite formation

Avdeiko G.P., Paluyeva A.A., *Institute of Volcanology and Seismology FED RAS, Russia*
Kuvikas O.V., kuvikas@mail.ru*, Department of Natural History Science, Graduate School of Science, Hokkaido Univ., Japan; Institute of Volcanology and Seismology FED RAS, Russia*

Review and analysis of genesis conditions for adakites and magnesian andesites with adakite properties showed that there are various tectonic and geodynamic settings within subduction zones of the Pacific Ring. These settings provide additional heating sufficient for slab melting in subduction zones.

The model of the adakite formation in Kurile-Kamchatka zone is created. In difference to previous models, this model operates with the melting of the cold subduction slab with age more than 95 Ma. As a rule, on the initial stage of subduction process a front part of a new slab suffered

melting caused by heat from hot asthenosphere. In this case, their association with NEB type can be traced. A large number of adakite location depend on additional heating and slab melting in slab windows regardless geodynamic conditions. Moreover, formation of adakites may probably be caused by subduction of hot spreading centers. Oblique subduction and transform interactions between plates may generate additional heating sufficient for adakite volcanism. This model can be used for any subduction systems with age more than 5Ma (Figs. 1.4.1.1.1 and 1.4.1.1.2).
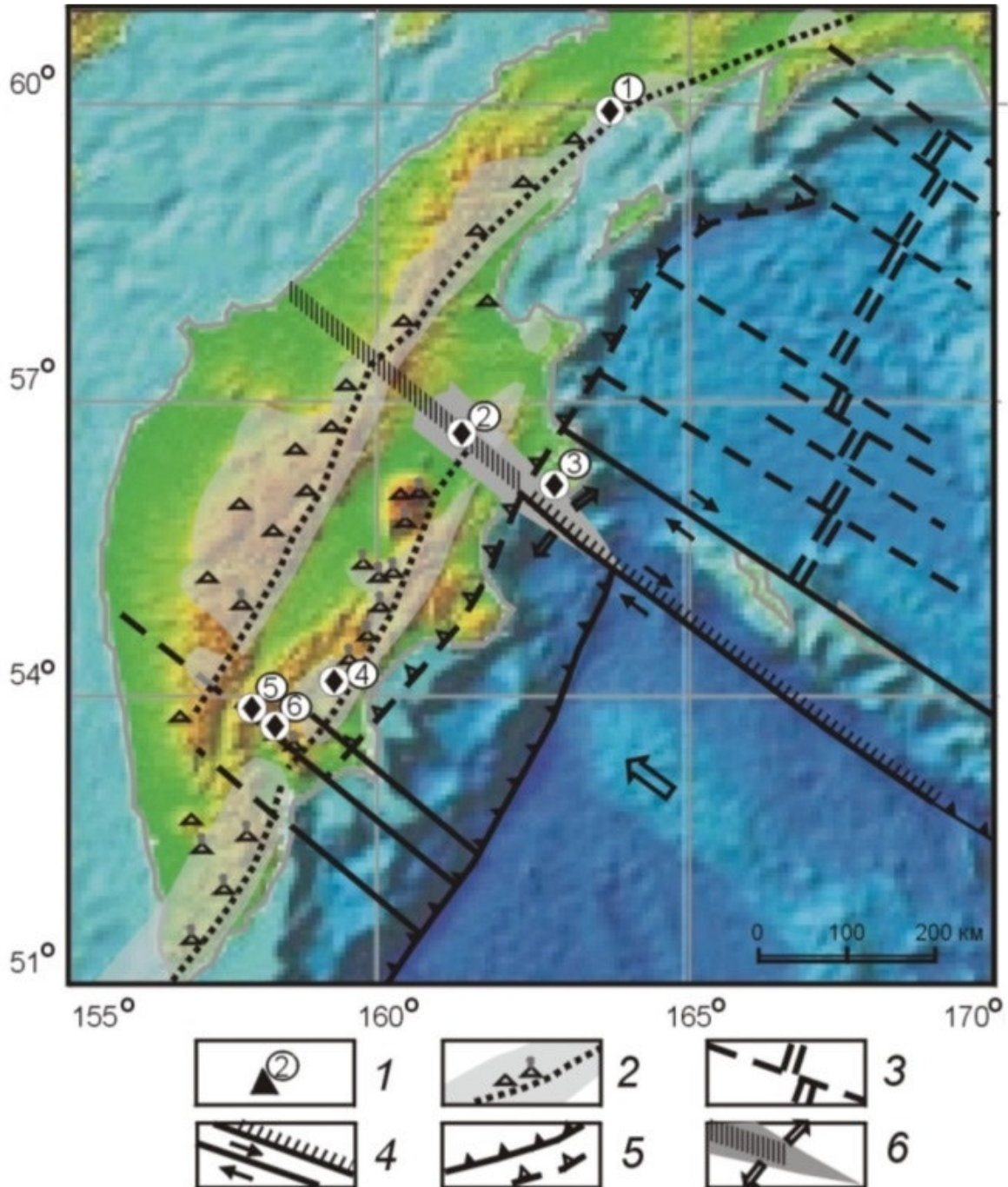
Fig. 1.4.1.1.1. Tectonic setting of the adakite edifices at Kamchatka peninsula. 1 – adakite location;, 2 – volcanic belts, volcanoes and volcanic front; 3 – Paleorifts and transform faults; 4 – old and recent trenches; 5 – fault; 6 – subduction window.
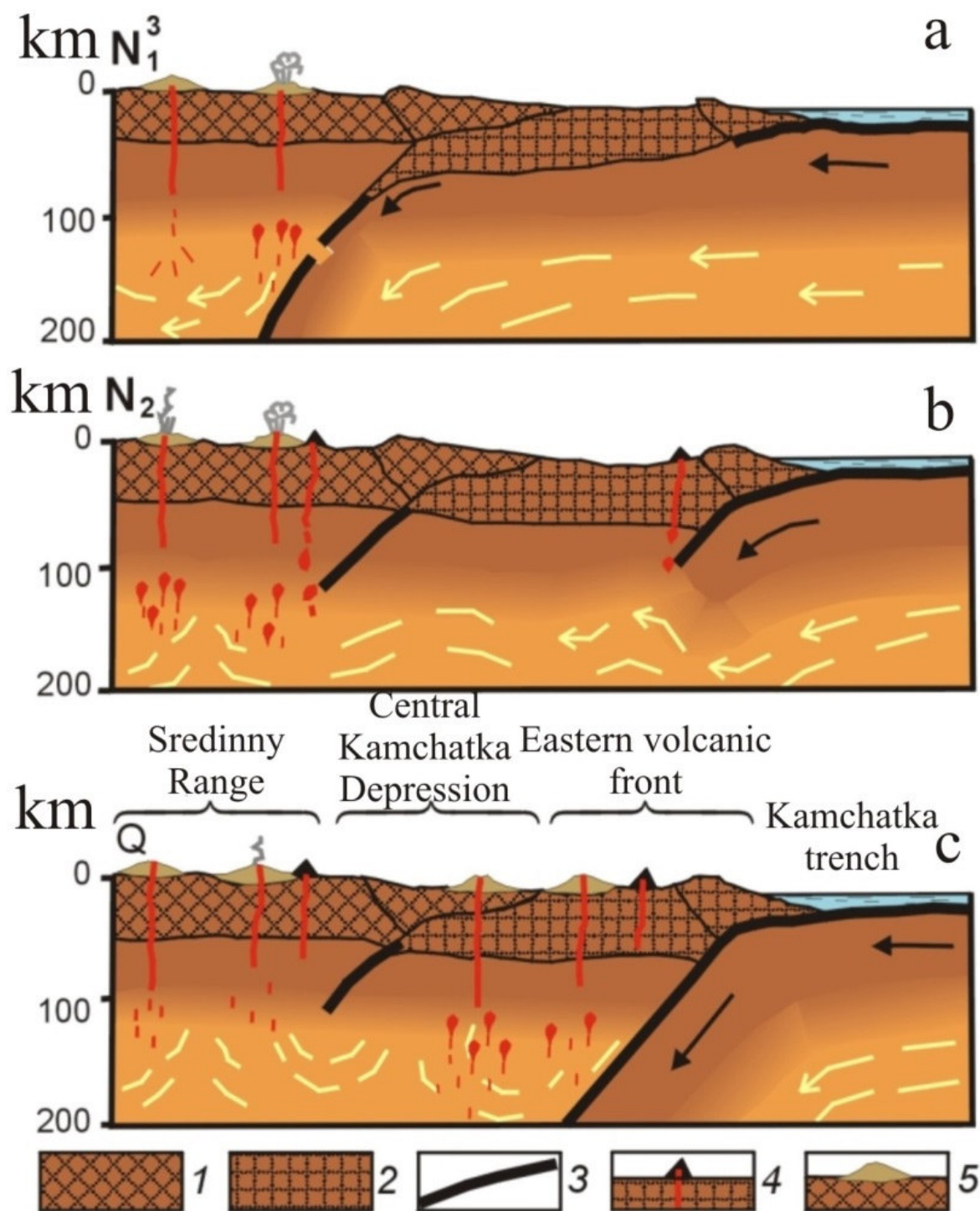
Fig. 1.4.1.1.2. The model of Miocene-Qaternary geodynamical evolution and adakite formation. 1 – continental crust, 2 - continental crust of the Kronotskaya paleo-arc; 3 – oceanic crust, 4 – adakite edifices, 5 – volcanoes.

Avdeiko G. P., Paluyeva A. A., & Kuvikas O. V. (2011). Adakites in subduction zones of the Pacific ring: review and analysis of geodynamic genesis conditions. Bulletin of Kamchatka regional association "Educational-Scientific Center". Earth sciences, 1(17), 45-60. (In Russian). http://www.kscnet.ru/kraesc/2011/2011_17/art5.pdf

1.4.1.2.   Sr-Nd-Pb isotop distribution along the North-Eastern Pacific

Koloskov A.V., kolosav@kscnet.ru, *Institute of Volcanology and Seismology FED RAS, Petropavlovsk-Kamchatski, Russia*

Sr-Nd-Pb systematics of the volcanic rocks of Upper-Cretatious – Cenozoic ages along the North-Eastern Pacific edge was achived based on original and earlier published data (Kay et al., 1978; Davis et al., 1993; Yogodzinski et al., 1993, 1994, 1995; Moll-Staleap, 1995; Kersting, Arculus, 1995; Tatsumi et al., 1995; Johnson et al., 1996; Kepezhinskas et al., 1997; Volynets et al., 1997; Apt et al., 1998; Turner et al., 1998; Dorendorf et al., 2000; Churikova et al., 2001; Bindeman et al., 2004; George et al., 2004; Jieda et al., 2004; Akinin et al., 2005; Portnyagin et al., 2005; Fedorov, 2006; Volynets et al., 2010). Nd-Pb isotopes suggest that volcanic rocks at Kamchatka Peninsula and Kurile-South-Okhotsk regions were originated from Indian MORB mantle (I-MORB) while volcanic rocks of Komandor-Aleutian island arcs were originate from Pacific MORB mantle (N-MORB)(Fig. 1.4.1.2.1).
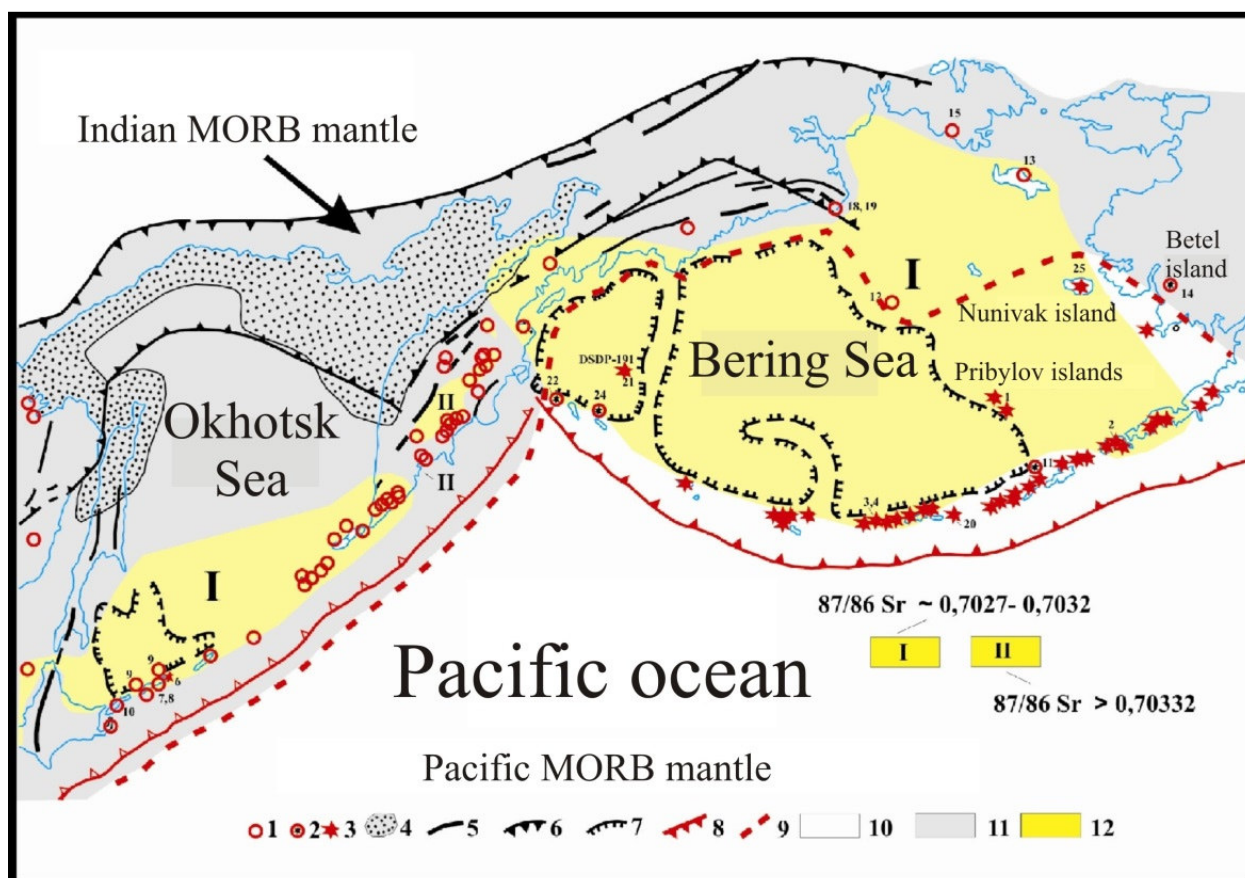
Fig. 1.4.1.2.1. Schematic sketch of the Late- Cenozoic volcanic rocks manifestations and local isotope anomalies for the Okhotsk, Kamchatka and Bering Sea regions. 1-3 – volcanic centres with isotopes of I-MORB-type (1), intermediate (2) and N-MORB type (3); 4 – Late- Cenozoic valleys; 5 – tectonic faults; 6 – the border of Eastern-Asian graben belt; 7 – the borders of the deep-sea trenches; 8 – deep-sea trenches; 9 – The border between the different mantle areas: 10 – N-MORB type, 11 – Indian MORB type; 12 – local anomalies of Sr isotopes (I and II).

Koloskov A.V. (2012) Isotope-geochemical features of Late-Cenozoic volcanics of the north-eastern Asian margin and subduction-related problems of geodynamics Volcanism and related processes. Annual regional scientific conference dedicated to the Volcanologist Day. Proceedings of the conference. March 29-30, 2012, Petropavlovsk-Kamchatsky.

Petropavlovsk-Kamchatsky: Institute of volcanology and seismology FED RAS, 50-55. (In Russian). http://www.kscnet.ru/ivs/publication/volc_day/2012/art8.pdf

1.4.1.3. Siberian mantle

Konc Z., zoltankonc@iact.ugr-csic.es, **Marchesi C., Hidas K., Garrido C. J.,** *Instituto Andaluz de Ciencias de la Tierra (IACT), CSIC-UGR, Armilla, Granada, Spain*
Szabo C., *Lithosphere Fluid Research Lab, Eötvös University, Budapest, Hungary*
Sharygin V. V., *S. Sobolev Institute of Geology and Mineralogy SD RAS, Novosibirsk, Russia*

We present new data on spinel peridotite xenoliths hosted in Agardag alkaline lamprophyres from the Sangilen Plateau (Tuva, South Siberia, Russia), sampling at similar to 450 Ma the subcontinental lithospheric mantle of the Tuva-Mongolian micro-continent that belongs to the accretionary Central Asian orogenic belt at the southern edge of the Siberian craton. Xenoliths are spinel lherzolites principally showing poikilitic and subordinately coarse granular and coarse equigranular textures. Geothermobarometric calculations for pyroxene yield a narrow range of equilibration temperature (ca. 1000-1100 °C) that corresponds to lithospheric depths from 43 to 53 km (1.3-1.6 GPa) along a hot intracontinental geotherm. Variation of mean Mg# [$100*Mg/(Mg + Fe)$] of olivine (87.9-90.9) with mean Cr# [$100*Cr/(Cr + Al)$] of spinel (9.5-45.7) indicates that spinel lherzolites are mostly residues of up to 10% melting of a fertile peridotite source. In terms of normalized REE (Rare Earth Element) and incompatible trace element patterns of clinopyroxene, the Sangilen xenoliths can be classified into three types: Type I characterized by convex-upward REE patterns depleted in LREE (0.10 <= La/Yb-N <= 0.49), and with relative negative anomalies of Rb, Pb. Hf, Zr and Ti and positive spikes of U and Sr; Type II displaying variable LREE/HREE ratios (0.53 < La/Yb-N < 2.17) but generally flatter REE patterns) and similar abundances of other trace elements compared to Type I; and Type Ill showing a LREE enriched pattern [(La/Sm)(N) = 2.22; (La/Yb)(N) = 8.42], high REE contents and no relative anomalies of U and Sr. The elevated Yb-N concentration of one Type II clinopyroxene and the variable fractionation of LREE-MREE relative to HREE in most xenolith types indicate Sangilen xenoliths underwent variable metasomatic enrichment. This enrichment is well accounted by percolation-reaction between depleted peridotite and small-melt fractions of alkaline mafic melts precursor to the Agardag alkaline lamprophyres. The lack of correlation with depth of modal variations, textural types, inferred degrees of melting and trace element patterns in xenoliths indicates the absence of a texturally or compositionally layered lithospheric mantle sampled by Ordovician lamprophyres beneath the Sangilen plateau. The observed compositional variations are better accounted by depleted lithosphere variably metasomatized along a network of percolating alkaline mafic melts heterogeneously distributed throughout the Sangilen lithospheric mantle section.

Konc, Z., Marchesi, C., Hidas, K., Garrido, C. J., Szabó, C., & Sharygin, V. V. (2012). Structure and composition of the subcontinental lithospheric mantle beneath the Sangilen Plateau (Tuva, southern Siberia, Russia): Evidence from lamprophyre-hosted spinel peridotite xenoliths. Lithos, 146–147, 253-263. Doi: http://dx.doi.org/10.1016/j.lithos.2012.05.012.

1.4.2. Geochronological and geodynamical regional studies

1.4.2.1. Arctic and Pacific paleoclimatic records

Ponomareva V., vera.ponomareva1@gmail.com, *Institute of Volcanology and Seismology, Petropavlovsk-Kamchatsky, Russia*

Portnyagin M., mportnyagin@ifm-geomar.de, *V.I. Vernadsky Institute of Geochemistry and Analytical Chemistry, Moscow, Russia. Helmholtz-Zentrum für Ozeanforschung Kiel (GEOMAR), Kiel, Germany*

Derkachev A., *V.I.Il'ichev Pacific Oceanological Institute, Vladivostok, Russia*

Juschus O., *Faculty of Landscape Management and Nature Conservation, Eberswalde University of Sustainable Development, Eberswalde, Germany*

Garbe-Schönberg D., *Institute of Geoscience, Christian-Albrechts-University of Kiel, 24118 Kiel, Germany*

Nürnberg D., *Helmholtz-Zentrum für Ozeanforschung Kiel (GEOMAR), Kiel, Germany*
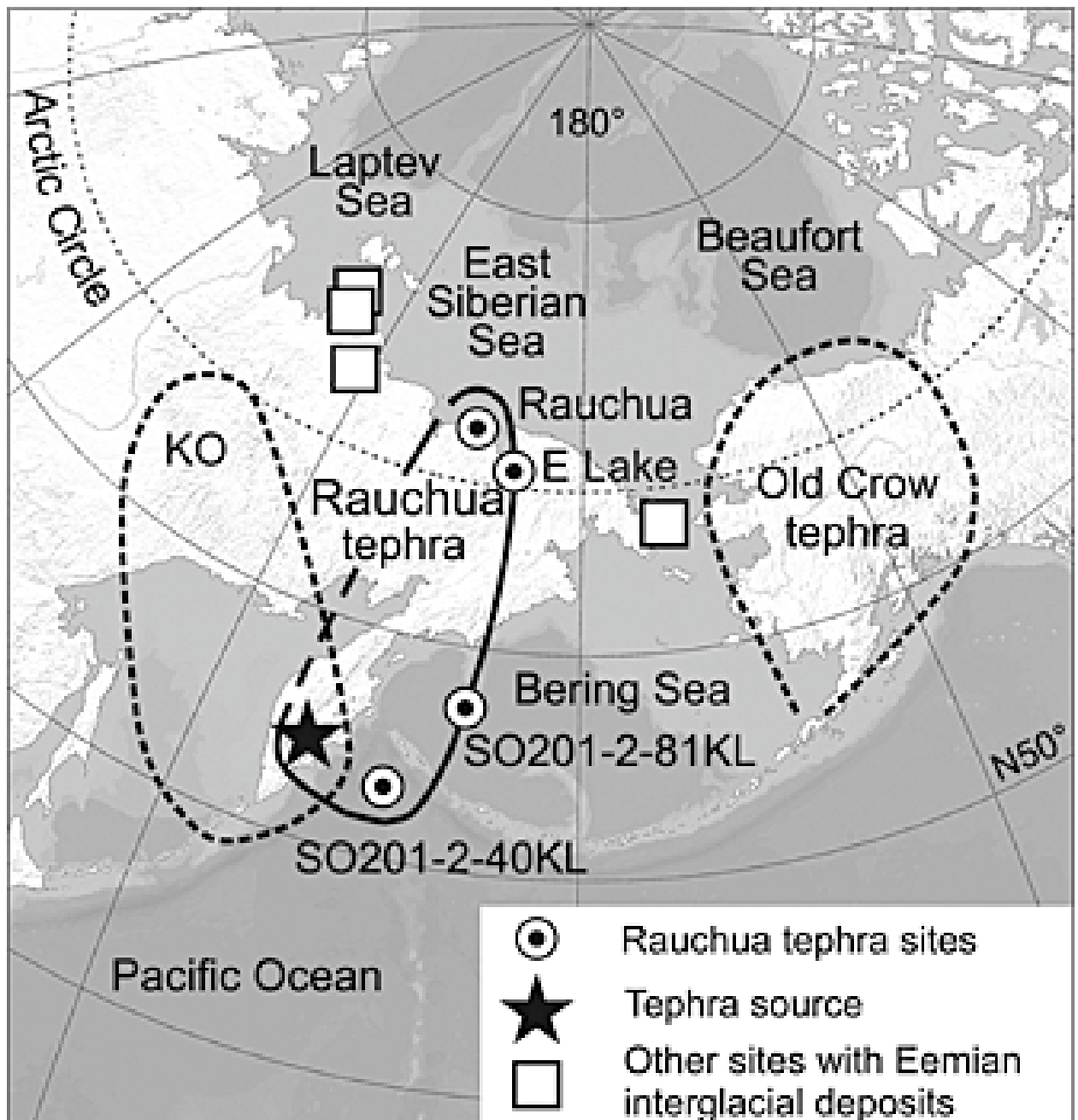
Fig. 1.4.2.1.1. Location of the Rauchua tephra sites and its minimum outline (solid line); with Old Crow (~124 ka) [Preece et al., 2011] and Kurile Lake (KO, ~8.4 ka) [Ponomareva et al., 2004] tephras outlines (dashed) for comparison. Karymsky volcanic center is shown with the star. Some other sites with the MIS 5e (Eemian) interglacial deposits according to Brigham-Grette et al. [2001], Kaplina [2011], and Schirrmeister et al. [2011]. Long axis of the Rauchua tephra outline is ~1800 km

Very few age controls exist for Quaternary deposits over the vast territory of the East Russian Arctic, which hampers dating of major environmental changes in this area and prevents their correlation to climatic changes in the Arctic and Pacific marine domains. We report a newly identified ~177 ka old Rauchua tephra, which has been dispersed over an area of >1,500,000 km^2 and directly links terrestrial paleoenvironmental archives from Arctic Siberia with marine cores in the northwest Pacific, thus permitting their synchronization and dating (Fig. 1.4.2.1.1). The Rauchua tephra can help to identify deposits formed in terrestrial and marine environments during the oxygen isotope stage 6.5 warming event. Chemical composition of volcanic glass from the Rauchua tephra points to its island-arc origin, while its spatial distribution singles out the Kamchatka volcanic arc as a source. The Rauchua tephra represents a previously unknown, large (magnitude >6.5) explosive eruption from the Kamchatka volcanic arc.

Ponomareva, V., Portnyagin, M., Derkachev, A., Juschus, O., Garbe-Schönberg, D., & Nürnberg, D. (2013) Identification of a widespread Kamchatkan tephra: a middle Pleistocene tie-point between Arctic and Pacific paleoclimatic records. Geophysical Research Letters. 40(14), 3538–3543, Doi: 10.1002/grl.50645.

Ponomareva, V., Polyak, L., Portnyagin, M., Abbott, P., & Davies S. (2014). A Holocene cryptotephra record from the Chukchi margin: the first tephrostratigraphic study in the Arctic Ocean. Proceedings of the II PAST Gateways International conference and workshop, Trieste, Italy, May 19-23, 2014, c. 69-70. http://pastgateways2014.inogs.it/sites/default/files/PAST-Gateways_2014_0.pdf

1.4.2.2. Sediment cores extracted from Lake El'gygytgyn, in the Far East Russian Arctic

van den Bogaard C., cbogaard@geomar.de, *GEOMAR Helmholtz-Zentrum für Ozeanforschung Kiel, Wischhofstr. 1–3, 24148 Kiel, Germany*
Jensen B. J. L., Froese D. G., *Department of Earth and Atmospheric Sciences, 1–26 Earth Sciences Building, University of Alberta, Edmonton, AB, T6G 2E3, Canada*
Pearce N. J. G., *Department of Geography and Earth Sciences, Aberystwyth University, Llandinam Building, Penglais Campus, Aberystwyth, SY23 3DB, Wales, UK*
Portnyagin M., mportnyagin@ifm-geomar.de, *V.I. Vernadsky Institute of Geochemistry and Analytical Chemistry, Moscow, Russia. Helmholtz-Zentrum für Ozeanforschung Kiel (GEOMAR), Kiel, Germany*
Ponomareva V., vera.ponomareva1@gmail.com, *Institute of Volcanology and Seismology, Petropavlovsk-Kamchatsky, Russia*
Garbe-Schönberg D., *Institute of Geoscience, Christian-Albrechts-University of Kiel, 24118 Kiel, Germany*
Wennrich V. *University of Cologne, Institute for Geology and Mineralogy, Cologne, Germany*
now at: School of Geography, Archaeology and Palaeoecology, Queen's University Belfast, UK

Ash layers from explosive volcanic eruptions (i.e. tephra) represent isochronous surfaces independent from the environment in which they are deposited and the distance from their source. In comparison to eastern Beringia (non-glaciated Yukon and Alaska), few Plio-Pleistocene distal tephra are known from western Beringia (non-glaciated arctic and subarctic eastern Russia), hindering the dating and correlation of sediments beyond the limit of radiocarbon and luminescence methods (Fig. 1.4.2.2.1). The identification of eight visible tephra layers (T0–T7) in sediment cores extracted from Lake El'gygytgyn, in the Far East Russian Arctic, indicates the feasibility of developing a tephrostratigraphic framework for this region (Fig. 1.4.2.2.2). These tephra range in age from ca. 58 ka to 2.2 Ma, and each is described and characterized by its major-, minor-, trace-element and Pb isotope composition. These data show that subduction zone related volcanism from the Kurile–Kamchatka–Aleutian–Arc and Alaska Peninsula is the most likely

source, with Pb isotope data indicating a Kamchatkan volcanic source for tephra layers T0–T5 and T7, while a source in the Aleutian Arc is possible probable for Tephra T6. The location of Lake El'gygytgyn relative to potential source volcanoes (> 1000 km) suggests these tephra are distributed over a vast area. These deposits provide a unique opportunity to correlate the high-resolution paleoenvironmental records of Lake El'gygytgyn to other terrestrial paleoenvironmental archives from western Beringia and marine records from the northwest Pacific and Bering Sea. This is an important first step towards the development of a robust integrated framework between the continuous paleoclimatic records of Lake El'gygytgyn and other terrestrial and marine records in NE Eurasia.
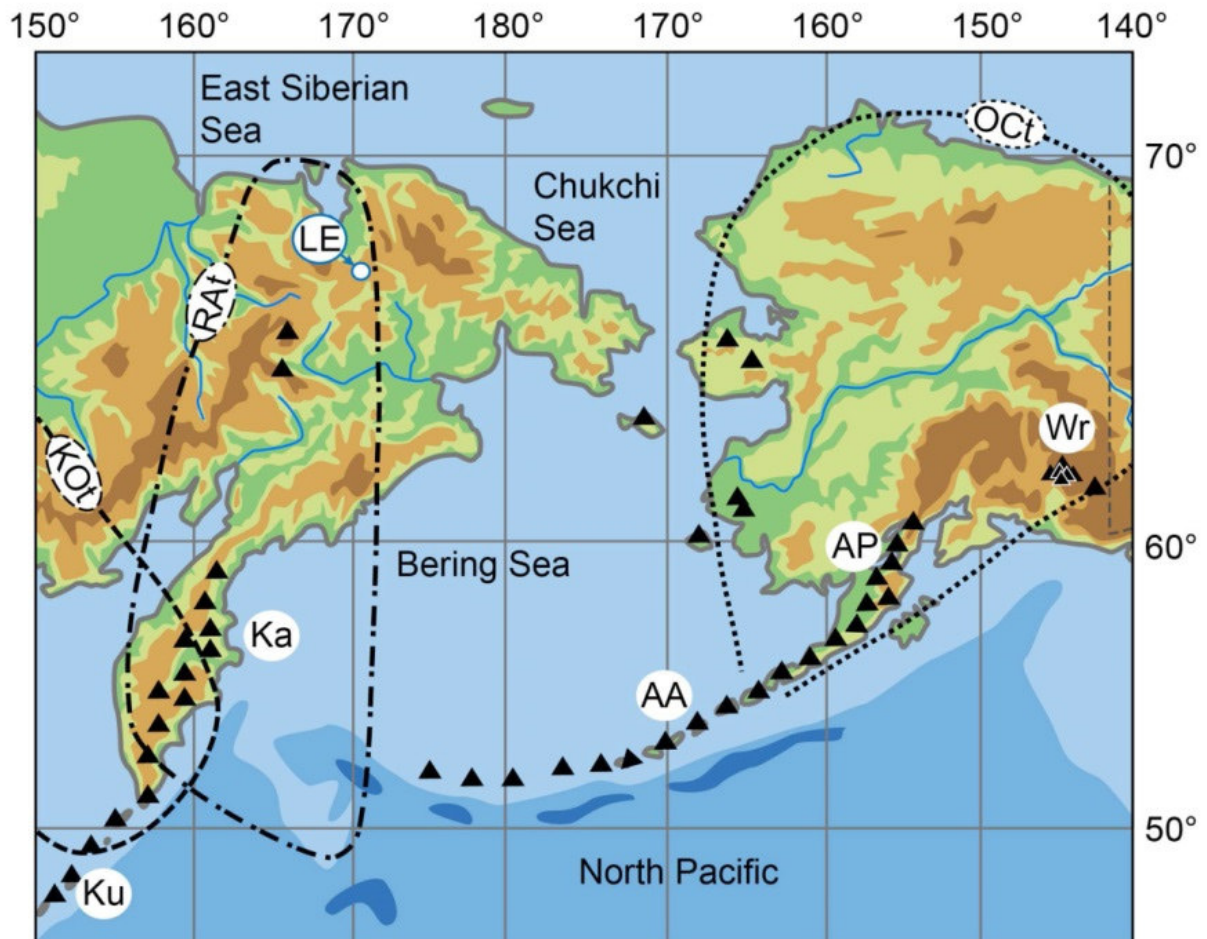
Fig. 1.4.2.2.1. Location of Lake El'gygytgyn (LE) in relation to volcanic areas in the Kuriles (Ku), Kamchatka (Ka), Aleutian Arc (AA) and Alaska Peninsula (AP). Reconstructed distribution patterns of Old Crow Tephra (OCt; -124 ka; Preece et al., 2011), Raucha Tephra (RAt; -177 ka; Ponomareva et al., 2013b) and KO Tephra (KOt; -7 ka; Derkachev et al., 2004) illustrate the potential for widespread tephra distribution in this region. The Wrangell volcanic field (Wr) and other smaller cinder cones and maars, indicated by additional markers, are either to far afield and/or do not produce the type of tephra deposits that are found in Lake El'gygytgyn. During glacial times, the Bering shelf between Russia and Alaska was exposed, and only mountainous areas in this region experienced limited glaciation, creating the glacial refugium known as Beringia. As a result, Beringia contains terrestrial paleoenvironmental records that rival marine deposits in their richness and length.
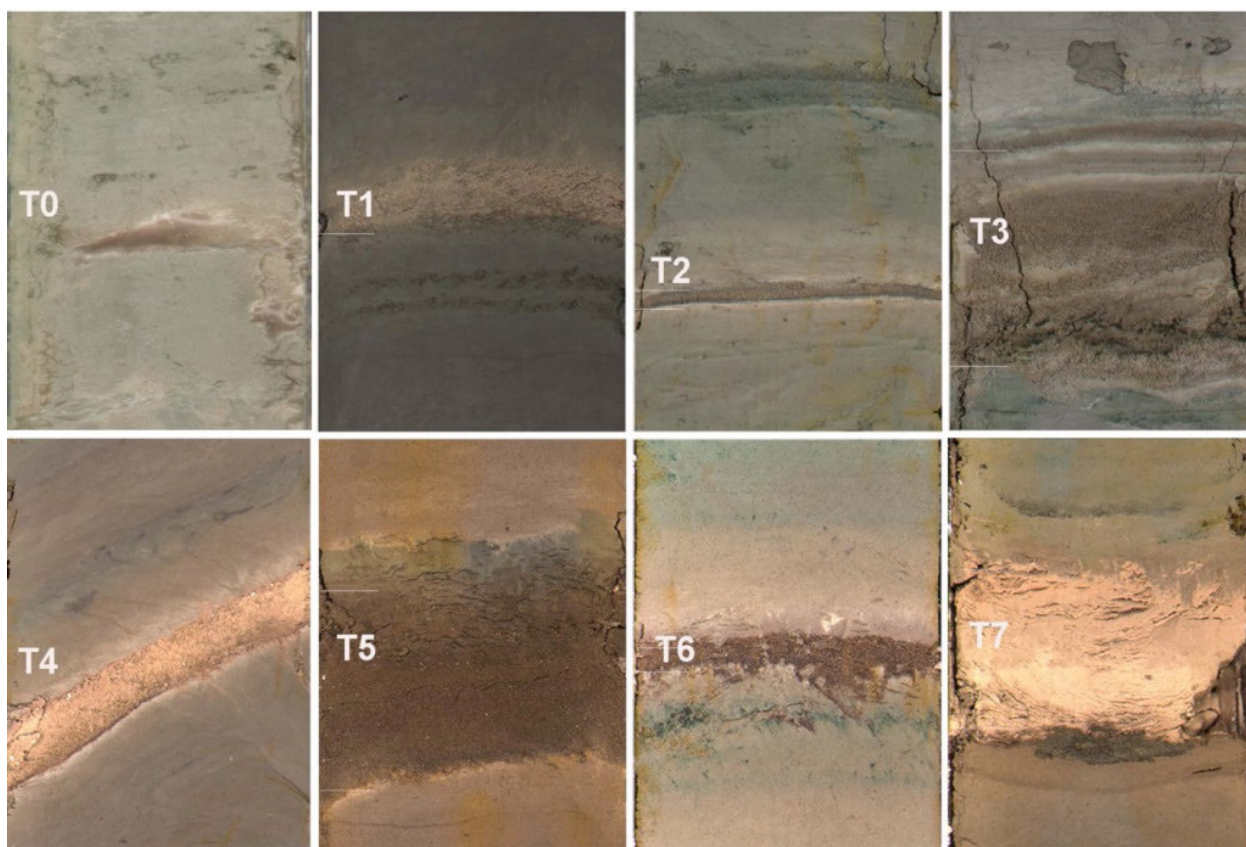
Fig. 1.4.2.2.2. Photos of the sections of cores with the detected tephra layers from Lake El'gygtgyn: T0 (5011-4D-2H1), T1 (5011-1B-1H2), T2 (5011-1B-7H2), T3 (5011-1B-10H2), T4 (5011-1A-19H1), T5 (5011-1A-19H2), T6 (5011-1A-25H1), T7 (5011-1A-35E1). Length of each segment is 12 cm.

Van den Bogaard, C., Jensen, B. J. L., Pearce, N. J. G., Froese, D. G., Portnyagin, M. V., Ponomareva, V. V., & Wennrich, V. (2014). Volcanic ash layers in Lake El'gygytgyn: eight new regionally significant chronostratigraphic markers for western Beringia, Clim. Past, 10, 1041-1062, Doi: 10.5194/cp-10-1041-2014, http://www.clim-past.net/10/1041/2014/cp-10-1041-2014.pdf

1.4.2.3. Vegetation dynamics and climate change in Kamchatka Peninsula during last 11.5 ka

Dirksen V., dirksen@kscnet.ru, **Dirksen O.,** dirksen@kscnet.ru, *Institute of Volcanology and Seismology FED RAS, 9 Piip Blvd, 683006 Petropavlovsk-Kamchatsky, Russia*
Diekmann B., Bernhard.Diekmann@awi.de, *Alfred-Wegener-Institute für Polar- und Meeresforschung (AWI), Telegrafenberg A43, 14473 Potsdam, Germany*

We re-examined sixteen pollen records from non-volcanic areas in the Kamchatka Peninsula to reconstruct vegetation and climate changes during the Holocene. Pollen records were first summarized and evaluated for each of three main physiographic regions: (1) Western Lowland (WL), open to the Sea of Okhotsk (6 records); (2) Central Kamchatka Depression (CKD), bordered by mountains (4 records); and (3) Eastern Coast (EC), facing the Pacific Ocean (6 records), and then compared over the peninsula. The synthesized data suggest that the climate over Kamchatka was generally wet and mild before ca. 5.8 ka (1 ka=1000 cal. yrs BP) due to strong and prolonged maritime influence. The first forest maximum in the CKD started at ca. 8.9, indicating a warmer climate; however, forest spread along the both coasts was delayed until ca. 7 ka, suggesting a possible modulation of greater effective moisture on the coastal sites (Fig. 1.4.2.3.1). The warmest period at ca. 7–5.8 ka is defined by the evidence of maximal forest extension overall the peninsula.

During that time, birch (Betula) prevailed over alder (Alnus) in forest everywhere except in the EC. Since ca. 5.8 ka, divergent vegetation patterns became evident in northern vs. southern and coastal vs. interior sites that correspond with a shift from warmer/maritime climate to cooler/continental climate. Also, greater climate variability accompanied the Neoglacial cooling since 5.8 ka. This climate cooling, indicated by drastic shrub expansion, advanced southward from the northern coasts (ca. 5.8 ka) to the central interior and coastal areas (ca. 5 ka) and then to the south (ca. 3.5 ka). Subsequent warming, suggested by the evidence of a second forest maximum, advanced westward from the EC (ca. 5.2 ka) to the CKD (ca. 3.2 ka) and then to the WL (ca. 1.9 ka). An advance of larch (Larix) in the CKD since ca. 3.2 ka points to increased climate continentality and larger seasonal variations. In contrast, alder forest spread after ca. 1.7 ka, reported only from the southern EC and CKD sites, indicates a mild, maritime-like climate that also agrees with the first apparent advance of spruce (Picea) in the interior. The latest cooling event, indicated by another shrub expansion, shows eastward trend: it occurred much earlier at the WL (ca. 2.4–1.6 ka) then at the EC (ca. 900–350 cal. yrs BP), and was less evident in the CKD. Instead, there was a remarkable coniferous expansion during the last millennium when both larch and spruce invaded and replaced deciduous forests so that by ca. 450–320 cal. yrs BP, an extensive coniferous forest ("Coniferous Island") appeared in the interior of Kamchatka. Since ca. 300 cal. yrs BP, spruce expanded most rapidly what broadly coincides with the beginning of the Little Ice Age.
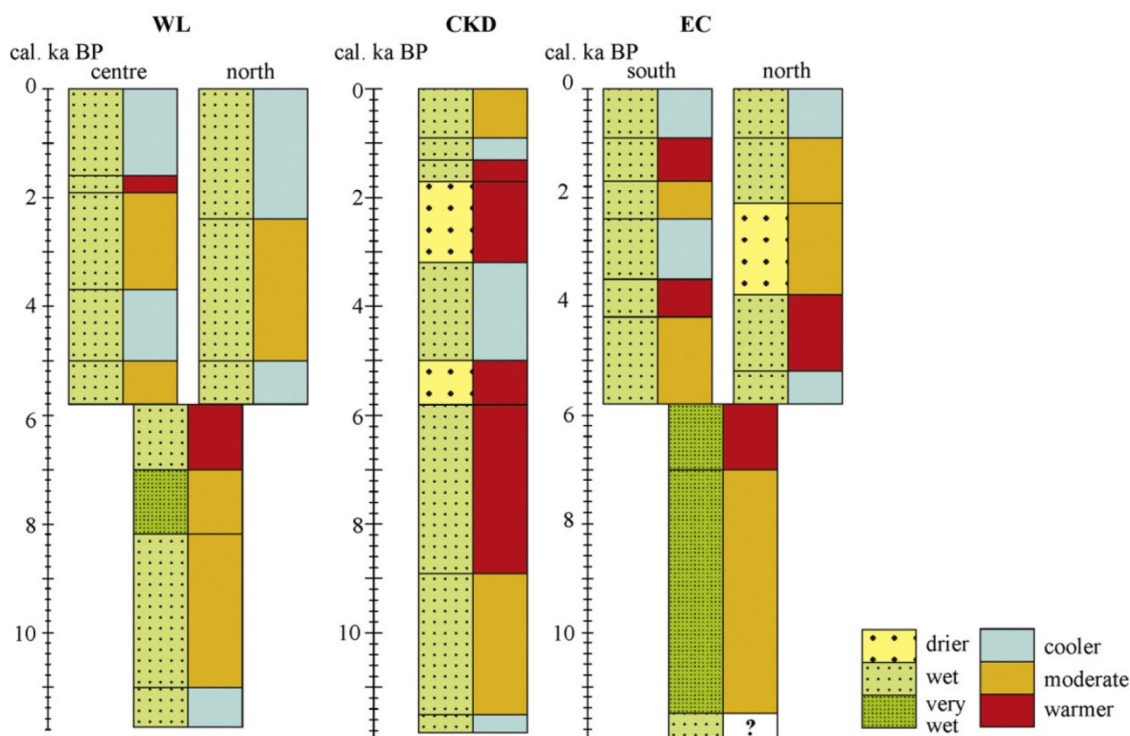
Fig. 1.4.2.3.1. Comparison of climate changes over Kamchatka.

Dirksen, V., Dirksen, O., & Diekmann, B. (2013). Holocene vegetation dynamics and climate change in Kamchatka Peninsula, Russian Far East. Review of Palaeobotany and Palynology, 190, 48-65. Doi: http://dx.doi.org/10.1016/j.revpalbo.2012.11.010

1.4.2.4.   Geogynamics in North-West of Pacific region: results from marine terraces investigations

Pinegina T.K., pinegtk@kscnet.ru, pinegtk@yandex.ru, **Kravchunovskaya E.A.,** *Institute of Volcanology and Seismology, FED, RAS, Petropavlovsk-Kamchatsky, Russia*

Bourgeois J. jbourgeo@uw.edu, *Department of Earth and Space Sciences, University of Washington, Seattle, WA, USA*

Lander A.V., land@mitp.ru, *Institute of Earthquake Prediction Theory and Mathematical Geophysics RAS, Moscow 117997, Russia*

Arcos M.E.M., beth.arcos@amec.com, *AMEC, 2101 Webster Street, Oakland, California 94612, USA*

Pedoja K., kevin.pedoja@unicaen.fr, **Nexer M., Delcaillau B.,** *Department of Geosciences, Normandie University, Caen, France, UCBN, Caen, France, CNRS, UMR 6143, Caen, France*

MacInnes B.T. macinnes@geology.cwu.edu, *Department of Geological Sciences, Central Washington University, Ellensburg, Washington 98926, USA*

Authemayou C., *Université de Brest,UMR 6538/CNRS Domaines océaniques, Plouzané, France*

Regard V. *Université de Toulouse, UPS (OMP), LMTG, Toulouse, France, IRD, LMTG, Toulouse, France, CNRS, LMTG, Toulouse, France*
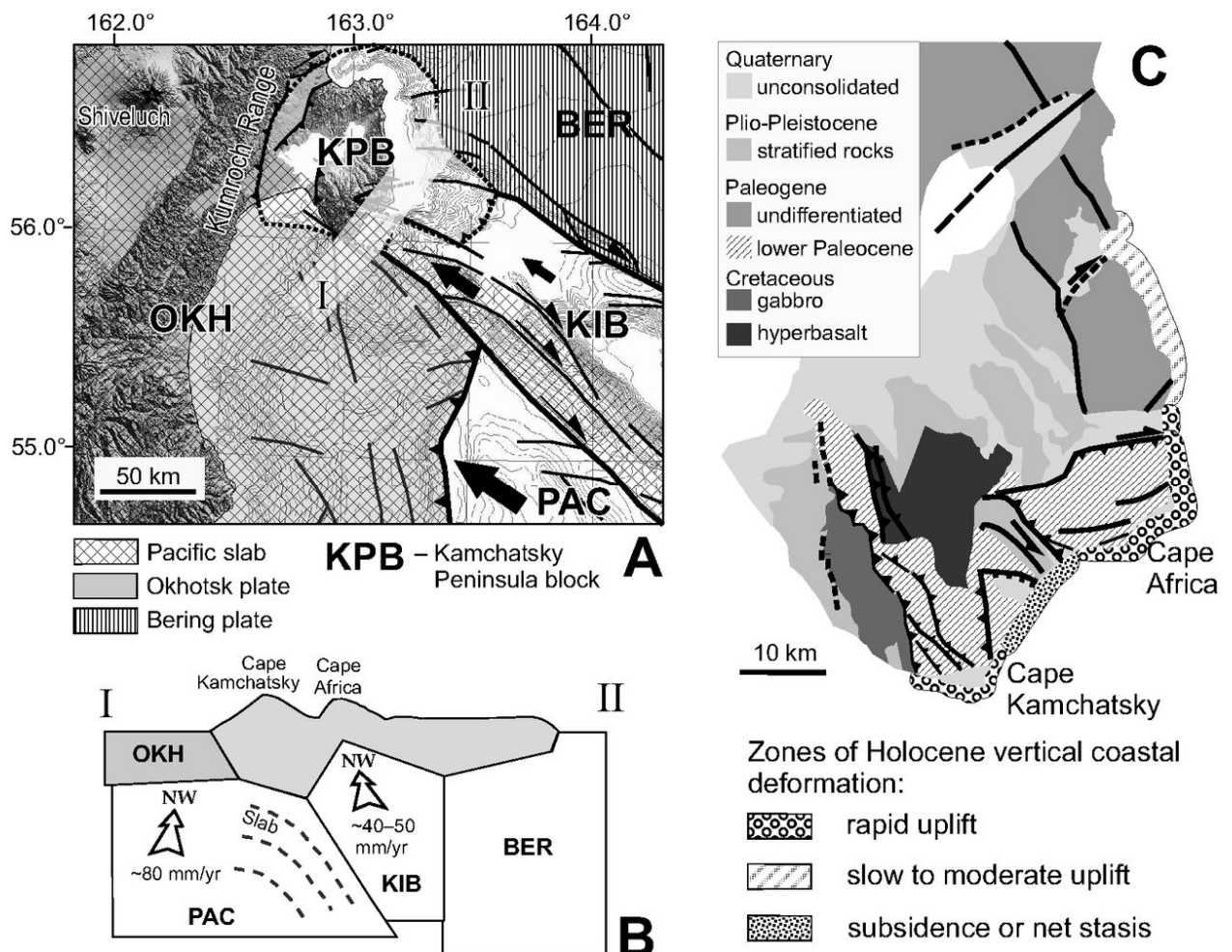
Fig. 1.4.2.4.1. Proposed geodynamic model for the Kamchatsky Peninsula region. (A) Proposed boundary of Kamchatsky Peninsula block (KPB): Western onshore boundary is after Kozhurin (2009) and Kozhurin and Pinegina (2011); other boundaries are shown schematically; southern boundary is after Bourgeois et al. (2006) and Pedoja et al. (2006); northern and eastern boundaries are shown along the base of the continental slope (margin). I-II—position of the schematic cross section shown on B. (B) Schematic cross section of the Kamchatsky Peninsula region divided into plates. PAC—Pacific plate, BER—Bering plate, OKH—Okhotsk plate, KIB— Komandorsky [Commander] Island block. Okhotsk and Pacific plates extend to the northwest, Komandorsky Island and Bering plates are limited by the Kamchatsky Peninsula block. (C) Geological map of Kamchatsky Peninsula (modified from Freitag et al., 2001), showing its main structural features and main faults, both active and old and zones of Holocene vertical coastal deformation. Note that the faults in C are based on different interpretations than in A.

Kamchatsky Peninsula lies within a complex meeting place of tectonic plates, in particular, the orthogonal interaction of the west-moving Komandorsky Island block with mainland Kamchatka. Examining the Holocene history of vertical deformation of marine wave-built terraces along the peninsular coast, we differentiated tectonic blocks undergoing uplift and tilting separated by zones of stable or subsided shorelines. We analyzed about 200 excavations along >30 coastal profiles and quantified vertical deformation on single profiles as well as along the coast using paleoshorelines dated with marker tephras. For the past 2000 yr, the average rates of vertical deformation range from about –1 to +7 mm/yr. Uplift patterns are similar to those detected from historical leveling and from mapping of the stage 5e Quaternary marine terrace (ca. 120 ka). Average vertical deformation in the Holocene is highest for the shortest studied time period, from ca. A.D. 250 to 600, and it is several times faster than rates for marine oxygen isotope stage (MIS) 5e terraces. Vertical displacements observed along the coast are most likely coseismic and probably have included subsidence as well as uplift events. Because subsidence is generally associated with erosion, almost surely more prehistoric large earthquakes occurred than are recorded as topographic steps in these terraces. We suggest that the distribution of coastal uplift and subsidence observed along the Kamchatsky Peninsula coastline is qualitatively explained by the squeezing of the Kamchatsky Peninsula block between the Bering and Okhotsk plates, and the Komandorsky Island block.

Vertical deformation of the southeast Kamchatsky Peninsula averaged over the past 2000 yr ranges from approximately –1 to +7 mm/yr. The most intensive and continuous Holocene vertical uplift has taken place around Capes Africa and Kamchatsky, consistent with their being uplifted mountainous massifs generated over a longer time scale. Sharp changes in rate of uplift in the Holocene correspond to three known active faults along the Pikezh, First, and Second Pereval'naya Rivers.

In individual locations, the average rate of vertical deformation varies over different time intervals and even changes from net uplift to subsidence. Through comparison of our data with seismological and geodetic data, we hypothesize that deformation of marine terraces was most likely coseismic. Earthquake source locations might be on mapped onshore and offshore faults as well as on unmapped faults under the continental shelf. Some coseismic deformation could be realized during the slip of the Pacific slab at its NW corner. The highest gradients of rate change along the coast took place during the shortest time interval we analyzed (about 350 yr long). This supports our conclusion that it is coseismic deformation rather than slow tectonic movement. There is some suggestion that the net rates for the past 2000 yr include episodes of both uplift (raised terraces) and subsidence (completely or partly eroded terraces).

We see no reason to assign the same rate of lateral displacement to the Cape Africa block as to Krutoberegovo station (as in Baranov et al., 2010); also, it seems clear that the Cape Africa block is not moving at the same rate as the Komandorsky Island block. If the GPS measurements represent a longer-term trend (such as the Holocene or longer), then the shortening could be taken up either offshore (suggested by Baranov et al., 2010) or onshore or, most likely, both. The dramatic difference in uplift between Cape Africa and the subsiding area to the south suggests to us that there should be a thrust fault bounding the southern side of the cape.

We propose a qualitative explanation for the variety of vertical movements observed on the Kamchatsky Peninsula coastline. The shallow parts of the Kamchatsky Peninsula are pressed (squeezed) between three bounding plates—Bering, Okhotsk, and Komandorsky Island block—whereas the base is partly coupled with the Pacific slab (Fig. 1.4.2.4.1). We think that in the northern and northeastern part of the peninsula, deformation is primarily the result of interaction with the Bering plate, resulting in slow to moderate uplift. Cape Africa rises rapidly as a result of collision with the Komandorsky Island block. The southern and western parts of the peninsula are under the influence of two plates: interaction with the Okhotsk plate and tangential stress on the base as result of coupling with the Pacific slab. This geodynamic model helps explain the pattern of coastal uplift and subsidence described in detail in this paper.

At the NW corner of the Pacific region, just south of the Kamchatsky Peninsula, the northern tip of the Pacific plate subduction and associated volcanic arc interacts with the western end of the Aleutian-Komandorsky dextral transform plate boundary and associated arc. Study of both Holocene and Pleistocene sequences of uplifted marine terraces and also of fluvial drainage patterns on the Kamchatsky Peninsula allows us to highlight active tectonics produced by complex plate interaction. Our results show that the central eastern coast of the peninsula is currently divided into four different zones consisting in uplifted blocks associated with various uplift rates in front of a fold-and-thrust zone to the west. Our main tectonic benchmark—the altitude of the shoreline correlated to the Last Interglacial Maximum (Marine Isotopic Stage 5e)—yields late Pleistocene uplift rates ranging from 0.2 to 2.74 mm/yr. One of the main active faults bounding the coastal blocks is dextral and is interpreted as a prolongation of an offshore fault of the Aleutian-Komandorsky dextral transform plate boundary. We suggest that structures on the Kamchatsky Peninsula accommodate a part of the transform motion, but that mainly, the arc-continent collision of the Aleutian arc against Kamchatka produces a "bulldozer" effect on the Kamchatsky Peninsula.
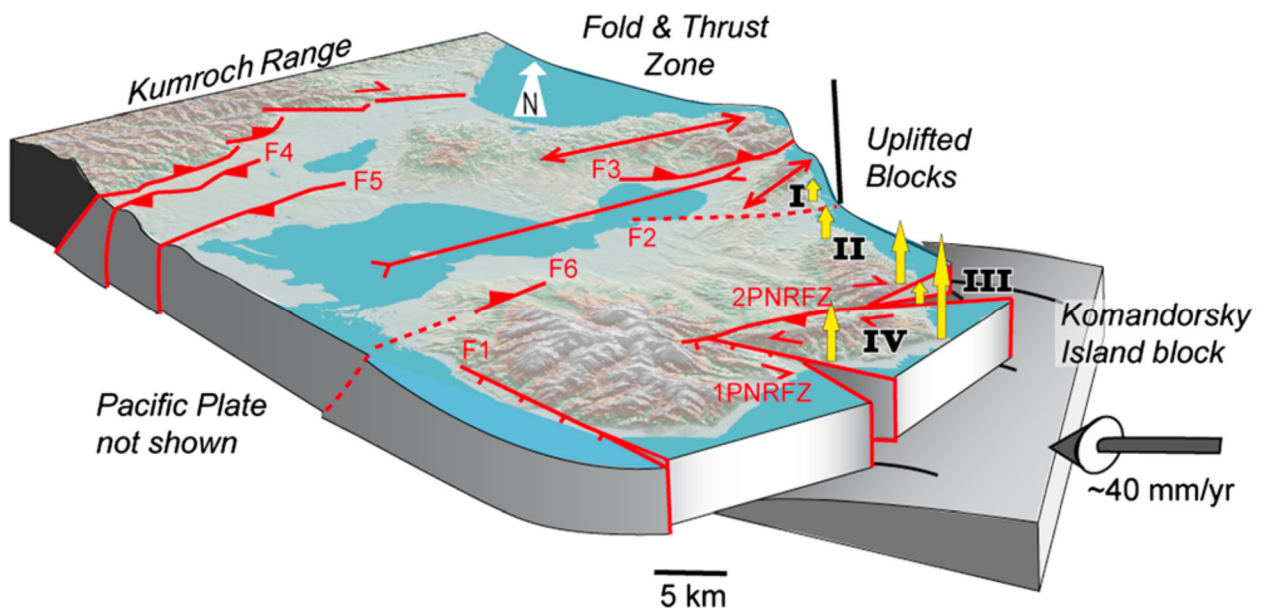
Fig. 1.4.2.4.2. Cartoon representing the "encroachment" of the Komandorsky Island block on the Kamchatsky Peninsula.

Our results show marked tectonic segmentation of the coastal fringe of the Kamchatsky Peninsula (Fig. 1.4.2.4.2). Late Pleistocene uplift rates along the coast vary in space with marked rapidity, ranging from 0.2 to 2.74 mm/yr. Geomorphic analysis suggests folding and thrusting in the hinterland of the Kamchatsky Peninsula and tilting of the coastal blocks associated with vertical and strike-slip displacements along faults at the block boundaries. Since the Kamchatsky Peninsula is located near the western end of the large dextral transform system associated with the western Aleutian-Komandorsky arc, the structures on the peninsula likely accommodate westward convergence of the Komandorsky Island block and its collision with the continent, producing the effect of a bulldozer.

This deformation pattern indicates that the Kamchatsky Peninsula actively undergoes arc-continent collision with the Aleutian arc at the triple junction between the Okhotsk, North American, and Bering plates, as suggested by several earlier studies. On the other hand, the pattern, in particular the shortening in the hinterland associated with Kumroch Range blocking, contravenes an active, rigid, clockwise rotation of the entire Kamchatsky Peninsula as proposed by Kozhurin [2007]. Also, the connection between onshore faults of the peninsula and offshore faults of the Aleutian-Komandorsky transform boundary suggested by Gaedicke et al. [2000] is not supported by our results, except for the fault zone of the second Pereval'naya River valley, which can be linked to a proposed splay of the Bering fault zone. This independence of onshore faults was also proposed

by Kozhurin [2007], although our kinematic model does not agree with some details of his analysis.

In this study, uplift rates and active deformation of the Kamchatsky Peninsula—located at the intersection of the Pacific subduction zone and the Komandorsky-Aleutian dextral transform boundary—have been estimated using a combined field and map analysis of Pleistocene marine terraces, drainage anomalies, and active faults. Extensive field data accompanied by morphotectonic analysis using several remote-sensing techniques have permitted us to refine a neotectonic model for the entire Kamchatsky Peninsula as affected by this very active and complex collision zone.

Pinegina, T. K., Bourgeois, J., Kravchunovskaya, E. A., Lander, A. V., Arcos, M. E. M., Pedoja, K., & MacInnes, B. T. (2013) A nexus of plate interaction: Vertical deformation of Holocene wave-built terraces on the Kamchatsky Peninsula (Kamchatka, Russia). Geological Society of America Bulletin*, 125(9-10), 1554-1568. Doi:10.1130/B30793.1*

Pedoja, K., Authemayou, C., Pinegina, T., Bourgeois, J., Nexer, M., Delcaillau, B., & Regard, V. (2013) "Arc-continent collision" of the Aleutian-Komandorsky arc into Kamchatka: insight into Quaternary tectonic segmentation through Pleistocene marine terraces and morphometric analysis of fluvial drainage. Tectonics, 32(4), 827-842. Doi:<u>10.1002/tect.20051</u>

1.4.2.5.   Rate of collisional deformations in Kamchatsky Peninsula

Kozhurin A. I., <u>anivko@yandex.ru,</u> **Zelenin E. A.,** <u>egorzelenin@mail.ru</u>**,** *Geological Institute, Russian Academy of Sciences, Pyzhevskii per. 7, Moscow, 119017 Russia*

Pinegina   T.K., <u>pinegtk@kscnet.ru,</u>   <u>pinegtk@yandex.ru,</u>   **Ponomareva   V.   V.,** <u>vera.ponomareva1@gmail.com</u>, *Institute of Volcanology and Seismology, Petropavlovsk-Kamchatsky, Russia*

Mikhailyukova P. G., *Faculty of Geography, Moscow State University, Moscow, 119234 Russia*

Detailed data are discussed on the rate of Holocene horizontal and vertical movements along a fault in the southeastern Kamchatsky Peninsula, which is situated between the converging Aleutian and Kamchatka island arcs. The fault is the northern boundary of the block invading into the peninsula under pressure of the Komandorsky Block of the Aleutian arc. The rate of right-lateral slip along the fault was increasing in the Holocene and reached 18–19 mm/yr over the last 2000 years and 20 mm/yr by contemporary time. Comparison of these estimates with those that follow from offsets of older rocks also indicates acceleration of horizontal movements along the fault from the early Quaternary to the present. The results obtained from rates of GPS station migration show that about half the rate of the northwestern drift of the Komandorsky Block is consumed for movement of the block of the southern side of the fault. The remainder of movement of the Komandorsky Block is consumed for movements (probably, underthrusting) at the eastern continental slope of the Kamchatsky Peninsula (Figs. 1.4.2.5.1 and 1.4.2.5.2).

The horizontal movements along the Second Pereval'naya Fault in the Holocene were characterized by a high rate. For comparison, it can be seen that the mean rate over the last 2000 years (18–19 mm/yr) and the suggested modern rate (~20 mm/yr) are equal to the rate of horizontal movements in the Holocene along the North Anatolian Fault (18 ± 5 mm/yr) and that it only slightly yields to the rate of movements along some segments of San Andreas Fault (24 ± 3 mm/yr) over the last 14000 years. The fast propagation of the southern side of the Second Pereval'naya Fault is apparently determined by the geodynamic situation, especially by the closeness to the contact of the western Aleutian arc and Pacific Plate as a source of motion. Comparison of the estimated rates of horizontal movements along the above fault and the rates of GPS station migration suggests that the southern side of the fault should be limited in the east and west by zones of horizontal shortening of the crust; i.e., it is a separate block. This implies, first, the

possibility, to a certain degree, of independent movement of the southeastern part of the Kamchatsky Peninsula relative to the Komandorsky Block, and second, that the Second Pereval'naya River Fault is not an immediate onshore extension of the right-lateral Bering Fault on land.
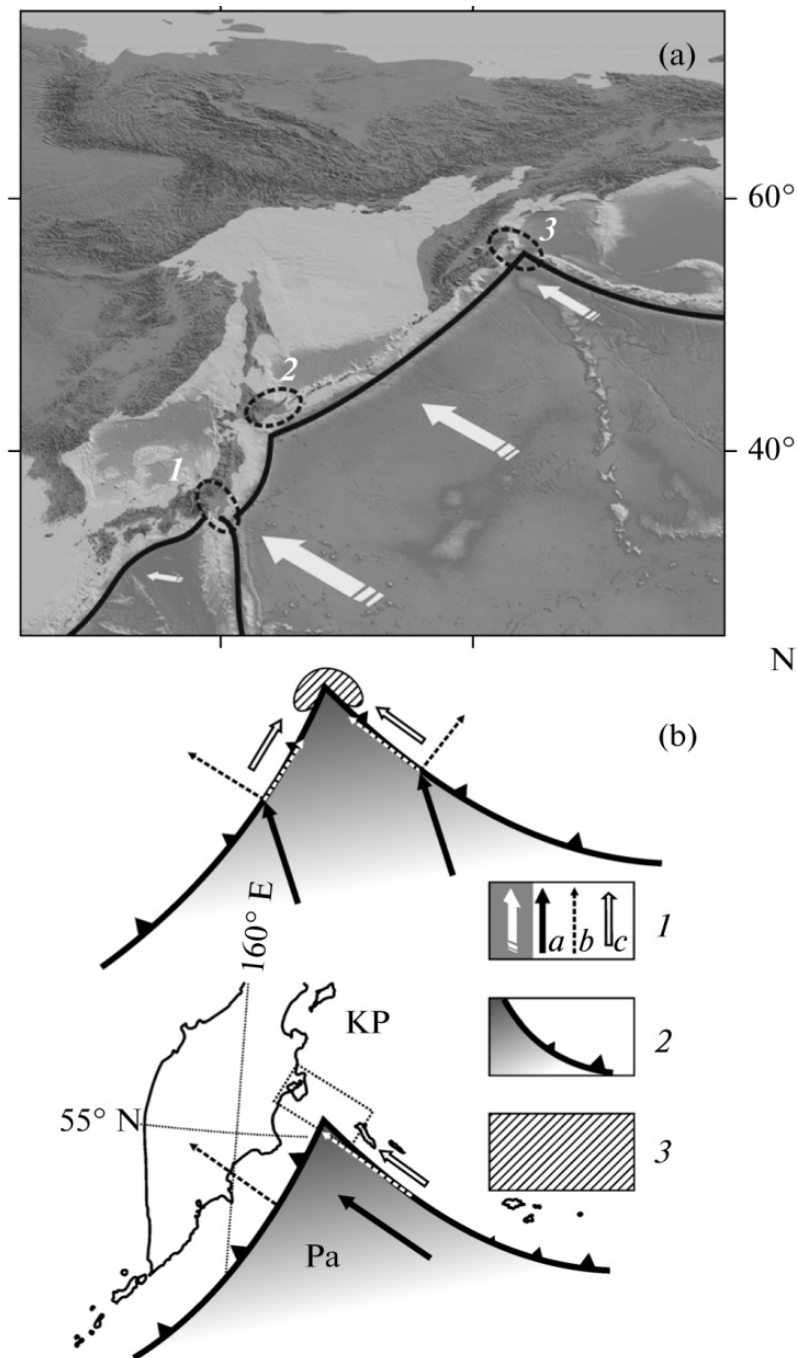
Fig. 1.4.2.5.1. (a) Collisional interaction of island arcs in the northwestern Pacific: 1, Izu–Bonin and Japan; 2, Japan and Kurile–Kamchatka; 3, Kurile–Kamchatka and Aleutian; bathymetry and topography, after SRTM30-PLUS; (b) conceptual scheme of tangential and normal components of oceanic plate motion relative to island arcs (above) and their relationships in the junction of Kamchatka and Aleutian island arcs (below). (1a) Direction of the Pacific Plate motion, (1b) orthogonal and tangential components of plate motion relative to island arcs, (1c) direction of motion of part of island arc toward collisional zone; (2) subduction zone; size of triangular ticks shows increase (decrease) of underthrusting (normal) component; (3) collisional domain. KP, Kamchatsky Peninsula; Pa, Pacific Plate.
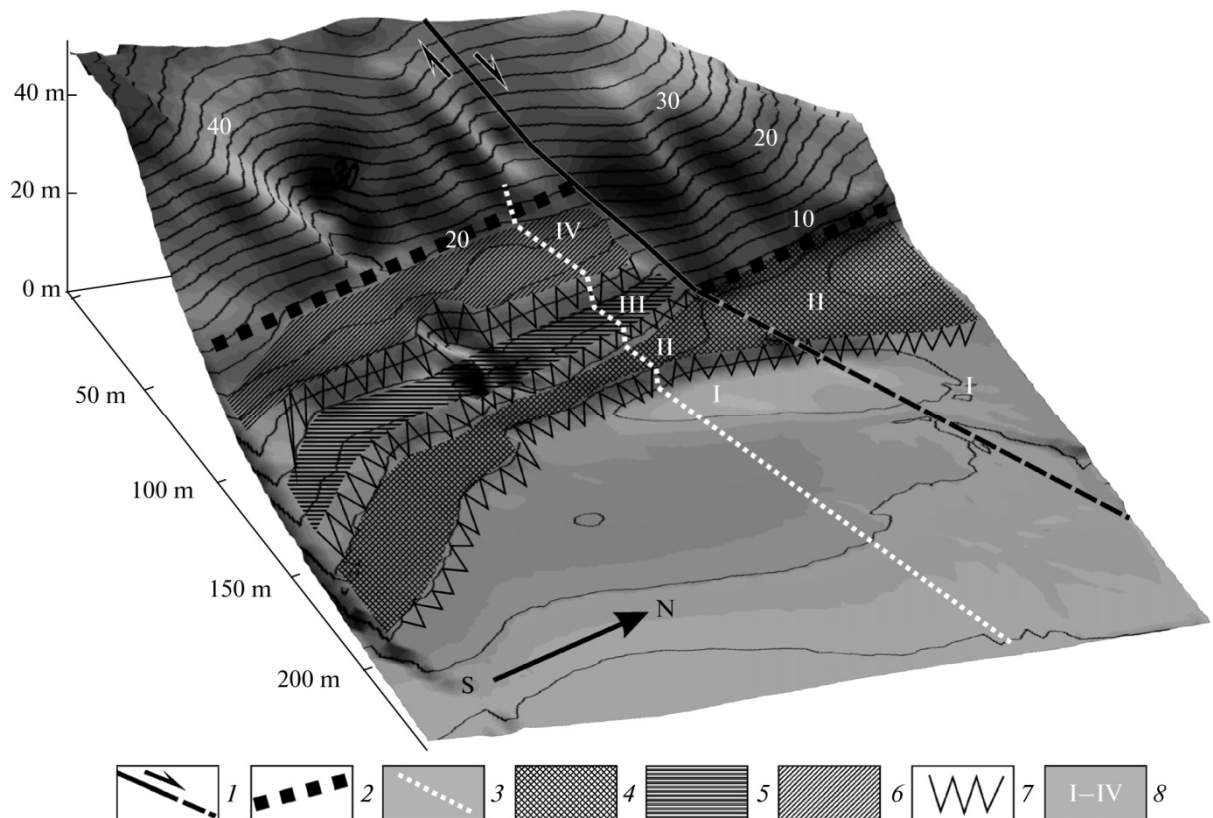
Fig. 1.4.2.5.2. 3D model of topography of wave built marine terrace cut by the Second Pereval'naya Fault. (*1*) Fault line along which landforms and sediments have been deformed; dashed line is segment of fault where young marine terrace remains undeformed; (*2*) abrasion cliff displaced along fault 30–32 m; (*3*) topographic profile; (*4*) terrace level II undeformed by fault; (*5, 6*) terrace levels III and IV retained only in southern uplifted side of fault; (*7*) scarps separating terrace levels; (*8*) terrace level number. Contour lines are spaced at 2 m.

From the two-thirds of the transform movement rate related to the northwestern drift of the western Aleutians, almost half is consumed by collisional deformation of the Kamchatsky Peninsula, which is a buffer in the zone of interaction between the Aleutian arc and Kamchatka. The remaining motions of the Komandorsky Block are apparently consumed by movements (probably underthrusting) in the zone of tectonic contact at the eastern continental slope of the peninsula established by Geist and Scholl.

The increase in mean rate of horizontal movements along the Second Pereval'naya River Fault reflects the acceleration of movement of the southern side of this fault (southeastern block of the Kamchatky Peninsula) since the onset of its motion in the early Quaternary.

Kozhurin, A. I., Pinegina, T. K., Ponomareva, V. V., Zelenin, E. A., & Mikhailyukova, P. G. (2014). Rate of collisional deformation in Kamchatsky Peninsula, Kamchatka. Geotectonics, 48(2), 122-138. Doi: 10.1134/S001685211402006X

1.4.3. Volcano monitoring and geoinformation systems

1.4.3.1. Kamchatkan Volcanic Eruption Response Team (KVERT)

Gordeev E.I., gordeev@kscnet.ru**, Girina O.A.,** girina@kscnet.ru**,** *Institute of Volcanology and Seismology, Petropavlovsk-Kamchatsky, Russia*

In March 2013, the Kamchatkan Volcanic Eruption Response Team (KVERT) celebrated the 20th anniversary of its activity. This team, which was created by the joint efforts of Russian and American scientists, analyzes on a daily basis the data supplied by the complex (seismic, video, visual, and satellite) monitoring system of volcanoes of Kamchatka and the Northern Kuril Islands to notify airline companies and all interested organizations about potential hazards.

Kamchatka is one of the most active volcanic regions on the planet. Large explosive volcanic eruptions, in which the ash elevates up to 8-15 km above sea level, occur here every 1.5 years. Study of eruptions precursors in order to reduce a volcanic risk for the population is an urgent problem of Volcanology. The available precursor of strong explosive eruptions of volcanoes, identified from satellite data (thermal anomaly), as well as examples of successful prediction of eruptions using this precursor, are represented in this research.

The Alaska Volcano Observatory (AVO) staff also participated in hazard communication and monitoring of multiple eruptions at ten volcanoes in Russia as part of its collaborative role in the Kamchatka and Sakhalin Volcanic Eruption Response Teams

Gordeev, E. I., & Girina, O. A. (2014). Volcanoes and their hazard to aviation. Herald of the Russian Academy of Sciences, 84(1), 1-8. Doi: 10.1134/S1019331614010079

Girina, O. A. (2012). On precursor of Kamchatkan volcanoes eruptions based on data from satellite monitoring. Journal of Volcanology and Seismology, 6(3), 142-149. Doi: 10.1134/S0742046312030049

McGimsey, R.G., Neal, C.A., Girina, O.A., Chibisova M.V., & Rybin A.V. (2014) 2009 Volcanic activity in Alaska, Kamchatka, and the Kurile Islands—Summary of events and response of the Alaska Volcano Observatory: U.S. Geological Survey Scientific Investigations Report 2013–5213, 125 p. Doi: http://dx.doi.org/10.3133/sir20135213

1.4.3.2.   Information system «Volcanoes of the Kurile-Kamchatka island arc»

Romanova I.M., roman@kscnet.ru, **Girina O.A.,** girina@kscnet.ru, **Melekestsev I.V., Maximov A.P.,** maximov@kscnet.ru, *Institute of Volcanology and Seismology, Petropavlovsk-Kamchatsky, Russia*
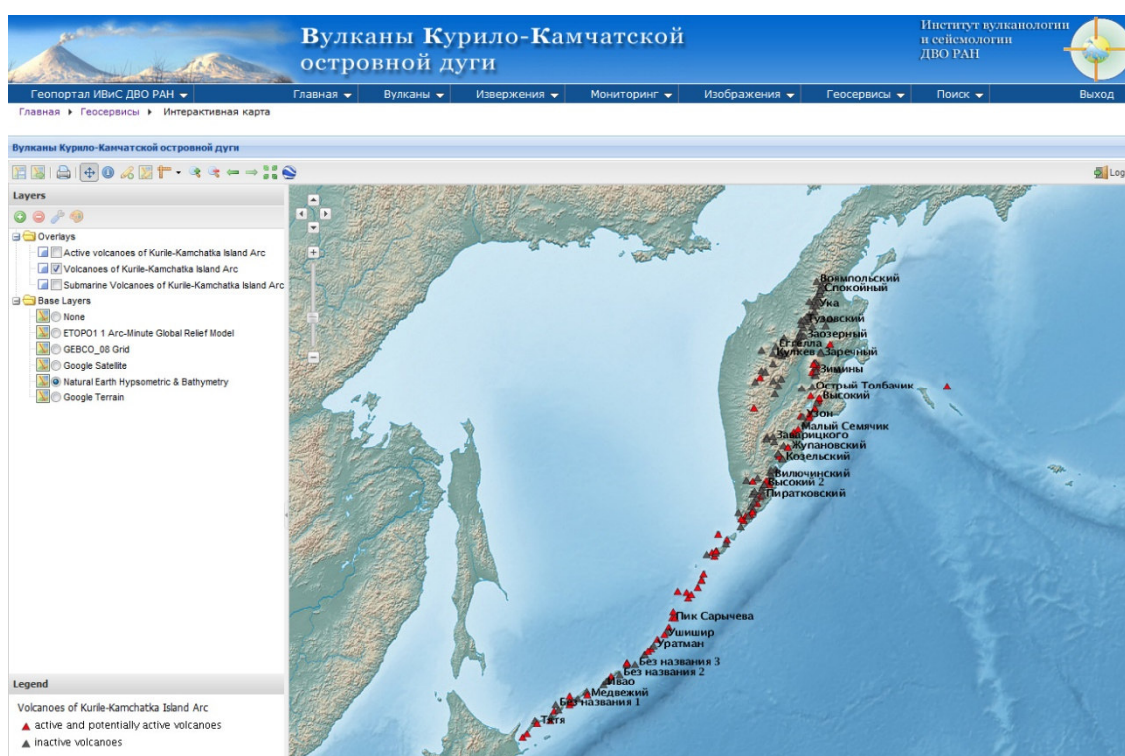
Fig. 1.4.3.2.1. WMS-service «Volcanoes of the Kurile-Kamchatka island arc».
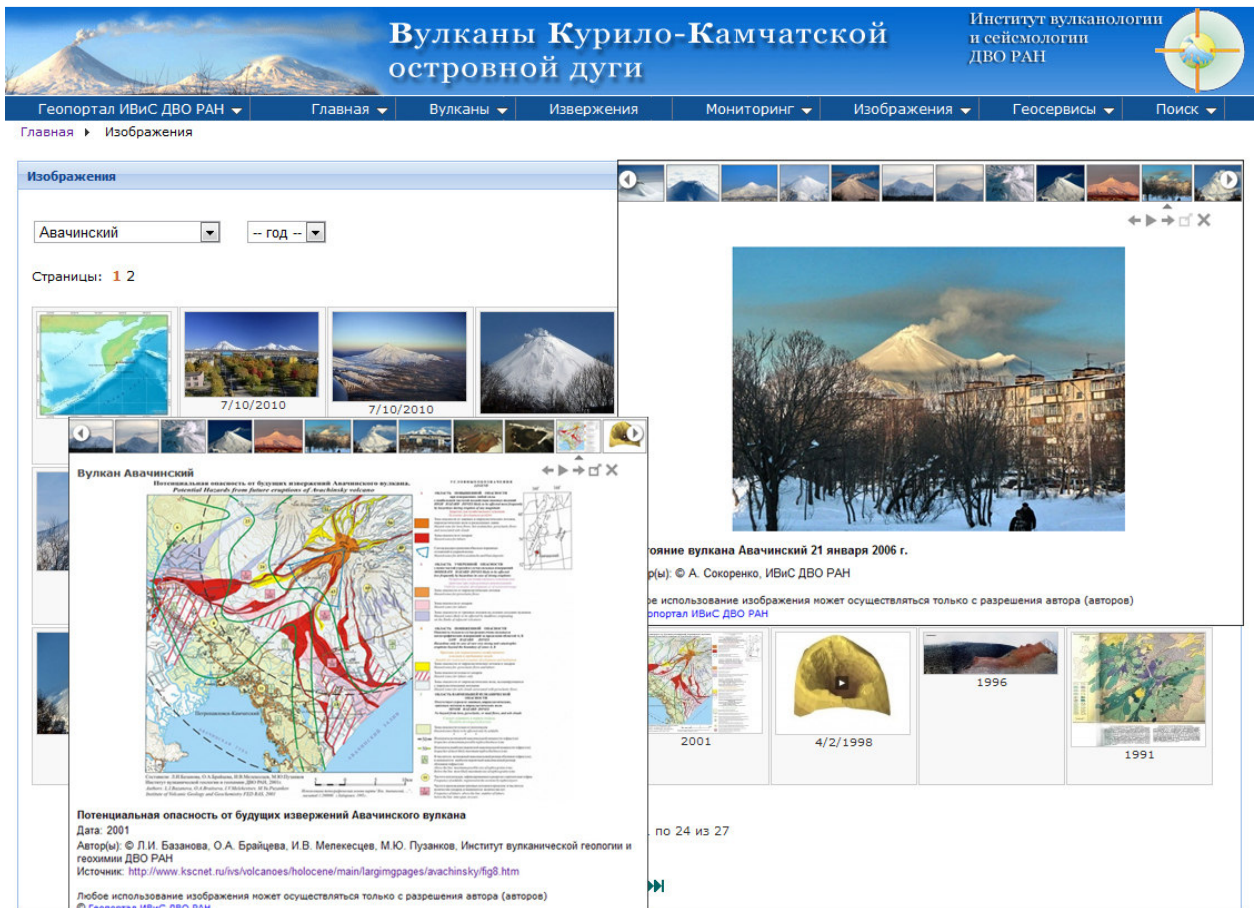
Fig. 1.4.3.2.2. Example of the the web page «Images» (Avachinsky volcano).

This research was conducted with aim to create the information system «Volcanoes of the Kurile-Kamchatka island arc» which is being developed in the Institute of Volcanology and Seismology FEB RAS. The system will allow integration of wide range of data on volcanoes in Kamchatka, Kurile Islands and adjacent seas into a single information environment available for the world scientific community and for Internet users. The general interface of the system is shown on Figs. 1.4.3.2.1 and 1.4.3.2.2.

Romanova, I. M., Girina, O. A., Melekestsev, I. V., & Maximov, A. P. (2012). Information system "Volcanoes of the Kurile-Kamchatka island arc. Bulletin of Kamchatka regional association "Educational-Scientific Center". Earth sciences, 1(19), 128-137. (In Russian). http://www.kscnet.ru/kraesc/2012/2012_19/art9.pdf

Romanova, I.M., Girina, O.A., Maximov, A.P., & Melekestsev, I.V. (2012) The creation of a comprehensive web-based information system "Volcanoes of the Kurile-Kamchatka island arc" (VOKKIA). Information science and control systems, no. 3 (33), 179-187. . (In Russian). http://ics.khstu.ru/media/2012/N33_19.pdf

Romanova, I. M., Girina, O. A., Maximov, A. P., & Melekestsev, I. V. (2013). Volcanoes of Kurile-Kamchatka Islands Arc information system. Forecasting Volcanic Activity - Reading and translating the messages of nature for society. IAVCEI 2013 Scientific Assembly, July 20-24, Kagoshima, Japan. http://www.kazan-g.sakura.ne.jp/iavcei2013/iavcei_hp/PDF/4H.pdf

1.4.3.3. V□□□n □m□nit□ring s□st□ms

Gordeev E.I., gordeev@kscnet.ru, **Girina O.A.,** girina@kscnet.ru,, **Mel'nikov D.V.,** dvm@kscnet.ru, **Manevich A.G.,** lav217@kscnet.ru, **Romanova I.M.,** roman@kscnet.ru, *Institute of Volcanology and Seismology, Far East Branch, Russian Academy of Sciences, Petropavlovsk-Kamchatsky, Russia*
Efremov V.Yu., evgeny@iki.rssi.ru, **Lupyan E.A. , Matveev A.M., Proshin A.A., Flitman E.V.,** *Space Research Institute of RAS, Moscow, Russia*
Kramareva L.S., kramareva@dvrcpod.ru, *Far-Eastern Center of State Research Center for Space Hydrometeorology «Planeta», Khabarovsk, 680000, Russia*
Sorokin A.A., alsor@febras.net, **Korolev S.P.,** *Computer Center of Far East Branch, Russian Academy of Sciences, Khabarovsk, 680063, Russia*
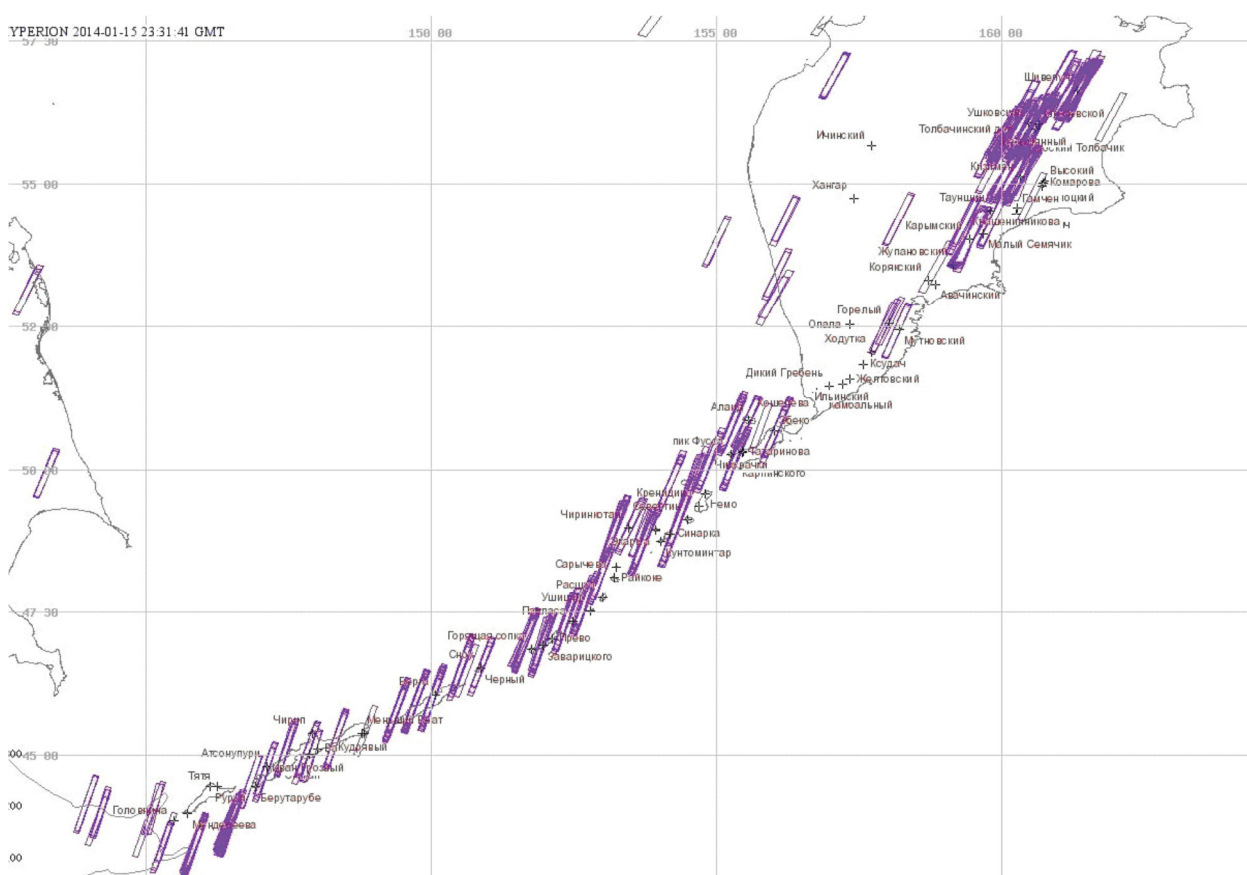
Fig. 1.4.3.3.1. The area of coverage by the Hyperion equipment along the Kurile-Kamchatka arc available for the information system VolSatView at January 2014.

Annual Kamchatkan strong explosive eruptions with ash emissions of 8–15 km above the sea level represent a real threat to modern jet aviation. To reduce the risk of aircraft encounters with volcanic ash clouds in the North Pacific region, the KVERT team of the Institute of Volcanology and Seismology of Far Eastern Branch RAS (IVS FEB RAS) conducts daily satellite monitoring of Kamchatkan volcanoes. In 2011, experts of IVS FEB RAS, Space Research Institute RAS, Computing Center of Far Eastern Branch RAS and Far Eastern Center of "Planeta" Research Center for Space Hydrometeorology created and put into trial operation an information service "Monitoring of volcanic activity of Kamchatka and the Kurile Islands" (VolSatView). This service allows working with different satellite data, including hyperspectral data, as well as meteorological and ground information. VolSatView will be able to provide volcanologists with the possibility of continuous monitoring and study of volcanic activity in Kamchatka and the Kurile Islands. The

paper presents examples of hyperspectral satellite data use in the VolSatView environment to analyze different volcanic processes.

The coverage area for "Monitoring of volcanic activity of Kamchatka and the Kurile Islands" information system is shown on Fig. 1.4.3.3.1, and the examples of satellite images for the active volcanoes of Kamchatka are shown on Fig. 1.4.3.3.2 and 1.4.3.3.3.
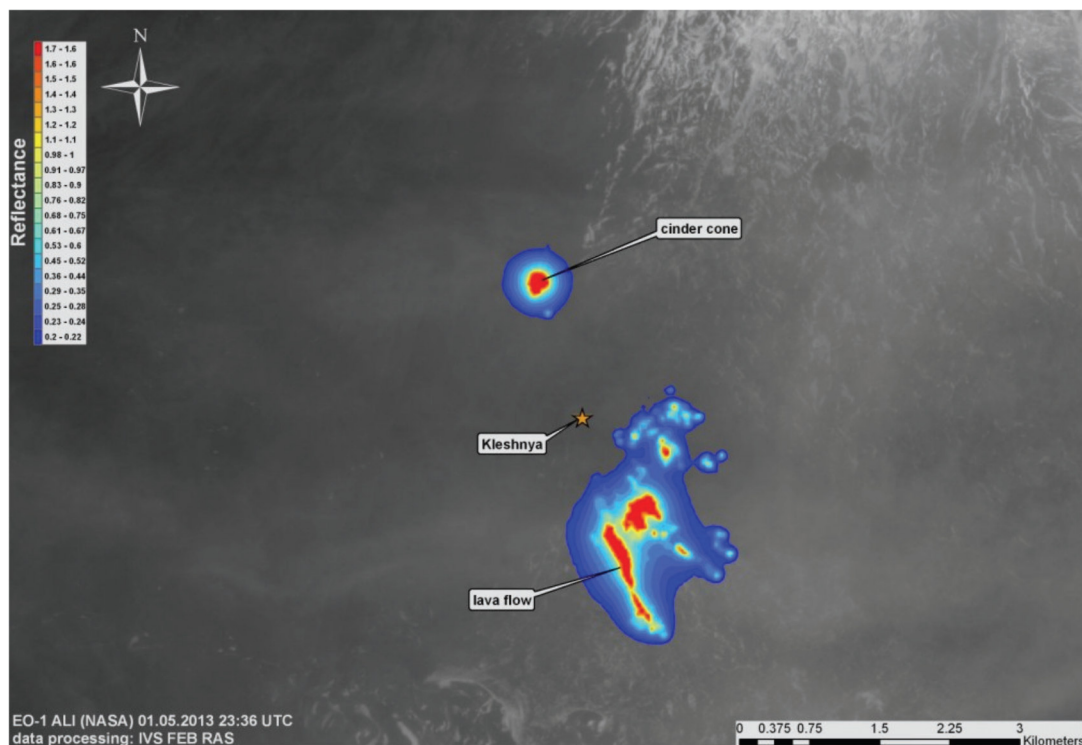
Fig. 1.4.3.3.2. Reflectance of the lava flows of the Tolbachik eruption 2012-13 in spectral diapazone 2.08-2.35 mkm from space image EO-1 ALI (NASA) from 23:36 UTC 01.05.2013.
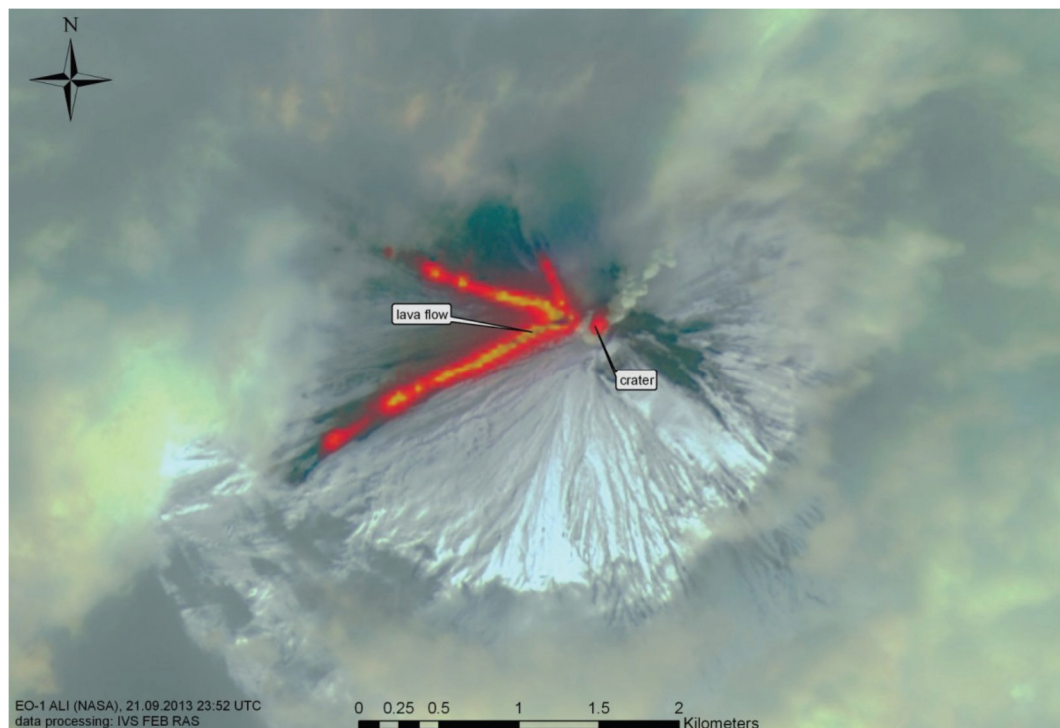
Fig. 1.4.3.3.3. Reflectance of the Klyuchevskoy lava flows from space image EO-1 ALI (NASA) from 21.09.2013 in IR diapason (combination of channels 10, 9, 8).

Gordeev, E. I., Girina, O. A., Lupyan, E. A. , Sorokin, A. A., Efremov, V. Yu., Mel'nikov,, D. V., Manevich, A. G., Romanova, I. M., Korolev, S. P., & Kramareva, L. S. (2014). Possibility of using hyperspectral data from satellite observations to study activity of Kamchatka volcanoes on the basis of the VolSatView geoportal. Current problems in remote sensing of the earth from space, 11(1), 267-284. (In Russian). http://d33.infospace.ru/d33_conf/sb2014t1/267-284.pdf

Efremov, V. Yu., Girina, O. A., Kramareva, L. S., Lupyan, E. A. , Manevich, A. G., Matveev, A. M., Mel'nikov, D. V., Proshin, A. A., Sorokin, A. A., & Flitman, E. V. (2012). Creating an information service "Remote monitoring of active volcanoes of Kamchatka and the Kuril Islands", Current problems in remote sensing of the earth from space, 9(5), 155-170. http://d33.infospace.ru/d33_conf/sb2012t5/155-170.pdf

1.4.3.4. Database of marker tephra layers from major Holocene eruptions in Kamchatka

Kyle Ph.R., kyle@nmt.edu, **Rourke Schluep R.,** *Department of Earth and Environmental Science, New Mexico Institute of Mining and Technology, Socorro, NM, USA*

Ponomareva V., vera.ponomareva1@gmail.com, *Institute of Volcanology and Seismology, Petropavlovsk-Kamchatsky, Russia*

Kamchatka Peninsula is one of the most active volcanic regions in the world. Many Holocene explosive eruptions have resulted in widespread dispersal of tephra-fall deposits. The largest layers have been mapped and dated by the ^{14}C method. The tephra provide valuable stratigraphic markers that constrain the age of many geological events (e.g. volcanic eruptions, palaeotsunami, faulting, and so on). This is the first systematic attempt to use electron microprobe (EMP) analyses of glass to characterize individual tephra deposits in Kamchatka. Eighty-nine glass samples erupted from 11 volcanoes, representing 27 well-identified Holocene key-marker tephra layers, were analysed. The glass is rhyolitic in 21 tephra, dacitic in two, and multimodal in three. Two tephra are mixed with glass compositions ranging from andesite/dacite to rhyolite. Tephra from the 11 eruptive centres are distinguished by their glass K_2O, CaO, and FeO contents. In some cases, individual tephra from volcanoes with multiple eruptions cannot be differentiated. Trace element compositions of 64 representative bulk tephra samples erupted from 10 volcanoes were analysed by instrumental neutron activation analysis (INAA) as a pilot study to further refine the geochemical characteristics; tephra from these volcanoes can be characterized using Cr and Th contents and La/Yb ratios.

Unidentified tephra collected at the islands of Karaginsky (3), Bering (11), and Attu (5) as well as Uka Bay (1) were correlated to known eruptions. Glass compositions and trace element data from bulk tephra samples show that the Karaginsky Island and Uka Bay tephra were all erupted from the Shiveluch volcano. The 11 Bering Island tephra are correlated to Kamchatka eruptions. Five tephra from Attu Island in the Aleutians are tentatively correlated with eruptions from the Avachinsky and Shiveluch volcanoes.

Using these data the geochemical database on glass composition was created. This batabase includes analyses of 1000 ash samples from the Kamchatka's volcanoes and represented by 15000 microprobe analyses and by 360 LA-ICPMS analyses (Fig. 1.4.3.4.1).

This database allows correlate the ash between remote sections and thus allows to compare paleoclimate, paleooceanic, volcanic and paleoseismological events as well as the scales of past explosive eruptions.

At present time the geospatial database of Kamchatka Holocene volcanism is in development. This database will include information on volcanic deposits distribution, their ages, chemical composition, location of calderas, craters, cinder cones and metadata for single volcanoes or group of volcanoes.
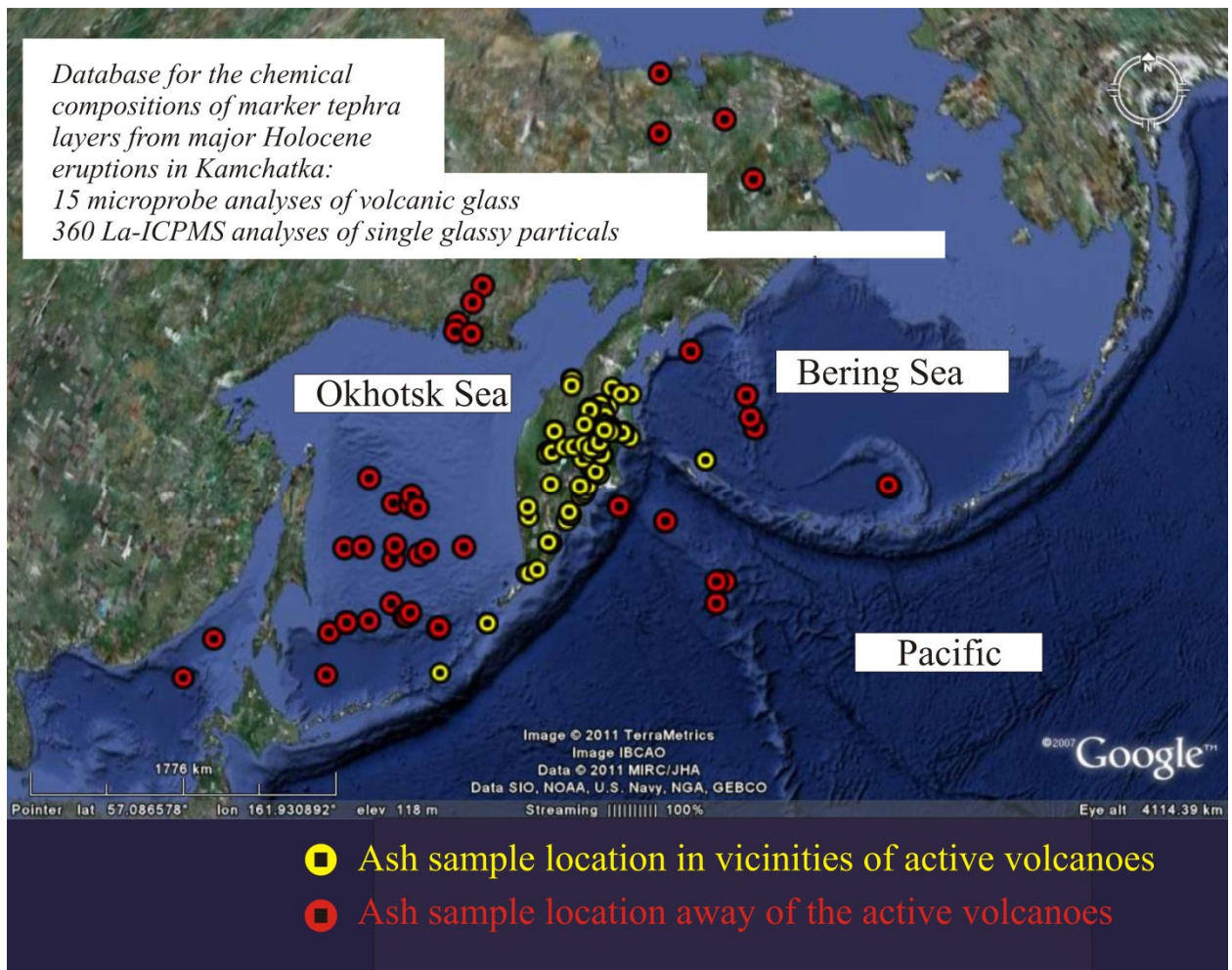
Fig. 1.4.3.4.1. The location of ash sampling.

Kyle, Ph. R., Ponomareva, V. V., & Schluep, R. R. (2011). Geochemical characterization of marker tephra layers from major Holocene eruptions in Kamchatka, Russia. International Geology Review, 53(9), 1059–1097. Doi: 10.1080/00206810903442162

Zelenin, E. A., Ponomareva, V. V., & Mikhaylyukova, P. G. (2014). The geospatial database of Kamchatka Holocene volcanism: structure and implementation using PostgreSQL/PostGIS. Modern Information Technologies in Earth Sciences: Materials of the International Conference, Petropavlovsk-Kamchatsky, September 8-13, 2014, 158. Vladivostok, Dalnauka. http://kamchatka2014.fegi.ru/images/abstracts1.pdf

1.4.3.5. Integrated Instrumental Monitoring of Volcanoes

Chebrov V.N., chebr@emsd.iks.ru, **Droznin D.V., Droznina S.Ya., Kugaenko Yu.A.,** ku@emsd.ru, **Nuzhdina I.N., Senyukov S.L.,** ssl@emsd.ru, **Sergeev V.A., Serovetnikov S.S., Titkov N.N., Firstov P.P.,** firstov@emsd.ru, **Yaschuk V.V.,** *Geophysical Survey, Kamchatka Branch, Russian Academy of Sciences (GS KB RAS), Petropavlovsk-Kamchatsky, Russia*

Zakharchenko N.Z., Mishatkin V.N., *Geophysical Survey, Russian Academy of Sciences, Obninsk, Kaluga oblast, Russia*

Melnikov D.V., dvm@kscnet.ru, **Murav'ev Ya.D.,** murjd@kscnet.ru, *Institute of Volcanology and Seismology, Far East Branch, Russian Academy of Sciences, Petropavlovsk-Kamchatsky, Russia*

Rybin A. V., *Institute of Marine Geology and Geophysics, Far East Branch, Russian Academy of Sciences, Yuzhno-Sakhalinsk, Russia*

This work presents the project of the first stage of implementation of the integrated instrumental system of volcanic activity monitoring in Kamchatka and the Kuril Islands (Fig. 1.4.3.5.1). The system of monitoring was designed for the purpose of ensuring public safety, aviation safety, and reducing economic losses caused by volcanic eruptions. The most active and dangerous volcanoes in Kamchatka (North and Avacha groups of volcanoes) and the Kuril Islands (volcanoes on the islands of Kunashir and Paramushir) are of first priority for monitoring. For this purpose, special observation points are planned to be installed on the volcanoes. The system of monitoring will include a complex of observations (broadband seismic station with a large dynamic range, tiltmeter, devices for gas, acoustic, and electromagnetic observations, and video camera). All the data will be passed to information processing centers in real time. New methods and algorithms of automatic and automated identification of the volcanic activity level and the probabilistic volcano hazard assessment have been developed.
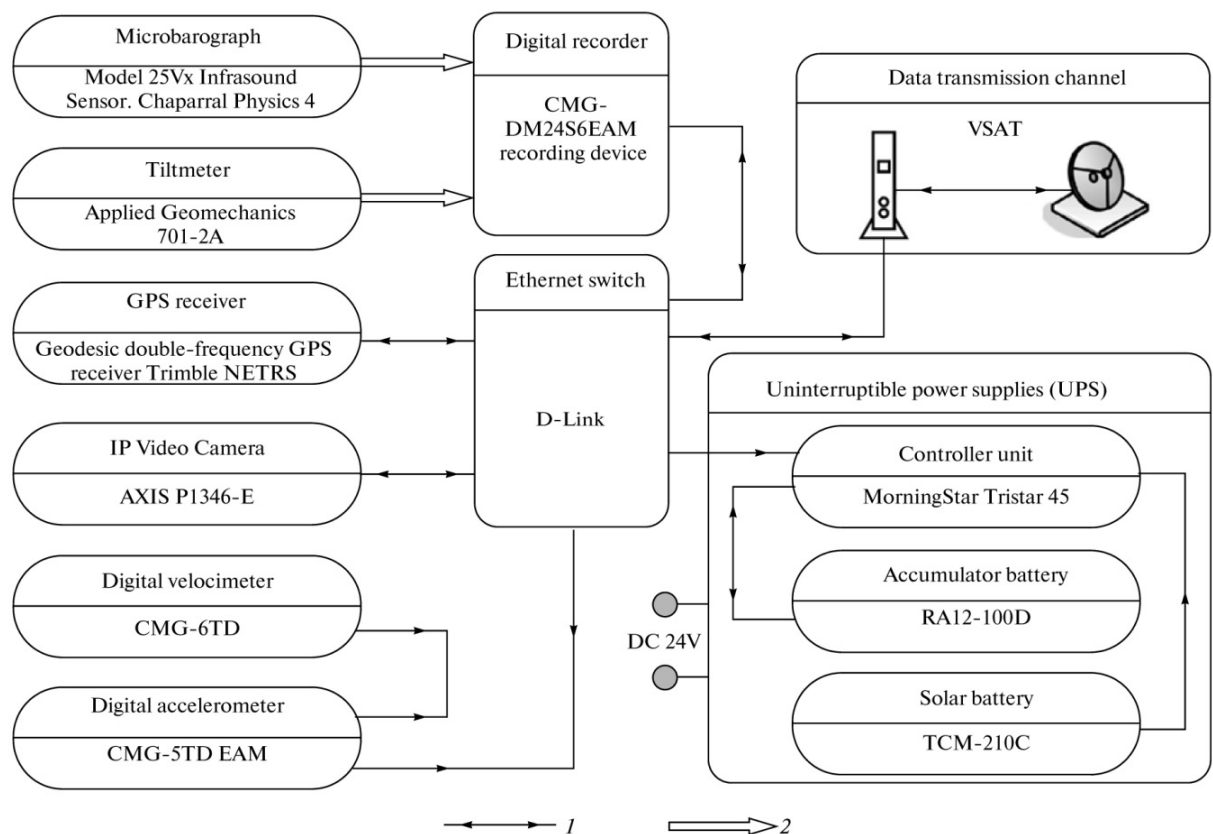
Fig. 1.4.3.5.1. The block diagram of a typical volcano observation point. 1 – Ethernet lines, 2 – analog signals.

Chebrov, V. N., Droznin, D. V., Droznina, S. Y., Zakharchenko, N. Z., Kugaenko, Y. A., Melnikov, D. V., Mishatkin, V. N., Murav'ev, Ya. D., Nuzhdina, I. N., Rybin, A. V., Senyukov, S. L., Sergeev, V. A., Serovetnikov, S. S., Titkov, N. N., Firstov, P. P.,. & Yaschuk, V. V. (2013). The development of the system of integrated instrumental monitoring of volcanoes in the Far East Region. Seismic Instruments, 49(3), 254-264. Doi: 10.3103/S0747923913030055

1.4.4. The phenomenon of the Khailinskoe earthquake in the South-West of the Koryak highland. Tectonic conditions of formation and localization

Yarotskij G.P. *Institute of Volcanology and Seismology, Far East Branch, Russian Academy of Sciences, Petropavlovsk-Kamchatsky, Russia*

We determined the tectonic setting of the Khailinskoe earthquake (1991, M>6.6) in Koryak seismic belt. This earthquake had unusual north-west cloud orientation, which cross cut the regional NE structures (Fig. 1.4.4.1). The earthquake was localized in the area of longitudinal deep NW fault, which was formed in the axis of graben-sinclinal of the Olutorsky bay crust. This fault cross cut at some depth the area were two terraines joined producing on the top of it the column of heterogeneity with pores, voids, and so on. Koryak seismic belt is located on the northern edge of the Bering plate. Due to rotation of Bering plate on the depth of 35 km the relaxation was occur. Khailinskoe earthquake was a foreshock of the Olutor earthquake which happened in 2006 (M>7.6). The deep modelling was confirmed by Ilpirsky (2013) and Ust'-Kamchatsky earthquakes (1971) and can be considered as a part of the seismical forecast for this area.
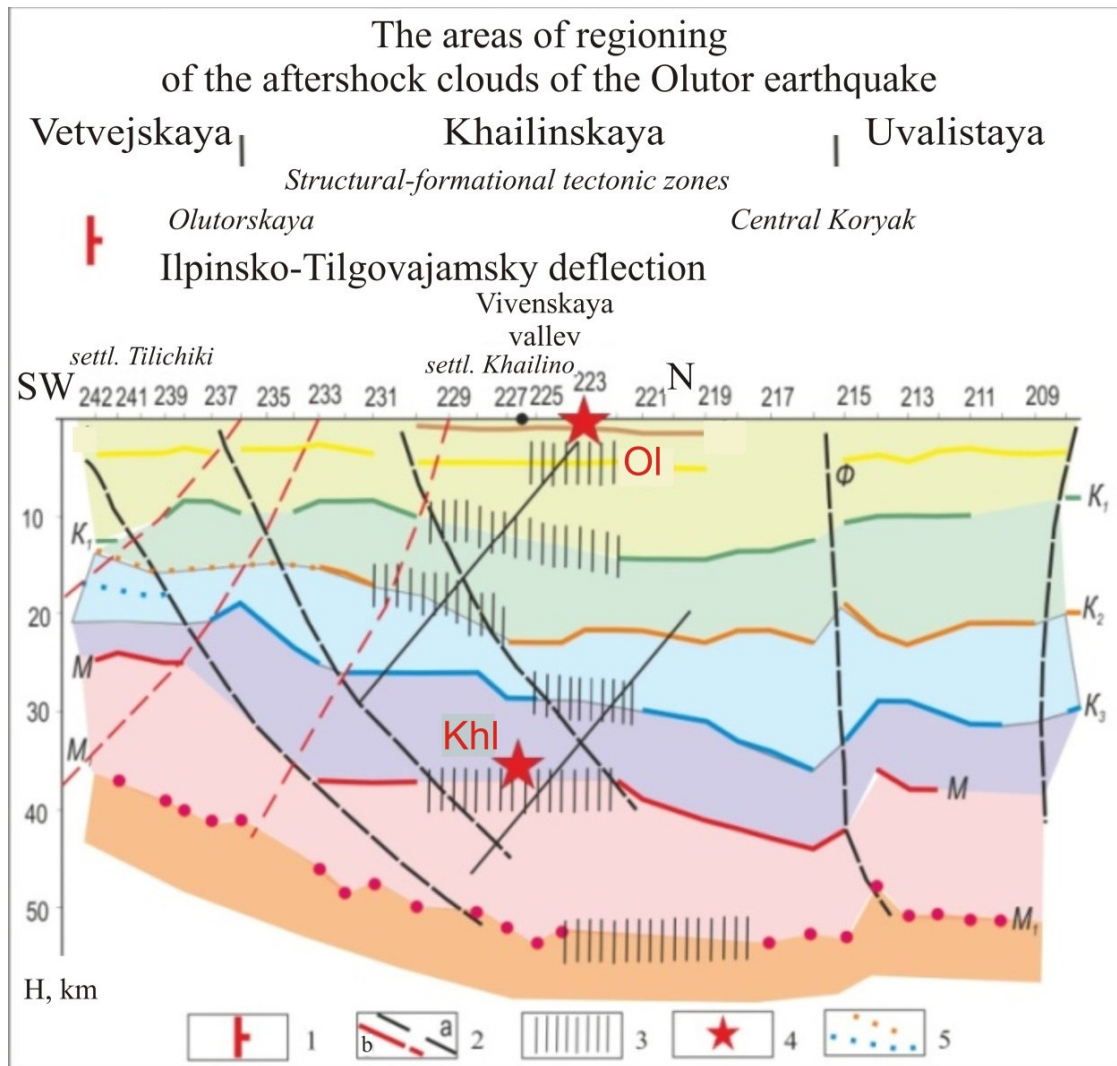
Fig. 1.4.4.1. The model tectonic structure of the Khailinsky earthquake. (1) transverse transcrust faults; (2) faults determined by the loss of correlation in the boundaries at the basement, crust, Moho and upper mantle (a), author interpretatzion (b); (3) the areas of the loss of correlation in the crust and upper mantle (Fedotov et al., 2011) and zones of loss of converted waves (Beliavsky et al., 2007); (4) the main epicenters (Ol – Olutorsky earthquake, Khl – Khailinskoe earthquake); 5 – supposed borders.

Yarotskij G. P. (2013). The phenomenon of the Khailinskoe earthquake in the South-West of the Koryak highland. Tectonic conditions of formation and localization. Geodynamics, Lviv city, Ukraine, "Lvovskaja politekhnika", 14, 95-101. (In Russian).

2. COMPLEX RESEARCHES ON THE VOLCANOES OF THE KURILE ISLAND ARC

2.1. Volcanological studies along the Kurile island arc

2.1.1. Bubbled lava from the floor of the Sea of Okhotsk

Baturin G.N., gbatur@ocean.ru, *Shirshov Institute of Oceanology, Russian Academy of Sciences, Moscow, Russia*
Dubinchuk V.T., *Fedorovskii Russian Scientific Research Institute of Mineral Resources, Moscow, Russia*
Rashidov V.A., rashidva@kscnet.ru, *Institute of Volcanology and Seismology, Far East Branch, Russian Academy of Sciences, Petropavlovsk-Kamchatsky, Russia*
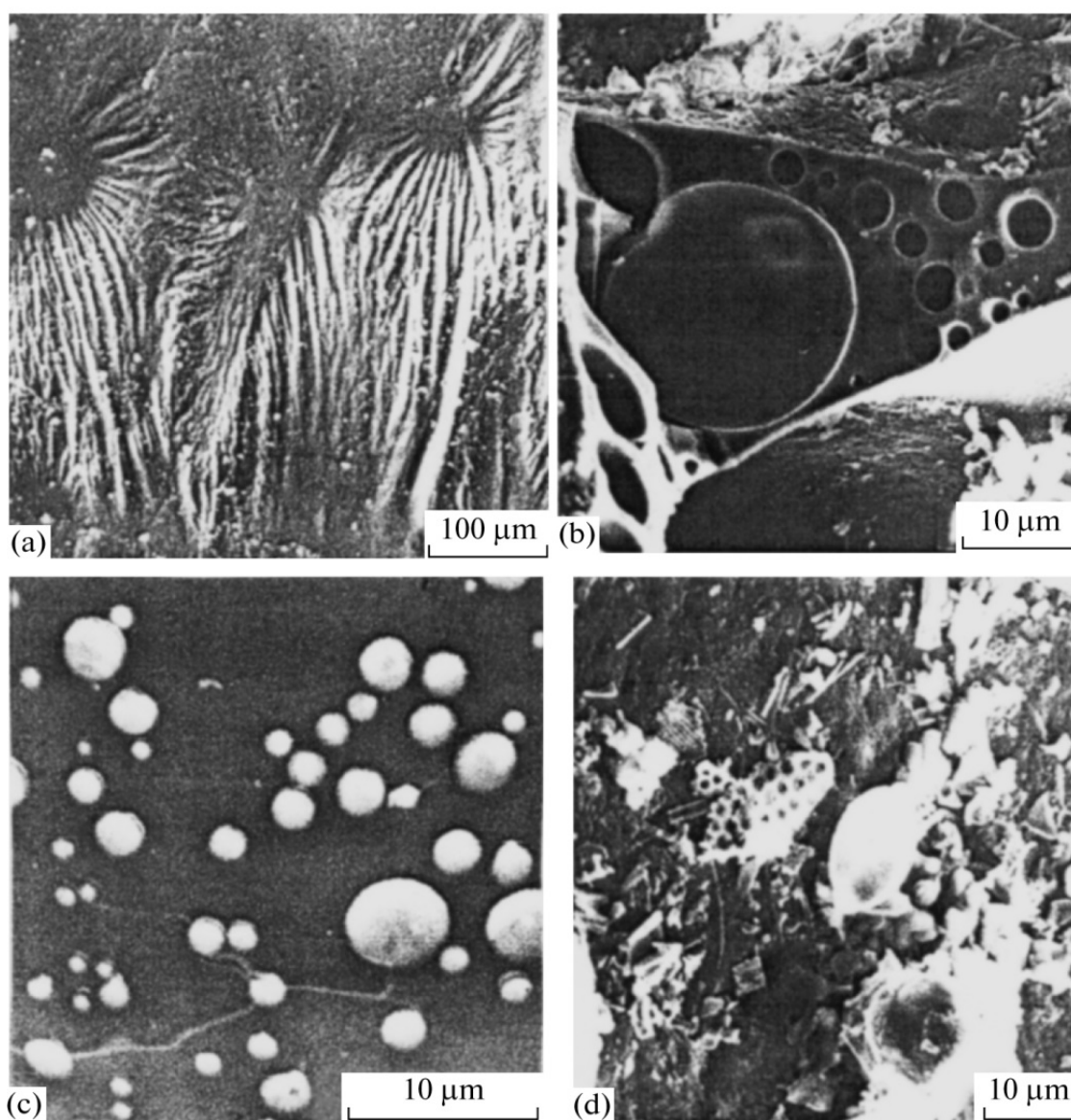
Fig. 2.1.1.1. Microstructure of the lava: (a) liquation microstructure of the inner part of the sample; (b) porous microstructure of the outside of the sample; (c) microglobules within the porous mass; (d) organic residues on the surface of the lava.

A sample of bubbled lava (Fig. 2.1.1.1) raised from a submarine volcano in the Sea of Okhotsk was analyzed by means of electron microscopy and the ICP–MS technique. The outside of the sample is flecked with rounded micro- and macrocavities, and the inner part is characterized by a liquation structure. Along with this, the unstructured mass of the rock contains globular particles of nearly the same diameters as the cavities. The lava is close to andesites and volcanic ashes of Kamchatka Peninsula in the macro- and microelemental composition but different in the somewhat increased content of barium, strontium, lithium, niobium, tungsten, uranium, and thorium. It is suggested that the cavities were formed during the eruption of the submarine volcano owing to contact of the boiling gas-saturated lava with seawater accompanied by the ejection of ash, which was spread by marine currents over long distances.

Baturin, G. N., Dubinchuk, V. T., & Rashidov, V. A. (2014). Bubbled lava from the floor of the Sea of Okhotsk. Doklady Earth Sciences, 456(1), 579-584. Doi: 10.1134/S1028334X14050225

## 2.1.2. Origin of spatial compositional variations of volcanic rocks from the Northern Kurile Islands, Russia: Geochemical studies of active volcanoes on the Paramushir, Atlasov, Antsiferov islands and adjacent submarine volcanoes

Kuvikas O.V., olgakuvikas@gmail.com, *Department of Natural History Science, Graduate School of Science, Hokkaido Univ., Japan. Institute of volcanology and seismology FEB RAS, Piip boulevard 9, Petropavlovsk-Kamchatsky 683006, Russia*
Nakagawa M., mnakagawa@mail.sci.hokudai.ac.jp, *Department of Natural History Science, Graduate School of Science, Hokkaido Univ., Japan*
Avdeiko G.P., gavdeiko@kscnet.ru, **Rashidov V.A.,** rashidva@kscnet.ru, *Institute of volcanology and seismology FEB RAS, Piip boulevard 9, Petropavlovsk-Kamchatsky 683006, Russia*

The Northern Kurile Islands located on the Northern part of the Kuril Arc, on the boundary between continental Southern Kamchatka basement and oceanic Kurile Arc. Investigated area includes active volcanoes of Paramushir, Atlasova, Antsiferova islands and adjacent submarine volcanoes (Fig. 2.1.2.1). We newly determined major and trace element compositions, Sr-Nd isotopic variations.

Peculiarities of petrography and whole-rock chemistry enable us to divide all volcanoes into three main zones: frontal, intermediate and rear ones. Frontal zone include Chikurachki, Tatarinova, Lomonosova, 1.3 volcanoes. The rocks are Ol-Cpx bearing Opx basaltic andesite. Fuss, Shirinki and Ebeko volcanoes locate at the intermediate zone. Hbl-Cpx-Ol-bearing Opx andesite (SiO_2 ~ 49-63%) are commonly characterized by the presence of hornblende phenocryst. Alaid, Grigoreva volcanic group locate at the rear zone. Ol-bearing Cpx basalts and basaltic andesite are typical (SiO_2 ~ 48-52%). In addition, Alaid and Grigorev volcanic group is characterized by the largest eruptive volume (150 km^3). Analyzed rocks have subduction origin, about it suggest Ta, Nb minimum on the spider diagrams and naturally enriched of the LILE, LREE and depleted of the HFSE, HREE from front to back arc zone (Fig. 2.1.2.2). Frontal zone is characterized by lowest contents of incompatible elements (e.g. Rb, Ba, K) and LREES (e.g. Nd, Ce).

Isotopic variations have the highest value of $^{143}Nd/^{144}Nd$ and $^{87}Sr/^{86}Sr$ as 0.7031-0.7034 (Fig. 2.1.2.3). In the opposite, rear and intermediate zones show narrower lower contents of $^{143}Nd/^{144}Nd$ and $^{87}Sr/^{86}Sr$ as 0.7029-0.7031. The rocks of rear zone show highest contents of LILE (e.g. K, Rb), LREES (e.g. La, Gd, Nd, Sm) and HFSEE (e.g. Nb, Ta). Both $^{143}Nd/^{144}Nd$ and $^{87}Sr/^{86}Sr$ ratios of the rocks from intermediate and frontal zones increase with increasing of silica contents. These suggest that andesitic and dacitic rocks from these zones are possibly affected by crustal

component. In contrast, crustal assimilation might be minor process in the case of the rear zone, because basaltic rocks are predominant in the zone. Geochemical features of the mafic rocks investigate the spatial difference in magma sources of three zones. Rocks from rear zone are systematically enriched in Nb/Y, Th/Yb, Ta/Yb, Nb/Yb, La/Yb ratios (Fig. 2.1.2.2a). These data are implied by the fact that magma in the rear zone more enriched with comparing depleted frontal zone. In addition, chemical variations of fluid-mobile elements (e.g. Cs, Ba, U, Th, Sr) and immobile elements (e.g. Nd, Nb, Zr, Hf) of the mafic rocks will be explained by different types of subduction components (Fig. 2.1.2.2 b).
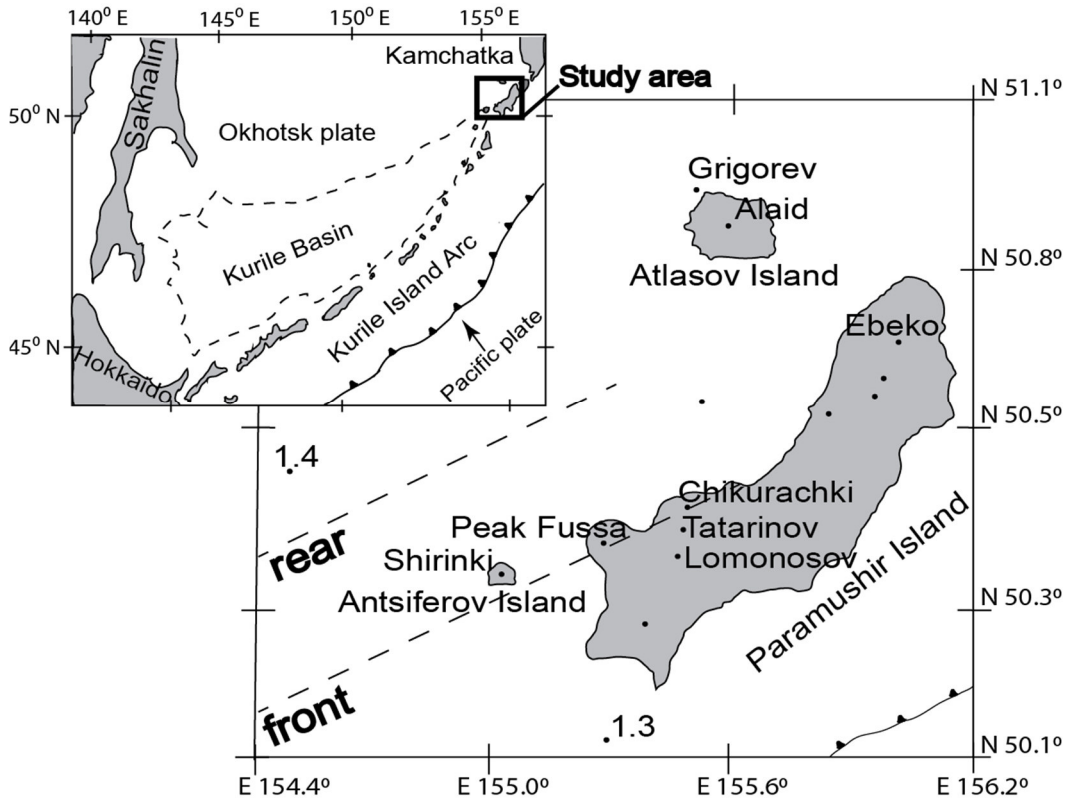
Fig. 2.1.2.1. Index map of the NKI and surrounding areas (inset). Small points denote volcanoes. Dash lines define tectonic zones relatively to slab depth: 120-140 km frontal zone, 140-160 km rear zone.
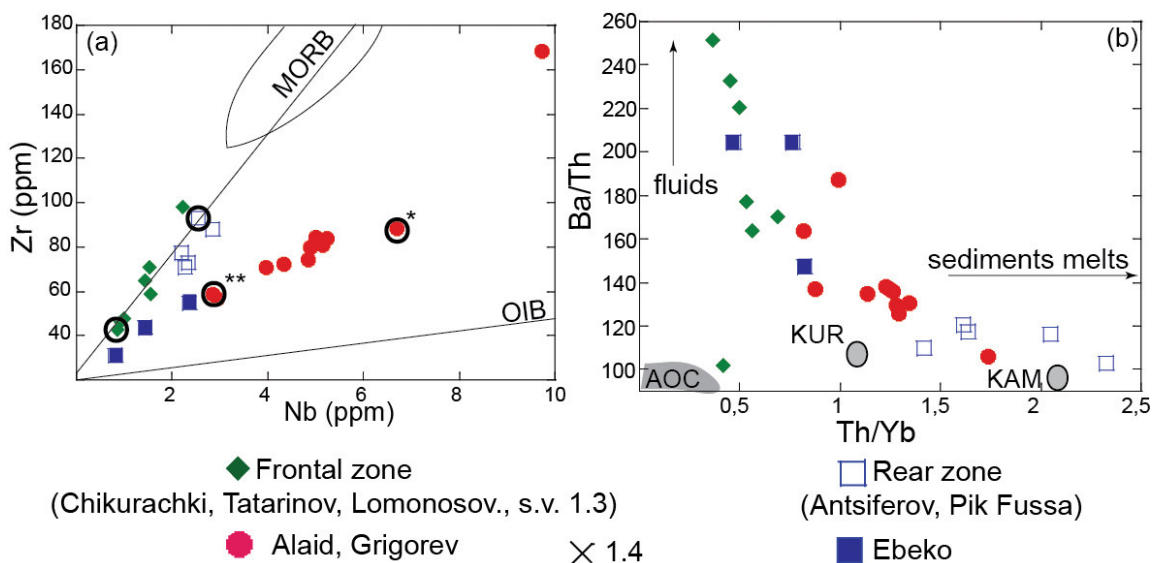
Fig. 2.1.2.2. Inter-element ratios with less fluid-mobile or immobile elements (a) and strongly fluid-mobile (b). Data source are: N-MORB (Sun, 1989), AOC (Duggen et al., 2007), sediments subducted beneath the Kurile (KUR) and Kamchatka (KAM) (Plank and Langmuir, 1998).

128
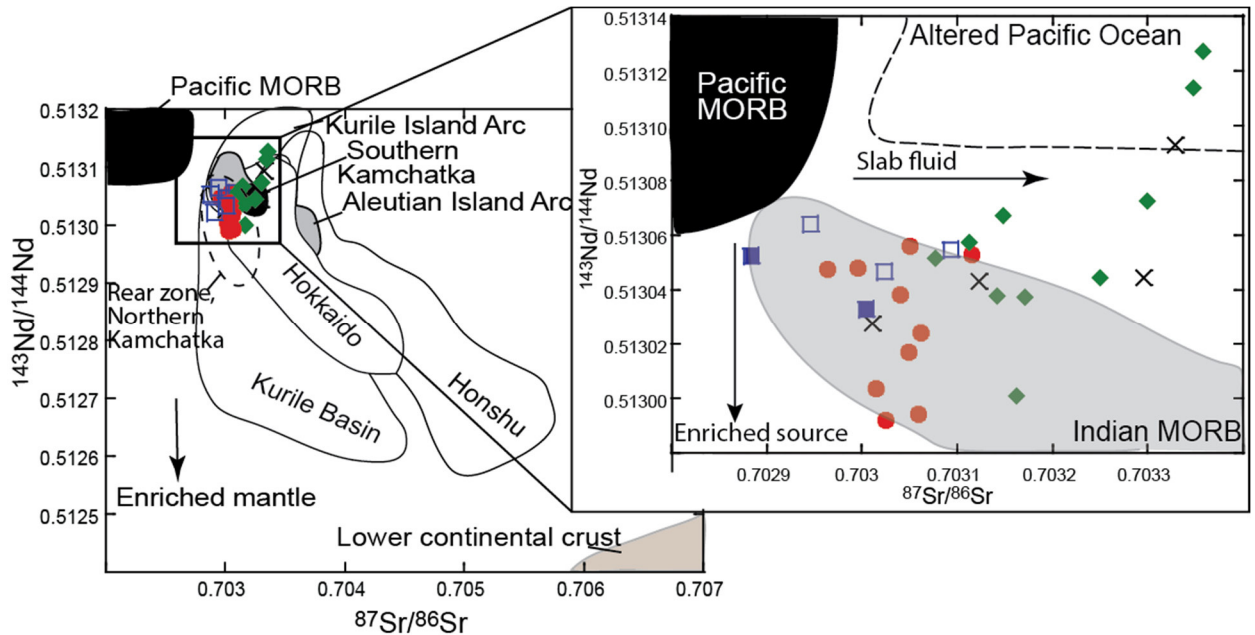
Fig. 2.1.2.3. Isotopic compositions 87Sr/86Sr versus 143Nd/144Nd for rocks from NKI and Pacific Island Arc systems. With using data from Yogodzinski et al. (2001), Duggen et al. (2007), Martynov et al. (2010) and Kosugi and Nakagawa (201X). Symbols are the same as in Fig. 2.1.2.2.

Besides across arc variations the along arc variations is defined. It is determined in enriched mantle source to northward. Maximum concentrations of the high incompatible elements (Th/Ta, Th/Yb, Nb/ Yb) are typically for Alaid, Grigorev and Ebeko volcanoes. The highest contents of isotopic ratios ($^{143}Nd/^{144}Nd$ 0.51303-0.51314 and $^{87}Sr/^{86}Sr$ 0.7301-0.7304) characterized southern frontal and intermediate zones. In the opposite, lowest isotopic ratios distinguish northern intermediate and rear ones. Various types of subduction component of intermediate zone can be explained by differences in distance to slab and corresponding processes. Ebeko volcano formed by dehydration fluid, because distance to slab smaller and temperature in mantle wedge is not enough for sediment melting. In contrast Peak Fussa and Shirinki volcanoes are located on the farther distance to trench and formed by sediment melting, since temperature and pressure are enough for this process.

In summary, the following parameters have mainly affected the observed geochemical zonation in the primary magma; variably depleted and enriched mantle source, the different types of the fluid flux from the slab to the mantle wedge.

Kuvikas, O. V., Nakagawa, M., Avdeiko, G. P., & Rashidov V. A. (2011). Spatial compositional variations in quaternary volcanics from the norhern Kuril Islands, Russia. 7th Biennual Workshop on Japan-Kamchatka-Alaska Subduction Processes: Mitigating Risk Through International Volcano, Earthquake, and Tsunami Science. JKASP-2011. Petropavlovsk-Kamchatsky, Russia. August 25-30, 2011. Abstracts. – Petropavlovsk-Kamchatsky: Institute of Volcanology and Seismology FEB RAS, Kamchatkan Branch of Geophysical Service RAS, 284-285. http://www.kscnet.ru/ivs/slsecret/jkasp_2011/abstr/abs130.pdf

Kuvikas, O. V., Nakagawa, M., Avdeiko, G. P., & Rashidov, V. A. (2011) Geochemical features of volcanic centers from the Northern Kurile Islands, Russia. The volcanological society of Japan. October 2-4, 2011 Fall Meeting. 80 p. https://www.researchgate.net/publication/272170588_Geochemical_features_of_volcanic_centers_from_the_Northern_Kuril_Islands_Russia

Kuvikas O.V., Nakagawa M., Avdeiko G.P. (2012) Peculiarities of across arc variations of volcanic rocks from Northern Kuriles: Estimation of subduction component in magma genesis // Modern problem of metamorphism and magmatism. Sankt-Peterburg, October

1-2, 2012. Sankt-Peterburg. 318-319. (In Russian). http://window.edu.ru/resource/124/79124

Kuvikas O.V., Nakagawa M., Avdeiko G.P. (2013) *Origin of spatial compositional variations of volcanic rocks from Northern Kurile Islands: Geochemical studies of active volcanoes on Paramushir, Atlasova, Antsiferova islands and submarine volcanoes Forecasting Volcanic Activity - Reading and translating the messages of nature for society. IAVCEI 2013 Scientific Assembly, July 20-24, Kagoshima, Japan. 4W_1B-P20.* http://www.kazan-g.sakura.ne.jp/iavcei2013/iavcei_hp/PDF/4W_1B-P20.pdf

Kuvikas O.V., Nakagawa M., Avdeiko G.P.. (2013) *Origin of spatial compositional variations of volcanic rocks from Northern Kurile Islands. Japan Geoscience Union Meeting 2013. Chiba. Japan.*

Kuvikas O.V., Nakagawa M., Avdeiko G.P. (201X) *Origin of spatial compositional variations of volcanic rocks from the Northern Kurile Islands: Geochemical studies of active volcanoes on the Paramushir, Atlasova, Antsiferova islands and adjacent submarine volcanoes. Contribution of Mineralogy and Petrology. (In submission)*

2.2. Geophysical studies along the Kurile island arc

2.2.1. Modern techniques for interdisciplinary investigation of submarine volcanoes in the Kurile island arc

Blokh Yu.I., yuri_blokh@mail.ru, *Moscow, Russia*
Bondarenko V.I., *Nekrasov State University in Kostroma, 156000, Russia*
Dolgal A.S., Novikova P.N., *3Mining Institute of the Ural Branch of the RAS, Perm, 614007, Russia*
Pilipenko O.V., *Schmidt Institute of Physics of the Earth RAS; Moscow, 123995, Russia*
Rashidov V.A., rashidva@kscnet.ru, *Institute of Volcanology and Seismology FEB RAS, Petropavlovsk-Kamchatsky, 683006, Russia*
Trusov A.A., *CJSC «GNPP Aerogeofizika», Moscow, 107140, Russia*

The Kuril Island Arc with submarine volcanoes on the side of Okhotskoye Sea slope is a key element of a transit zone between Asia continent and the Pacific Ocean. Scientists carried out 11 systematic and multidisciplinary investigations of submarine volcanic activity within the Kuril Islands Arc onboard R/V «Volcanolog». The volcanologic investigation included echo-sounding survey, continuous seismoacoustic profiling, hydromagnetic survey, and geologic sampling, and consisted of two phases. In the first phase we carried out profiling and areal survey. During the second phase we carried out dredging within zones determined from results of geophysical survey. Geophysical research at the monitored area was carried out using profile network which were chosen according to goals of volcanological investigation.

The authors used various profile networks extending the monitored area during following cruises. Unfortunately, profiles were irregular and their density was low. In order to process the data from irregular networks, we created a high-performance technology for quantitative interpretation of data from hydromagnetic survey using continuous seismoacoustic profiling, echo-sounding survey, and analysis of remnant magnetization and chemical composition of dredged rocks. This technology allows interpretation using benchmark data and avoids gridding (Blokh et al., 2010a, b). The technology consists of a method of singularity using SINGULAR software (Blokh et al., 2010a), 2.5D modeling on single profiles, followed by 3D modeling for all profiles using SIGMA-3D (Blokh et al., 2011) software. This technology uses a model of sub-horizontal layer which suffers fluctuation of magnetization along lateral. In order to correct vector direction of magnetization of a volcanic edifice we use IGLA software (Blokh et al., 2007) which uses initial magnetic field.
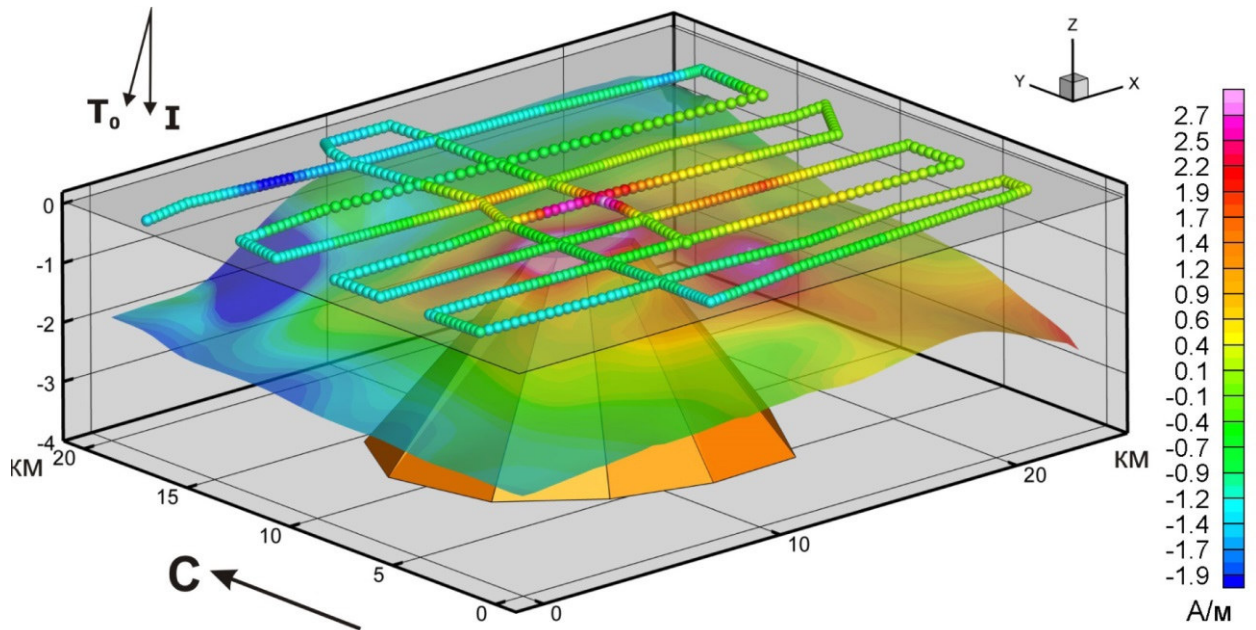
Fig. 2.2.1.1. Clarification of the orientation of the magnetization vector of the rocks frpm submarine volcano 6.13, using the IGLA program.

For modeling the authors used a true relief of volcanic edifices determined by echo-sounding survey and continuous seismoacoustic profiling. In order to locate attitude position of submarine volcanoes conduits an assembly method was used (Blokh et al., 2011).
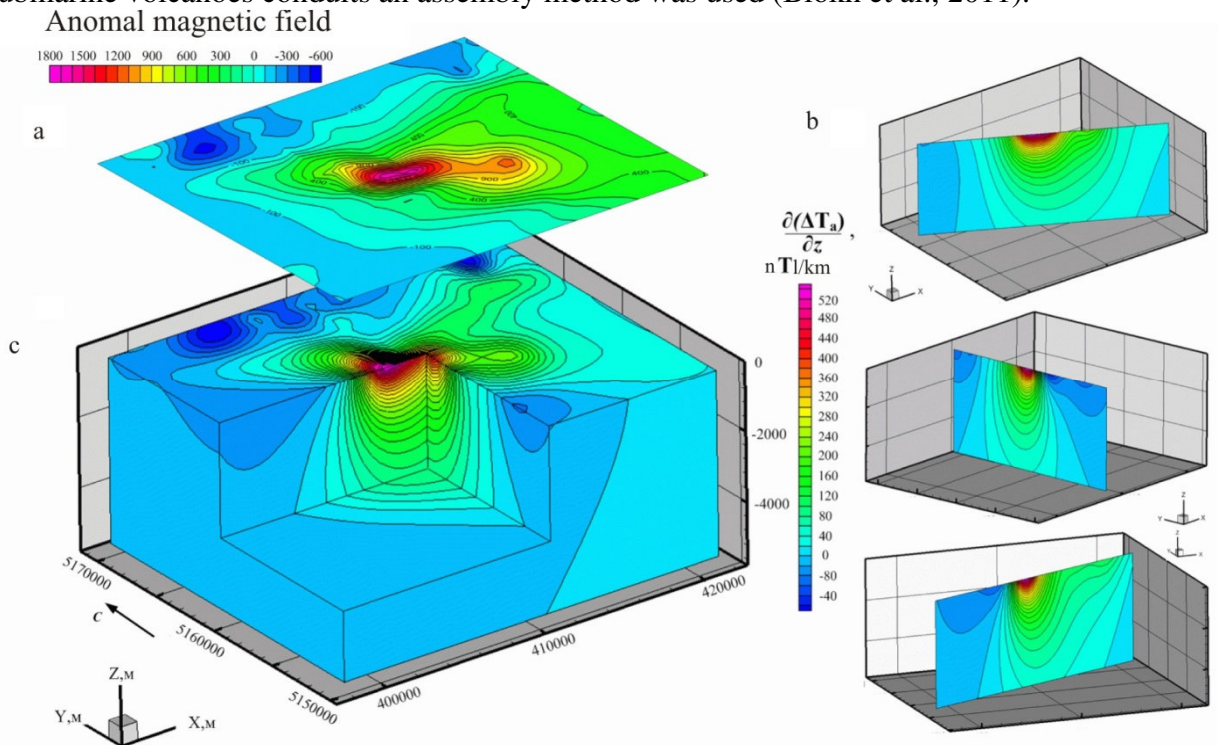
Fig. 2.2.1.2. Contours of the anomaly magnetic field ΔTa (a) 3D plot (b) showing the spatial distribution of quasimagnetization of the rocks of the submarine volcano 6.13 and its orthogonal cross-sections (c).

Modern techniques allowed distinguishing single lava flows, summit calderas, lateral volcanic cones, active volcanic centers, peripheral magmatic chambers, conduits and estimating magnetic properties of rocks in natural deposits within large volcanic edifices of the Kuril Islands Arc. Multidisciplinary method allows creating the most accurate geomagnetic model.

New submarine volcanoes, calderas and zones of mud volcanic and hydrothermal activity were revealed within the Kuril Islands Arc. The authors traced evolution of certain isolated volcanoes and volcanic massifs as well as estimated zones, types and, in some cases, duration of submarine volcanic activity.

During 2011-2014 these methods provides results from application of authors' modern computer technology designed for interpretation of materials from complex geophysical investigation of submarine volcanic centre near the south-western coast of Simushir Island, the Kurile island arc. Estimated magnetic properties of rocks in natural deposits showed that the most magnetized is the part of the volcanic centre 6.13 within the depth interval 480 to 950 m, where productive magnetization is about 3 A/m. The authors suggest a subvertical direction of feeding channels and a solidified peripheral magmatic chamber at a depth of 2.5 km (Figs. 2.2.1.1, 2.2.1.2). The main ferromagnetic carriers of magnetization are single-domain and pseudo-single-domain poor anisotropic grains of titano-magnetite and magnetite. Besides, the authors created an interpolation 3D model of the causative magnetic body (Blokh et al., 2014).

Another example was shown in (Blokh et al., 2013) for submarine volcanoes 2.7 and 2.8, which are located west of the south-western coast of Onekotan Island in the Kurile island arc (Fig. 2.2.1.3). The research resulted in estimation of rock magnetic properties in natural deposits and revealed that the south-western flanks of submarine volcano 2.8 are the most magnetized with their productive magnetization of about 2 A/m. The authors suggested that the feeding channels of volcano 2.7 stretch southwest, while the feeding channels of volcano 2.8 stretch subvertically, southwest and southeast. A peripheral magma chamber of the volcano was revealed at the depth of about 650 m.
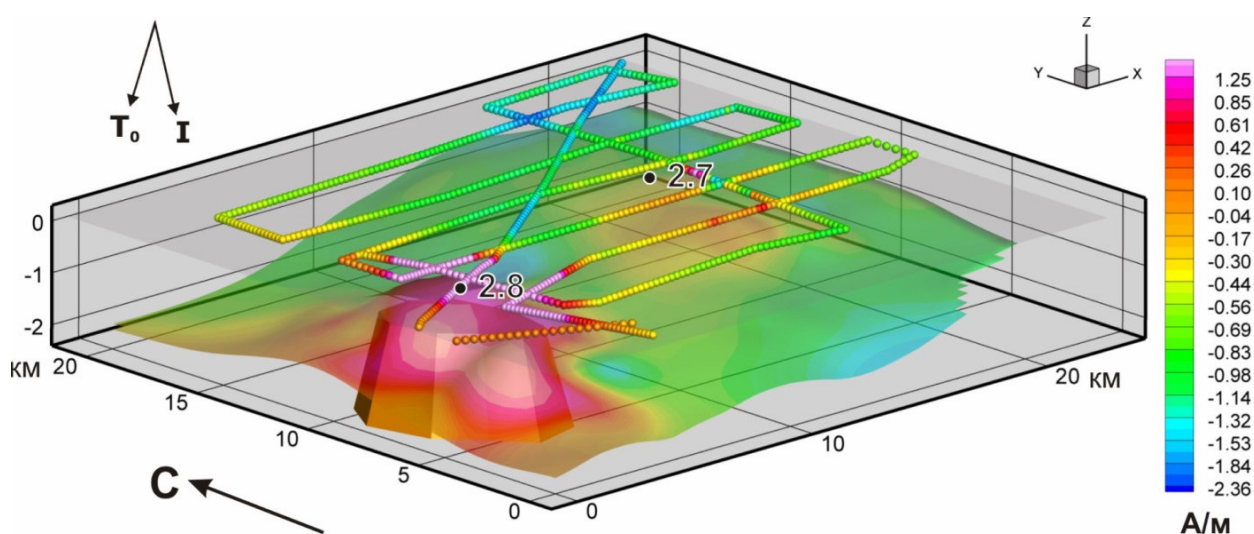

Fig. 2.2.1.3. Clarification of the orientation of the magnetization vector of the rocks frpm submarine volcanoes 2.7 and 2.8, using the IGLA program.

Blokh, Yu. I., Bondarenko, V. I., Dolgal, A. S., Novikova, P. N., Rashidov, V. A., & Trusov, A. A. (2013). Complex modeling of submarine volcanoes 2.7 and 2.8, the Kurile island arc. Bulletin of Kamchatka regional association "Educational-Scientific Center". Earth sciences, 1(21), 77-85. (In Russian). http://www.kscnet.ru/kraesc/2013/2013_21/art9.pdf

Blokh, Yu. I., Bondarenko, V. I., Dolgal, A. S., Novikova, P. N., Pilipenko, O. V., Rashidov, V. A., & Trusov, A. A. (2014). Application of modern computer technologies for investigation of submarine volcanic centre near the south-western coast of Simushir island, the Kurile island arc. Bulletin of Kamchatka regional association "Educational-Scientific Center". Earth sciences, 2(24), 27-40. (In Russian). http://www.kscnet.ru/kraesc/2014/2014_24/art3.pdf

Blokh Yu.I., Bondarenko V.I., Dolgal A.S., Novikova P.N., Rashidov V.A., Trusov A.A. Geophisicheskiye issledovaniya podvodnogo vulkana 6.1 (Kurilskaya ostrovnaya duga).

Voprosy teorii i praktiki geologicheskoy interpretatsii geophisicheskikh poley. Materialy tridtsat vosmoy sessii Mezhdunarodnogo nauchnogo seminara imeni D.G. Uspenskogo, Perm, 24-28 yanvarya 2011 goda. Perm, GI UrO RAN, 2011. P. 32-35. (In Russian).

Blokh Yu.I., Bondarenko V.I., Rashidov V.A., Trusov A.A. Primeneniye integrirovannoy sistemy SINGULYAR dlya izucheniya glubinnogo stroeniya podvodnikh vulkanov Kurilskoy ostrovnoy dugi. Voprosy teorii i praktiki geologicheskoy intepretttatsii gravitatsionnikh, magnitnikh i elektricheskikh poley. Materialy tridtsat vosmoy sessii Mezhdunarodnogo nauchnogo seminara imeni D.G. Uspenskogo, Moskva, 25-29 yanvarya 2010 goda. M: IPhZ RAN, 2010a. P. 62-65. (In Russian).

Blokh, Yu. I., Bondarenko, V. I., Rashidov, V. A., Trusov, A. A. (2010). Istoriya geomagnitnikh issledovaniy podvodnikh vulkanov Kurilskoy ostrovnoy dugi. Materialy Vserossiyskoy konferintsii, posvyashonnoy semidesyatipyatiletiyu Kamchatskoy vulkanologicheskoy stantsii. Otv. red. akademik E.I. Gordeev. Petropavlovsk-Kamchatskiy. Izdatelstvo IViS DVO RAN, 2010. P. 6-10. http://www.kscnet.ru/ivs/slsecret/75-KVS/Material_conferenc/art2.pdf

Blokh Yu.I., Trusov A.A. Programma IGLA dlya interaktivnoy ekspress-interpretatsii lokalnikh gravitatsionnikh i magnitnikh anomaliy. Voprosy teorii i praktiki geologicheskoy interpretatsii gravitatsionnikh, magnitnikh i elektricheskikh poley: materialy tridtsat chetvyortoy sessii mezhdunarodnogo seminara imeni D.G. Uspenskogo. M: IPhZ RAN, 2007. P. 36-38. (In Russian).

2.2.2. Ancient subduction zone in Sakhalin Island

Rodnikov A.G., rodnikov@wdcb.ru, **Sergeyeva N.A., Zabarinskaya L.P.,** *Geophysical Center, Russian Academy of Sciences, Moscow, Russia*

The northern part of Sakhalin Island is an area of recent intensive tectonic movements and hydrothermal processes, as well as a place of accumulation of useful minerals. The deep structure of the lithosphere beneath the region of the Neftegorsk earthquake of May 27, 1995 in North Sakhalin, which killed residents and caused significant destruction, is examined in this paper. Our geodynamic model shows that North Sakhalin consists of the North Sakhalin Basin, Deryugin Basin and an ophiolite complex located between them. The Deryugin Basin was formed in place of an ancient deep trench after subducting the Okhotsk Sea Plate under Sakhalin in the Late Cretaceous–Paleogene. The North Sakhalin Basin was formed on the side of the back-arc basin at that time. The ophiolite complex is fixed in the position of ancient subduction zone that was active in the Late Cretaceous–Paleogene. Approximately in the Miocene, the subduction of the Okhotsk lithosphere apparently ceased. The remains of the subduction zone in the form of an ophiolite complex have been identified from geological and geophysical data. On the surface, the subduction zone is manifested as deep faults stretched along Sakhalin. It is probable that the Neftegorsk earthquake was a result of activation of this ancient subduction zone.

The constructed model for a deep structure of lithosphere under the Neftegorsk earthquake region shows that North Sakhalin consists of the North Sakhalin sedimentary basin, Deryugin Basin and ophiolite complex located between them. The Deryugin Basin was formed in the position of an ancient deep trench after subducting the Okhotsk Sea Plate under the volcanic arc along Sakhalin in the Late Cretaceous–Paleogene. The North Sakhalin Basin was formed in the place of a back-arc basin at that time. The ophiolite complex combined with the ultrabasic rocks, fixing the position of an ancient subduction zone from the Late Cretaceous–Paleogene. On the surface, the subduction zone manifests itself as deep faults running along Sakhalin. The center of the Neftegorsk earthquake was directly produced from a burst of activity in this ancient subduction zone. Due to the position of the ancient subduction zone under Sakhalin, which is a cause of strong earthquakes there, the region is one of the most seismically dangerous in Russia.
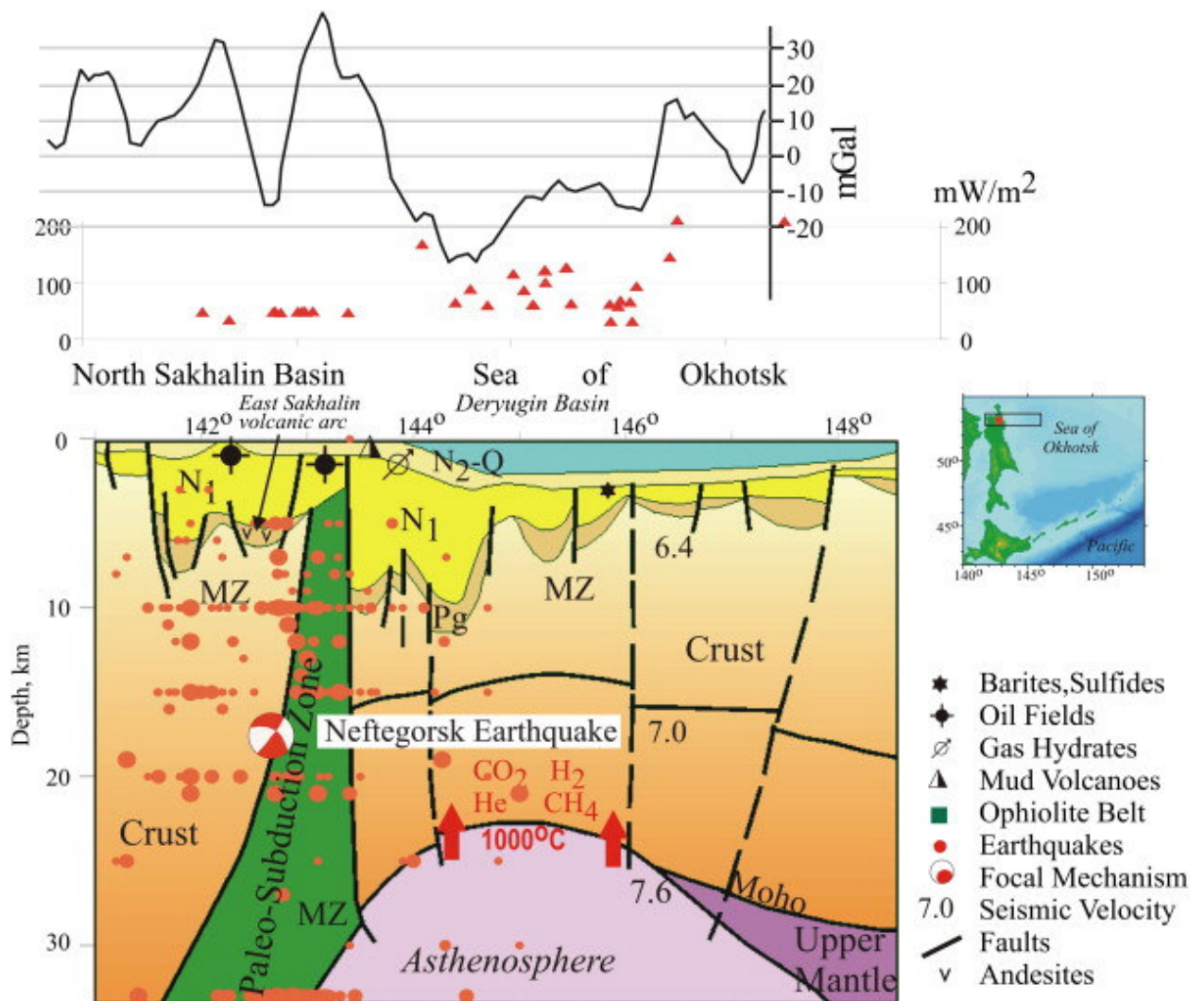
Fig. 2.2.2.1. Geodynamic model of the deep structure of the Neftegorsk earthquake region with the area scheme (see upper right). The Deryugin Basin was formed on the side of an ancient deep trench after the subduction of the Okhotsk Sea Plate under Sakhalin which had been completed in the Neogene. The basin is located above a hot plume in the mantle that is an asthenosphere diapir of partial melting revealed at a depth of 25 km. The ophiolite belt of ultramafic magmatic rocks is an ancient (Late Cretaceous to Paleogene) paleo-subduction zone separating the Deryugin Basin from the North Sakhalin Basin. The North Sakhalin Basin was formed on the side of the Late Cretaceous–Paleocene back-arc basin. Observed gravity in mGal and measured heat flow values in mW/m^2 are shown along the profile (see top) (Rodnikov et al., 1996).

Constructed on a basis of complex interpretation of the geological and geophysical data, geodynamic models of active continental margins give the chance to: (a) study the deep structure of the Earth under seismically dangerous zones, volcanic areas, mineralization regions and sedimentary basins; (b) investigate the role of deep processes in the mantle that influence the formation of crust units; (c) represent the dynamics of the development of continental margins; (d) ascertain the correlation between geological features, tectonomagmatics, hydrothermal activity and processes in the upper mantle; and (e) plot detailed maps identifying zones of increased risk to prevent active construction or other economic activities in highly dangerous regions.

Rodnikov, A. G., Sergeyeva, N. A., & Zabarinskaya, L. P. (2013). Ancient subduction zone in Sakhalin Island. Tectonophysics, 600, 217-225. Doi: http://dx.doi.org/10.1016/j.tecto.2012.12.014

3. INVESTIGATIONS OUTSIDE RUSSIA

3.1.   A comparative analysis of magnetic properties in rocks: five active submarine volcanoes in the Western Pacific

Rashidov V. A., *rashidva@kscnet.ru, Institute of Volcanology and Seismology, Far East Branch, Russian Academy of Sciences, Petropavlovsk-Kamchatsky, Russia*
Pilipenko O. V., *Institute of Physics of the Earth, Russian Academy of Sciences, Moscow, Russia*
Ladygin V. M. *Department of Geology, Moscow State University, Moscow, Russia*

We studied the petrophysical and magnetic properties of dredged rocks that compose the edifices of five active submarine volcanoes in the Pacific Ocean, viz., the Fukujin, Esmeralda, Kovachi, and Simbo at island arcs, and Ile des Cendres in a marginal sea. We measured the standard petrophysical and magnetic characteristics and performed three kinds of thermomagnetic analysis as well as an electron-probe analysis. Comparative analysis of magnetic properties in rocks showed that they are strongly differentiated by the value of natural remnant magnetization and of magnetic susceptibility. The greatest values are shown by the Esmeralda aphyric basaltic andesites, the lowest occur in the Ile des Cendres xenoliths. The principal carriers of magnetization in the rocks are grains of unaltered and/or oxidized titanomagnetite with varying domain structures. All the samples are magnetically isotropic.

Our study was concerned with the petrophysical and petromagnetic properties of erupted rocks that compose the edifices of five active submarine volcanoes in the Pacific Ocean, viz., Fukujin, Esmeralda, Kovachi, Simbo (all of the island-arc type) and Ile des Cendres (in a marginal sea).

A comparative analysis of the magnetic properties in the rocks showed that the rocks are strongly differentiated as to NRM and K. The highest NRM and K values are shown by the Esmeralda aphyric basaltic andesites and the lowest by the Ile des Cendres xenoliths. All the samples studied here are magnetically isotropic and contain comparatively low coercive magnetic minerals with varying domain structures.

The magnetic properties of these rocks are typical of young oceanic basalts. The main carriers of magnetization in the rocks are grains of unaltered and/or oxidized titanomagnetite with varying domain structures. The high NRM values are largely due to the single domain structure of titanomagnetite. Magnetite is the main magnetization carrier in the Fukujin sample. It may be hypothesized that the original titanomagnetite was already oxidized in this sample under natural conditions.

These studies made a substantial contribution to the available information on petromagnetic characteristics of the rocks that compose the active submarine volcanoes in the Pacific Ocean. The results may be used for both a better understanding and comparative analysis of magnetization in the rocks that compose young submarine volcanic edifices and for interpreting materials from geomagnetic surveys of the world ocean.
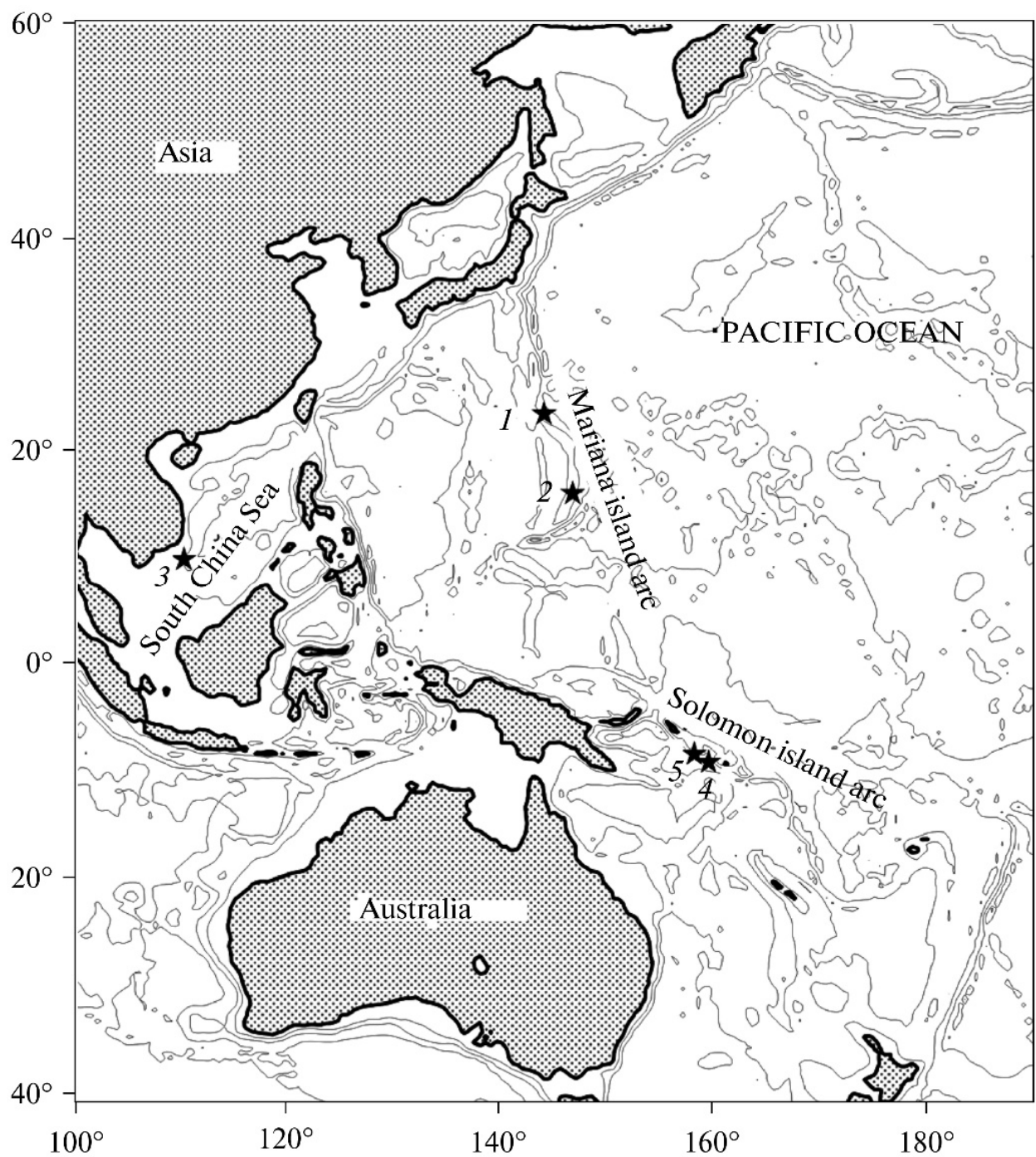
Fig. 3.1.1. The locations of the submarine volcanoes studied here. Stars mark the following submarine volcanoes: (1) Fukujin; (2) Esmeralda submarine volcano; (3) Ile des Cendres; (4) Kovachi; (5) Simbo.

136

3.2. An outstanding achievement of the Russian Academy of Sciences: the successful forecast of the earthquake of March 11, 2011, in Japan

Sidorin A.Ya., sidorin@ifz.ru, *Schmidt Institute of Physics of the Earth, Russian Academy of Sciences, Moscow, Russia*

The seismic catastrophe in Japan was forecasted far ahead of time by scientists from the Russian Academy of Sciences. The most reliable forecast was made by A.A. Lyubushin, a leading researcher at the Schmidt Institute of Physics of the Earth. Over the 2008–2010 period, at a number of the most important international conferences, including that of the Seismological Society of Japan, Lyubushin warned that an earthquake with a magnitude of 8.5–9.0 could occur in Japan; it was published in English in leading scientific journals all over the world. On April 26, 2010, Lyubushin officially informed the Russian Advisory Council on Earthquake Prediction and Seismic Hazard Assessment of his forecast. One distinctive feature of this fore cast is that it is based on large bodies of data on microseismic oscillations for the territory of Japan, which were mathematically treated using presentday methods. This forecast has a reliable physical justification and a visual interpretation. Brief information on the results of other Russian studies on the precursors of the main shock and aftershocks of the earthquake of March 11, 2011, in Japan is given.

3.3. Explosive interaction of lava flows with ice

Belousov A., belousov@mail.ru, *Earth Observatory of Singapore, Nanyang Technological University, Singapore. Institute of Volcanology and Seismology, Far East Division, Russian Academy of Sciences, Petropavlovsk-Kamchatsky, Russia*
Boris Behncke, *Istituto Nazionale di Geofisica e Vulcanologia, Sezione di Catania, Italy*
Marina Belousova, *Institute of Volcanology and Seismology, Far East Division, Russian Academy of Sciences, Petropavlovsk-Kamchatsky, Russia*

We describe a new type of secondary rootless phreatomagmatic explosions observed at active lava flows at volcanoes Klyuchevskoy (Russia) and Etna (Italy). The explosions occurred at considerable (up to 5 km) distances from primary volcanic vents, generally at steep (15–35°) slopes, and in places where incandescent basaltic or basaltic-andesitic lava propagated over ice/water-saturated substrate. The explosions produced high (up to 7 km) vertical ash/steam-laden clouds as well as pyroclastic flows that traveled up to 2 km downslope. Individual lobes of the pyroclastic flow deposits were up to 2 m thick, had steep lateral margins, and were composed of angular to subrounded bomb-size clasts in a poorly sorted ash–lapilli matrix. Character of the juvenile rock clasts in the pyroclastic flows (poorly vesiculated with chilled and fractured cauliflower outer surfaces) indicated their origin by explosive fragmentation of lava due to contact with external water. Non-juvenile rocks derived from the substrate of the lava flows comprised up to 75% in some of the pyroclastic flow deposits. We suggest a model where gradual heating of a water-saturated substrate under the advancing lava flow elevates pore pressure and thus reduces basal friction (in the case of frozen substrate water is initially formed by thawing of the substrate along the contact with lava). On steep slope this leads to gravitational instability and sliding of a part of the active lava flow and water-saturated substrate. The sliding lava and substrate

disintegrate and intermix, triggering explosive "fuel–coolant" type interaction that produces large volume of fine-grained clastic material. Relatively cold steam-laden cloud of the phreatomagmatic explosion has limited capacity to transport upward the produced clastic material, thus part of it descends downslope in the form of pyroclastic flow. Similar explosive events were described for active lava flows of Llaima (Chile), Pavlof (Alaska), and Hekla (Iceland) indicating that this type of explosions and related hazard is common at snow/ice-clad volcanoes.

Fig. 3.3.1. Pre-climactic stage of 1994 eruption of Klyuchevskoy volcano on September 30; cloud of the secondary rootless phreatomagmatic explosion originates at front of the active lava flow at 3 km a.s.l. and rises up to 7 km a.s.l. (much higher than eruption cloud of the Strombolian eruption in the summit crater).
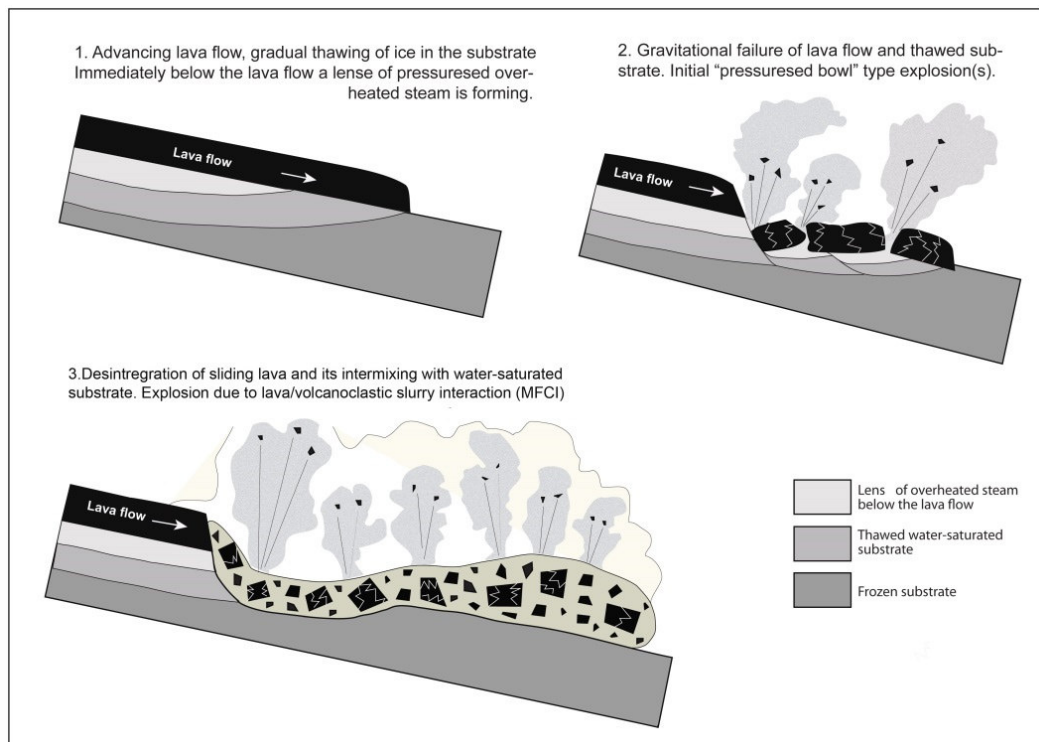
Fig. 3.3.2. Sketch illustrating the mechanism of secondary explosions and PF generation at Klyuchevskoy volcano. The processes shown on the sketch can occur on any part of active lava flow (not only at the front).

Belousov, A., Behncke, B., & Belousova, M. (2011). Generation of pyroclastic flows by explosive interaction of lava flows with ice/water-saturated substrate. Journal of Volcanology and Geothermal Research, 202(1–2), 60-72. Doi: http://dx.doi.org/10.1016/j.jvolgeores.2011.01.004

3.4.   Volcanic tsunamis

3.4.1. Volcanic tsunami: a review of source mechanisms

Paris R., R.Paris@opgc.univ-bpclermont.fr, *CNRS, UMR 6524, Magmas et Volcans, 63038 Clermont-Ferrand, France. Clermont Universite´, Universite´ Blaise Pascal, BP 10448, 63000 Clermont-Ferrand, France*

Ulvrova M., *Clermont Universite´, Universite´ Blaise Pascal, BP 10448, 63000 Clermont-Ferrand, France*

Switzer A. D., *Earth Observatory of Singapore, Nanyang Technological University, Singapore, Singapore. Division of Earth Sciences, Nanyang Technological University, Singapore, Singapore*

Belousova M., belousov@mail.ru, **Belousov A.,** *Earth Observatory of Singapore, Nanyang Technological University, Singapore, Singapore. Institute of Volcanology and Seismology, Far East Division, Russian Academy of Sciences, Petropavlovsk-Kamchatsky, Russia*

Whelley P. L., *Earth Observatory of Singapore, Nanyang Technological University, Singapore, Singapore*

Ontowirjo B., *BPDP BPPT, Jakarta 10340, Indonesia*
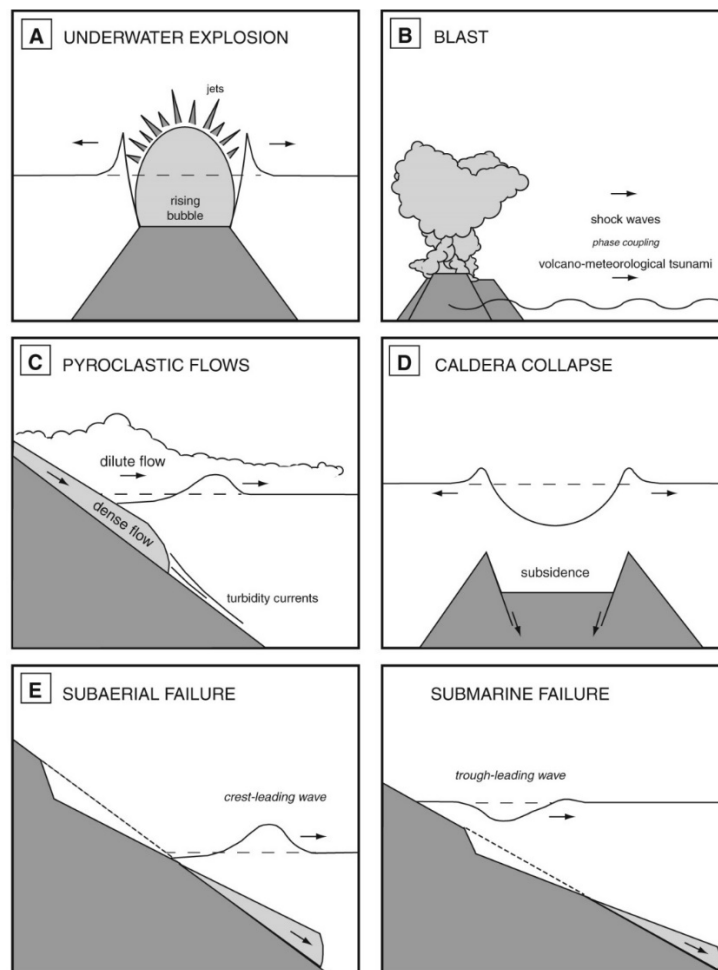
Fig. 3.4.1.1. Principal source mechanisms of tsunami at volcanoes: underwater explosions, air wave generated by blast, pyroclastic flow, caldera collapse, flank failures.

Southeast Asia has had both volcanic tsunamis and possesses some of the most densely populated, economically important and rapidly developing coastlines in the world. This contribution provides a review of volcanic tsunami hazard in Southeast Asia. Source mechanisms of tsunami related to eruptive and gravitational processes are presented, together with a history of past events in the region. A review of available data shows that many volcanoes are potentially tsunamigenic and present often neglected hazard to the rapidly developing coasts of the region. We highlight crucial volcanic provinces in Indonesia, the Philippines and Papua New Guinea and propose strategies for facing future events.

Paris, R., Switzer, A., Belousova, M., Belousov, A., Ontowirjo, B., Whelley, P., & Ulvrova, M. (2014). Volcanic tsunami: a review of source mechanisms, past events and hazards in Southeast Asia (Indonesia, Philippines, Papua New Guinea). Natural Hazards, 70(1), 447-470. Doi: 10.1007/s11069-013-0822-8

3.4.2. Coupling the eruption and tsunami record: the 1883 Krakatau case study, Indonesia

Paris R., R.Paris@opgc.univ-bpclermont.fr, **Benbakkar M.**, *Clermont Université, Université Blaise Pascal, BP 10448, 63000 Clermont-Ferrand, France. Magmas et Volcans, CNRS, UMR 6524, 63038 Clermont-Ferrand, France*
Wassmer P., *UMR 8591, Laboratoire de Géographie Physique, CNRS, 92195 Meudon, France. Faculté de Géographie et d'Aménagement, Université de Strasbourg, Strasbourg, France*
Lavigne F., *UMR 8591, Laboratoire de Géographie Physique, CNRS, 92195 Meudon, France. Université Paris 1 Panthéon-Sorbonne, PRES HESAM, Meudon, France*
Belousov A., belousov@mail.ru, **Belousova M.**, *Institute of Volcanology and Seismology, Far East Division, Russian Academy of Sciences, Petropavlovsk-Kamchatsky, Russia*
Iskandarsyah Y., *Laboratorium Geologi Lingkungan dan Hidrogeologi, Fakultas, Teknik Geologi, Universitas Padjadjaran (UNPAD), Bandung, Indonesia. Laboratoire Image, Ville, Environnement (LIVE), UMR 7362 CNRS, Université de Strasbourg, Strasbourg, France*
Mazzoni N., *Clermont Université,GEOLAB, Université Blaise Pascal, BP 10448, 63000 Clermont-Ferrand, France. GEOLAB, UMR 6042, CNRS, 63057 Clermont-Ferrand, France*
Ontowirjo B., *BPDP BPPT, Jakarta 10340, Indonesia*

The well-documented 1883 eruption of Krakatau volcano (Indonesia) offers an opportunity to couple the eruption's history with the tsunami record. The aim of this paper is not to re-analyse the scenario for the 1883 eruption but to demonstrate that the study of tsunami deposits provides information for reconstructing past eruptions. Indeed, though the characteristics of volcanogenic tsunami deposits are similar to those of other tsunami deposits, they may include juvenile material (e.g. fresh pumice) or be interbedded with distal pyroclastic deposits (ash fall, surges), due to their simultaneity with the eruption.
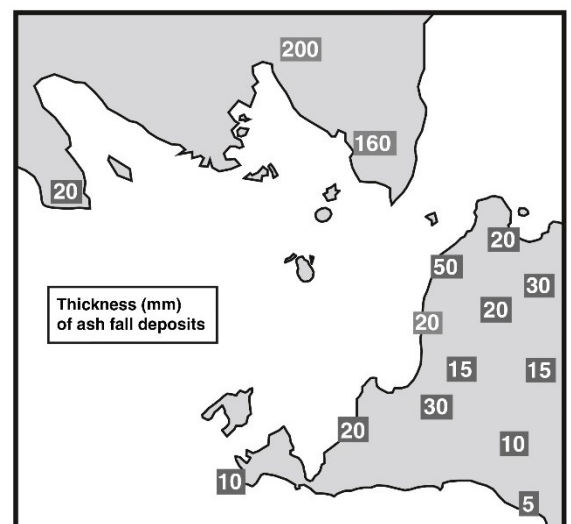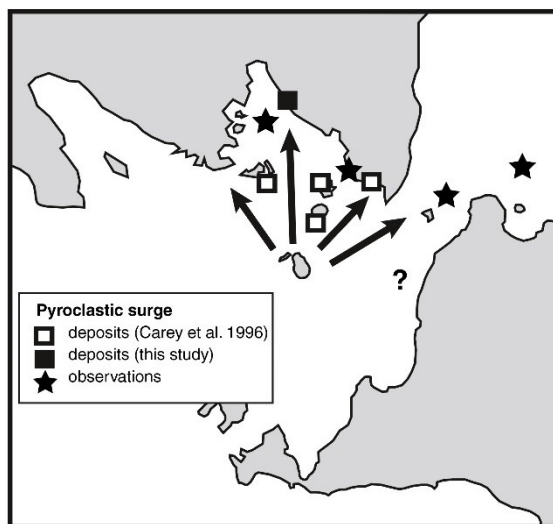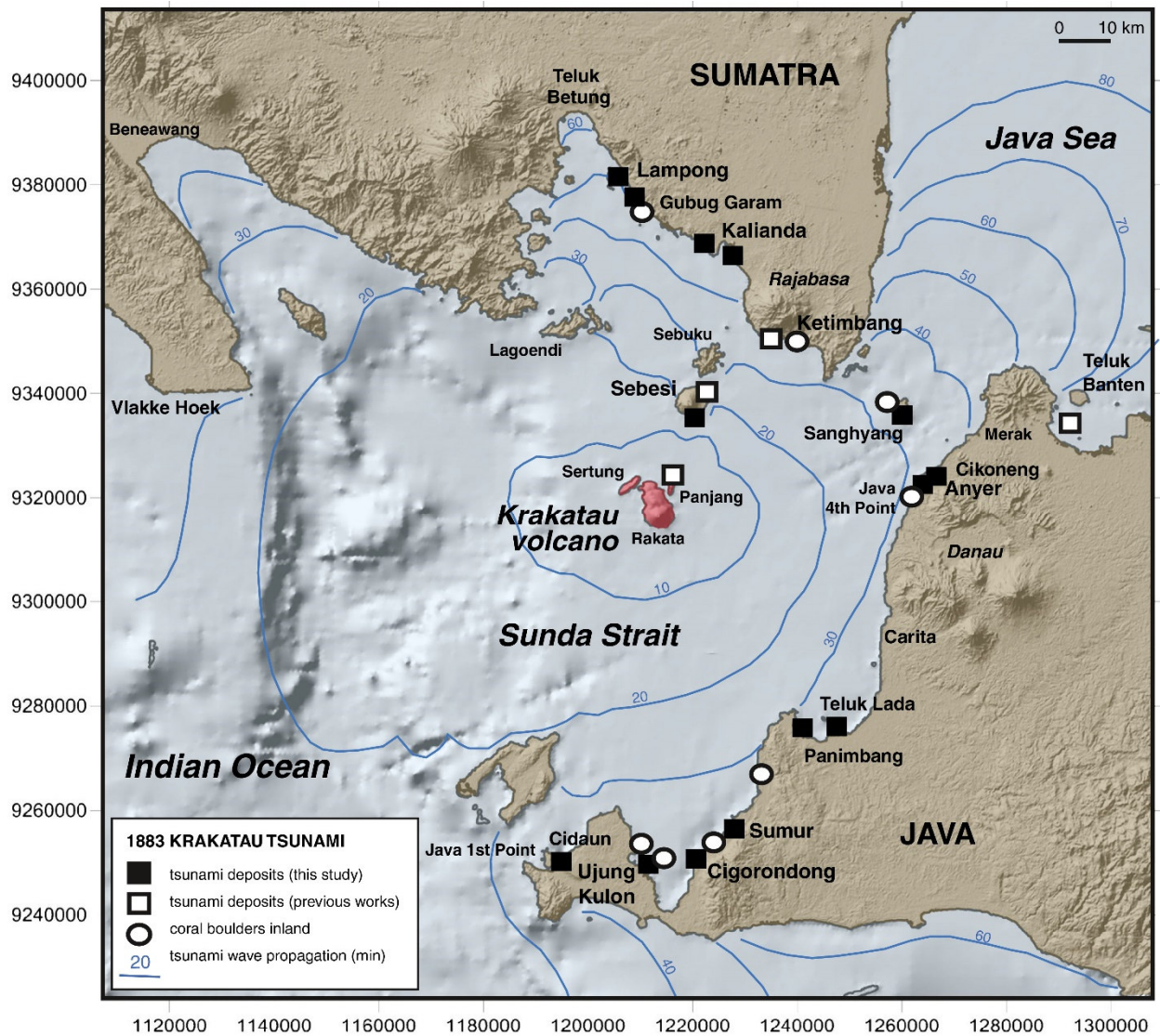
Fig. 3.4.2.1. Maps showing distribution of 1883 Krakatau tsunamis, pyroclastic surges and ash fall deposits in Sunda Strait region (Indonesia), after previous works on tsunami deposits by Williams (1941), Ongkosongo (1983), Bronto (1990), Carey et al. (2001) and Van den Berg et al. (2003). Distribution of coral boulders after Umbgrove (1947), Verstappen (1956) and Setjaatmadja (2007). Typical tsunami wave propagation time in Sunda Strait (in minutes) was estimated by Yokoyama (1981), Giachetti et al. (2012) and Maeno and Imamura (2011).

Paris, R., Wassmer, P., Lavigne, F., Belousov, A., Belousova, M., Iskandarsyah, Y., Benbakkar, M., Ontowirjo, B., Mazzoni, N. (2014). Coupling eruption and tsunami records: the Krakatau 1883 case study, Indonesia. Bulletin of Volcanology, 76(4):814, 1-23. Doi: 10.1007/s00445-014-0814-x

3.4.3. Volcanic tsunamis: from Krakatau to Karymskoye

Belousov A., belousov@mail.ru, **Belousova M.**, *Institute of Volcanology and Seismology, Far East Division, Russian Academy of Sciences, Petropavlovsk-Kamchatsky, Russia*

In this paper we describe tsunamis connected with volcanic eruptions but of different scale: the great 1883 Krakatau eruption and comparatively small underwater explosions in Karymskoye lake in 1996. The results of this comparative study are very important, such as they allow to predict danger from underwater explosions happened in shallow water basins (lakes or sea bays) which coastal areas are usually densely populated.
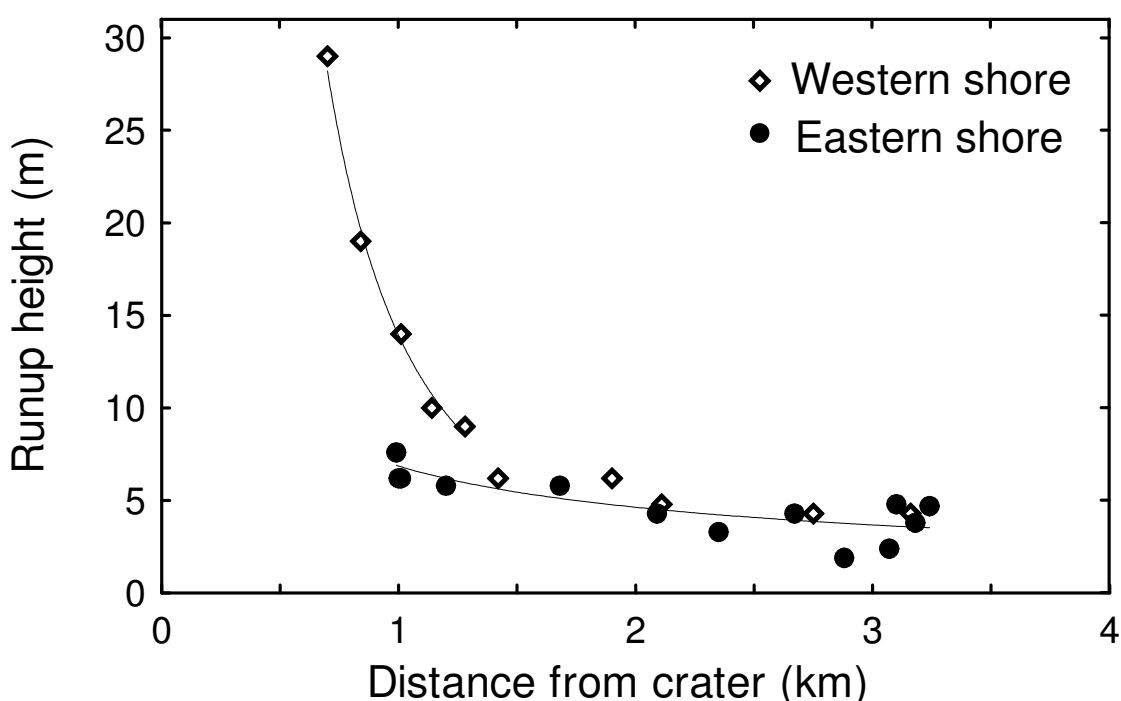
Fig. 3.4.3.1. Runup height vs. distance from the crater. Note change in trend about 1.3 km from the crater, Dotted line gives log decay as discussed in text. Dashed line is best fit to our data that approximately matches 1/distance1/2 decay.

Belousov A, Belousova M. (2011) Volcanic tsunamis: from Krakatau to Karymskoye. Priroda 6, 26-34. (In Russian). http://www.ras.ru/publishing/nature.aspx

3.5. Reconstruction of modern eruptive history of Tatun Volcanic Group, Northern Taiwan

3.5.1. Deposits, character and timing of recent eruptions and gravitational collapses in Tatun Volcanic Group, Northern Taiwan: Hazard-related issues

Belousov A., belousov@mail.ru, **Belousova M.,** *Institute of Earth Sciences, Academia Sinica, 128 Academia Road Sec. 2, Nankang, Taipei 11529, Taiwan. Earth Observatory of Singapore, Nanyang Technological University, N2-01a-15, 50 Nanyang Avenue, 639798 Singapore. Institute of Volcanology and Seismology, Far East Division, Russian Academy of Sciences, Petropavlovsk-Kamchatsky, Russia*
Chen C.-H., *Institute of Earth Sciences, Academia Sinica, 128 Academia Road Sec. 2, Nankang, Taipei 11529, Taiwan*
Zellmer G. F., Institute of Earth Sciences, Academia Sinica, 128 Academia Road Sec. 2, Nankang, Taipei 11529, Taiwan. Lamont-Doherty Earth Observatory, 61 Route 9W, Palisades, NY10964, USA

Taipei City, with a population of around 8 million, as well as two nuclear power plants is located in close proximity to the Quaternary, dominantly andesitic Tatun Volcanic Group (TVG) of Northern Taiwan. We have investigated the stratigraphy of the youngest volcaniclastic deposits, as well as the morphology of lava flows and domes of the TVG in order to reconstruct the character and timing of the most recent eruptions and related hazardous events in the area.

Fig. 3.5.1.1. At the foreground – downtown of Taipei, at background – Tatun volcanic group.

Our data indicate that recent eruptions of the group were dominated by long-term, voluminous extrusions of crystal-rich, very viscous lavas. These eruptions formed closely spaced monogenetic domes and lava flows. Based on morphological parameters of the lava flows (thicknesses 80–150 m, lengths up to 5.6 km, and volumes up to 0.6 km^3), average rates of magma effusion ranged from 1 to 10 m^3/s, eruption durations from 500 to 1800 days, and lava front speeds from 0.5 to 6 m/h.

Explosive activity of TVG was diverse, ranging from weak phreatic to highly explosive (VEI 4) Plinian eruptions; vulcanian activity with deposition of lithic ashes was most common. Interaction of rising magma with ground water frequently occurred during the eruptions.

This study presents the first radiocarbon dates of various volcaniclastic deposits of the TVG, which indicate that Cising, Siaoguanyin, and possibly Huangzuei volcanoes had magmatic eruptions in the period 13,000–23,000 years ago. In addition, Mt. Cising had a phreatic eruption 6000 years ago, and possibly an effusive eruption just before that. Gravitational collapses of volcanic edifices with volumes 0.01–0.1 km^3 and H/L 0.16–0.25 were also common. They occurred on intersections with tectonic faults and may have been triggered by seismic activity. The youngest collapses occurred at Mt. Siaoguanyin (23,000 BP) and Mt. Cising (6000 BP).

It is concluded that the TVG should be considered volcanically active. The results of this study provide a basis for volcanic hazard assessment and mitigation in the area.
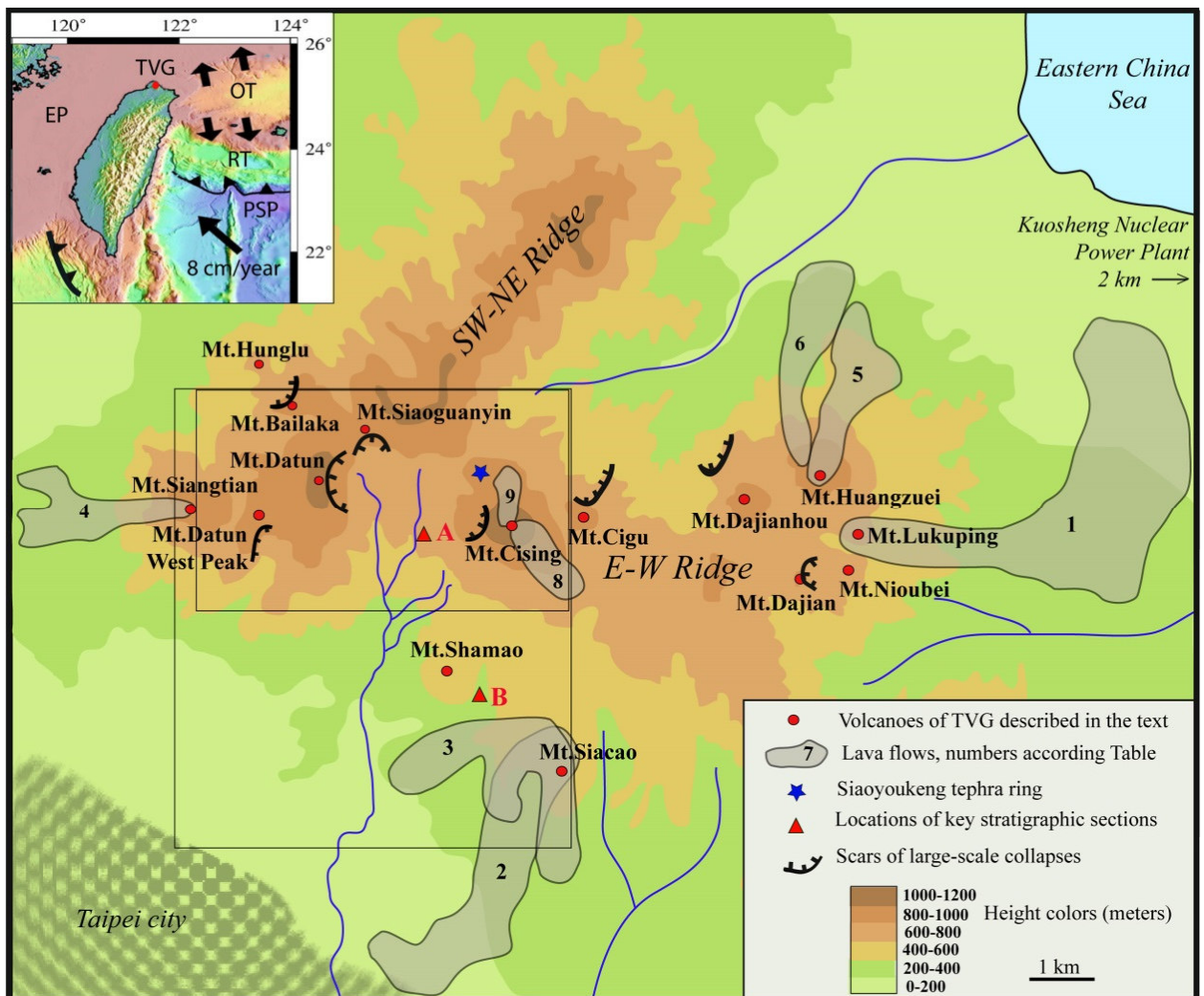
Fig. 3.5.1.2. Sketch map of Tatun Volcanic Group (TVG), Northern Taiwan. Locations of the main volcanic ridges, volcanoes, lava flows, collapse scars and key outcrops are indicated. Location of the TVG as well as the tectonic regime of Taiwan is shown in the inset. EP— Eurasian Plate, PSP —Philippine Sea Plate, OT—Okinawa Trough, RT —Ryukyu Trench.

Belousov, A., Belousova, M., Chen, C.-H., & Zellmer, G. F. (2010). Deposits, character and timing of recent eruptions and gravitational collapses in Tatun Volcanic Group, Northern Taiwan: Hazard-related issues. Journal of Volcanology and Geothermal Research, 191(3–4), 205-221. Doi: http://dx.doi.org/10.1016/j.jvolgeores.2010.02.001

3.5.2. Generation of calc-alkaline andesitic rocks of the Tatun volcanic group (Taiwan) by shallow crystal fractionation within an extensional environment

Shellnutt G., Department of Earth Sciences, National Taiwan Normal University, Taipei, Taiwan
Belousov A., belousov@mail.ru, *Belousova M., Institute of Volcanology and Seismology, Far East Division, Russian Academy of Sciences, Petropavlovsk-Kamchatsky, Russia*
Wang K.-L, Institute of Earth Sciences, Academia Sinica, Taipei, Taiwan
Zellmer G., Soil and Earth Sciences Group, Massey University, Palmerston North, New Zealand

Rocks collected from the Tatun volcanic group include basaltic to andesitic rocks. The basalt is compositionally similar to within-plate continental tholeiitic whereas the basaltic andesite and andesite are calc-alkaline. Petrological modelling and the Sr-Nd isotope results indicate that the volcanic rocks from Tatun volcanic group are derived from the same mantle source and that the andesites are the product of fractional crystallization of a parental magma similar in composition to the basaltic andesites. Furthermore, our results indicate that, in some cases, calc-alkaline andesites may be generated by crystal fractionation of mafic magmas derived in an extensional back-arc setting rather than a subduction zone setting.

3.6. Influence of pre-eruptive degassing and crystallization on the juvenile products of laterally directed explosions

Neill Owen K., Department of Geology & Geophysics, University of Hawaii - Manoa, 1680 East West Road, Honolulu, HI, USA, 96822. Geophysical Institute, University of Alaska Fairbanks, 903 Koyukuk Drive, Fairbanks, AK, USA, 99775-7320
Hammer Julia E., Department of Geology & Geophysics, University of Hawaii - Manoa, 1680 East West Road, Honolulu, HI, USA, 96822
Izbekov Pavel E., Geophysical Institute, University of Alaska Fairbanks, 903 Koyukuk Drive, Fairbanks, AK, USA, 99775-7320
Belousova Marina G., Belousov Alexander B., belousov@mail.ru, Earth Observatory of Singapore, Nanyang Technological University, 50 Nanyang Avenue, Block N2-01a-15, Singapore 639798. *Institute of Volcanology and Seismology, Far East Division, Russian Academy of Sciences, Petropavlovsk-Kamchatsky, Russia*
Clarke Amanda B., School of Earth and Space Exploration, Arizona State University, P.O. Box 871404, Tempe, AZ, USA, 85287-1404
Voight Barry, College of Earth and Mineral Sciences, Pennsylvania State University, University Park, PA, USA, 16802

Strikingly similar examples of edifice collapse and directed blast are the 18 May 1980 eruption of Mount St. Helens (MSH) and the 30 March 1956 eruption of Bezymianny Volcano (BZ), Kamchatka. In these cases, flank failures led to near-instantaneous decompression and fragmentation of intra-edifice cryptodome magma, which produced catastrophic, laterally directed blasts. In both instances, the blast products consisted of juvenile material with bimodal density/vesicularity distributions: low- and high-density modes at 1900 and 2400 kg m−3 for BZ, 1600 and 2300 kg m−3 for MSH, although the proportion of high-density material is greater at BZ. Blast materials also exhibit striking variety in groundmass crystallinity (b40 to N90 vol.%)

despite having fairly uniform phenocrystallinities, suggesting that degassing-driven groundmass crystallization occurred to varying extents within cryptodome magma at both volcanoes. New bulk-rock H2O and ∂D measurements confirm that progressive open-system outgassing occurred prior to both blasts. The correlations between crystallinity, clast density, and bulk H2O contents suggest that syn-blast magma expansion was modulated both by non-uniform volatile distribution within the cryptodome and rheological controls associated with non-uniform crystal content.

Neill, O. K., Hammer, J. E., Izbekov, P. E., Belousova, M. G., Belousov, A. B., Clarke, A. B., & Voight, B. (2010). Influence of pre-eruptive degassing and crystallization on the juvenile products of laterally directed volcanic explosions. Journal of Volcanology and Geothermal Research, 198(1–2), 264-274. Doi: http://dx.doi.org/10.1016/j.jvolgeores.2010.09.011

3.7.   New Petrological Data on the Volcanic Rocks of the Chichinautzin Region: The Sources of the Magmatic Melts and the Origin of the Trans-Mexican Volcanic Belt

A.V. Koloskov, *kolosav@kscnet.ru*, **S.A. Khubunaya,** *Institute of Volcanology and Seismology, Far East Branch, Russian Academy of Sciences, Petropavlovsk–Kamchatsky, Russia*
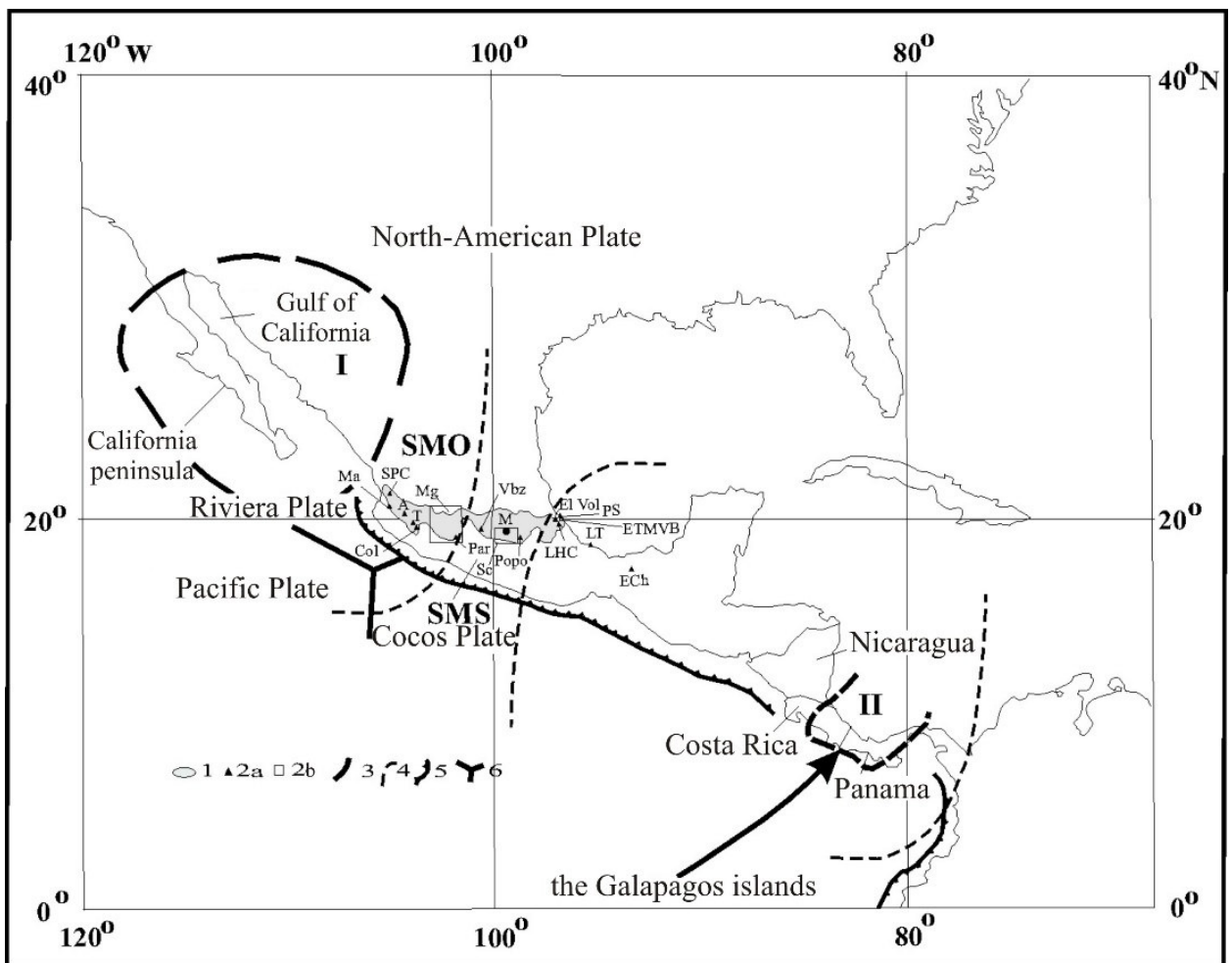
Fig. 3.7.1. Sketch of Trans-Mexican volcanic belt. 1 - TMVB, 2a and 2b – local and square volcanic structures. 3 – Californian ring structure (I) and Galapagos «slab window» (II), 4 – boundaries of mantle plumes, 5 – trenches, 6 – boundaries of plates

New petrographic, isotopic–geochemical, and mineralogical data are presented for the volcanic rocks of the Chichinautzin region of the (TMVB). The geological setting and the peculiarities of the composition of the volcanic rocks from different regions of the belt are compared to the plume-related volcanic rocks from the areas of the Gulf of California, Central America, and the Galapagos hot spot. It was concluded that the composition of the intraplate rocks from the western and eastern parts of the TMVB was subjected to the Californian and Galapagos plumes, respectively. In its turn, the ascending mantle plumes provoke melting of the subcontinental lithospheric mantle related to Trans-Mexican volcanic belt the formation of island-arc rocks. The model of the consecutive propagating rifting in the eastward direction suggested by some researchers (Marquez et al., 1999; Verma, 2001) instead of the subduction hypothesis is in agreement with the geological and geophysical data and the isotopic–geochemical peculiarities of the volcanic rocks within the TMVB.

Koloskov, A. V., & Khubunaya, S. A. (2013). New petrological data on the volcanic rocks of the Chichinautzin region: The sources of the magmatic melts and the origin of the Trans-Mexican volcanic belt. Russian Journal of Pacific Geology, 7(4), 247-261. Doi: 10.1134/S1819714013040052

3.8. Rhonite in alkali basalts: silicate melt inclusions in olivine phenocrysts

Sharygin, V. V., sharygin@igm.nsc.ru**, Timina, T. J.,** *V.S. Sobolev Institute of Geology and Mineralogy, Siberian Branch of the Russian Academy of Sciences, pr. Akademika Koptyuga 3, Novosibirsk, 630090, Russia*
Kóthay, K., Szabó, C., *Lithosphere Fluid Research Lab, Department of Petrology and Geochemistry, Eötvös University, Pázmány Péter sétány 1/C, H-1117 Budapest, Hungary*
Török, K., *Lithosphere Fluid Research Lab, Department of Petrology and Geochemistry, Eötvös University, Pázmány Péter sétány 1/C, H-1117 Budapest, Hungary. Research Group for Environmental Physics and Geophysics of the Hungarian Academy of Sciences, Department of Geophysics, Eötvös University, Pázmány Péter sétány 1/C, H-1117 Budapest, Hungary*
Vapnik, Y., *Department of Geological and Environmental Sciences, Ben-Gurion University of the Negev, P.O. Box 653, 84105 Beer-Sheva, Israel*
Kuzmin, D. V. *V.S. Sobolev Institute of Geology and Mineralogy, Siberian Branch of the Russian Academy of Sciences, pr. Akademika Koptyuga 3, Novosibirsk, 630090, Russia. Geochemistry Division, Max Planck Institute für Chemie, Joh.-Joachim-Becher-Weg 27, Mainz, 55128, Germany*

Silicate melt inclusions containing rhonite $Ca_2(Mg,Fe^{2+})_4Fe^{3+}Ti[Al_3Si_3O_{20}]$ were studied in olivine phenocrysts from alkali basalts of six different volcanic regions: Udokan Plateau, North Minusa Depression, Tsagan-Khurtei Ridge (Russia), Bakony-Balaton Highland, Nograd-Gomor Region (Hungary) and Makhtesh Ramon (Israel). Rhonite-bearing silicate melt inclusions are relatively common phenomena in alkali basalts and usually coexist with inclusions containing no rhonite. Inclusions with rhonite generally occur in the core of the olivine phenocrysts. According to heating experiments and CO_2 microthermometry, all the rhonite-bearing inclusions in core of the olivine phenocrysts were trapped as silicate melt at T > 1300 °C and P > 3-5 kbar. Rhonite crystallized in a narrow temperature range (1180-1260 °C) and P < 0.5 kbar. The petrography and thermometry of rhonite-bearing silicate melt inclusions show a general crystallization sequence: Al-spinel -> rhonite -> clinopyroxene -> apatite -> +/- amphibole, Fe-Ti oxide (ilmenite or Ti-magnetite) -> glass.

Majority of rhonites from melt inclusions have $Mg/(Mg + Fe^{2+}) > 0.5$ and belong to Mg-rich species $Ca_2Mg_4Fe^{3+}Ti[Al_3Si_3O_{20}]$. There are no essential differences in chemistry among rhonites from olivine-hosted silicate melt inclusions from phenocryst, from groundmass of alkali

basalts, from alteration products of kaersutitic amphibole mega/xenocrysts and of kaersutite in deep-seated xenoliths in alkali basalts. The rare occurrence of rhonite as essential constituent in rocks may be explained from its microstructural peculiarities. This mineral is an intermediate member of the polysomatic spinel-pyroxene series. Possibly, the structural feature of rhonite does explain why it is an unstable mineral in under changing crystallization conditions. In general, the presence and chemistry of rhonite may be used for rough estimation of temperature, pressure and oxygen fugacity during crystallization of alkali basalts.
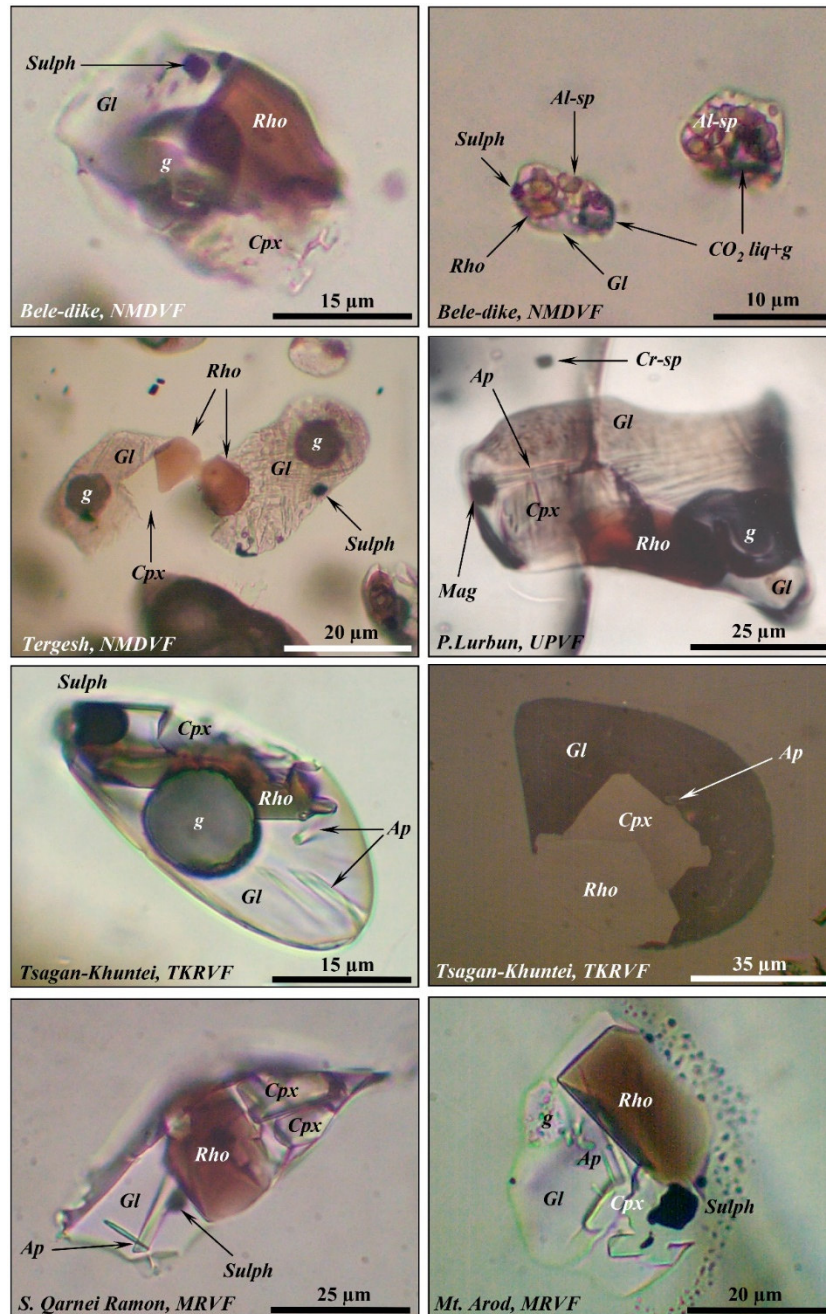
Fig. 3.8.1. Photomicrographs of primary rhonite-bearing silicate melt inclusions in phenocrystal olivine from alkali basalts of NMDVF, UPVF, TKRVF, and MRVF. Ordinary and reflected lights.

Sharygin, V. V., Kóthay, K., Szabó, C., Timina, T. J., Török, K., Vapnik, Y., & Kuzmin, D. V. (2011). Rhönite in alkali basalts: silicate melt inclusions in olivine phenocrysts. Russian Geology and Geophysics, 52(11), 1334-1352. Doi: http://dx.doi.org/10.1016/j.rgg.2011.10.006

3.9. Silicate-natrocarbonatite liquid immiscibility in 1917 eruption combeite-wollastonite nephelinite, Oldoinyo Lengai Volcano, Tanzania: Melt inclusion study

Sharygin, V. V., sharygin@igm.nsc.ru, *V.S. Sobolev Institute of Geology and Mineralogy SB RAS, Koptyuga prospect 3, Novosibirsk 630090, Russia*
Kamenetsky, V. S., Kamenetsky, M. B., *ARC Centre of Excellence in Ore Deposits and School of Earth Sciences, University of Tasmania, Hobart, Tasmania 7001, Australia*
Zaitsev, A. N., *Department of Mineralogy, Faculty of Geology, St. Petersburg State University, University Emb. 7/9, St. Petersburg 199034, Russia. Department of Mineralogy, Natural History Museum, Cromwell Road, London, SW7 5BD UK*
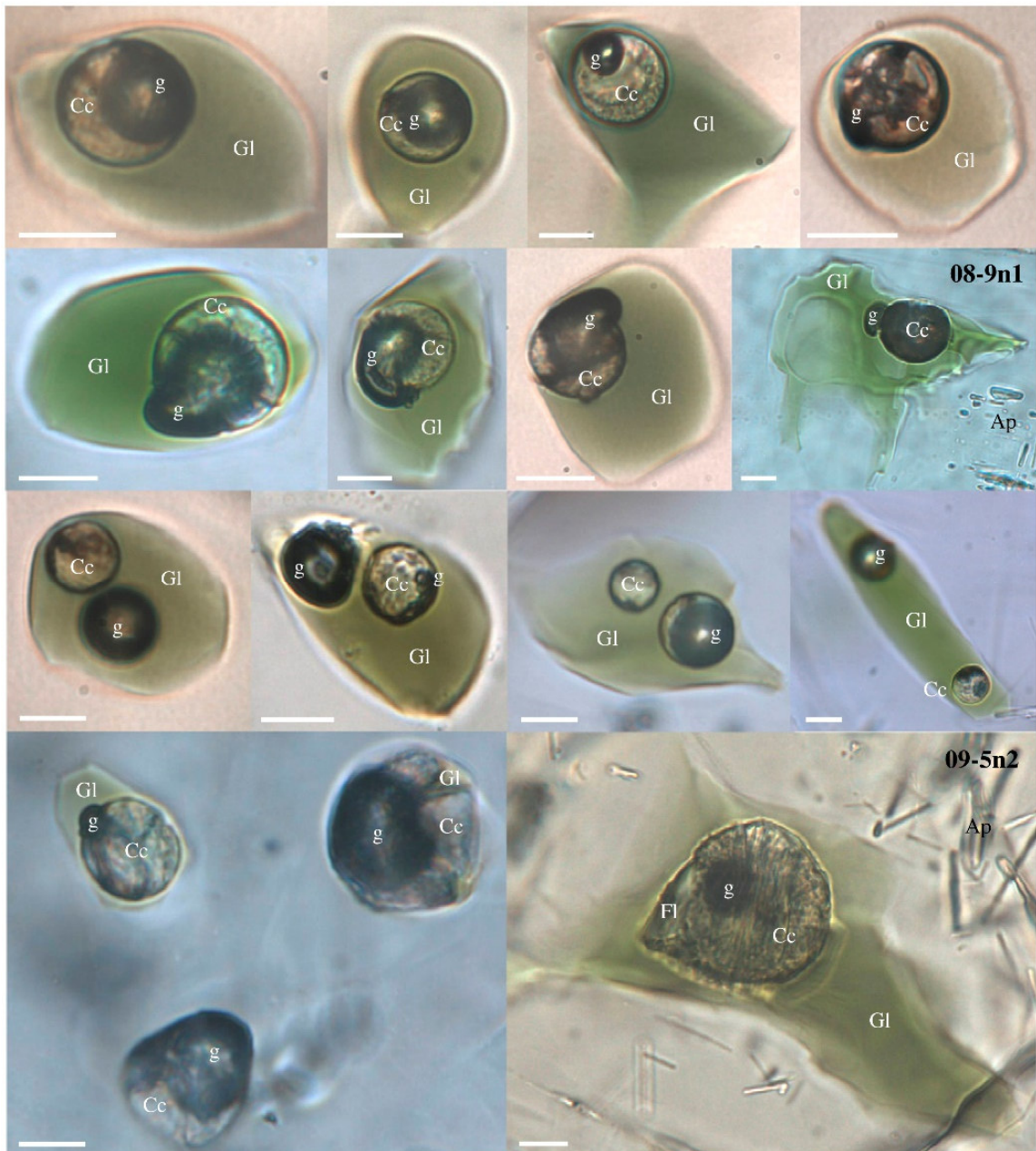
Fig. 3.9.1. Variable relationships between gas and natrocarbonatite in silicate–melt inclusions without daughter silicate minerals, nepheline phenocrysts, sample Ol 7/2000, CWN, Oldoinyo Lengai.Scale bar is 10 μm. Inclusions with numbers refer to data in Tables 4 and 6. Symbols: Gl — silicate glass; g — gas bubble; Cc — natrocarbonatite aggregate; Ap — fluorapatite; Fl — fluorite.

Primary silicate-melt and carbonate-salt inclusions occur in the phenocrysts (nepheline, fluorapatite, wollastonite, clinopyroxene) in the 1917 eruption combeite-wollastonite nephelinite at Oldoinyo Lengai. Silicate-melt inclusions in nepheline clearly show liquid immiscibility phenomena expressed in the presence of carbonate globules in silicate glass. The coexistence of inclusions with markedly different proportions of silicate glass + vapor-carbonate globule in the core of nepheline phenocrysts, the presence of carbonate-salt inclusions in fluorapatite and our heating experiments strongly suggest that their entrapment began at temperatures higher than 1130 °C in an intermediate chamber when initial carbonated nephelinite melt was heterogeneous and represented a mixture of immiscible liquids. Silicate-natrocarbonatite melt immiscibility took place at high temperature and immiscible nephelinite and carbonatite liquids coexisted over a wide temperature range from >= 1130 °C to 600 °C. Homogenization of a carbonate globule (dissolution of the gas bubble in carbonate melt) at 900-940 °C indicates that after separation from silicate magma the natrocarbonatite represented homogeneous liquid in the 900-1130 °C temperature range, whereas below these temperatures immiscible melts of different composition and fluid phase have separated from it. The bulk composition of homogeneous natrocarbonatite melt may be estimated as approximate to 20% CaF_2, 40-60% $(Na, K)_2CO_3$ and 20-40% $CaCO_3$ based on the coexistence of nyerereite, calcite and fluorite and the rapid phase transition (carbonate aggregate -> carbonate liquid) at 550-570 °C observed in vapor-carbonate globules of nepheline-hosted silicate-melt inclusions and on the Na_2CO_3-$CaCO_3$-CaF_2 phase diagram. Silicate glasses of nepheline-hosted immiscible inclusions drastically differ from host nephelinite in the abundance of major and trace elements. They are high peralkaline ((Na + K)/Al - up to 9.5) and virtually free of water (H_2O<0.6 wt.%). Their very high Zr/Hf and Nb/Ta ratios and Li contents indicate that these silicate glasses represent the most evolved compositions at Oldoinyo Lengai. The peralkaline character of nephelinite melt is expressed in the composition of the daughter mineral assemblage within silicate-melt inclusions in nepheline (delhayelite, leucite, mica, clinopyroxene). These minerals show strong deficiency in Al and enrichment in Fe^{3+} that is also common to the groundmass of the Oldoinyo Lengai combeite-wollastonite nephelinites.

Sharygin, V. V., Kamenetsky, V. S., Zaitsev, A. N., & Kamenetsky, M. B. (2012). Silicate–natrocarbonatite liquid immiscibility in 1917 eruption combeite–wollastonite nephelinite, Oldoinyo Lengai Volcano, Tanzania: Melt inclusion study. Lithos, 152, 23-39. Doi: http://dx.doi.org/10.1016/j.lithos.2012.01.021

3.10. Mineralogy, geochemistry and petrology of the phonolitic to nephelinitic Sadiman volcano, Crater Highlands, Tanzania

Zaitsev A.N., burbankite@gmail.com, *Department of Mineralogy, Faculty of Geology, St. Petersburg State University, University Emb. 7/9, St. Petersburg, 199034, Russia. Department of Mineralogy, Natural History Museum, Cromwell Road, London, SW7 5BD, UK*
Marks M.A.W., Wenzel T., Markl G., *Universität Tübingen, Mathematisch-Naturwissenschaftliche Fakultät, FB Geowissenschaften, Wilhelmstrasse 56, D-72074 Tübingen, Germany*
Spratt J., Strekopytov S., *Department of Mineralogy, Natural History Museum, Cromwell Road, London, SW7 5BD, UK*
Sharygin V.V., *V.S. Sobolev Institute of Geology and Mineralogy, Siberian Branch of Russian Academy of Sciences, Koptuga pr. 3, Novosibirsk, 630090, Russia*

Sadiman volcano is located in the Crater Highlands area of northern Tanzania, which lies next to the western escarpment of the Gregory rift-a part of the eastern branch of the East African Rift system. It consists of inter-layered phonolitic tuffs, tuff breccias (with blocks of nephelinites)

and nephelinitic lava flows. Rare xenoliths of phonolite lava and ijolite were observed within the nephelinite lavas with ijolite blocks occurring in phonolitic tuffs. No evidence for the presence of melilite-bearing and/or carbonatitic rocks was found during this study.
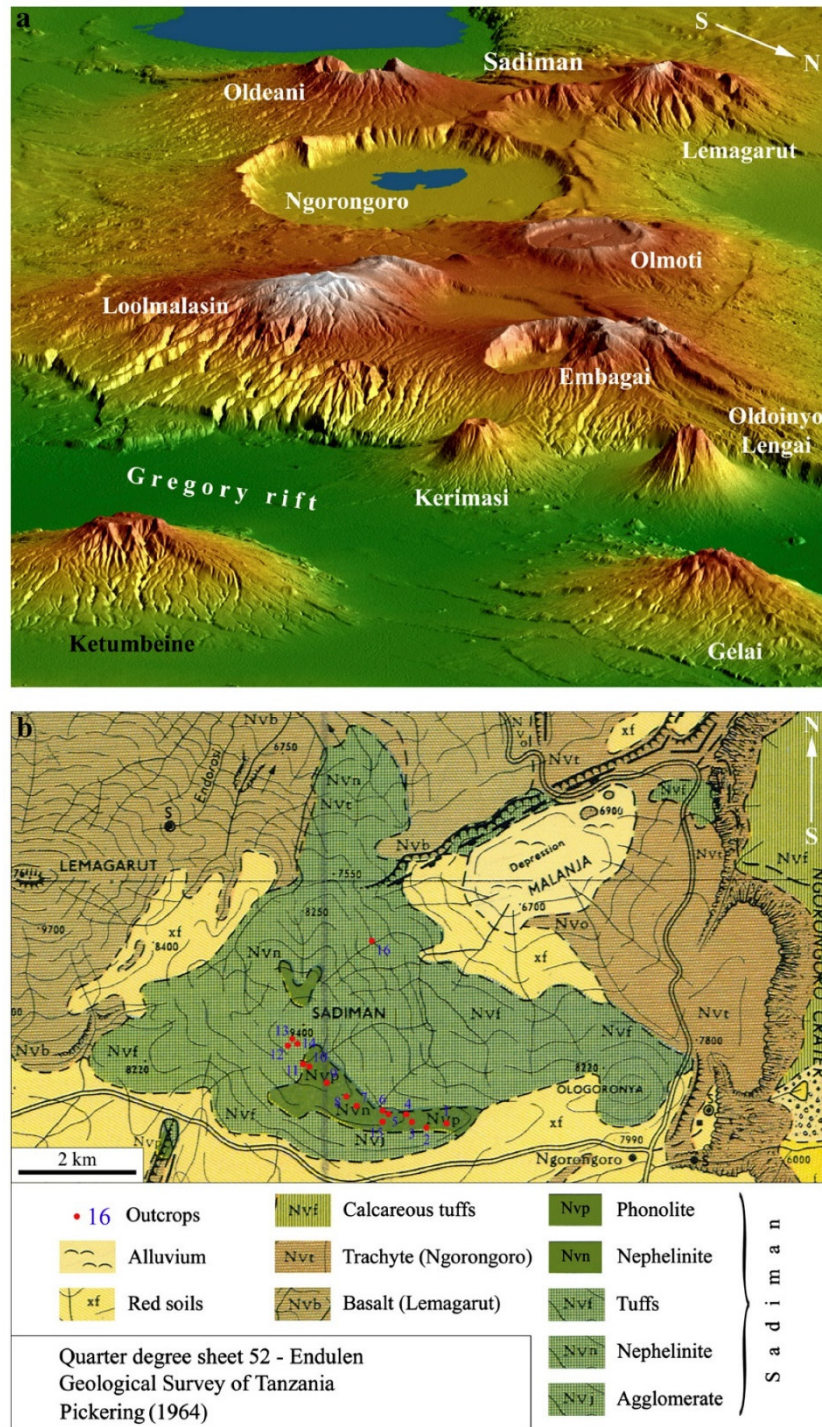
Fig. 3.10.1. (a) Volcanoes in the Crater Highlands area and the Gregory rift in northern Tanzania. SRTM data (February 2000); view size: 44.5 km wide by 142.5 km distance; location: 3° South latitude, 36° East longitude; orientation: View 35° south of west, 15° below horizontal; image courtesy NASA/JPL/NGA Shuttle Radar Topography team. (b) Pickering's (1964) geological map of Sadiman volcano, with lithologies as identified by Pickering. Abbreviations: Nv = Neogene volcanic rocks, f = tuffs, t = trachyte, b = basalt, p = phonolite, n =nephelinite, j = agglomerate Numbered outcrops (red dots) represent samples collected for the current study.

On the basis of petrography, mineralogy and geochemistry the nephelinites are divided into highly porphyritic nephelinite, wollastonite nephelinite and phonolitic nephelinite, the latter of

151

which is the dominant variety at Sadiman. Nepheline + clinopyroxene + titanite +/- perovskite +/- andradite-schorlomite +/- wollastonite +/- sanidine +/- sodalite are the principle pheno- and microphenocryst phases. The nephelinites are highly evolved (Mg# = 0.17-0.26) alkaline to peralkaline (Al = 0.88-1.21) rocks enriched in incompatible elements such as Rb, Ba, Th, U, Nb, Pb, Ta, Sr and light REEs, and strongly depleted in P and Ti. This suggests derivation from an enriched mantle source and fractionation of apatite and Ti-rich mineral(s). Primary melt inclusions in nepheline phenocrysts (T-homogenization = 860-1100 °C) indicate enrichment of volatile components in the melts, particularly of fluorine (up to 1.8 wt % in silicate glass) resulting in the formation of daughter fluorite in partly and complete crystallized inclusions. The Sadiman nephelinites crystallized under relatively oxidizing conditions (above the FMQ buffer), which differ from the reducing conditions reported for trachytic and pantelleritic rocks from other parts of the Gregory rift. Similar rock types and relatively oxidizing conditions are known from Oldoinyo Lengai and other localities, all of which are closely associated with carbonatites. By analogy, we conclude that andradite-schorlomite-rich nephelinites may indicate a pre-stage on the evolutionary path towards carbonatitic magmatism.

Zaitsev, A. N., Marks, M. A. W., Wenzel, T., Spratt, J., Sharygin, V. V., Strekopytov, S., & Markl, G. (2012). Mineralogy, geochemistry and petrology of the phonolitic to nephelinitic Sadiman volcano, Crater Highlands, Tanzania. Lithos, 152, 66-83. Doi: http://dx.doi.org/10.1016/j.lithos.2012.03.001

3.11. Rhyolite xenolith from the neovolcanic basalts of the rift valley of the Juan de Fuca Ridge, northeastern pacific: reconstruction of interaction between MOR silicic rocks and basic magmas

Sharapov, V. N., *vik@igm.nsc.ru*, **Tomilenko, A. A., Smirnov, S. Z., Sharygin, V. V., Kovyazin, S. V.** *Sobolev Institute of Geology and Mineralogy, Siberian Branch, Russian Academy of Sciences, pr. Akademika Koptyuga 3, Novosibirsk, 630090 Russia*

This paper discusses the conditions of rhyolite crystallization and interaction of its fragment with later portions of basic magmas on the basis of the investigation of melt and fluid inclusions in minerals. This study was focused on the rhyolite xenolith and host basalts of the Cleft segment of the Juan de Fuca mid-ocean ridge (East Pacific). The basic rocks of the southern part of this segment are typical MOR basalts in terms of bulk chemistry and the compositions of melt inclusions in phenocrysts. Olivine, clinopyroxene, and plagioclase crystallized at temperatures of 1160-1280 °C and pressures of 20 and 100 MPa. The xenolith represents a leucocratic rock with negligible amounts of mafic minerals, which clearly distinguishes it from the known occurrences of silicic rocks in the rift valleys of MOR. The rhyolite melt crystallized at temperatures of 900-880 °C. At 780-800 °C the final stages of rhyolite melt crystallization were accompanied by release of a saline aqueous fluid with high chloride contents. On the basis of melt inclusion and rhyolite melting products geochemistry it is suggested that they were produced by hydrous melting of metamorphosed oceanic crust of the Cleft segment under the influence of saline aqueous fluid occupying pore and interstitial space of the melting rocks. The xenolith represents latest products of those melt differentiation. The final portions of the melts show high volatile contents: $H_2O >$ 3.0 wt %, Cl ~2.0 wt %, and F ~ 0.1 wt %. The interaction of the xenolith with the host basaltic melt occurred at temperatures equal or slightly higher than those of ferrobasalt melts (1190-1180 °C). During the ascent the xenolith residence time in the high-temperature basic magma were few tens of hours and xenolith started to melt. Meanwhile, diffusion exchange between the basaltic and silicic melts was very minor.
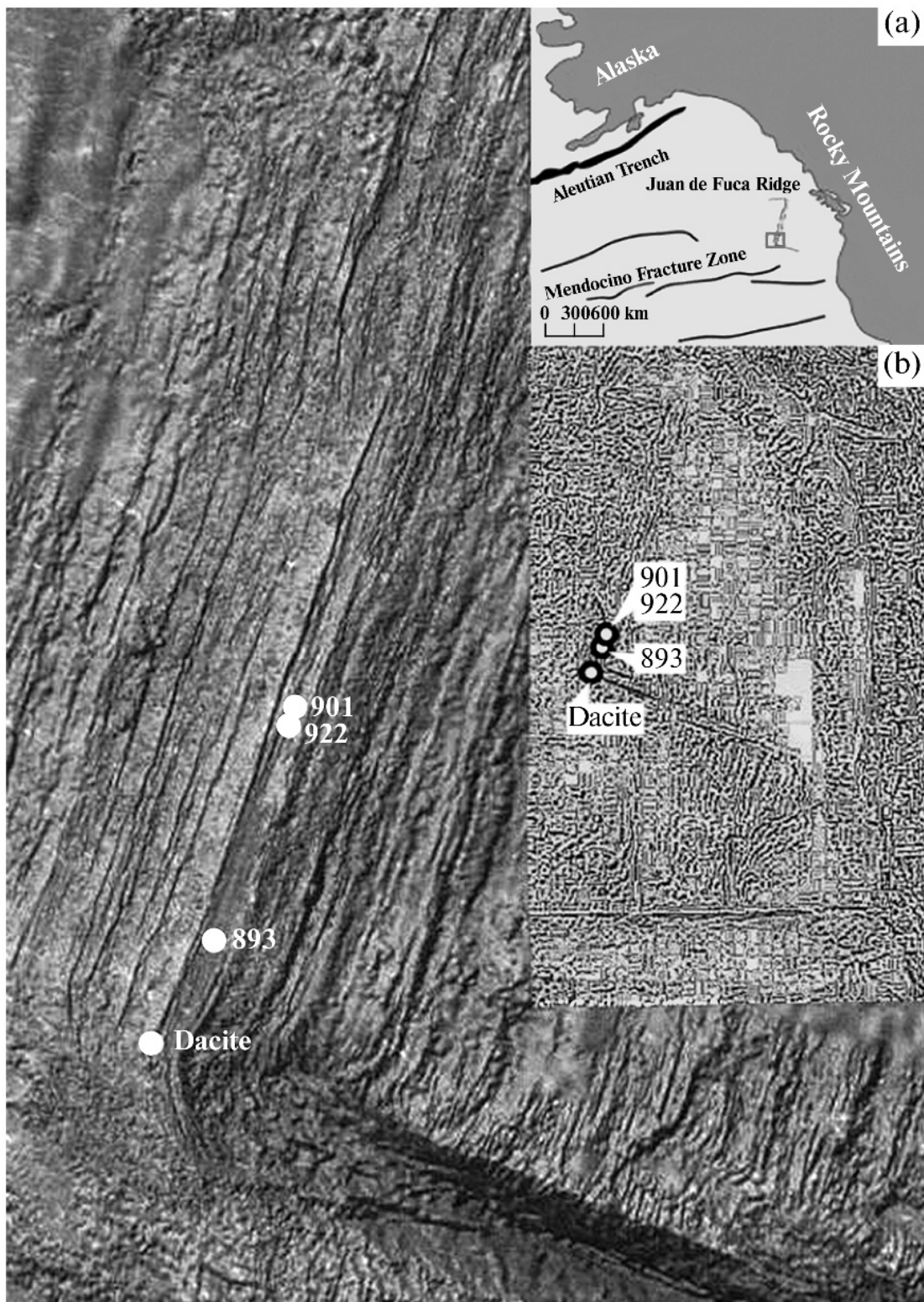
Fig. 3.11.1. Sampling sites of rocks in the axial rift valley of the Cleft segment of the Juan de Fuca Ridge. Dacite is an exposure of the andesite–dacite extrusion described by Cotsonika (2006); 893 and 922 are dredge stations; and 901 is the area of the valley where the rhyolite sample was recovered. Insets show (a) the location of the area of interest in the system of ridges and (b) the distribution of lineaments in the Juan de Fuca Ridge and adjoining regions obtained by the graphical processing of the Google map of the region.

Sharapov, V. N., Tomilenko, A. A., Smirnov, S. Z., Sharygin, V. V., & Kovyazin, S. V. (2013). Rhyolite xenolith from the neovolcanic basalts of the rift valley of the Juan de Fuca Ridge, northeastern pacific: Reconstructsen MOR silicic rocks and basic magmas. Petrology, 21(5), 427-453. Doi: 10.1134/S0869591113050044

4. INVESTIGATIONS OF ORE DEPOSITS

4.1. The study of crystallization conditions, melt and fluid compositions of rare-metal ore magmatic systems

4.1.1. Ongonite-elvan magmas of the Kalguty ore-magmatic system (Gorny Altai): composition, fluid regime, and genesis

Sokolova E.N., Smirnov S.Z., ssmr@igm.nsc.ru, *V.S. Sobolev Institute of Geology and Mineralogy, Siberian Branch of the Russian Academy of Sciences, pr. Akademika Koptyuga 3, Novosibirsk, 630090, Russia. Novosibirsk State University, ul. Pirogova 2, Novosibirsk, 630090, Russia*
Astrelina E.I., Kotler P.D., *Novosibirsk State University, ul. Pirogova 2, Novosibirsk, 630090, Russia*
Annikova I.Y., *V.S. Sobolev Institute of Geology and Mineralogy, Siberian Branch of the Russian Academy of Sciences, pr. Akademika Koptyuga 3, Novosibirsk, 630090, Russia*
Vladimirov A.G. *Novosibirsk State University, ul. Pirogova 2, Novosibirsk, 630090, Russia*

The Kalguty ore-magmatic system (OMS) is a complex combination of a granite pluton, a hydrothermal Mo-W deposit, pegmatites, greisens, and a belt of rare-metal (RM) and ultra-rare-metal (URM) elvan and ongonite dikes.

Studies of melt inclusions (MI) in quartz phenocrysts in the dike rocks have demonstrated that quenched glass has major element contents close to those of the dike rocks but rare elements (Li, Rb, Be, Cs) and P contents. This suggests that the MI represent magma at the stage preceding the dike emplacement. The MI in quartz from the URM rocks are poorer in Si, Fe, Mg, and REE than those in quartz from the RM rocks but richer in Cs, Rb, Nb, and Ta, like the URM rocks themselves. This indicates that the melts had segregated into RM and URM ones before the studied quartz phenocrysts began to crystallize. The composition of MI glass corresponds to "the albite trend" of differentiation, suggesting that the initial melt compositions were ongonitic, while their K enrichment and formation of elvan magma followed the crystallization of the quartz phenocrysts.

According to our estimates, the melt contained 6-7 wt % H_2O. The quartz phenocrysts crystallized in a heterogeneous medium consisting of a silicate melt and an aqueous fluid. The latter was a high-density supercritical fluid with 3-12 wt % NaCl equiv. Variations in the gas and salt compositions of the fluid inclusions (FI) are attributed to the interaction between fluids of magmatic and hydrothermal systems. This possibility is confirmed by ample evidence of their coeval formation.

Quartz crystallization from the RM melts took place at 630-650 degrees C, whereas quartz from the URM melts formed at 20-30 degrees C lower temperatures. Quartz phenocrysts crystallized at 4.5-5.5 kbar. Additional estimates with regard to the mineral composition and quartz compressibility yielded values of 3-6.5 kbar.

A petrogenetic model of some crystallization stages of the dike rocks within the Kalguty OMS was constructed on the basis of the results obtained in this study. The melts which formed the dikes of the East Kalguty belt are derivatives of the same magma which formed the major-stage granite pluton. Quartz is present as intratelluric phenocrysts, which crystallized at considerably greater depths than those of the dike emplacement. Differentiation of the parental magma was accompanied by rare element and P accumulation. The compositions of the FI and MI confirm that the magma and hydrothermal system of the Kalguty OMS exchanged their substances. It is associated with the increasing K content of the melts and the subsequent elvan crystallization as well as considerable variations in the salt and gas compositions of the magmatic fluid inclusions.

Sokolova, E. N., Smirnov, S. Z., Astrelina, E. I., Annikova, I. Y., Vladimirov, A. G., & Kotler, P. D. (2011). Ongonite–elvan magmas of the Kalguty ore-magmatic system (Gorny Altai): composition, fluid regime, and genesis. Russian Geology and Geophysics, 52(11), 1378-1400. Doi: http://dx.doi.org/10.1016/j.rgg.2011.10.017

4.1.2. Petrology of the tin-bearing granite-leucogranites of the Pia Oak Massif, Northern Vietnam

Vladimirov A. G., vladimir@igm.nsc.ru, *Sobolev Institute of Geology and Mineralogy, Siberian Branch, Russian Academy of Sciences, pr. Akad. Koptyuga, Novosibirsk, 630090 Russia. Novosibirsk State University, ul. Pirogova 2, Novosibirsk, 630090 Russia. Tomsk State University, pr. Lenina 36, Tomsk, 634050 Russia*

Anh P. L., luuanhphan@yahoo.com, *Institute of Geological Sciences, Vietnam Academy of Sciences and Technologies, Hanoi, Vietnam*

Kruk N. N., Annikova I. Y., Pavlova G. G., Kuibida M. L., Moroz E. N., *Sobolev Institute of Geology and Mineralogy, Siberian Branch, Russian Academy of Sciences, pr. Akad. Koptyuga, Novosibirsk, 630090 Russia*

Smirnov C. Z., Sokolova E. N., *Sobolev Institute of Geology and Mineralogy, Siberian Branch, Russian Academy of Sciences, pr. Akad. Koptyuga, Novosibirsk, 630090 Russia. Novosibirsk State University, ul. Pirogova 2, Novosibirsk, 630090 Russia*

Astrelina E. I., *Novosibirsk State University, ul. Pirogova 2, Novosibirsk, 630090 Russia*
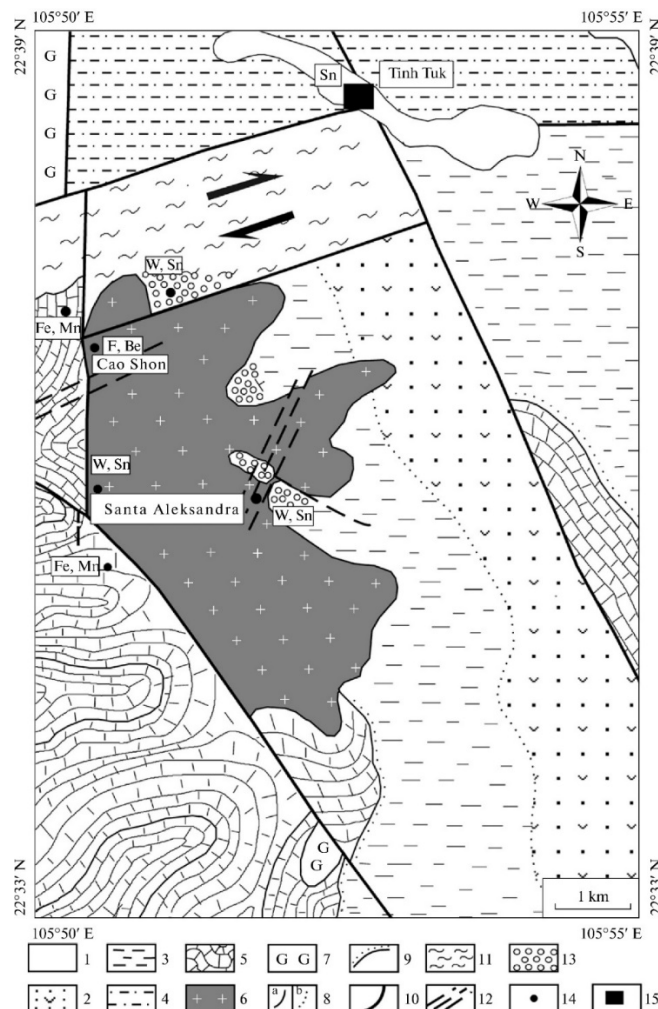
Fig. 4.1.2.1. Geological scheme of the Piaoak rare-metal granite massif and related ore deposits (Northern Vietnam). Compiled by Phan Luu Anh and A.G. Vladimirov using materials (Bourret, 1924; Lacroix, 1933;

Lazarev, 1958; Izokh et al., 1986; Nguyen Van Quyen et al., 1986), as well as the State Geological maps of Vietnam on scales of 1 : 1000000 (Chan Van Chi et al., 1977) and1 : 500000 (Chan Dyk Lyong et al., 1992). (1) Quaternary deposits; (2) volcanogenic–terrigenous sequences (conglomerates, gravelstones, sandstones, and mudstones) with intercalations of felsic tuffs, tuff rhyolites, and rhyolites of the Middle Triassic age; (3) Early Triassic deep-water black shales; (4) undivided Permian massive and oolithic shales with bauxite interbeds; (5) undivided Early Devonian substantially carbonate sequences with interbeds of dolomites, shales, and siliceous rocks; (6) Late Cretaceous Piaoak granite–leucogranite complex; (7) gabbrodolerite (congo-diabases) of the contingently Early Triassic Caobang Complex; (8) geological boundaries: (a) observed, (b) inferred; (9) boundaries of structural unconformities of stratified sequences; (10) faults; (11) shear zone with brittle ductile flowing of the matter; (12) zones of intense fracturing with signs of greisenization (after granites), (13) greisenized hornfels in the roof and contacts of the Piaoak granite–leucogranite massif; (14) occurrences and deposits (Fe, Mn—postmagmatic magnetite veins, (Sn,W) tin–tungsten-bearing quartz vein–greisen occurrences; (F, Be) fluorite-bearing metasomatites and occurrences); (15) Tinh Tuk open pit cassiterite deposit.

The Pia Oak tin-bearing granite-leucogranites located in the Caobang Province of Northern Vietnam compose a stock-like hypabyssal body. Host rocks are represented by Early Devonian carbonate sequences and Early Triassic "black" shales. The geochronological age of the Piaoak granite-leucogranites corresponds to the Late Cretaceous: T = 83.5 +/- 6.2 Ma, Rb-87/Sr-86 method; T = 89.7 +/- 1.0 Ma, Ar-39/Ar-40 method. The massif has a simple basic to acid order: two-mica and muscovite granite-leucogranite -> raremetal aplites, pegmatites -> tin-bearing greisens and hydrothermal veins. The petrographic and microstructural studies revealed a sharp change in crystallization conditions of the granite-leucogranite magma at the late magmatic stage and formation of muscovite via incongruent melting of protolithionite. The study of melt and coexisting fluid inclusions showed that solidus crystallization occurred under fluid-saturated conditions at 635-600 °C. In composition, the granite-leucogranites of the Piaoak Massif correspond to the rare-metal-plumasite geochemical type (according to L.V. Tauson), and reach Li-F facies in terms of their rare-element composition. The composition of aplites and pegmatites demonstrates that granite-leucogranite magma did not accumulate lithophile and volatile components in the residual melt during differentiation, but was initially enriched in rare-metals. It is most probable that the melt was generated from Proterozoic lithotectonic complexes and overlaying Lower Triassic "black" shales.

Vladimirov, A. G., Anh, P., Kruk, N. N., Smirnov, C. Z., Annikova, I. Y., Pavlova, G. G., Kuibida, M. L., Moroz, E. N., Sokolova, E. N., & Astrelina, E. I. (2012). Petrology of the tin-bearing granite-leucogranites of the Piaoak Massif, Northern Vietnam. Petrology, 20(6), 545-566. Doi: 10.1134/S0869591112050074

4.1.3. Melt compositions and fluid regime of crystallization of rare-metal granite and pegmatites from the Sn-W Tigrinoe deposit (Primor'e)

Smirnov S. Z., ssmr@igm.nsc.ru**,** *Sobolev Institute of Geology and Mineralogy, SiberianBranch, Russian Academy of Sciences, Novosibirsk, Russia. Novosibirsk State University, Novosibirsk, Russia. Tomsk State University, Tomsk, Russia*
Bortnikov N. S., Gorelikova N. V., *Institute of Geology of Ore Deposits, Petrography, Mineralogy, and Geochemistry, Russian Academy of Sciences, Moscow, Russia*
Gonevchuk V. G., *Far East Geological Institute, Far East Branch, Russian Academy of Sciences, Vladivostok, Russia*

The Tigrinoe deposit is located in the central part of SikhoteAlin (Primor'e). The small intrusions of biotite bearing porphyry granite of the Bolshoi stock and medium grained, sometimes porphyric, protolithionite–zinnwaldite granite of the Malyi stock related to the first and second intrusive phases of rare-metal granite magma, respectively, occur in the junction zone between the

Sikhote Alin and Tigrinskii faults. Drilling in the Malyi stock revealed a body of porphyric zinnwaldite granite interpreted as the third phase. These bodies contain wide greisenization zones, vein stockworks, and ore breccias composing the large Sn–W deposit. The Malyi stock also contains small bodies of pegmatites (stocksheiders) observed at the contacts with magmatic rocks of different phases and along their contacts with host sedimentary rocks replaced by hornfels, and with greisen bodies in granites. The paper reports new data on fluid regime of crystallization of rare-metal granites and constrains conditions of pegmatite formation.

The melt and fluid inclusion study revealed that the crystallization of granites and pegmatites occurred from the same Li and F-rich granitic melts at 550-600 °C. The crystallization of pegmatites was related to heterogeneous mixture of the silicate melts and aqueous fluid enriched in CH_4. No traces of CO_2 were detected. melt and fluid inclusion petrography implies that crystallization occurred under high water pressure. Pegmatites may be considered as a result of crystallization of relatively small areas of the magma chamber containing a high portion of the methane–hydrous fluid phase. The presence of this phase, most likely of a complex "crust–mantle" nature, could explain the input of extra potassium to the pegmatite forming batches. Magmatic methane-rich aqueous fluids with no or traces of CO_2 actively participated in the processes of transport and accumulation of Sn, W, and Mo in hydrothermal veins of the deposit.
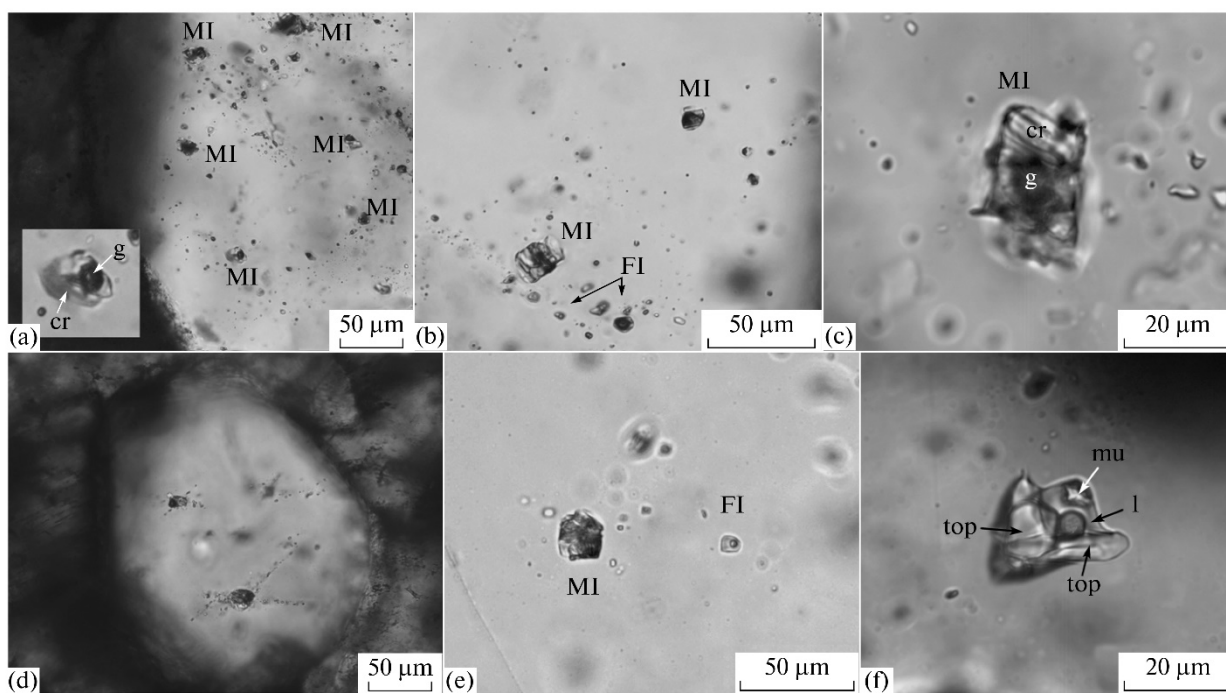
Fig. 4.1.3.1. Melt and fluid inclusions in quartz from rare-metal granite and pegmatites of the Tigrinoe deposit. (a–c) Inclusions in quartz from the Bolshoi (a, b) and Malyi (c) stocks; (d–f) inclusions in quartz from pegmatites: decrepitated melt inclusions (d), syngenetic melt (MI) and fluid (FI) inclusions (e), and combined fluid (gas (g) + liquid (l)) inclusion with trapped topaz (top) crystals and probably daughter muscovite (mu) crystals (f).

Smirnov, S. Z., Bortnikov, N. S., Gonevchuk, V. G., & Gorelikova, N. V. (2014). Melt compositions and fluid regime of crystallization of rare-metal granite and pegmatites from the Sn-W Tigrinoe deposit (Primor'e). Doklady Earth Sciences, 456(1), 558-562. Doi: 10.1134/S1028334X14050201

4.1.4. Geochemistry and age of rare-metal dyke belts in eastern Kazakhstan

Khromykh S. V., serkhrom@mail.ru, *Sobolev Institute of Geology and Mineralogy, Siberian Branch, Russian Academy of Sciences, Novosibirsk, Russia. Novosibirsk State University, Novosibirsk, Russia*

Sokolova E. N., Smirnov S. Z., *Sobolev Institute of Geology and Mineralogy, Siberian Branch, Russian Academy of Sciences, Novosibirsk, Russia. Novosibirsk State University, Novosibirsk, Russia. National Research Tomsk State University, Tomsk, Russia*

Travin A. V., *Sobolev Institute of Geology and Mineralogy, Siberian Branch, Russian Academy of Sciences, Novosibirsk, Russia*

Annikova I. Y. *Sobolev Institute of Geology and Mineralogy, Siberian Branch, Russian Academy of Sciences, Novosibirsk, Russia. National Research Tomsk State University, Tomsk, Russia*

The results of studies of the Chechek and Akhmirovka dyke belts (the Kalba-Narym zone of Eastern Kazakhstan) constituted by rare-metal Li-F-granitoids (ongonites) are presented. The results of geochemical mapping of dyke belts are given, as are the first-obtained data on the rare-metal composition of rock-forming minerals and melt inclusions. The data on precision dating of rocks by means of the Ar-40/Ar-39-isotope technique are presented. It is shown that the dyke belts were formed from the melts of three different geochemical types. The existence of these types might be caused by differentiation within the deep-seated magma chambers. The data of geochronology permit us to conclude that the centers of rare-metal Li-F-magmatism characteristic of the large magma provinces that appeared under the impact of mantle plumes on the arisen continental crust might have been formed at the final stages of the formation of the Kalba-Narym batholith. This allows one to assume the rare-metal Li-F-granitoids (ongonites) of the dyke belts in Eastern Kazakhstan belong to the large Late-Paleozoic magma province that appeared in the region of Central Asia as a result of the activity of the Tarim plume.
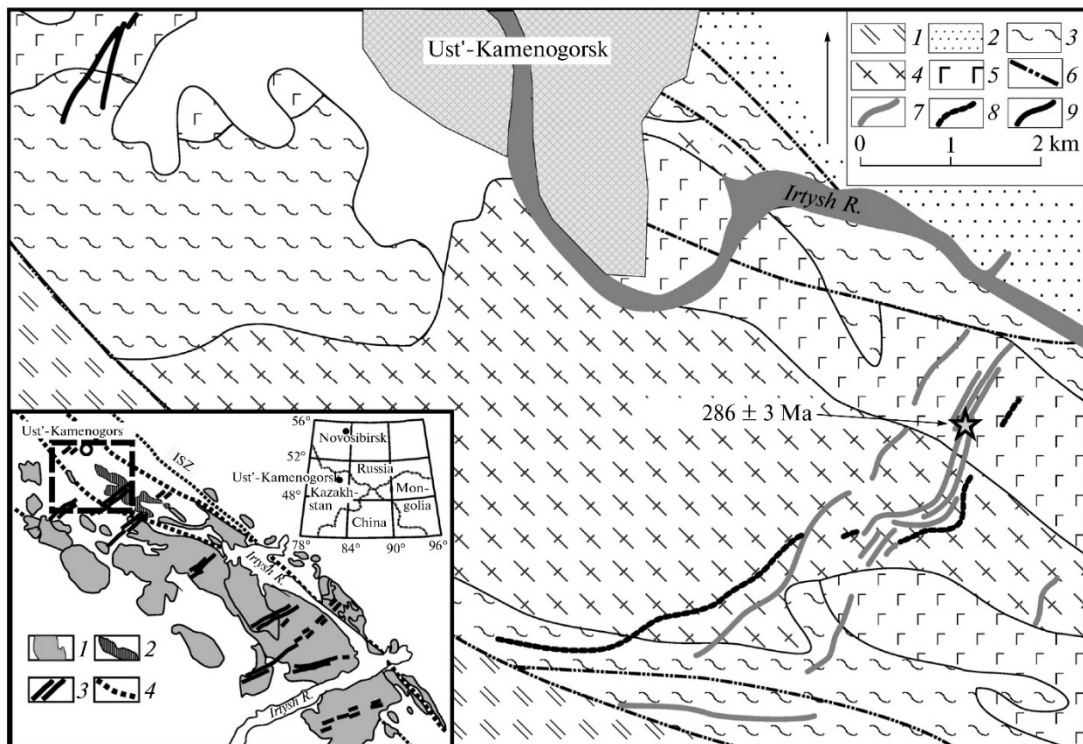
Fig. 4.1.4.1. Scheme of the dislocation of the Chechek and Akhmirovo rare-metal dyke belts (by [7] with corrections). The positions of dykes are mapped by the decoded data of the Google Earth satellite images.

1, 2 — Siltstones, sandstones, and schists (D2); 3 — gneisses, amphibolites, and crystalline schists of the Irtysh contortion zone (D3–C1?); 4 — gneiss–granodiorites and gneiss–granites (C2); 5 — gabbros, diorites, gabbronorites (C2-3?); 6 — faults; 7, 8 — Chechek dyke belt: 7 — highly rare-metal rocks, 8 — rare-metal rocks; 9 — rare-metal dyke rocks of the Akhmirovo belt. The asterisk marks the sampling site for dating. In the inset: 1 — granitoids of the Kalba–Narym batholith (undivided); 2 —g abbroids (C2-3?); 3 – dyke belts of the Mirolyubovo complex; 4 — faults (ISZ is the Irtysh shear zone).

Khromykh, S. V., Sokolova, E. N., Smirnov, S. Z., Travin, A. V., & Annikova, I. Y. (2014). Geochemistry and age of rare-metal dyke belts in eastern Kazakhstan. Doklady Earth Sciences, 459(2), 1587-1591. Doi: 10.1134/S1028334X14120174

4.2. The study of deep seated processes related to alkaline magmatism

Kamenetsky V. S., Dima.Kamenetsky@utas.edu.au**, Kamenetsky M. B.,** *ARC Centre of Excellence in Ore Deposits and School of Earth Sciences, University of Tasmania, Hobart, Tasmania 7001, Australia*
Golovin A. V., Sharygin V. V., *VS Sobolev Institute of Geology and Mineralogy, SB RAS, Novosibirsk, Russia*
Maas R. *School of Earth Sciences, University of Melbourne, Vic 3010, Australia*
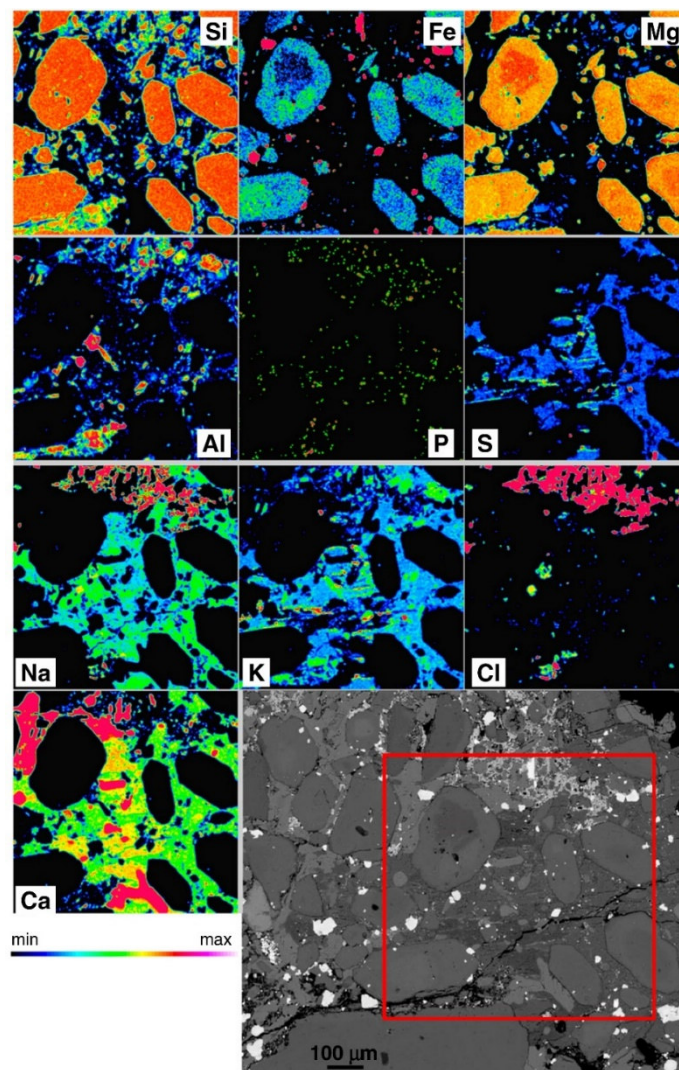
Fig. 4.2.1. Backscattered electron image and X-ray element maps showing euhedral zoned crystals of olivine (Si, Fe, Mg maps) set in the groundmass composed of S-bearing Na–K–Ca carbonates, calcite

159

(highest intensity on Ca-map), halite, phlogopite (Al, Mg and K maps), sodalite (Al and Cl maps), apatite (P map), Fe-oxides and Cr–spinel (highest intensity on Fe-map). The maps are recorded on the electron microprobe JEOL JXA-8200 (Max Planck Institut für Chemie, Mainz).

An ultrabasic/ultramafic composition of kimberlite magmas is difficult to reconcile with existing models of the kimberlite mantle source and melting conditions, inferred magma temperatures and rheological properties, and the style of magma ascent and emplacement. The inconsistencies in current thinking indicate serious flaws in understanding kimberlite magma compositions. Much of the uncertainty over true kimberlite compositions may stem from almost ubiquitous hydration and leaching of kimberlite rocks. This study presents petrographic and geochemical data for kimberlite samples largely unaffected by postmagmatic modification, from the Devonian Udachnaya-East pipe in Siberia. These samples are unusually enriched in chlorine and sodium, yet they are essentially anhydrous. These features are consistent with the phase composition of the groundmass which is dominated by minerals such as Na-Ca carbonates, Na-K chlorides and sulphates which appear to be - in our samples - co-magmatic with common silicates and oxides, but are unknown in other kimberlites, or rarely found within magmatic assemblages. We suggest that a kimberlite parent melt of essentially non-silicate composition, with high concentrations of alkalis, CO_2 and Cl may be a viable alternative to the currently favoured water-rich, high-Mg model primary melt. Entrainment of mantle silicates into such a melt en route to the surface, followed by gravitational accumulation of mantle olivine and liquidus oxides (perovskite, Cr-spinel) at the bottom of vertically extensive magma bodies after emplacement, would explain the observed properties of kimberlite magma/rock, notably enrichment in olivine and trace elements in the hypabyssal kimberlite facies. A carbonate melt composition would retain attributes of the standard model such as trace element enrichment via low degrees of partial melting, it would explain low temperatures of crystallisation and the exceptional rheological properties that enable kimberlite primary melts to segregate from the lithospheric source and buoyantly ascend at high speed, while mixing and reacting with country rocks.

Kamenetsky, V. S., Kamenetsky, M. B., Golovin, A. V., Sharygin, V. V., & Maas, R. (2012). Ultrafresh salty kimberlite of the Udachnaya–East pipe (Yakutia, Russia): A petrological oddity or fortuitous discovery? Lithos, 152, 173-186. Doi: http://dx.doi.org/10.1016/j.lithos.2012.04.032

4.3. The study of ferromanganese crusts from the Sea of Okhotsk

4.3.1. Distribution of microelements in ferromanganese crusts of the Sea of Okhotsk

Baturin, G. N., *gbatur@ocean.ru, Shirshov Institute of Oceanology, Russian Academy of Sciences, pr. Nakhimovskii 36, Moscow, 117997 Russia*
Dubinchuk, V. T., *Fedorovskii All-Russian Institute of Mineral Resources (VIMS), per. Staromonetnyi 29, Moscow, 119017 Russia*
Rashidov, V. A., *Piip Institute of Volcanology and Seismology, Far East Branch, Russian Academy of Sciences, bul'v. Piipa 9, Petropavlovsk-Kamchatsky, 683006 Russia*

The contents of 60 macro- and microelements were determined by inductively coupled plasma mass spectrometry in the samples of ferromanganese crusts collected on submarine slopes of the Kuril Islands. Along with a pronounced variability in the chemical composition of the crusts, the contents of several microelements vary according to the values of the europium anomaly. A positive value points to local volcanogenic hydrothermal activity, which provides for the

accumulation of manganese and iron at the expense of the accumulation of some nonferrous and rare metals.
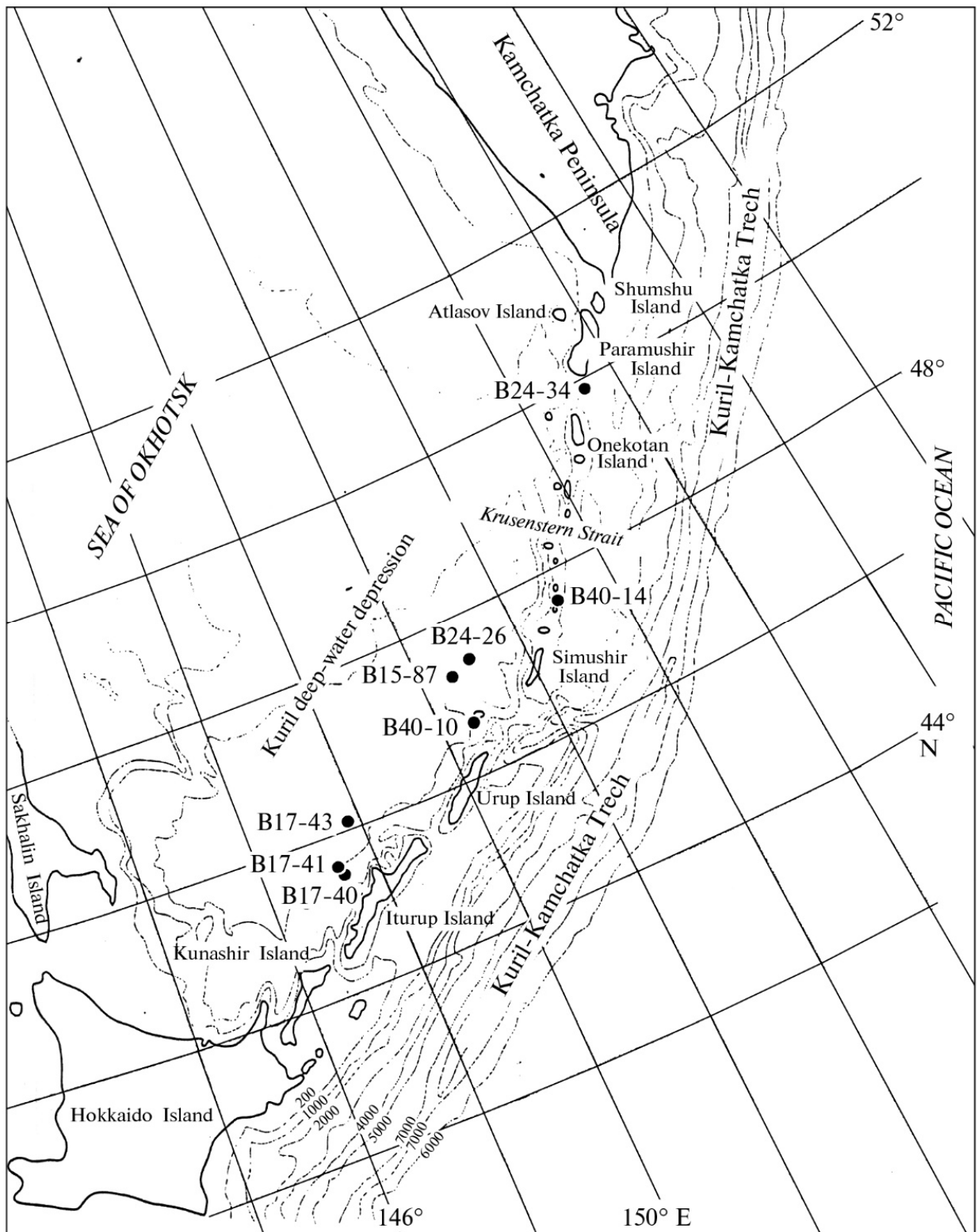
Fig. 4.3.1.1. Scheme of the location of sampling stations.

Baturin, G. N., Dubinchuk, V. T., & Rashidov, V. A. (2011). Distribution of microelements in ferromanganese crusts of the sea of Okhotsk. Doklady Earth Sciences, 440(1), 1291-1297. Doi: 10.1134/S1028334X11090121

4.3.2. Ferromanganese Crusts from the Sea of Okhotsk

Baturin, G. N., *gbatur@ocean.ru, Shirshov Institute of Oceanology, Russian Academy of Sciences, pr. Nakhimovskii 36, Moscow, 117997 Russia*
Dubinchuk, V. T., *Fedorovskii All-Russian Institute of Mineral Resources (VIMS), per. Staromonetnyi 29, Moscow, 119017 Russia*
Rashidov, V. A., *Piip Institute of Volcanology and Seismology, Far East Branch, Russian Academy of Sciences, bul'v. Piipa 9, Petropavlovsk-Kamchatsky, 683006 Russia*
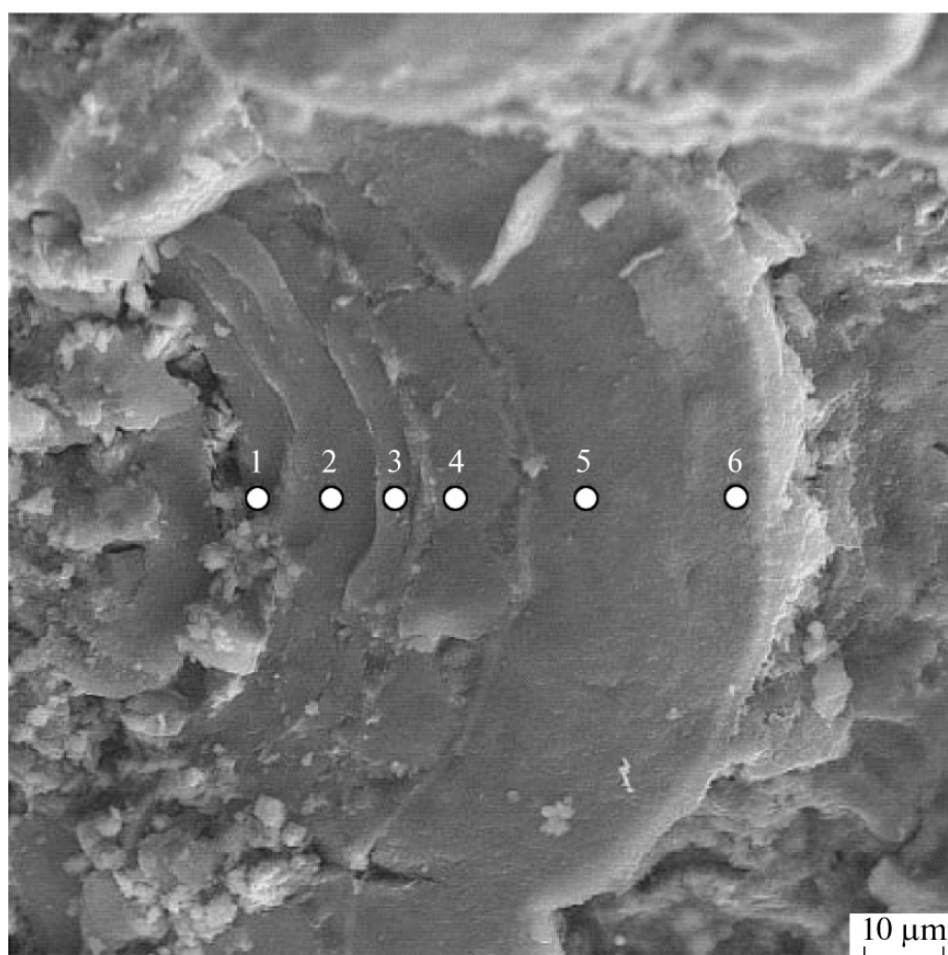
Point number	Al_2O_3	SiO_2	ClO_2	K_2O	CaO	MnO	Fe_2O_3
1	0	2.02	1.08	1.79	3.65	82.16	9.30
2	0	1.60	0.98	1.00	3.65	83.76	10.09
3	0	1.02	1.08	1.12	3.50	84.91	10.07
4	0	2.41	0.68	1.80	3.95	83.16	6.20
5	0	0	1.08	1.10	4.34	84.16	11.22
6	0	2.72	1.08	1.09	0.65	84.16	11.30

Fig. 4.3.2.1. The microlaminated area of the crust under a scanning electron microscope.

New data on the microstructures and the mineral and chemical compositions of ferromanganese crusts obtained from the western slope of the Kuril Island Arc in the Sea of Okhotsk during cruises of the R/V "Volcanolog" are discussed. The study of the crusts using analytical electron microscopy methods revealed that their manganese phase is represented by vernadite, Fe-vernadite, todorokite, asbolane, and asbolane–buserite, while the iron phase consists of hematite, hydrohematite, ferroxyhite, and magnetite. The assemblage of lithic minerals includes apatite, quartz, epidote, and montmorillonite. According to the chemical analysis, most of the crusts contain a significant share of volcanogenic and hydrothermal material, which is evident from the elevated values of the Mn and Ti modules, the low concentrations of some trace elements, and the positive Eu anomaly in the rare earth elements composition.

Baturin, G. N., Dubinchuk, V. T., & Rashidov, V. A. (2012). Ferromanganese crusts from the Sea of Okhotsk. Oceanology, 52(1), 88-100. Doi: 10.1134/S0001437012010031

4.4. Nizhne-Koshelevsky geothermal field south Kamchatka: neomorphic minerals on surface of the pyrite grains

Rychagov S.N., *Institute of Volcanology and Seismology, Far East Division, Russian Academy of Sciences, Petropavlovsk-Kamchatsky, Russia*
Schegolkov Yu.V. *Central Research Institute of Geological Prospecting for Base and Precious Metals, Varshavskoe sh., 129 korpus1, Moscow, 117545 Russia*
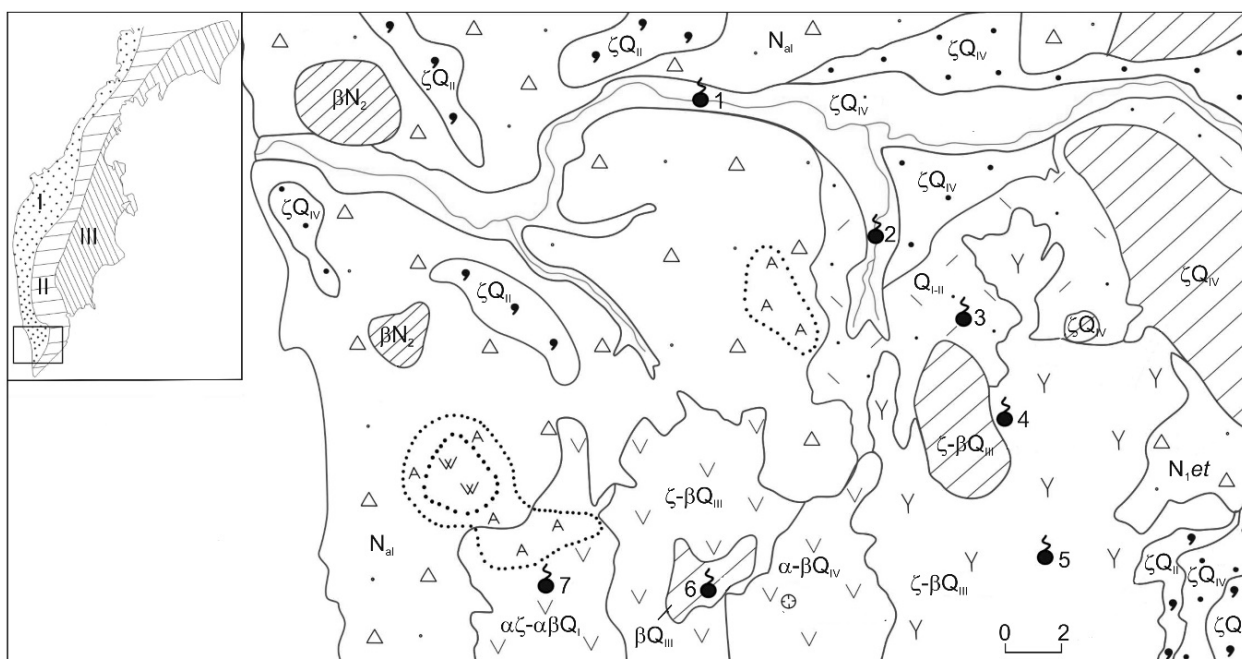
Fig. 4.4.1. Geological sketch map Pauzhetskaya-Kambalny-Koshelevo geothermal (ore) areas at a scale of 1: 200 000:

XPS and AES studies of the pyrite grains extracted from hydrothermal clays underlying Nizhne-Koshelevsky geothermal field in the Kamchatka Peninsula demonstrated that mineral films coat surfaces of these grains. Such films are several nm through several hundred nm thick and consist of two layers. The lower one consists of thiosulfate complexes of iron containing reduced nitrogen, whereas the upper one is a Ti-bearing oxide-silicate phase. Presumably, formation of such mineral substance coating the pyrite grain surfaces displays influence of a deep

metal-bearing reducing fluid on the physicochemical processes in the near-surface part of the geothermal field.

Rychagov S.N., Schegolkov Yu.V. (2011) Nizhne-Koshelevsky geothermal field south Kamchatka: neomorphic minerals on surface of the pyrite grains. Rudy I Metally 2, 52-57. (In Russian). http://www.tsnigri.ru/?q=node/24

4.5. Native metals in voicanic ashes

Karpov G.A. *Institute of Volcanology and Seismology, Far East Division, Russian Academy of Sciences, Petropavlovsk-Kamchatsky, Russia*
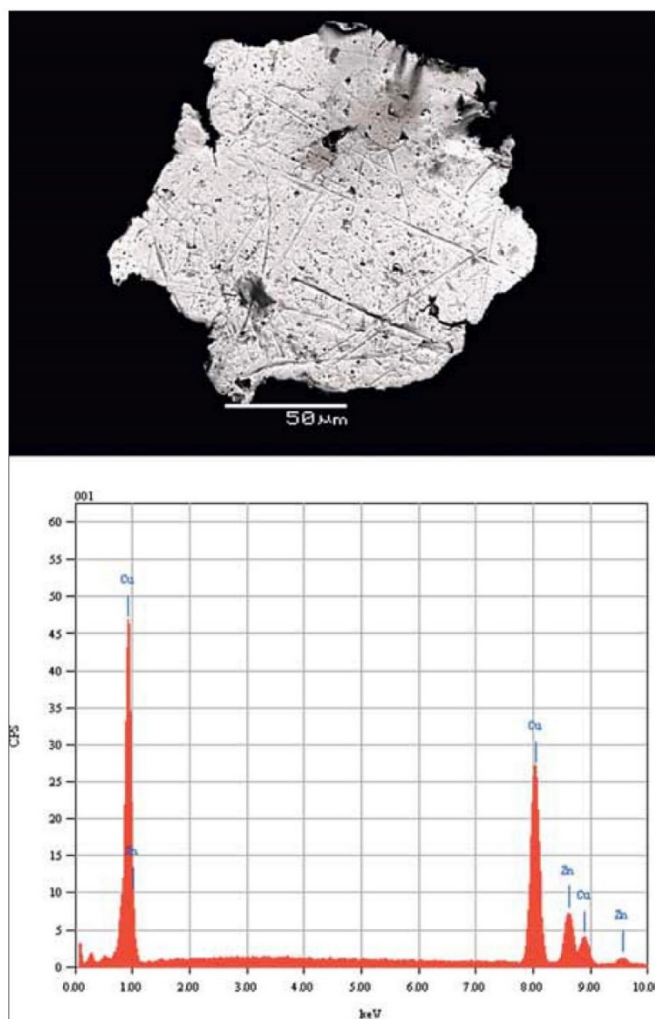
Fig. 4.5.1. Particle native copper from the ashes of the volcano Sn. Helens and its X-ray spectrum.

Based on the research of accessory ore minerals ash active volcanoes of Kamchatka concluded that modern volcanic fluid systems have ore load, ie, are mineralized. Frequently observed in the composition of the same sample different-ash (from the maximum reduction to the oxidized) state ore components show complex redox conditions in the area of fluid transport and on - apparently for emergency heterogenetic conditions of the gas-transport reactions in gas - ash column during the eruption. Transfer ore material takes the form of native elements and intermetallic compounds, possibly in the form of clusters or nanoparticles.

Karpov G.A. (2014) Native metals in voicanic ashes. Science in Russia 4, 19-28. (In Russian).

5. THEORETICAL EVIDENCES IN VOLCANOLOGY

5.1. Geochemical evidences

5.1.1. Therholites formation

Simakin A.G., simakin@iem.ac.ru, *Institute of Experimental Mineralogy RAS, Chernogolovka, 142432, Russia. Physics of the Earth RAS, Moscow, D-242, Russia, 123995*
Bindeman I.N., bindeman@uoregon.edu, *Geological Sciences, 1272 University of Oregon, OR 97403-1272, USA*

Process of rhyolites formation by the basalts underplating of the ancient (Precambrian) silicic rocks and young siliceous pyroclastics is actual in many important occasions including formation of Spervolcanoes of Snake River Plate (USA). Convective melting dynamics at the underplating was theoretically considered in the limited number of publications with overwhelming citation leadership of (Huppert and Sparks, 1985). We extend simple analytical model to include realistic melting diagram and multi-phase magma rheology. At the relatively large Rayleigh numbers of 106-108 typical for magma sills dimensions chaotic plumes convection develops. Resolution with grid size around 20 cm is required to properly resolve flow field even for granitic magma. Low viscosity basaltic magma needs even finer resolution. For technical reasons we model melting of the silicic protolith by the superheated rhyolitic magma. This system can represent relocated rhyolitic magma or just upper part of the underplating pair at the properly defined bottom heat flux. First of all we define at what melt and rock temperatures convecting melting occurs (Fig. 5.1.1.1).
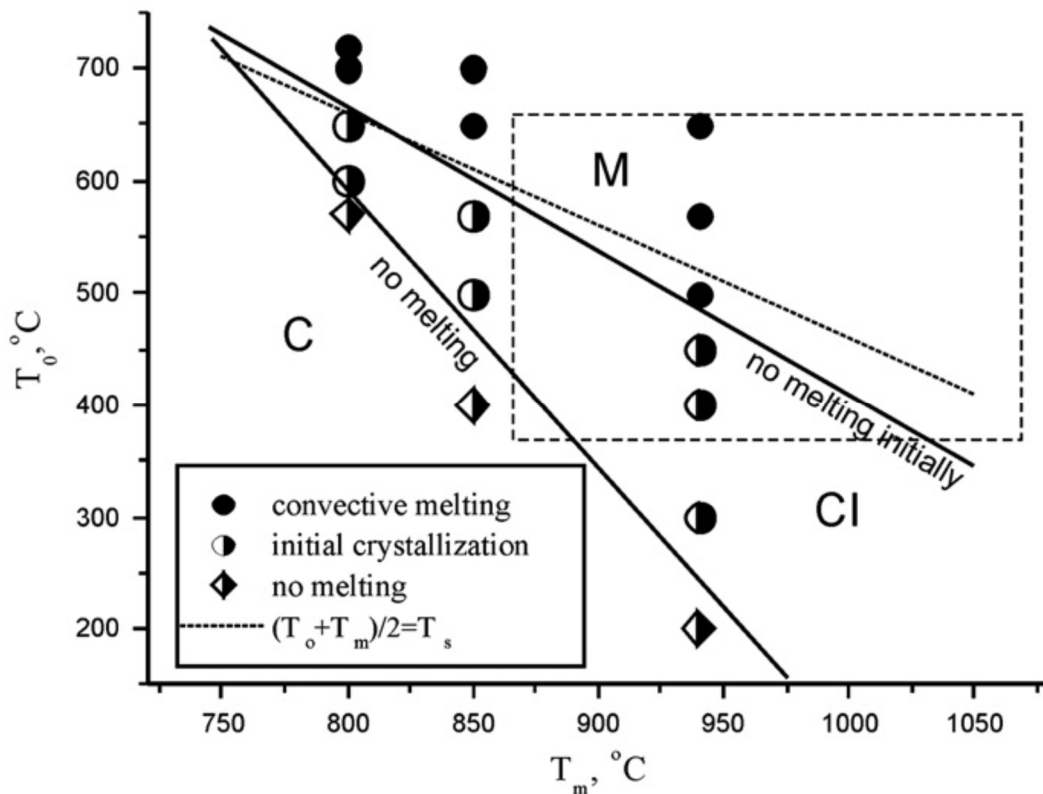

Fig. 5.1.1.1. Dynamic diagram of melting regimes for rhyolite magma with 4 wt.% H_2O in coordinates melt ($T_m^o C$) and surrounding rocks ($T_0^o C$) temperatures. Regimes: C- crystallization, CI – initial crystallization following by melting, M – melting. Dotted line theoretical boundary of the conductive melting regime (T_0+T_m)=T_s (solidus temperature).

On the dynamic diagram crystallization, initial crystallization followed by the roof melting and roof melting fields are defined. It follows that superheated in the contact with basalts rhyolitic magma will assimilate country rocks with temperatures as low as 400-500°C. The most important result consists in the evaluation of the melting front propagation rate (Fig. 5.1.1.2).
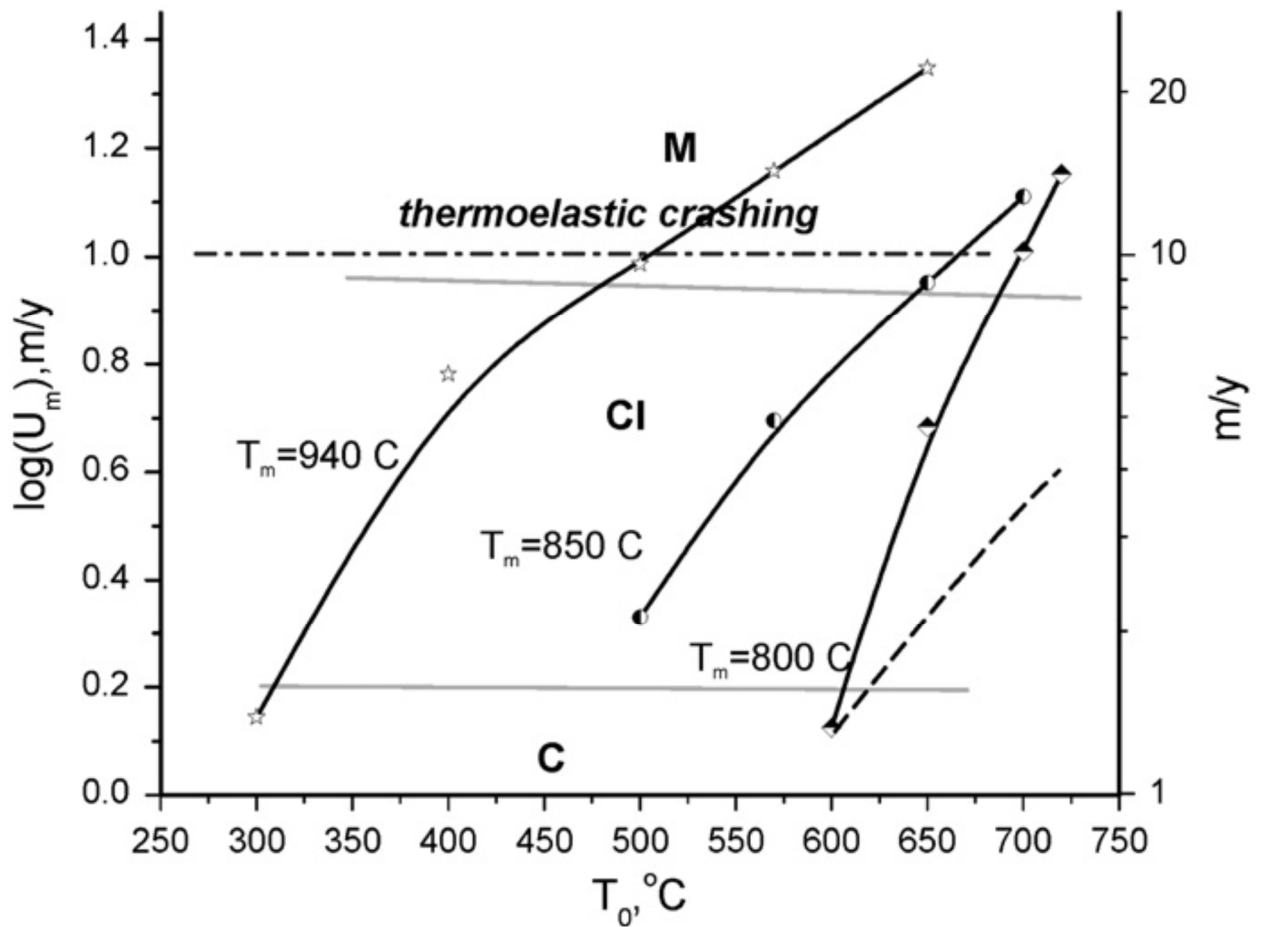
Fig. 5.1.1.2. Initial melting linear rates (Um) for different rock and magma temperatures (indicated at the bottom of the correspondent curves). Strong accelerating two-phase effect (magma + crystals) is observed only for the low temperature magma and hot surrounding rocks (dashed line correspond to the trend of Um for descending plumes with negligibly low crystal content)

It follows that melting proceeds with really high rates of several meters per year. We expect thermoelastic failure at the melting front to occur at the melting rates above approximately 10 m/yr. These calculations explain quite short time of high silica rhyolites formation in the siliceous pyroclastics underplated by basalts in Iceland discovered at the drilling during hydrothermal exploration (). These estimates implies also that formation of the large volumes of the rhyolites required for the super-eruptions with volume 1000-3000 km^3 can take geologically short time and is constrained only by the basaltic magma supply rate.

Our results demonstrates that convection is intensive enough to thoroughly mix rhyolite and melted roof. Effective mixing is provided by the chaotic nature of plume convection (Fig. 5.1.1.3). Heads of the descending from the roof plumes rotate, simple shear with rotational component occurs in the plume tail. Thus the liquid particles chaotically travel in the set of the closely packed swirls several meters diameter rotated in opposite directions that topologically resembles mixing in the turbulent flow.

166
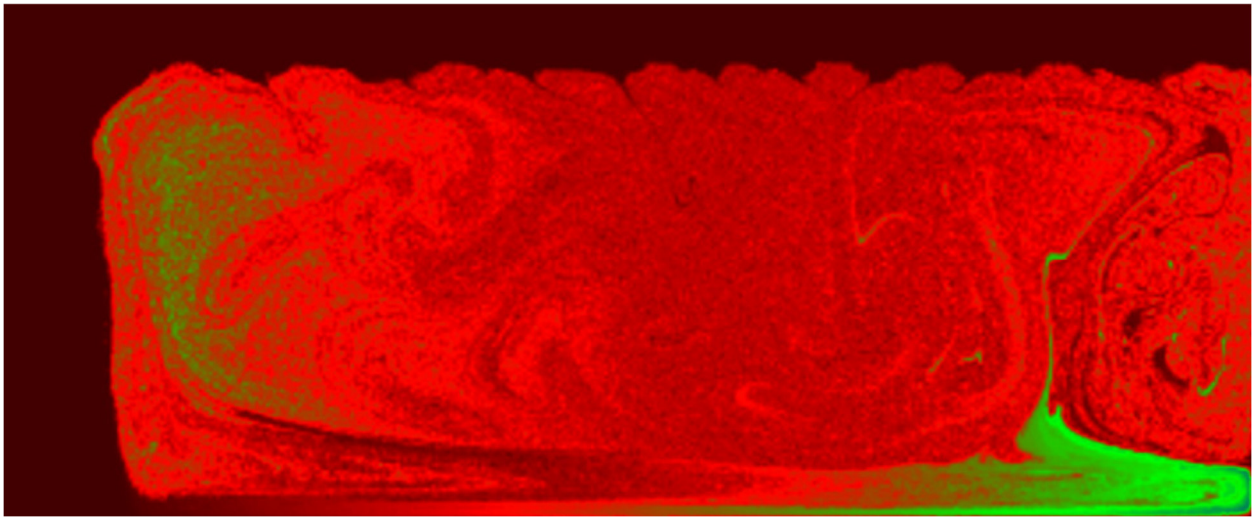
Fig. 5.1.1.3. Distribution of horizontal displacements δX(x,y) of the 5 × 5 cm averaged markers after 5 days of convective melting in the rhyolitic magma chamber Image is 25 × 50 m and color scale signifies the magnitude of horizontal displacement in meters. Brown color corresponds to the surrounding unmelted (static) rocks, static condition, δX(x,y) = 0; green stripes correspond to the maximum relative horizontal displacement of markers.

We calculate the size distribution of the inclusions of melted roof within superheated rhyolite characterized by the mean length 4-6 cm close to the field observations of the granodiorite inclusions in granites (). The current velocity resolution permits modeling of the splitting in the flow of the small inclusions only with negligible yielding stress.

Simakin, A. G., & Bindeman, I. N. (2012). Remelting in caldera and rift environments and the genesis of hot, "recycled" rhyolites. Earth and Planetary Science Letters, 337–338, 224-235. Doi: http://dx.doi.org/10.1016/j.epsl.2012.04.011

Bindeman, I. N., & Simakin, A. G. (2014) Rhyolites—Hard to produce, but easy to recycle and sequester: Integrating microgeochemical observations and numerical models. Geosphere, *10(5), 930-957. Doi: 10.1130/GES00969.1*

5.1.2. Am☐hib☐☐g☐-b☐r☐m☐t☐r d☐v☐☐☐m☐nt

Simakin A.G., simakin@iem.ac.ru, *Institute of Experimental Mineralogy RAS, Chernogolovka, 142432, Russia. Physics of the Earth RAS, Moscow, D-242, Russia, 123995*
Zakrevskaya O., Salova T., Gordeychik B., gordei@mail.ru, *Institute of Experimental Mineralogy RAS, Chernogolovka, 142432, Russia*
Churikova T., tchurikova@mail.ru**.** *Institute of Volcanology and Seismology, Far East Division, Russian Academy of Sciences, Petropavlovsk-Kamchatsky, 683006, Russia*

Amphibole with quite complex crystallo-chemistry still lacks quantitative thermodynamic model. Nevertheless numerous empirical mono-mineral amphibole geobarometers were proposed for the last decades. In these models correlation of the total aluminum content of the experimental amphiboles and pressure was mainly used in calibration. Only in the most recent barometer proposed by Ridolfi (2012) full composition regression with pressure was performed. Our model is based on our own experimental data on the amphibole crystallization from high magnesium andesites of Shiveluch at 2-5 kbar and published data for the higher pressures. We find that the most equilibrated amphibole forms at the low undercoolings. Kinetic effects and disequilibrium fractionation strongly affect amph composition at the undercoolings above 20-30°C while reequilibration eliminating disequilibrium features is usually incomplete in the experiments with several hours-days duration.

Octahedral aluminum (Al^6) content in the melt increases with rise of pressure and Mg^{2+} content. Through the portioning of Al^6 between melt and crystal amphibole composition reflects pressure variations. Low magnesium dacitic and rhyolitic magmas contain very few Al^6 therefore mono-amphible barometer and construction of an accurate mono-mineral barometer is only possible for the constrained magma composition range. Our calibration accounts for the preferable occupation of M2 position in amphibole by the high charge cations Al^{3+}, Ti^{4+}, Fe^{3+} along with Mg^{2+} and Fe^{2+}. Octahedral aluminum competes with essentially Fe^{3+} for M2 position so that in the oxidized environment Fe^{3+} prevails with maximum content approaching 2 apfu (really 18-1.9 apfu). To exclude influence of fO_2 on the Al^6 content in amphibole we use linear regression $Al^6(Fe^{3+}+Ti)$ for given amphibole compositions set to estimate ideal maximum Al^6 content at $Fe^{3+}+Ti=0$. This maximum Al^6 is linked with pressure for the basic to andesite-basalt magmas. Liquidus temperature of the amph in the basic magmas is higher (950-1100°C) than in the more silicious ones (750-850°C) and some researcher link spikes of Al in the zoned amph with heating episodes.

Currently barometer of Ridolfi is widely used in volcanologic applications, however, its accuracy is overestimated by the author. We make independent test on the geologic objects where numerous independent estimates of the pressure exit.
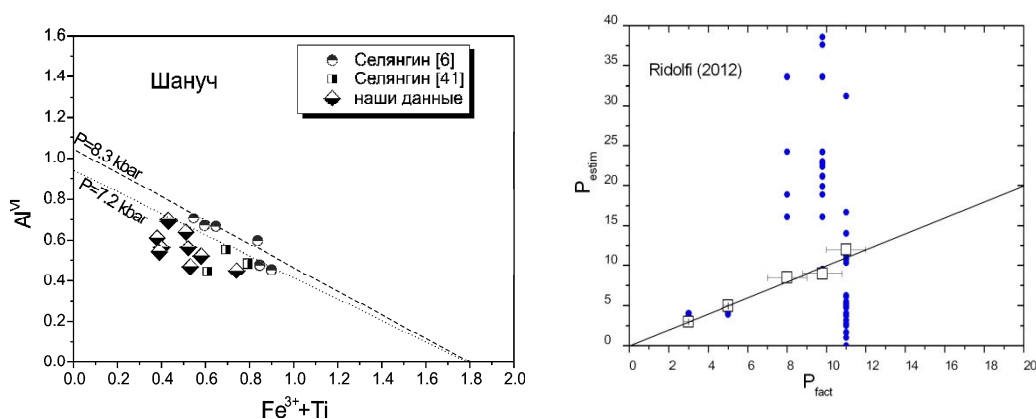
Fig. 5.1.2.1. Comparison of barometers a) an example of application of our barometer to the amphiboles from cartlandite intrusion Shanuch (Kamchatka) b) filled circles results of application of Ridolfi (2012) barometer to the different objects, P_{fact}=3 and 5 kbar corresponds to our runs conditons, for values see text. Error bars reflects uncertainty of P_{fact}, squares are our estimates.

Our experimental data obtained at P=3 and 5 kbar are reproduced more or less well while high pressure magmatic amphiboles compositions are treated unsatisfactorily with large systematic error and extremely wide spread. For testing we use amphiboles from kortlandites Central Ridge, Kamchatka (P=8 kbar), basaltic xenoliths from Dish Hill, California (P=9.8 kbar) and Pikulney ultrabasic-basic complex (P=11 kbar). Fig. 5.1.2.1a illustrates application of our barometer to the magmatic amphiboles of Ni-bearing Shanuch kortlandite intrusion. Composition of the amphibole is recalculated into the cations distribution by positions in accordance with IMA-1997 classification scheme. Indicating regression lines are drawn through the upper points of the sets of analysis and extreme point ($Fe^{3+}+Ti$ =1.8; Al^6=0), asymptotic values of Al^6 are read at the intersections with ordinate axis. Those values give estimates of pressure.

We apply our novel geobarometer to Shiveluch amphiboles. An example of application to basalts from the center located at the western slope of Old Shiveluch caldera (Gorbach center) is in Fig. 5.1.2.2.
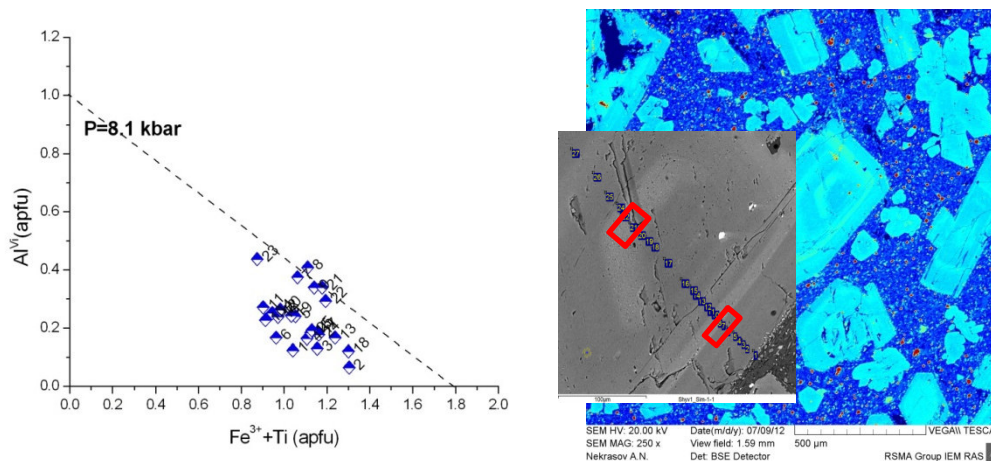
Fig. 5.1.2.2. Amphibole from the basaltic center on the western flank of Shiveluch (Kamchatka).

The indicating line (P=8 kbar) is drawn through the high T compositions near the recovered dissolution-decomposition surface in the center of the zoned crystal. Other parts of crystals were grown from the more silicious magma depleted in MgO. While using all available published and our data on amphiboles from Shiveluch we get histogram with peaks at P=2.6 and 5.8 kbar. The high pressures are grouped around 9.8 kbar (with the highest P=11 kbar). These three values mark preferable levels of magma accumulation (near surface, mid-crustal and near Moho depths).

Simakin, A., Zakrevskaya, O., & Salova, T. (2012) Novel aphibole geo-barometer with application to mafic xenoliths. Earth Science Research, 1(2), 82-97. Doi:10.5539/esr

Simakin, A., Salova, T., Gordeychik, B., & Chyurikova, T. (2013) Shiveluch volcano: mineralogical records of geodynamic complexity. Mineralogical Magazine, 77(5), 2213. (Abstract of Goldschmidt Conference, 2013 August 25-30 Florence, Italy). Doi:10.1180/minmag.2013.077.5.19

5.1.3. Experimental study of melt and fluid inclusions and development of new methods for deciphering P-T-X conditions of fluid-rich magmatic processes

Smirnov S.Z., ssmr@igm.nsc.ru, **Tomas V.G., Kupriyanov I.N.,** *Institute of Geology and Mineralogy, Siberian Branch of the Russian Academy of Sciences, pr. Akademika Koptyuga 3, Novosibirsk, 630090, Russia*
Sokolova E.N., *Novosibirsk State University, ul. Pirogova 2, Novosibirsk, 630090, Russia*

The paper is devoted to the experimental study of the leak-tightness of water-containing melt inclusions heated in the autoclave at high temperature and under the pressure of D_2O. Quartz-hosted silicate-melt inclusions from the rhyolite tuffs of the Taupo volcanic zone (New Zealand) and a tourmaline-pegmatite vein from the SW Pamirs were heated at 650 degrees C and 3 kbar. The penetration of heavy water into the inclusions was controlled by IR spectroscopy. The studies have demonstrated that the inclusions can remain leak-tight under these conditions and not exchange water with the environment even if the confining pressure is 1.5-3 times above their internal pressure. The influence of water diffusion through the quartz lattice and dislocations on the leak-tightness can be neglected in the thermometry of water-containing melt inclusions. The crucial factors determining the water exchange between the inclusions and the environment in the experiments performed are mechanical defects (open and healed cracks). Using D_2O as a pressurizing medium makes it possible to control the leak-tightness of the heated inclusions. To

do this, it is recommended that melt inclusions be homogenized under the pressure of D_2O above the expected entrapment pressure and studied by IR spectroscopy after the heating.

Smirnov, S. Z., Tomas, V. G., Sokolova, E. N., & Kupriyanov, I. N. (2011). Experimental study of the leak-tightness of water-containing silicate-melt inclusions under the pressure of D_2O at 650 °C and 3 kbar. Russian Geology and Geophysics, 52(5), 537-547. Doi: http://dx.doi.org/10.1016/j.rgg.2011.04.006

5.1.4. Major element distribution in system basic-ultrabasic melt

Ponomaryov G.P., ponomarev@kscnet.ru, **Puzankov M.Yu.,** puzankov@kscnet.ru, *Institute of Volcanology and Seismology, Far East Division, Russian Academy of Sciences, Petropavlovsk-Kamchatsky, 683006, Russia*

This research shows the results of two interrelated lines in scientifi c investigation. 600 equations based on experimental data ≪INFOREX≫ resulted from the first line of scientific investigation. These equations allow calculating concentration of elements in melt, values of temperature and pressure estimating equilibrium of phases and melts. Many of them are unique and the analogous equations used by petrologists have worse statistical characteristics. The second line of the scientific investigation specifies and generalizes genetic peculiarities of bodies and massifs, composed of rocks of basite-hyperbasite series with different facial, formational and geodynamic characteristics by means of the obtained equations.

Among the results the most essential are re-equilibration of compositions of spinel–olivine associations in effusive rocks with basic-ultrabasic composition, except for paragenesis in basalts from the rift valley of the Mid-Ocean Ridge; limited depth of crystallization (not less than 15 kb, 40–45 km) of most magmas with basic-ultrabasic composition; characteristics of Ca behavior in olivine; non-magmatic genesis of diamantes from kimberlites.

A special attention was paid to the revealed patterns of calcium content in olivine crystals in the system "mafic-ultramafic melt–olivine" within a wide range of conditions, which are represented by 3 facial variations according to depths of formation. These patterns were revealed using processed experimental data from "INFOREX" database. The author separates two groups of parameters in the "melt–olivine" system, which are responsible for decrease or increase of calcium content in olivine. As appear during experiments low-calcium olivine is caused first of all by low calcium content in the melt regardless of the pressure and temperature. These data, in a view of patterns, obtained from experimental melts allow suggest that olivine crystals lost in certain cases initial calcium or they had not magmatic origin. Low-calcium olivines that represent all generations of this mineral in kimberlites give evidence for non-melt genesis of diamonds delivered by kimberlite magmas.

Ponomaryov, G. P., Puzankov. M. Yu., (2012) Distributions of rock forming elements in system basic-ultrabasic melt between melt and spinel, olivine, orthopyroxene, clinopyroxene, plagioclase. Geological application. Moscow, Petropavlovsk-Kamchatsky, Institute of Volcanology and Seismology, 668 p. (In Russian). http://www.kscnet.ru/ivs/bibl/sotrudn/puz/rpel.pdf

Ponomaryov G. P., (2014) The calcium content in olivine crystals grown from experimental melts. Part 1. Litosphere, 4, 66-79. (In Russian). http://www.lithosphere.igg.uran.ru/pdf/16819004_2014_4/16819004_2014_4_066-079.pdf

Ponomaryov G. P., (2014) Calcium content in crystals of natural olivine as a marker of their genesis. Part 2. Litosphere, 5, 57-70. (In Russian). http://www.lithosphere.igg.uran.ru/pdf/16819004_2014_5/16819004_2014_5_057-070.pdf

5.2. Geophysical Evidences

5.2.1. High-Frequency Radiation from an Earthquake Fault

Gusev A.A., gusev@emsd.ru, *Institute of Volcanology and Seismology, Far East Division, Russian Academy of Sciences, Petropavlovsk-Kamchatsky, 683006, Russia. Kamchatka Branch, Geophysical Service, Russian Ac. Sci 9 Piip Blvd., 683006 Petropavlovsk-Kamchatsky, Russia*
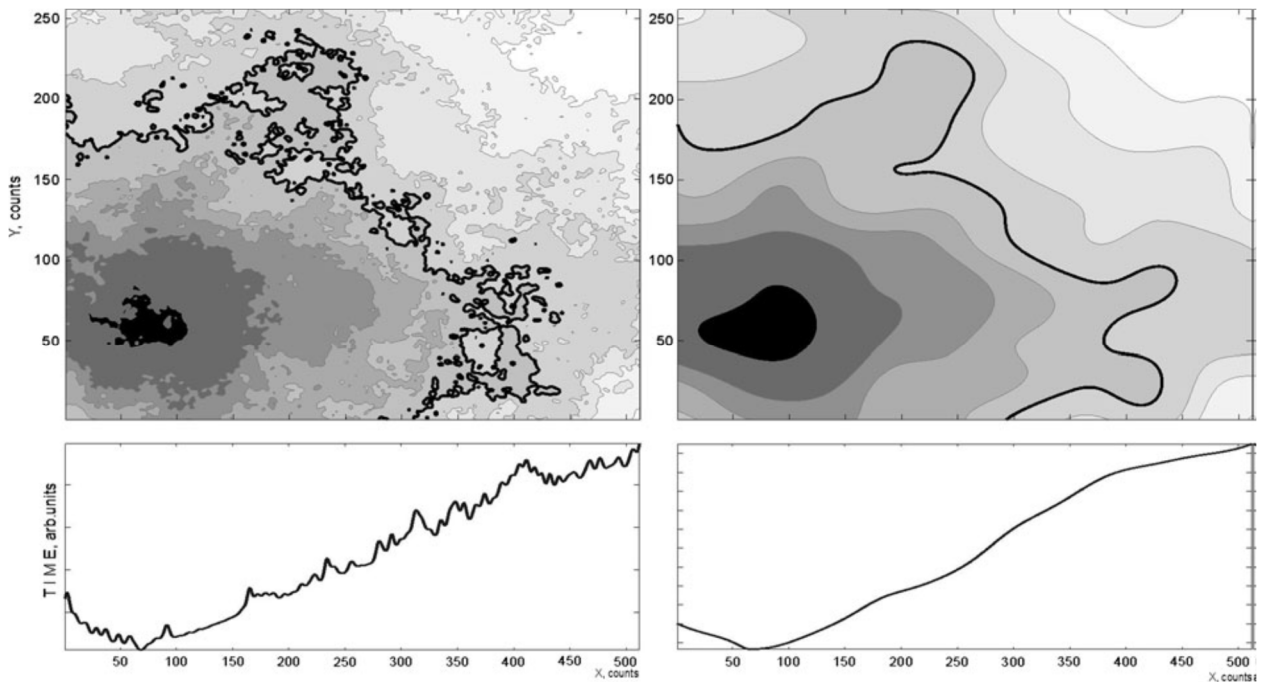
Fig. 5.2.1.1. Fault maps depicting hypothetic rupture evolution represented as a sequence of fractal isolines that show instant positions of the rupture front (top left). Black spot encircles the hypocenter; shades of grey represent time (the lighter, the later). The black line, tortuous and multiply connected, depicts a particular example instant position of the hypothetic rupture front; its timing is arbitrary and was selected to provide graphical clarity. At the top right, the smoothed variant of the same map is shown. Under the maps, corresponding plots for the arrival time of the rupture front are plotted for the line y = 60. Note non-monotonous dependence of onset time versus distance for the unsmoothed map; it is this non-monotonous behavior that generates random phases of contributions of fault spots at a receiver, creating incoherence

Observed high-frequency (HF) radiation from earthquake faults exhibits specific properties that cannot be deduced or extrapolated from low-frequency fault behavior. In particular: (1) HF time functions look like random signals, with smooth mean spectrum and moderately heavy-tailed probability distribution function for amplitudes; (2) well-known directivity of low-frequency radiation related to rupture propagation is strongly reduced at HF, suggesting incoherent (delta-correlated) behavior of the HF radiator, and contradicting the usual picture of a rupture front as a regular, non-fractal moving line; (3) in the spectral domain, HF radiation occupies a certain specific band seen as a plateau on acceleration source spectra $K(f) = f^2 M_0(f)$. The lower cutoff frequency f_b of $K(f)$ spectra is often located significantly higher than the common spectral corner frequency f_c, or f_a. In many cases, empirical $f_b(M_0)$ trends are significantly slower as compared to the simple $f_b \propto M_0^{-1/3}$, testifying the lack of similarity in spectral shapes; (4) evidence is accumulating in support of the reality of the upper cutoff frequency of $K(f)$: fault-controlled f_{max}, or f_{uf}. However, its identification is often hampered by such problems as: (a) strong interference between f_{uf} and site-controlled f_{max}; (b) possible location of f_{uf} above the observable spectral range; and (c) substantial deviations of individual source spectra from the ideal spectral shape; (5)

intrinsic structure of random-like HF radiation has been shown to bear significant self-similar (fractal) features. A HF signal can be represented as a product of a random HF ''carrier signal'' with constant mean square amplitude, and a positive modulation function, again random, that represents a signal envelope. It is this modulation function that shows approximately fractal behavior. This kind of behavior was revealed over a broad range of time scales, from 1 to 300 s from teleseismic data and from 0.04 to 30 s from near-fault accelerogram data. To explain in a qualitative way many of these features, it is proposed that rupture propagation can be visualized as occurring, simultaneously, at two different space–time scales. At a macro-scale (i.e. at a low resolution view), one can safely believe in the reality of a singly connected rupture with a front as a smooth line, like a crack tip, that propagates in a locally unilateral way. At a micro-scale, the rupture front is tortuous and disjoint, and can be visualized as a multiply connected fractal ''line'' or polyline. It propagates, locally, in random directions, and is governed by stochastic regularities, including fractal time structure. The two scales and styles are separated by a certain characteristic time, of the order of (0.07–0.15) x rupture duration. The domain of fractal behavior spans a certain HF frequency range; its boundaries, related to the lower and upper fractal limits, are believed to be manifested as f_b and f_{uf} (Fig. 5.2.1.1).

Gusev, A. A. (2013). High-Frequency Radiation from an Earthquake Fault: A Review and a Hypothesis of Fractal Rupture Front Geometry. Pure and Applied Geophysics, 170(1-2), 65-93. Doi: 10.1007/s00024-012-0455-y

5.2.2. A fractal earthquake source with a slip zone

Gusev A.A., gusev@emsd.ru, *Institute of Volcanology and Seismology, Far East Division, Russian Academy of Sciences, Petropavlovsk-Kamchatsky, 683006, Russia. Kamchatka Branch, Geophysical Service, Russian Ac. Sci 9 Piip Blvd., 683006 Petropavlovsk-Kamchatsky, Russia*
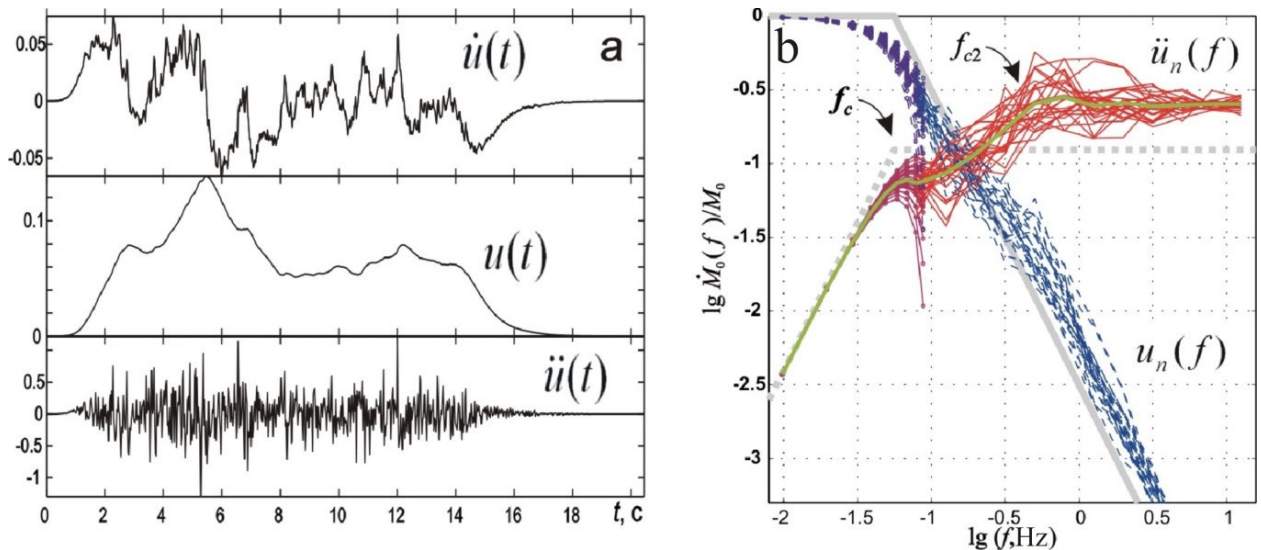
Fig. 5.2.2.1. Examples of simulation. (a) Examples of signal of velocity, displacement and acceleration ($\dot{u}(t)$, $u(t)$ и $\ddot{u}(t)$) of S-waves at the receiver. (b) Spectra $\ddot{u}_n(f)$ (solid) and $u_n(f)$ (dashes), initial and smoothed. The thick line is the geometrical average of $\ddot{u}_n(f)$ over 25 random tries. Gray lines are idealized spectra for the ω^{-2} model.

An important problem of the studies of earthquake sources is to clarify the mechanism of formation of radiated source spectra of the ω–2 ("omega-square") kind, or equivalently, of flat acceleration spectra. This spectral model is well established empirically and has the status of a classical one in source seismology; however, it lacks adequate theoretical foundation. It is shown

that spectra of the ω^{-2} kind can be explained by combining the following three concepts regarding source rupture: (1) the fault asperity model of Das-Kostrov; (2) the Andrews's concept that the field of the stress drop over the fault is a 2D flicker-noise with amplitude spectrum of the 1/k type; and (3) the hypothesis that the distance of propagation of Rayleigh waves from a failing spot on a fault is determined by the width of the slip zone associated with the rupture front (Fig. 5.2.2.1).

Gusev, A. A. (2013). A fractal earthquake source with a slip zone generates acceleration time histories with flat spectra. Doklady Earth Sciences, 448(2), 211-213. Doi: 10.1134/S1028334X13020049

5.2.3. Statistics of the normalized values of the shifts in points of the fault-earthquake

Gusev A.A., gusev@emsd.ru, *Institute of Volcanology and Seismology, Far East Division, Russian Academy of Sciences, Petropavlovsk-Kamchatsky, 683006, Russia. Kamchatka Branch, Geophysical Service, Russian Ac. Sci 9 Piip Blvd., 683006 Petropavlovsk-Kamchatsky, Russia*
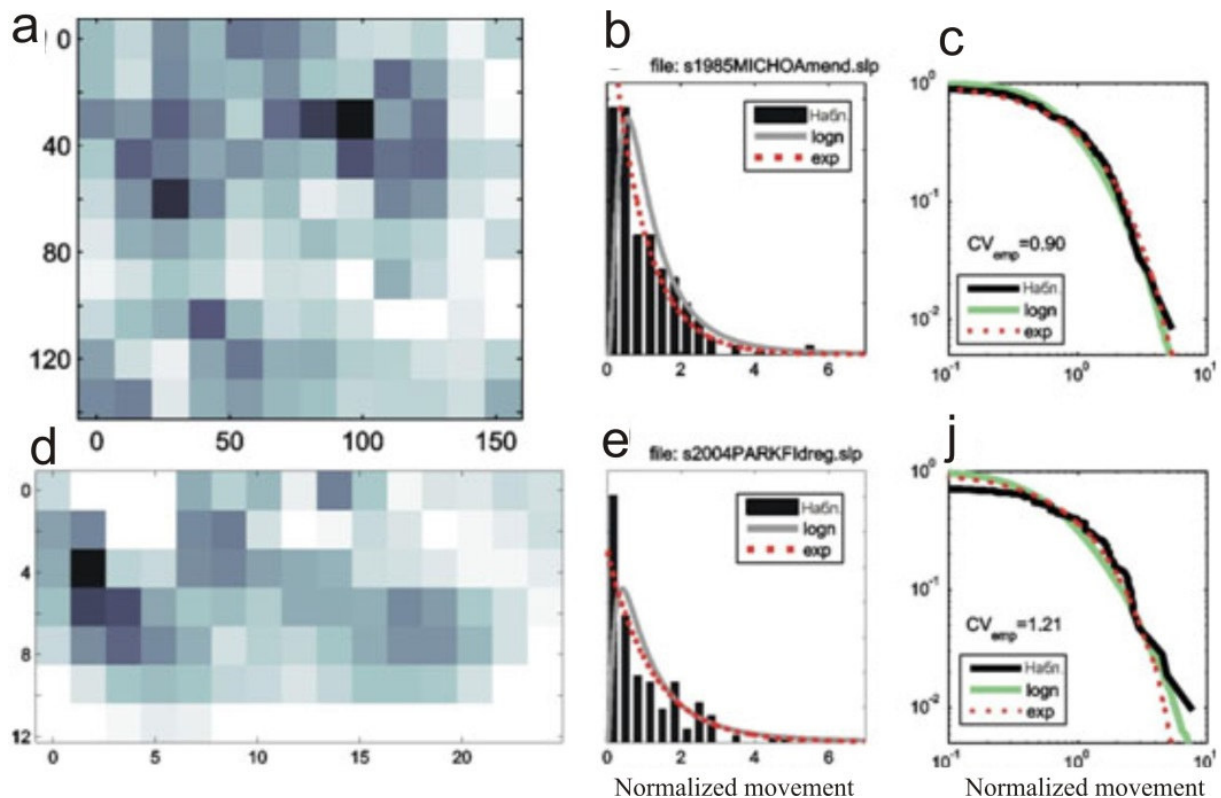
In order to develop a statistical description for the values of a final slip (dislocation) in different points of an area of an earthquake source fault, we analyzed the recently compiled collection extended-fault descriptions, obtained by solution of the corresponding inverse problem. The probability distribution function was studied for the normalized average slip in a subfault (an element of a large fault). Each large fault yielded by an individual inversion was normalized by division of the slip value in a subfault to the mean value averaged across the subfaults of a given fault. The processing included the following steps: informal rejection of less reliable inversions, normalization, and construction of empirical distribution functions for individual earthquakes and for the pooled sample. We estimated the parameters of the empirical functions and approximated them by simple standard distribution laws. The statistical structure of the values of the slip is found to be rather stable. The individual empirical samples have the coefficient of variation 0.98 ± 0.28 and, generally, resemble those with the exponential distribution law. The upper tail of the

distribution rather sharply tapers off, following, on average, the power law with the exponent α being approximately from −3.5 to −4. The composite distribution has a noticeable atom at zero with a weight of about 10%. The presence of this atom impedes approximation of the observed distribution by a simple law. We proposed a reasonable approximation by a modified lognormal law; the modification includes shifting to the left and winsorization at zero. The appearance of the atom at zero is possibly due to the unbreakable barriers at propagation of a rupture; at the same time, we cannot rule out the possibility for it to be an artifact generated by the procedure of inversion. Our results provide good grounds for practical simulations of the scenario earthquakes; they also are of interest for the physics of the earthquake source.

Fig. 5.2.3.1. The examples of the individual maps of movement and their distribution functions. a – the movement distribution in the earthquake source of Michoacan 1985 earthquake; the density of gray color show the value of the movement, white color corresponds to zero movement. The abscissa is the distance along the strike (km), the ordinate is the same for the drop; b and c – histograms and additional cumulate function of distribution for the normal movement in comparison with two modelled distributions; e, f, g – the similar graphs for the Parkfield 2004 earthquake.

Gusev, A. A. (2011). Statistics of the values of a normalized slip in the points of an earthquake fault. Izvestiya, Physics of the Solid Earth, 47(3), 176-185. Doi: 10.1134/S1069351310101015

5.2.4. The electrical conductivity of the lithosphere in the subduction zone

Moroz Yu.F., morozyf@kscnet.ru, **Moroz T.A.,** *Institute of Volcanology and Seismology, Far East Division, Russian Academy of Sciences, Petropavlovsk-Kamchatsky, 683006, Russia*
Smirnov S.E., *Institute of space physics and radio wave propagation, Far East Division, Russian Academy of Sciences, Paratunka, Kamchatka region, Russia*
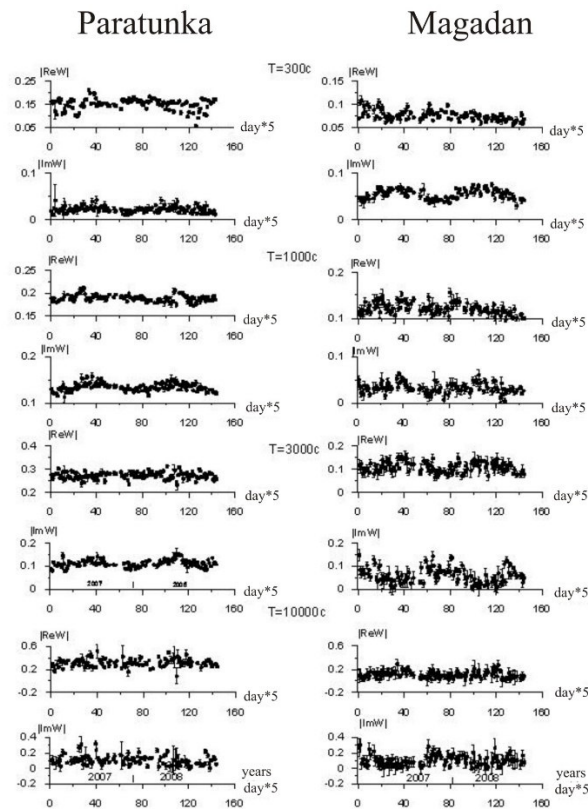
Fig. 5.2.4.1. The time series of the real and imaginary parts of tipper at periods of 300, 1000, 3000, and 10000 s.

Using electromagnetic monitoring data it was established that the electrical conductivity of the lithosphere in the subduction zone changes in time over the year period. These changes mostly occur in crustal conductive layer. Annual variation of the electrical conductivity of the lithosphere can be caused by turning of the Earth around the Sun, which is manifested by the annual cycles in the fracturing of the lithosphere, the degree of saturation of the hydrothermal fluids and the degree of tier mineralization. This result is important for geodynamics and volcanology when studying processes associated with earthquakes and volcanic eruptions (Fig. 5.2.4.1).

Moroz, Y. F., Moroz, T. A., & Smirnov, S. E. (2011). Results of monitoring the geomagnetic variations at the Magadan and Paratunka observatories. Izvestiya, Physics of the Solid Earth, 47(8), 698-710. Doi: 10.1134/S1069351311070068

5.2.5. The relationship between electrical conductivity of the lithosphere and earthquake

Moroz Yu.F., morozyf@kscnet.ru, **Moroz T.A.,** *Institute of Volcanology and Seismology, Far East Division, Russian Academy of Sciences, Petropavlovsk-Kamchatsky, 683006, Russia*

The data of long-term electromagnetic monitoring are used for studying the dynamics of electric conductivity of the medium and the electric field of the terrestrial sources. The electric conductivity of the medium is estimated from the magnetotelluric transfer functions (impedance tensor and telluric tensor). The electric field of terrestrial sources is identified by filtering the variations of the observed electric field of the Earth. The magnetotelluric parameters and the electric field of terrestrial sources feature anomalous changes of supposedly earthquake-related origin. The anomalies associated with the same earthquake are not simultaneous. It is shown that these anomalies are generated by processes occurring at different depths. The strong earthquake is preceded by the appearance of surface anomalies several months before the event and accompanied by a deep coseismic anomaly. The probable nature of the recognized anomalies is discussed.
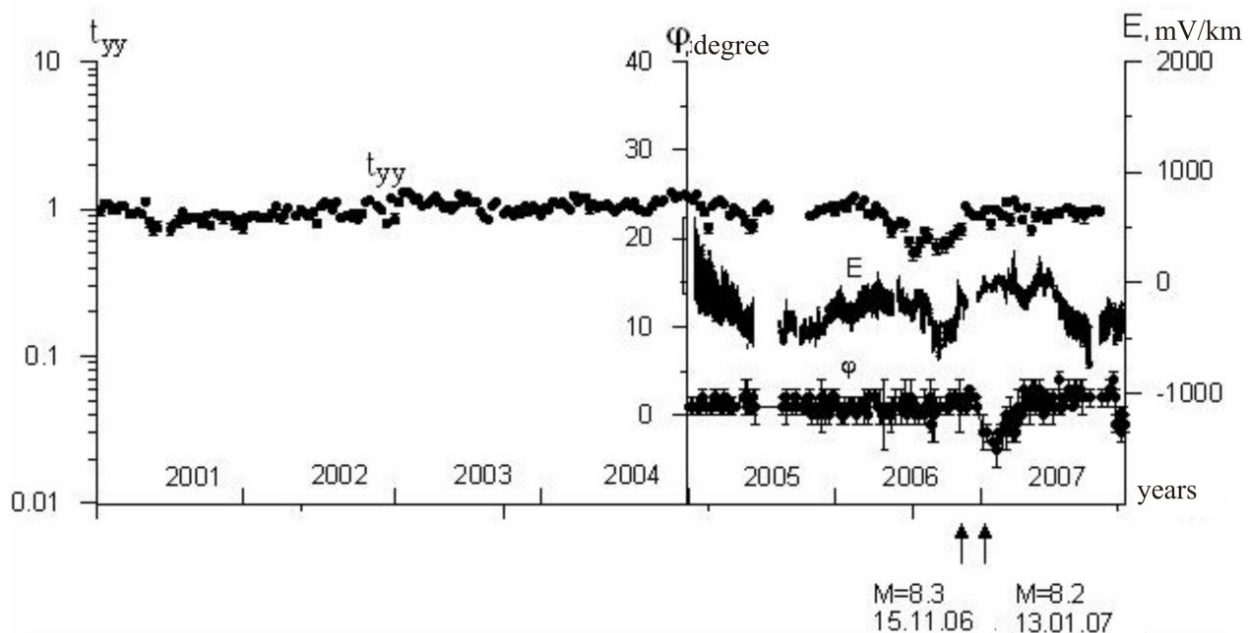

Fig. 5.2.5.1. The comparison of the impedance phase (ϕ_{yy}), the intensity of the electric field (E), and the modulus of the telluric tensor component (t_{yy}). The occurrence time, the magnitudes, and the dates of the strong earthquakes are shown by the arrows on the time axis.

Moroz, Y. F., & Moroz, T. A. (2012). Correlation of the anomalies in the electric field and electric conductivity of the lithosphere to earthquakes in Kamchatka. Izvestiya, Physics of the Solid Earth, 48(4), 287-296. Doi: 10.1134/S1069351312010090

5.2.6. Geophysical monitoring of stress-strain state of the geological environment

Gavrilov V.A., vgavr@kscnet.ru, **Morozova Yu.V.,** morozova@kscnet.ru, *Institute of Volcanology and Seismology, FEB RAS, Petropavlovsk-Kamchatsky, Russia*
Panteleev I.A., *Institute of Continuous Media Mechanics, UrB RAS, Perm, Russia*
Ryabinin G.V., *Kamchatka Branch of Geophysical Survey of RAS, Petropavlovsk-Kamchatsky, Russia*
Bogomolov L.M., *Institute of marine geology and Geophysics, FEB RAS, Yuzhno-Sakhalinsk, Russia*
Zakupin A.S., *Sientific station RAS, Beshkek city, Russia*

This work presents the results of studies of a physical basis of modulating effects of continuous exposure to electromagnetic radiation on intensity of geoacoustic processes in real geological media. The study is based on data from long-term borehole geoacoustic, electromagnetic, hydrogeochemical and hydrogeodynamic measurements performed in the Petropavlovsk-Kamchatsky geodynamic polygon. The authors have analyzed the physical reasons for the high correlation of the RMS signals of geoacoustic emission and external electromagnetic radiation at intervals of background seismicity and investigated the physical mechanism of the effect of degradation of geoacoustic emission response to the electromagnetic effects observed at the time of relatively close strong earthquakes.
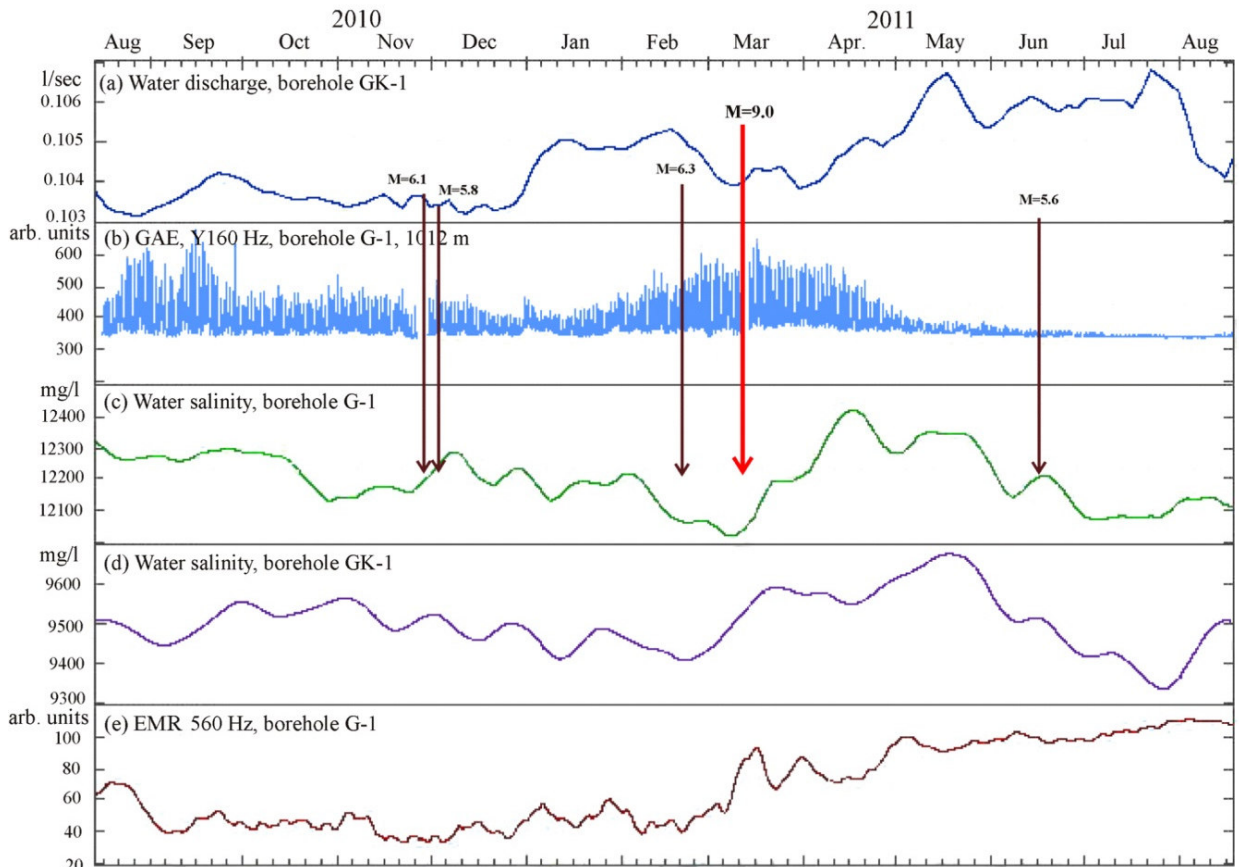

Fig. 5.2.6.1. Results of complex borehole measurements in time vicinity of the Tohoku mega-earthquake: (a) – water outflow of Borehole GK-1, averaging interval – 14 days; (b) – RMS of GAE at 1012 m; (c) –

water mineralization of Borehole G-1, averaging interval – 14 days; (d) – water mineralization of Borehole GK-1, averaging interval – 14 days; (e) – level of background EMR, averaging interval – 20 days. Dark arrows point at earthquakes of $MLH \geq 5.5$ in the zone of $R \leq 550$ km.

The nature of GAE response to external EMR in fluidsaturated geological media is defined by the values of density of the summed current, changing the values of DEL charges on the borders of fluid and solid phases. Generally a density of the summed current is a sum of three vector values – density of conductivity current, density of diffusive current and density of current of electro-kinetic nature. Regularities of changes of summed current are considerably connected with a stress-strain state of the geological media.

For seismically quiet periods changes of intensity of geoacoustic processes are directly connected with changes of intensity of external electric field and conductivity of rocks around a borehole (Fig. 5.2.6.1). It explains the physical reasons of high correlation of RMS values of GAE and EMR on such time intervals. Conductivity of rocks thus acts as the parameter defining geoacoustic sensitivity of the geological media to influence of external electric field.

Effect of degradation of GAE response to the influence of EMR in time vicinity of relatively close strong earthquakes is related to decrease in conductivity and porosity of rocks around a borehole at a stage of compressive stress.

At a stage of dilatancy increase of the volume of rocks surrounding a borehole, a significant increase of amplitudes of GAE response to external electromagnetic influence takes place. The physical reasons of the specified effect are connected with abrupt increase of a gradient of capacity of the current, increase in porosity of the geological media, growth of fluid saturation and increase in specific conductivity of rock, characteristic for the specified stage of stress-strain state of the geological media.

Gavrilov, V.A., Panteleev, I.A., Ryabinin, G.V., & Morozova, Yu.V. (2013) Modulating impact of electromagnetic radiation on geoacoustic emission of rocks. Russian journal of Earth sciences, 13(1): ES1002, 1-16. Doi: 10.2205/2013ES000527

Gavrilov, V. A., Bogomolov, L. M., & Zakupin, A. S. (2011). Comparison of the geoacoustic measurements in boreholes with the data of laboratory and in-situ experiments on electromagnetic excitation of rocks. Izvestiya, Physics of the Solid Earth, 47(11), 1009-1019. Doi: 10.1134/S1069351311100041

5.2.7. The long-term earthquake forecast for the Kuril-Kamchatka arc

Fedotov S.A., karetn@list.ru, *Institute of Volcanology and Seismology, Far East Division, Russian Academy of Sciences, Petropavlovsk-Kamchatsky, 683006, Russia. Institute of Physics of Earth, Russian Academy of Sciences, Moscow, 123995, Russia*
Solomatin A.V., alf55@mail.ru, **Chernyshev S.D.,** chernsd@gmail.com, *Institute of Volcanology and Seismology, Far East Division, Russian Academy of Sciences, Petropavlovsk-Kamchatsky, 683006, Russia*

More 40 years ago a number of essential regularities has been noted by S.A. Fedotov at research of the Kuril-Kamchatka seismogenic region seismicity. Major of them are «seismic gaps» and «seismic cycle» of the strongest earthquakes. In 1965-1968 the method of the long-term earthquake forecast for the Kuril-Kamchatka region and Northeast Japan on the basis these and some other regularities has been proposed by S.A. Fedotov [1]. This method is successfully applied till now.

The values of the seismic process parameters for previous 5 years in the most seismically active strip of the Kuril-Kamchatka seismogenic region (total length of 2100 km, width 100 km and depths of the hypocenters of 0-80 km) are the initial basis for the specified method long-term

earthquake forecasts. Now a number of values for 20 areas, comparable on the size with the strongest earthquakes areas, for the following fifth years is predicted:

the seismic cycle phase (I - the previous strongest earthquake aftershock period, II - the long stable seismic energy accumulation phase, III – the seismic activation before the following strongest earthquake);

the seismic gaps locations - areas in which a last strongest earthquake was more than 80 years ago;

the expected seismic activity A_{10} (the rationed number of the weak, $K_s=10$ or $M=3.6$, earthquakes);

the magnitude of the average magnitude earthquakes, which are expected with the probability equal to 0.8, 0.5, and 0.15;

the magnitude of the expected strongest earthquakes and the probability of the $M \geq 7.7$ earthquakes.

The D parameter (a released seismic energy rationed value) and A_{11} (a seismic activity defined on the basis of the average earthquakes with $K_s=11$ or $M=4.3$) are used together with the A_{10} parameter.

The seismic process has the complex, unstable character at the III phase. It is accompanied by the short-term quiescence periods. Nevertheless, the received for the extensive time and area intervals data show, that within the last 5-10 years of the seismic cycle the essential seismic process activation is observed. This fact is the basis for the seismic gaps danger definition. The III seismic cycle phase probability for the seismic gaps is proportional to $1-B = 1-P(A10)*P(D)*P(A11)$, where $P(A10)$, $P(D)$, and $P(A11)$ are the accidental appearance probabilities for the observable values A10, D, and A11 at the II (quiet) seismic cycle phase.

The earthquake forecasts are updated twice a year or more often. Their results are compared to the other methods forecasts data.

For the more than 40-year-old period of the method application the following strongest earthquakes have been successfully predicted: on Kuril islands (1969, 1973, 1978, 1994 and 2006), on Kamchatka (1971 and 1997). All these earthquakes filled the seismic gaps among the 2-3 most dangerous ones.

The last published forecast has been given in October, 2010. It has confirmed the earlier conclusions concerning the extremely high seismic danger for the Petropavlovsk-Kamchatskiy city.

From the method initial time it was applied also to the strongest earthquakes forecast in the Northeast Japan region. The place of the strongest earthquake 1968 near the island Honshu forecast was the first success of the method.

Afterwards the method was successfully used in 2004 at the retrospective Hokkaido 15.XI 2003, M=8.1 earthquake forecast, and in 2005 at construction of the long-term earthquake forecast for 2005-2010, when the extensive seismic gap near Honshu island has been detected (this gap was filled 11.III 2011 by the M = 9 catastrophic earthquake).

In connection with the earthquake 11.III 2011 ecological aftermath, when the atomic power station blocks in a province Fukushima (Japan) were damaged, it is necessary to notice, that in 1975-1976 under the director of Institute of Volcanology of S.A. Fedotov insisting the inadmissible dangerous building of an atomic power station near to Petropavlovsk-Kamchatsky has been stopped. The correctness of this decision is confirmed by the last long-term earthquake forecast. The important part of the long-term earthquake forecast method, concerning the probability of the strongest earthquakes foreshocks and aftershocks estimation - «the foreshocks and aftershocks scenario», was offered in 1994, and justified in practice. These estimations can be used at planning of the activity, concerning the seismic safety as directly ahead of the strongest earthquake - in the form of its short-term forecast, and after it - for the danger aftershock estimation at the rescue and restorative works.

This long-term earthquake forecast method can be used in other, similar on seismotectonic conditions, regions, and also for the long-term tsunami forecast.

The long-term earthquake forecasts data have been important as arguing for taking advance measures for seismic safety, seismic protection, and retrofitting. On their basis in 1986-2001 it were issued 6 of the USSR, RSFSR, and the Russian Federation Governmental Decisions and Orders. In 2006-2008 a number of the Commissions has been given by the Presidents of the Russian Federation V.V. Putin and D.A. Medvedev for purpose of enhancing the earthquake resistance of residential buildings, major facilities, life-support systems of the Kamchatsky Kray (Kamchatka area) and the Sakhalin area in 2009-2013. This works have begun in Petropavlovsk-Kamchatsky since October, 2010.

Fedotov, S. A., Solomatin, A. V., & Chernyshev, S. D. (2011). A long-term earthquake forecast for the Kuril-Kamchatka arc for the period from September 2010 to August 2015 and the reliability of previous forecasts, as well as their applications. Journal of Volcanology and Seismology, 5(2), 75-99. Doi: 10.1134/S0742046311020023
Fedotov, S. A., Solomatin, A. V., & Chernyshev, S. D. (2012). A long-term earthquake forecast for the Kuril-Kamchatka arc for the period from September 2011 to August 2016. The likely location, time, and evolution of the next great earthquake with M ≥ 7.7 in Kamchatka. Journal of Volcanology and Seismology, 6(2), 65-88. Doi: 10.1134/S0742046312020029

5.2.8. Investigations of the atmospheric electric field

Marapulets Yu.V., marpl@ikir.ru, **Larionov I.A., Mishchenko M.A.,** *Institute of Cosmophysical Research and Radiowave Propagation, Far East Branch, Russian Academy of Sciences, Kamchatsky krai, Paratunka, 684034 Russia*
Rulenko O.P., rulenko@kscnet.ru, *Institute of Volcanology and Seismology, Far East Branch, Russian Academy of Sciences, Petropavlovsk-Kamchatsky, 683006 Russia*
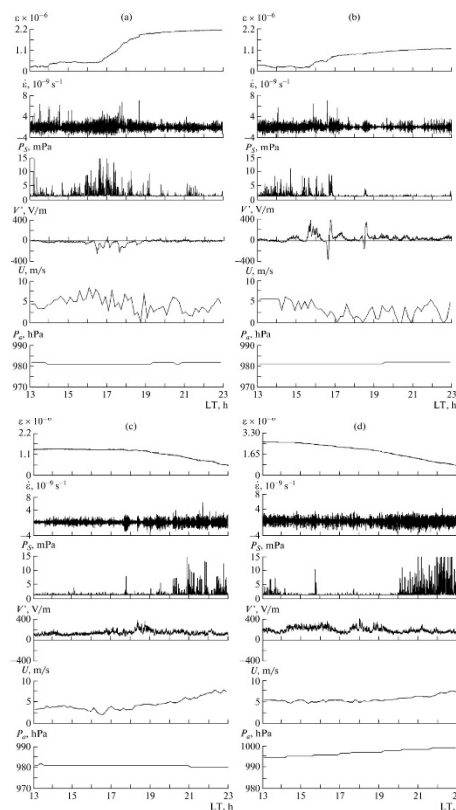
Fig. 5.2.8.1. Behavior of relative strain in near-surface rocks, ε, its rate, , acoustic pressure, *PS*, in the frequency range of 0.7–2.0 kHz, gradient of electric field's potential, *V*, wind speed, *U*, and atmospheric pressure, *Pa*, on October 14 (a), 16 (b), 15 (c), and 18 (d), 2009. The increase in ε corresponds to extension; the decrease, to compression.

During the period of October 1–18, 2009, 41 km southwest of Petropavlovsk-Kamchatsky, in the intersection zone of tectonic faults of various orders, simultaneous recording of the geoacoustic emission, gradient of the atmospheric electric field's potential, strains of the Earth's surface, atmospheric pressure, wind speed, and rain intensity was made. It was found for the first time that anomalous disturbances of high-frequency geoacoustic emission and atmospheric electric field near the Earth's surface originate as a simultaneous response to extension of near-surface sedimentary rocks. In the case of compression, only disturbances of geoacoustic emission occur. Anomalies were recorded under quiet weather conditions and with rocks strains being two orders greater than those of tidal ones (Fig. 5.2.8.1).

Marapulets, Y. V., Rulenko, O. P., Larionov, I. A., & Mishchenko, M. A. (2011). Simultaneous response of high-frequency geoacoustic emission and atmospheric electric field to strain of near-surface sedimentary rocks. Doklady Earth Sciences, 440(1), 1349-1352. Doi: 10.1134/S1028334X11090285

5.2.9. The finite-element method application for geophysical data

Dolgal A.S., dolgal@mi-perm.ru**, Michurin A.V., Novikova P.N., Christenko L.A., Sharkhimullin A.F.,** *Mining Institute of Ural branch of RAS, Perm, 614007, Russia*
Balk P.I., *Berlin, Germany*
Demenev A.G., *Permian State National Research University, Perm, 614990*
Rashidov V.A., rashidva@kscnet.ru, *Institute of Volcanology and Seismology FEB RAS, Petropavlovsk-Kamchatsky, 683006, Russia*
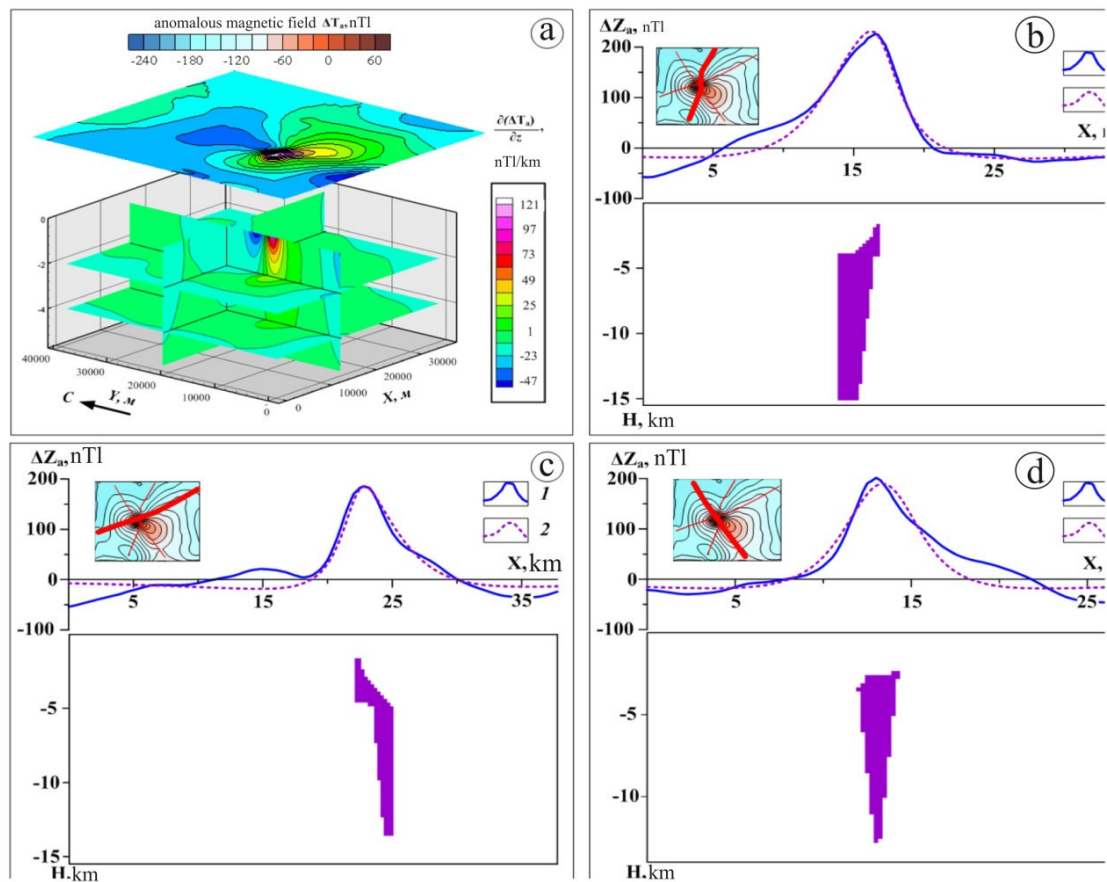
Fig. 5.2.9.1. Magnetic field of the submarine volcano 6.1 (Kurile arc) (*a*) and results of solving of the inverse problem of the magnetic by the mounting method for three gals (b-d); *1* – source field; *2* – modelled field.

In this research we consider finite-element interpretation technologies of gravity and magnetic data which are used to construct sourcewise approximations of fields and to determine parameters of field sources. A new algorithm of sourcewise approximations of gravity field is described in the paper. The computation process suggests solution of series of problems of one-dimensional optimization resulting in good match of observed and modeled fields with the number of sources lesser than the number of field points. The main characteristics of assembly method for solution of inverse gravity problem and the computing circuit are represented in the article. We suggest a new method of calculation of reliability estimation for interpretation of constructions on the basis of guaranteed approach. A new algorithm for determination of configuration of anomalous objects on interval value assignment of rock density (magnetization) is introduced in the paper. The article shows that application of high-performance computer clusters is productive. Model and practical examples for modeling of sources of geopotential fields are described (Fig. 5.2.9.1).

Dolgal, A. S., Balk, P. I., Demenev, A. G., Michurin, A. V., Novikova, P. N., Rashidov, V. A., Christenko, L. A., & Sharkhimullin, A. F. (2012). The finite-element method application for interpretation of gravity and magnetic data. Bulletin of Kamchatka regional association "Educational-Scientific Center". Earth sciences, 1(19), 108-127. (In Russian). http://www.kscnet.ru/kraesc/2012/2012_19/art8.pdf

5.2.10.   Geodynamical models of deep structures

Rodnikov A.G., Zabarinskaya L.P., Sergeyeva N.A. *Geophysical Center of the Russian Academy of Sciences, Moscow, Russia*
Rashidov V.A., rashidva@kscnet.ru, *Institute of Volcanology and Seismology FEB RAS, Petropavlovsk-Kamchatsky, 683006, Russia*

Numerous natural disasters, which have occurred in recent years, require the development of a new approach in research of modern geological processes. One of the directions of research in this domain of science includes creation of geodynamic models of the crust and upper mantle structure using the results from geological and geophysical studies. The area of research includes the transition zone between the Eurasian continent and the Pacific Ocean. Geodynamic models of deep structure were constructed for the Sea of Okhotsk, Sea of Japan, Philippine Sea and South China Sea regions, characterized by high seismicity, frequent volcanic eruptions and other natural hazards. The construction of these geodynamic models was based on the results of geological, geomorphological, seismic, seismological, petrological, geothermal, magnetic, electromagnetic and gravimetric researches; in addition the velocities of GPS stations and paleotectonic reconstruction were used for this. The development of geodynamic models of the deep structure of natural disaster regions can make a significant contribution to the general program studying the deep structure and geodynamic situation of the research areas, essential for a further assessment of risks in this or that zone and development of recommendations.

Rodnikov, A.G., Zabarinskaya, L.P., Rashidov, V.A., & Sergeyeva, N.A. (2014) Geodynamical models of the deep structure beneath the natural disaster regions of active continental margins. Moscow: Scientific World, 172 p. (In Russian). http://www.gcras.ru/?p=3046

5.2.11.   New model of the magma chamber

Vikulin A.V., vik@kscnet.ru, **Akmanova D.R.,** akmanova.dinara@mail.ru, *Institute of Volcanology and Seismology, Far East Division, Russian Academy of Sciences, Petropavlovsk-Kamchatsky, 683006, Russia*

In the frame of block representations on crust structure a fundamentally new model of thermal overheating of the magma chamber, located within the earth's crust has been proposed. The model that was the basis, developed in materials science for solid materials with intensive plastic deformations. These deformations at slow heat sink can lead to significant heating of the zone of plastic deformation until fracture of the body. The main arguments of the model are as follows.

The magnitude of localized plastic deformation may reach high values in slide zone, ≈ 1, and becomes close to zero outside such zones, ≈ 0. When the deformation rate of exponential manner depending on voltage and temperature, the plastic deformation can lead to temperature increases in the region of its localization at the expense of heat dissipation. In the case of small values of diffusivity, when compensation of heating does not occurs, the temperature in the zone of intensive plastic deformation will continue increase until the output mode of the thermal self-acceleration, which, usually, go to the destruction of the deformable part of the body, often as a result of its melting.

The thermodynamic calculations of the solid-state superheated above the melting point of the magma chamber, located at the depth boundaries of the crystalline basement H = 5-6 km (Kamchatka) were carried at low thermal conductivity of the earth's crust. When in this "superheated" chamber "germ" of the liquid phase is occur, in its solid part and adjacent to the chamber earth's crust created by the elastic stresses $\Delta P_l = 2,4 \cdot 109$ Pa. These elastic stresses are more than an order of magnitude above the lithostatic pressure $\Delta P_h = 10^8$ Pa. In our model of the magmatic chamber the condition $\Delta P_l \gg \Delta P_h$ is correct. It means that the thermodynamic conditions of the processes in superheated solid chamber is determined by the phase transition of magma "solid state – melt", which is accompanied by a volume increase, and does not depend on lithostatic pressure. This is an important conclusion, which enables a fundamentally new approach to the interpretation of the process of eruption.

This research proves the hypothesis of a constant and independent of the volcanic process thickness of the magma chamber as a property of the Earth crust. This idea is based on the most common distributions describing volcanic eruptions (recurrence curves, the squares, volumes of erupted material). The hypothesis is discussed in relation with the concept of block geomedium and its wave geodynamic movements.

Vikulin, A. V., & Akmanova, D. R. (2014). Magma chamber as a property of the Earth crust. Bulletin of Kamchatka regional association "Educational-Scientific Center". Earth sciences, 1(23), 213-230. (In Russian). http://www.kscnet.ru/kraesc/2014/2014_23/art17.pdf

5.2.12. Wave volcanic processes

Vikulin A.V., vik@kscnet.ru, **Akmanova D.R.,** akmanova.dinara@mail.ru, **Dolgaya A.A.,** adolgaya@kscnet.ru, *Institute of Volcanology and Seismology, Far East Division, Russian Academy of Sciences, Petropavlovsk-Kamchatsky, 683006, Russia*
Vikulina S.A., *Kamchatka branch, Geophysical Survey of the Russian Academy of Sciences 9, Boulevard Piip, Petropavlovsk-Kamchatsky 683006, Russia*

This research was based on author's catalogue of eruptions includes data on 627 volcanoes of the planet, which cover 6 850 eruptions in total through the past 12 thousand year, i.e. from 9650 BC to 2013. The energy characteristics of earthquakes are magnitudes, M, and of eruptions values W, where W = 1, 2, ..., 5, ..., 7 correspond to ejection volumes $10^{-(4-5)}$, 10^{-3}, ..., 1, ..., 10^2 km^3.

In studies of spatial and temporal distributions of events, such a configuraion of the zones (*Lmax>>Λ*) allows using two coordinates instead of three coordinates (latitude, longitude, and

time) of the plane with axes 'distance along the belt length *l* (0≤*l*≤*Lmax*) –time *t* (0≤*t*≤*T*$_{max}$), where T$_{max}$ – maximum duration catalogs of earthquakes (*ea*) and volcanic eruptions (*er*). Sets of the nodal points are determined for the most active areas (with the largest clusters of events), and thus they typically follow the junction lines of tectonic plates and the highest amounts of the volcanoes and earthquake sources (Fig. 5.2.12.1).
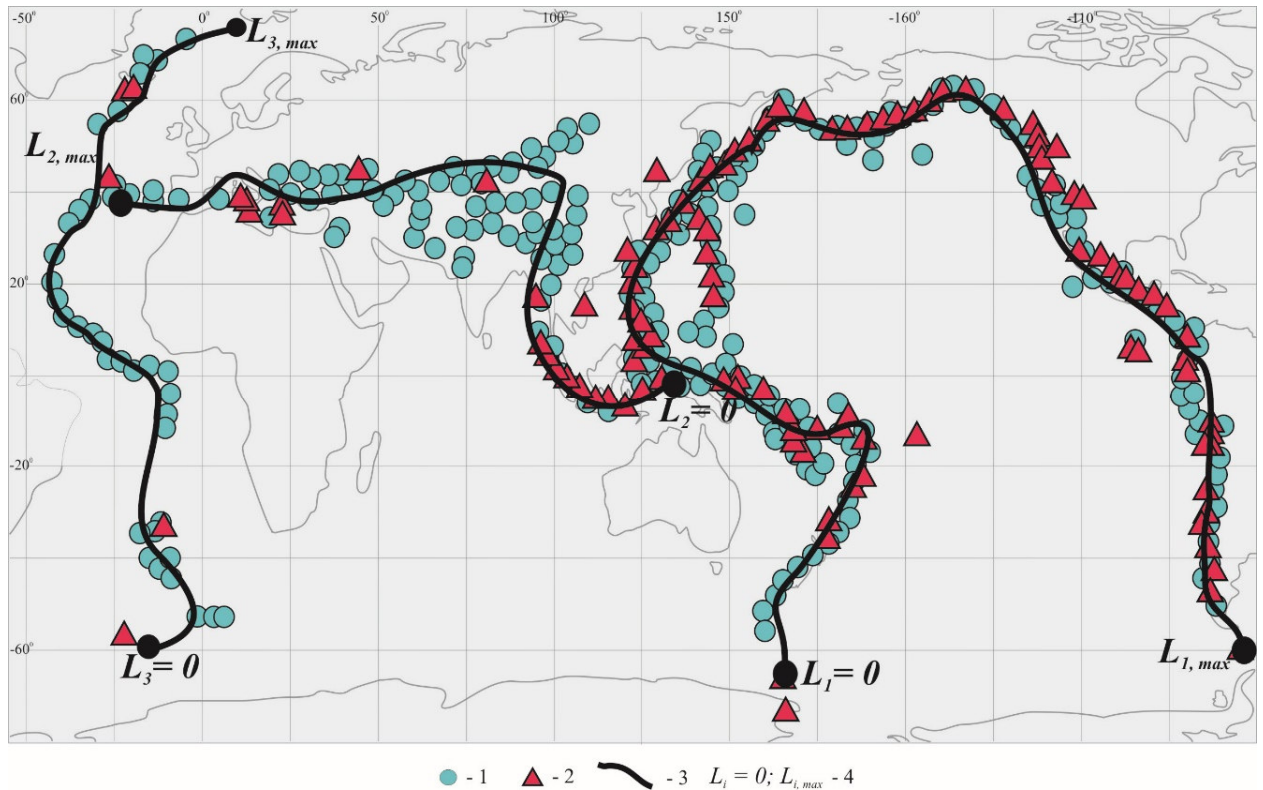

Fig. 5.2.12.1. Active zones of the planet [*Vikulin, et al., 2011*]. *1* – earthquake foci; *2* – volcanoes with eruptions; *3* – lines along the axes of the belts in reference to which coordinates *l* of earthquakes and volcanoes are calculated; *4* – terminations of zones ($L_i = 0$; $L_{i, max}$) (*i* = 1 – the Pacific margin; *i* = 2 – Alpine-Himalayan belt; *i* = 3 – Mid-Atlantic Ridge).

Lengths of the three most active belts of the Earth are determined as follows (Fig. 5.2.12.2): the Pacific margin from Buckle Island Volcano (Antarctica) L_1=0 to Desepson Volcano (South Shetland Islands) – L_1,max=45 000 km; the Alpine-Himalayan belt from Timor Island (Indonesia) L_2=0 to the Azores – L_2,max =20 500 km; the Mid-Atlantic Ridge from South Sandwich Islands (South Atlantic) L_3=0 to Iceland Island (North Atlantic) – L_3,max =18 600 km.

The events in the chains demonstrate the linear dependence between time of their occurrence and coordinates along the belt. (Fig. 5.2.12.2). The inclination of this line characterize the rate of movement of volcanic eruptions in space and time, which means rate of migration of volcanic activity (V).
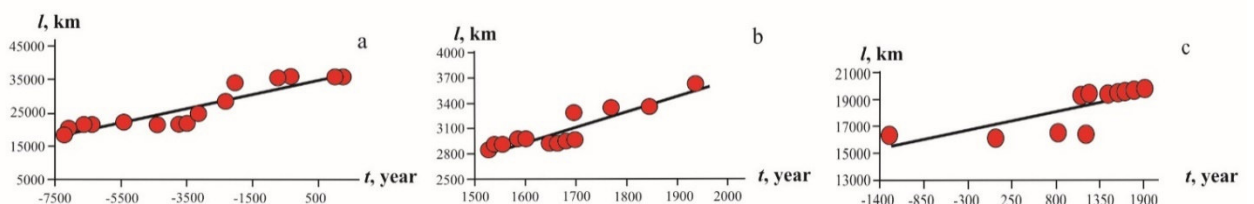

Fig. 5.2.12.2. Examples of migration chains: a) $W \geq 5$ within the Pacific margin; b) $W \geq 4$ within the Alpine-Himalayan Belt; c) $W \geq 4$ within the Mid-Atlantic Ridge. Migration velocities, *V for this chains* correspond to *V* = 90; 20; 2 km/year, respectively.

Within all energy ranges for all studied regions detected a large number of migration chains, which allows us to assume that migration is a characteristic feature of the volcanic activity of the Earth. The parameters of all the identified chains of seismic and volcanic activity are presented in the Table.1.

Table 1. Parameters of migration chains of volcanic eruptions revealed in the regions under study

W, km³	p	$N \pm \Delta N$	$T \pm \Delta T$, year	$L \pm \Delta L$, km	$V \pm \Delta V$, km/year
The Pacific margin					
$W \geq 1$	97	50 ± 16	2692 ± 3175	20468 ± 6956	62 ± 50
$W \geq 2$	90	44 ± 17	2833 ± 3256	19768 ± 8098	53 ± 43
$W \geq 3$	54	25 ± 9	4155 ± 3585	18014 ± 7789	27 ± 30
$W \geq 4$	34	15 ± 5	4953 ± 3058	15996 ± 5708	9 ± 10
$W \geq 5$	19	10 ± 3	5400 ± 2406	18426 ± 6179	12 ± 15
$W \geq 6$	12	5 ± 1	5534 ± 2387	11998 ± 6389	2 ± 1
The Pacific margin					
$W \geq 1$	38	31 ± 17	475 ± 465	3401 ± 2588	10 ± 4
$W \geq 2$	33	27 ± 14	475 ± 465	3586 ± 2859	9 ± 3
$W \geq 3$	11	11 ± 5	747 ± 470	3010 ± 2103	4 ± 2
$W \geq 4$	5	5 ± 1	877 ± 618	6034 ± 5642	5 ± 2
$W \geq 5$	2	5 ± 2	4336 ± 455	6936 ± 6909	1 ± 1
The Pacific margin					
$W \geq 1$	26	12 ± 8	2855 ± 3293	5570 ± 3682	27 ± 33
$W \geq 2$	24	11 ± 7	3061 ± 3407	5476 ± 3756	29 ± 35
$W \geq 3$	12	10 ± 7	5217 ± 3857	3282 ± 2565	2.5 ± 3
$W \geq 4$	6	11 ± 6	6214 ± 3304	4807 ± 2115	1 ± 0.6
$W \geq 5$	3	5 ± 3	7087 ± 1747	43 ± 28	0.002 ± 0.001

W – 'energy' of eruption; p – number of revealed migration chains; N – average number of volcanic eruptions in a migration chain; T – average timeline of a migration chain (year); L – average length of a migration chain (km); V – average migration velocity of volcanic eruptions of various 'energy' ranks (km/year).

It was found that the logarithm of velocity of the volcanic activity migration LgV within studied belts are relate to W characteristic (Fig. 5.2.12.3)

$$W \approx (-3.1 \pm 0.6)LgV; \quad W \approx (-3.9 \pm 1.0)LgV; \quad W \approx (-0.8 \pm 0.2)LgV$$
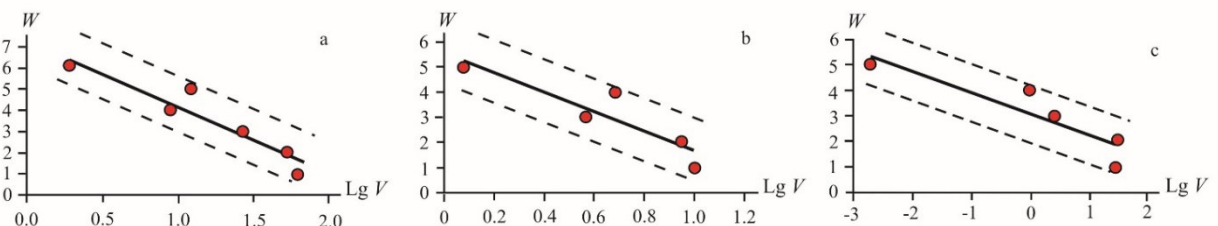

Fig. 5.2.12.3. Migration velocity V of volcanic eruptions vs. energy characteristic W: a) Pacific margin; b) the Alpine-Himalayan Belt; c) Mid-Atlantic Ridge

Presented here data obtained on a large statistical material. Despite the fact that there are eruptions of various different types of volcanoes that are located in regions with different geodynamic conditions, and each value of the velocity was determined with a wide range of deviations, the mean values of the rates of migration show a linear dependence on the energy performance of eruptions.

Slopes of volcanic curves LgV≈pWiW, showing specific features of migration of volcanic eruptions, are negative. Such a decrease of migration velocity of volcanic eruptions with increasing

184

values of W seems to be related to tension stresses within all the volcanic belts; the tension stresses are caused by magma penetration from the depth, which confirms the wave origin of volcanic process. This allows us to use the physics of wave processes to create models that describe the distribution of volcanic eruptions in space and time.

Vikulin, A. V., Akmanova, D. R., Vikulina, S. A., & Dolgaya, A. A. (2012) Migration of seismic and volcanic activity as display of wave geodynamic process. Geodynamics & Tectonophysics. 3(1). 1–18. Doi: 10.5800/GT-2012-3-1-0058

Dolgaya, A. A., Akmanova, D. R., Vikulina, S. A., & Vikulin, A. V. (2012) Volcanism as a wave process. Conference „Volcanism and rekated processes",Petropavlovsk-Kamchatsky, Institute of Volcanology and Seismology FED RAS, 2012, p. 112-115. (In Russian). http://www.kscnet.ru/ivs/publication/volc_day/2012/art18.pdf

Dolgaya, A. A., & Vikulin, A. V. On modeling of the systematics of the geodynamic process // Academical Journal of Western Siberia, 2014, v.10. №6 (55). p. 30-31. (In Russian).

Vikulin, A. V., & Melekestsev, I. V. Akmanova D.R., Dolgaya A.A. Vaschenko N.A. Catalog of seismic and volcanic events // The certificate of database registration № 2014620569 by 17.04.2014.